





# **Photoinduced Charge Transfer Processes in Triarylamine Based Redox Cascades**

Dissertation zur Erlangung des  
naturwissenschaftlichen Doktorgrades  
der Julius-Maximilians-Universität Würzburg

vorgelegt von

**Marco Holzapfel**

aus Aschaffenburg

Würzburg 2007

Eingereicht am: 5. Oktober 2007

bei der Fakultät für Chemie und Pharmazie

1. Gutachter: Prof. Dr. Christoph Lambert

2. Gutachter: Prof. Dr. Ingo Fischer

der Dissertation

1. Prüfer: Prof. Dr. Christoph Lambert

2. Prüfer: Prof. Dr. Ingo Fischer

3. Prüfer: Prof. Dr. Frank Würthner

des Öffentlichen Promotionskolloquiums

Tag des Öffentlichen Promotionskolloquiums: 3. Dezember 2007

Die vorliegende Arbeit wurde in der Zeit von September 2003 bis September 2007  
am Institut für Organische Chemie der Universität Würzburg angefertigt.

Mein besonderer Dank gilt

*Herrn Prof. Dr. Christoph Lambert*

für die Vergabe des vielseitigen Themas, die intensive Betreuung und Förderung und  
das mit vielen Anregungen und Diskussionen verbundene Interesse an dieser Arbeit.

*Falls Gott die Welt geschaffen hat, war seine Hauptsorge sicher nicht,  
sie so zu machen, dass wir sie verstehen können.*

Albert Einstein  
(1879 – 1955)

***meinen Eltern***

# Contents

<b>1</b>	<b>Introduction .....</b>	<b>1</b>
1.1	Fundamental Importance of Electron Transfer Processes ....	1
1.2	Theory .....	2
1.2.1	Diabatic and Adiabatic Electron Transfer .....	3
1.2.2	Marcus Theory .....	5
1.2.3	Extension of Marcus Theory .....	9
1.2.4	Electron Transfer Mechanisms .....	14
1.2.4.1	Superexchange Mechanism .....	14
1.2.4.2	Hopping Mechanism .....	15
1.3	State of the Art .....	16
1.3.1	Application of Suitable Redox Centres .....	16
1.3.2	Possible Approaches to Realise a Long-lived CS State ....	22
1.4	Project Aim .....	27
1.4.1	Design of the Cascades .....	27
1.4.2	Characterisation of CS States .....	29
<b>2</b>	<b>Transient Absorption Spectroscopy of Fluorescent Compounds in the ns Time Domain .....</b>	<b>30</b>
2.1	Introduction .....	30
2.2	Results and Discussion .....	31
2.3	Conclusion .....	35

<b>3 Photoinduced Charge Separation and Recombination in Acridine-Triarylamine Based Redox Cascades .....</b>	<b>36</b>
3.1 Introduction .....	36
3.2 Results and Discussion .....	39
3.2.1 Synthesis .....	39
3.2.2 Redox Properties .....	44
3.2.3 Stationary Spectroscopy .....	46
3.2.3.1 Steady State Absorption Spectroscopy .....	46
3.2.3.2 Steady State Emission Spectroscopy .....	48
3.2.4 Time Resolved Spectroscopy .....	51
3.2.4.1 Time Resolved Fluorescence Spectroscopy .....	51
3.2.4.2 Transient Absorption Spectroscopy .....	59
3.3 Conclusion .....	71
<b>4 Experimental Section .....</b>	<b>73</b>
4.1 Analytical Methods .....	73
4.1.1 General Analytical Methods .....	73
4.1.2 Cyclic Voltammetry .....	73
4.1.3 Spectroelectrochemistry .....	74
4.1.4 UV/Vis Spectroscopy .....	74
4.1.5 Fluorescence Spectroscopy .....	75
4.1.6 Transient Absorption Measurements .....	76
4.1.7 Synthesis .....	81



<b>4.2 Synthesis</b>	<b>81</b>
<b>4.2.1 General Experimental Procedures</b>	<b>81</b>
4.2.1.1 Palladium Catalysed Amination of Aryl Halides (GP1)	81
4.2.1.2 Hagihara-Coupling (GP2)	81
<b>4.2.2 Synthesis of Precursors</b>	<b>82</b>
<b>4.2.3 Synthesis of Reference Chromophores</b>	<b>102</b>
<b>4.2.4 Synthesis of Cascades</b>	<b>105</b>
<b>5 Literature</b>	<b>115</b>
<b>6 Table of Formulas</b>	<b>123</b>
<b>6.1 Reference Chromophores</b>	<b>123</b>
<b>6.2 Cascades</b>	<b>123</b>
<b>6.3 Precursors</b>	<b>124</b>
<b>7 Summary</b>	<b>127</b>
<b>8 Zusammenfassung</b>	<b>129</b>
<b>Appendix</b>	<b>131</b>
<b>Publikationen</b>	<b>131</b>
<b>Danksagung</b>	<b>132</b>
<b>Erklärung</b>	<b>135</b>

# Abbreviations

Ac	acridine
ATP	adenosine triphosphate
CR	charge recombination
CS	charge separation / charge separated
<sup>1</sup> CS	excited singlet charge separated
<sup>3</sup> CS	excited triplet charge separated
CT	charge transfer
<sup>1</sup> CT	excited singlet charge transfer
<sup>3</sup> CT	excited triplet charge transfer
CV	cyclic voltammetry / cyclic voltammogram
CW	continuous white light
dba	<i>trans,trans</i> -dibenzylideneacetone
DMF	dimethylformamide
DSSC	dye sensitised solar cells
ET	electron transfer
Fc	ferrocene
H	Hoechst 33258
HT	hole transfer
ISC	intersystem crossing
IVCT	intervalence charge transfer
LFP	laser flash photolysis
NADP	nicotinamide adenine dinucleotide phosphate
MeCN	acetonitrile
NIR	near infrared
OD	optical density
PET	photoinduced electron transfer
PhCN	benzonitrile
PMT	photomultiplier
S <sub>0</sub>	singlet ground state
S <sub>1</sub>	excited singlet state

SEC	spectroelectrochemistry
T	triplet state
TBAF	tetrabutylammonium fluoride
TBAH	tetrabutylammonium hexafluorophosphate
THF	tetrahydrofuran
UV	ultraviolet
Vis	visible

# 1 Introduction

## 1.1 Fundamental Importance of Electron Transfer Processes

Electron transfer processes are of fundamental relevance in chemistry as well as in biology. On earth, for organisms there exist only two different sources to gain energy. Chemotrophs use redox reactions to produce ATP whereas phototrophs convert sunlight into chemical energy. In both biochemical pathways several electron transfer processes are utilised to provide chemical energy.

As green plants (phototrophs) produce oxygen and are moreover considered to build the basis of the food chain, electron transfer steps in photosynthesis are essential for almost all life on earth. In the first of two steps light is required to generate energy-rich molecules. Photons are absorbed by the pigment chlorophyll which acts as a reducing agent in its excited state. Finally, at the end of several electron transfer steps NADP is reduced to NADPH/H<sup>+</sup> and a proton gradient across a membrane is generated which is used to synthesise ATP. In the following light-independent second step these high-energy substrates (NADPH/H<sup>+</sup> and ATP) are needed to generate small organic precursors for the main product glucose. To summarise, photosynthesis can be regarded as conversion of light into chemical energy with oxygen as a waste product.<sup>[1, 2]</sup>

Humans and most animals belong to the group of chemotrophic heterotrophs. They are not capable of producing energy-rich molecules on their own and depend on the ingestion of high-energy molecules produced by phototrophs. Intracellular electron transfer in mitochondria of eukaryotes from an energy-rich donor to an acceptor of lower energy occurs via several redox reactions along a cascade consisting of a directed redox gradient. Finally, the electron transfer reactions result in an electrochemical potential gradient across the mitochondrial inner membrane. This potential gradient (usually a proton gradient) powers the so-called enzyme ATP synthase to synthesise the universal energy carrier of cells, ATP.<sup>[3-5]</sup>

Due to their basic importance directed electron transfer processes along redox cascades have intensively been studied. Beyond learning fundamental aspects of photoinduced electron transfer reactions it is a general aim to mimic natural processes like photosynthesis to generate and store chemical energy. Research on (organic) solar cells is a timely field for several years and has attracted attention even in public since the discussion of climate warming has become a popular topic in the media. Development of solar cells with high efficiencies which are moreover cheap in fabrication and which exhibit no photodegradation would solve most of the world's energy problems. Solar energy conversion is a very clean energy generation using the sun as an effectively unlimited source.

In this work we report about the synthesis and the photophysical characterisation of acridine-triarylamine based redox cascades. These chromophores were designed in order to study directed photoinduced charge transfer processes in detail and to identify possible deactivation pathways depending on substituents and solvent polarity.

This chapter is organised as follows: at first, diabatic and adiabatic electron transfer reactions are explained followed by the discussion of different electron transfer theories. Then, hopping and superexchange mechanisms are outlined as two examples of electron transfer mechanisms. The next chapter deals with the state of the art and comprises a discussion of various redox centres as well as possible approaches to realise a long-lived charge separated state. The last part of the Introduction explains the design of the cascades and elucidates the importance of an accurate characterisation.

## 1.2 Theory

Generally, intramolecular electron transfer (ET) processes deal with electron transfers between a donor (D) and an acceptor (A) subunit of a dyad DA. In photoinduced electron transfer reactions one subunit is excited by light of appropriate wavelength. This results in a population of an excited state of either D\*A or DA\* in which either D\* or A\* is a better reducing or oxidising agent than its ground state. Provided that D<sup>+</sup>A<sup>-</sup> is lower in energy this excitation is followed by an electron transfer from the donor to the acceptor to form a charge separated (CS) state D<sup>+</sup>A<sup>-</sup> (see Equation 1.1 and Figure 1.1).



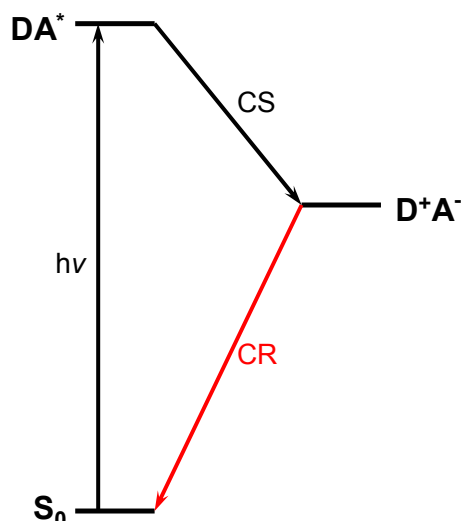


**Figure 1.1** Three-state model for a donor-acceptor dyad. Photoexcitation of DA is followed by charge separation (CS) resulting in a CS state and subsequent **charge recombination (CR)**.

### 1.2.1 Diabatic and Adiabatic Electron Transfer

The potential energy of the reactant DA is a function of many nuclear and solvent coordinates which results in a multidimensional potential-energy surface. For the product there exists a quite similar energy surface. To reduce the complex surface to a simpler energy profile, a reaction coordinate is introduced which is not only a cut within the surface but corresponds to a weighted distribution of all modes. Assuming that the Gibbs free energy  $\Delta G$  is given vertically, the energy profiles can be regarded as parabolas in the diabatic case with identical force constants (see Figure 1.2).<sup>[6]</sup>

Generally two types of electron transfer reactions are differentiated. In case of a large electronic coupling  $V$  compared to the thermal energy  $k_B T$  (with the Boltzmann constant  $k_B$  and the temperature  $T$ ) the ET reaction is of adiabatic nature, whereas in case of a small  $V$  the process is called diabatic.

$$\text{adiabatic: } V > k_B T \qquad \text{diabatic: } V < k_B T \qquad (1.2)$$

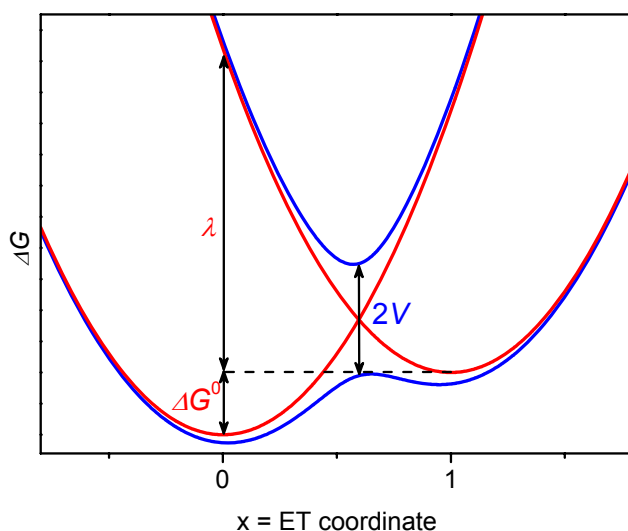


**Figure 1.2** Gibb's free energy of reactants and products as a function of the reaction coordinate for **diabatic** and **adiabatic** ET transfer.  $V$  = coupling energy,  $\lambda$  = Marcus reorganisation energy,  $\Delta G^0$  = difference of the free energy between the diabatic states and  $\Delta G^*$  = activation energy for the diabatic ET transfer.

The difference in  $\Delta G$  of the two adiabatic potential energy surfaces at the crossing point of the diabatic surfaces (regarded as parabolas) corresponds to  $2V$ . As it is shown in Equation 1.2 in the adiabatic case the electronic coupling is larger than the thermal energy. Consequently, the reaction occurs only on the lower potential surface and the upper one can be excluded from further considerations.<sup>[7]</sup> Due to very weak interactions in the diabatic case the reactant parabola cross the energy surface of the product.

Equation 1.3 is often used to calculate rate constants for diabatic ET processes. This equation is based on the Marcus theory which considers ET steps as thermally activated processes.<sup>[8]</sup> A derivation is given in the next chapter.

$$k_{\text{ET}} = 4\pi^2 hc^2 V^2 \sqrt{\frac{1}{4\pi\hbar c \lambda_o k_B T}} \exp\left[-\frac{\hbar c (\lambda_o + \lambda_i + \Delta G^0)^2}{4\lambda_o k_B T}\right] \quad (1.3)$$

In this equation  $h$  represents the Planck's constant,  $c$  the speed of light in vacuo and  $\lambda_o$  and  $\lambda_i$  the outer and the inner reorganisation energy, respectively.  $\Delta G^0$  corresponds to the Gibb's free energy.

In contrast, due to large distances separating opposite charges in the CS state of *extended* cascades, the electronic coupling should be quite small and consequently ET reactions should be diabatic in nature.

The proportionality according to Equation 1.3 between  $k_{\text{ET}}$  and  $V^2$  is only valid in case of a weak coupling  $V$  and a slow ET rate compared to nuclear motions along the reaction coordinate. With increasing electronic coupling the oscillation frequency  $\omega_C$  of the slowest nuclear motion becomes the rate determining step. Thus, the rate constant  $k_{\text{ET}}$  becomes independent of  $V$  and Equation 1.3 transforms into Equation 1.4 in which the prefactor now depends on the longitudinal solvent relaxation time  $\tau_L$ .<sup>[7]</sup>

$$k_{\text{ET}} = \frac{1}{\tau_L} \sqrt{\frac{hc\lambda_0}{16\pi k_B T}} \exp\left(-\frac{hc(\Delta G^0 + \lambda_0)^2}{4\lambda_0 k_B T}\right) \quad (1.4)$$

The longitudinal dielectric relaxation time  $\tau_L$  is given by the refractive index of the solvent  $n$ , the static dielectric constant of the solvent  $\epsilon_s$  and the Debye dielectric relaxation time  $\tau_D$ .<sup>[7]</sup>

$$\tau_L = \left(\frac{n^2}{\epsilon_s}\right) \tau_D \quad (1.5)$$

Because the electronic coupling  $V$  increases exponentially with decreasing distance of donor and acceptor subunits, ET reactions within compact molecules are more likely to refer to adiabatic processes. Even in chromophores with small electronic coupling electron transfer can occur adiabatically if nuclear motion along the reaction coordinate is slowed down as a result of low temperature or long relaxation times.<sup>[7, 9]</sup>

## 1.2.2 Marcus Theory

Although Marcus derived his theory primarily for outer sphere electron transfer reactions, it is probably the most widely applied theory for intramolecular electron transfer reactions by now.<sup>[10-15]</sup> This model considers ET steps as thermally activated processes with an activation barrier  $\Delta G^*$  (Equation 1.6). The prefactor  $k_0$  depends on the electronic coupling  $V$  of the corresponding subunits.<sup>[8]</sup>

$$k_{\text{ET}} = k_0 \exp\left(-\frac{\Delta G^*}{k_B T}\right) \quad (1.6)$$



The Marcus theory is based on the assumption of harmonic diabatic free-energy surfaces. The two intersecting parabolas which represent reactant and product states and which result from introducing a reaction coordinate have identical force constants. Marcus demonstrated the influence of the energies of the involved states on the rate constants for ET reactions.

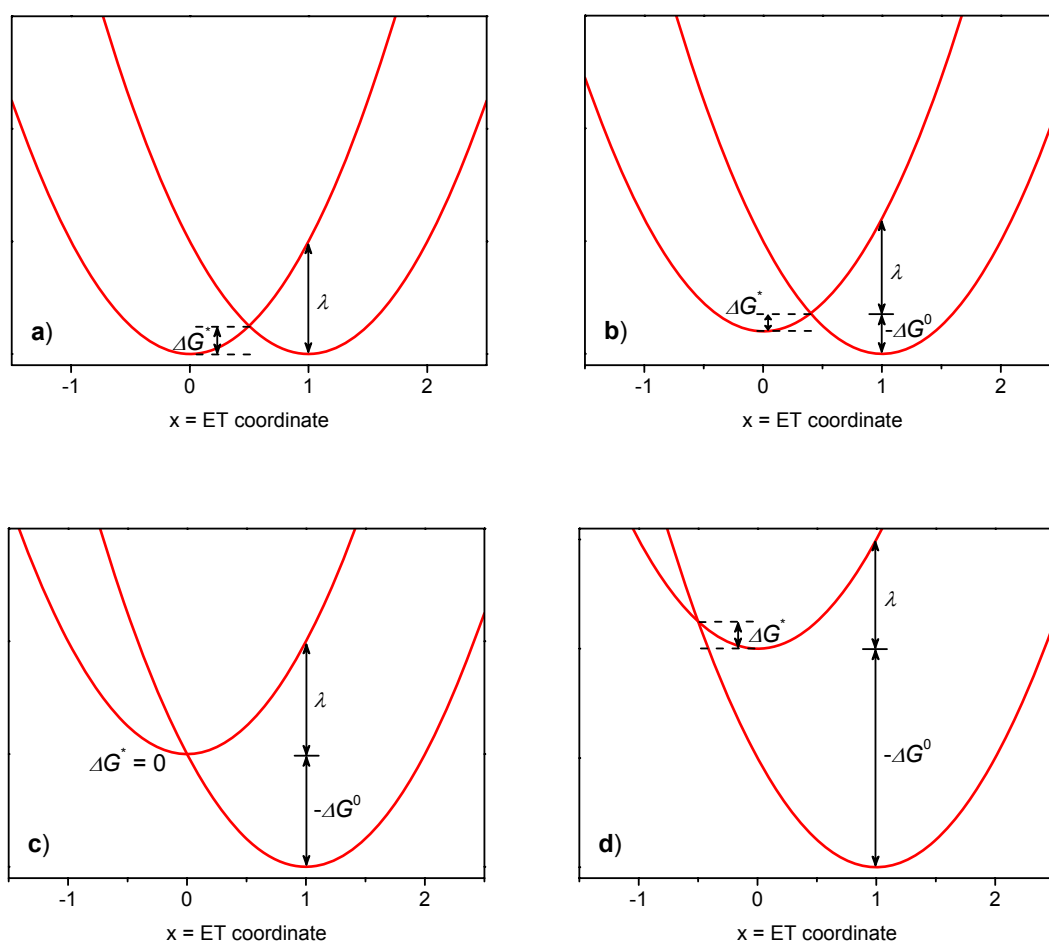


**Figure 1.3** Diabatic potentials in case of **a)** self-exchange reaction ( $-\Delta G^0 = 0$ ); **b)** the Marcus normal region ( $-\Delta G^0 < \lambda$ ); **c)** optimal conditions ( $-\Delta G^0 = \lambda$ ) and **d)** the Marcus inverted region ( $-\Delta G^0 > \lambda$ ).

Figure 1.3 illustrates four different situations which can generally underlie ET processes in case of very weak electronic coupling  $V$ . Figure 1.3a displays the case of a self-exchange reaction (or any other conditions where  $\Delta G^0 = 0$ ) where the energies of the equilibrium configurations of reactant and product are identical. Although  $\Delta G^0 = 0$  there is a significant barrier  $\Delta G^*$  for electron transfer. On the basis of geometrical considerations the activation barrier is calculated according to Equation 1.7.<sup>[8]</sup>

$$\Delta G^* = \frac{\lambda}{4} \quad (1.7)$$

For forward ET processes it is assumed that the product parabola is lowered vertically by  $-\Delta G^0$  (see Figure 1.3b). From Figure 1.3b it is evident that  $-\Delta G^0 < \lambda$ , which is called the Marcus normal region. Here, the activation barrier  $\Delta G^*$  is given by

$$\Delta G^* = \frac{(\lambda + \Delta G^0)^2}{4\lambda} \quad (1.8)$$

Substituting Equation 1.8 into 1.6 yields

$$k_{\text{ET}} = k_0 \exp\left[-\frac{hc(\lambda + \Delta G^0)^2}{4\lambda k_B T}\right] \quad (1.9)$$

In the case of diabatic conditions (weak electronic coupling  $V$ ) the prefactor  $k_0$  can be estimated by Equation 1.10.

$$k_0 = \frac{2\pi^{1.5} hc^2 V}{\sqrt{hc\lambda k_B T}} \quad (1.10)$$

With increasing  $-\Delta G^0$  the barrier  $\Delta G^*$  decreases and consequently the rate constant  $k_{\text{ET}}$  increases until it reaches its maximum when  $\Delta G^* = 0$  (see Figure 1.3c). The maximal rate constant is obtained if  $-\Delta G^0 = \lambda$ .

Figure 1.3d shows that a further increase of  $-\Delta G^0$  leads to an increase of  $\Delta G^*$  and consequently  $k_{\text{ET}}$  decreases. If ET is a highly exergonic process, i.e.  $-\Delta G^0 > \lambda$ , the reaction is located in the Marcus inverted region. Often it is desirable to design the chromophores in a way that charge recombination is located in that regime. It combines a slow recombination rate with an energy-rich excited CS state.

A crucial point in determining the rate constants on the basis of Marcus theory is the reorganisation energy  $\lambda$ .<sup>[6]</sup> It corresponds to the energy which is required to change the geometry of the chromophore as well as the orientation of the solvent molecules upon charge transfer. The configuration must change from the equilibrium of the reactant to the

equilibrium of the product that means from the minima of the left parabola to the minima of the right one. The overall reorganisation energy  $\lambda$  is the sum of the inner  $\lambda_i$  and outer  $\lambda_o$  reorganisation energy.

$$\lambda = \lambda_i + \lambda_o \quad (1.11)$$

The inner reorganisation energy  $\lambda_i$  refers to changes in bonding lengths and angles accompanying the ET process and is solvent independent. In contrast,  $\lambda_o$  is the part of the reorganisation energy caused by reorientation of the solvent molecules. Assuming that excited states are mostly of dipolar character, both  $\lambda_o$  and  $\Delta G^0$  depend strongly on solvent polarity. With increasing solvent polarity  $\Delta G^0$  decreases whereas  $\lambda_o$  increases. Thus, it is obvious that  $\lambda_i$  is the only parameter that can be affected by a proper design of the chromophore. As it is explained below, a small reorganisation energy is preferred to ensure fast charge separation and slow recombination processes. The inner reorganisation energy can be determined by Jortner fits of the absorption or emission bands of one compound in a given solvent.<sup>[16]</sup> The outer reorganisation energy can be calculated in the same way or by the Born equation 1.12.<sup>[17]</sup>

$$\lambda_o = \frac{e^2}{4\pi\epsilon_0} \left( \frac{1}{n^2} - \frac{1}{\epsilon_s} \right) \left( \frac{1}{2r_D} + \frac{1}{2r_A} - \frac{1}{R} \right) \quad (1.12)$$

In Equation 1.12  $e$  stands for the elementary charge,  $n$  for the refractive index and  $\epsilon_s$  for the static dielectric constant of the solvent.  $r_D$  and  $r_A$  are the radii of the donor and the acceptor subunit, respectively.  $R$  is the centre to centre distance of donor and acceptor. Although  $\lambda_o$  varies with temperature as  $n$  and  $\epsilon_s$  depend slightly on temperature, normally  $\lambda_o$  varies only within a 5 % range when changing the temperature for more than 100 K.<sup>[6]</sup>

In photoinduced electron transfer processes charge separation is expected to be in the Marcus normal region ( $-\Delta G^0 < \lambda$ ) and charge recombination in the inverted region ( $-\Delta G^0 > \lambda$ ). As fast charge separation and slow recombination rates are often preferred, a small internal reorganisation energy is appropriate to comply with these conditions. Figure 1.4 displays the effects of the reorganisation energy on the activation barrier and thus on the rates of electron transfer. A small reorganisation energy (blue curves) entails a small

activation barrier  $\Delta G^*$  for charge separation (Figure 1.4a) but impedes charge recombination (Figure 1.4b) due to a high activation barrier  $\Delta G^*$ .

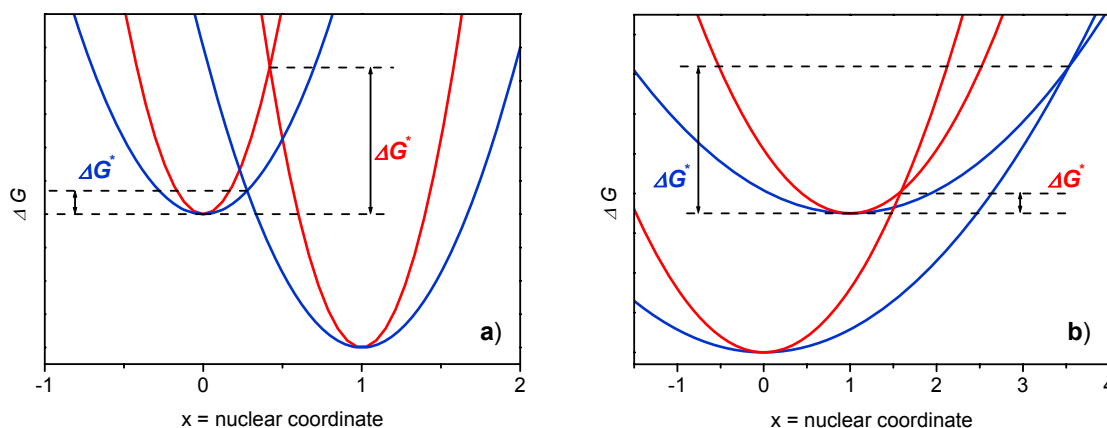


**Figure 1.4** Effect of **small** and **large** reorganisation energy on the activation barrier  $\Delta G^*$  for the processes of **a)** charge separation (normal region) and **b)** charge recombination (inverted region).

### 1.2.3 Extension of the Marcus Theory

It has been reported that the inverted region effect is less pronounced than predicted on basis of the classical Marcus theory. Slow recombination rates were explained by spin-forbidden transitions like intersystem crossing (ISC) which decelerates electron transfer processes.<sup>[8]</sup> Nuclear tunnelling reduces the high activation barrier for ET transfer in the inverted region and accelerates ET.<sup>[18, 19]</sup> However, the inverted region was confirmed experimentally by Miller *et. al.*<sup>[20]</sup> and must not be ignored completely. The effect of the inverted region is discussed controversially depending on the theory which is applied.

On the basis of the classical Marcus theory Levich<sup>[21]</sup> and Dogonadze<sup>[22]</sup> extended the electron transfer theory by taking nuclear tunnelling into account. The most important factors in this approach are the electronic coupling  $V$  and the overlap of the vibrational wavefunctions of reactant and product. The overlap integral at the transition state is a measure for the probability that ET occurs. Diabatic ET is possible in three cases.<sup>[6]</sup>

1. Higher levels near the intersection point of the energy surfaces are populated. Assuming that reactant and product state exhibit the same nuclear configuration electron tunnelling is possible even if the electronic coupling  $V$  is weak.

2. The overlap of the wavefunctions is below the transition state but it is large enough to ensure significant ET transfer.
3. In case of very low temperature only the lowest vibrational states are populated. Due to very small overlap of the wavefunctions electron transfer is extremely but not completely unlikely. Here, the ET rate is almost temperature independent.

Bixon and Jortner introduced the quantitative treatment of radiationless transitions.<sup>[23-26]</sup> Vibrations of the solvent are mostly of low frequency nature and are treated within one classical solvent mode. Moreover, in the Bixon-Jortner theory the high energy vibrations of the reactant state are represented by one averaged mode. The introduction of vibrational modes provides additional transitions channels from the reactant to the product (see Figure 1.5). Furthermore, with population of high-energy vibrational modes the difference in free energy between reactant and product states is reduced and consequently the rate constant for ET should increase. The total rate constant is calculated by the sum over all channels (see Equation 1.13).<sup>[24]</sup>

$$k_{\text{ET}} = \sum_{n=0}^{\infty} \left( \frac{k_{\text{NA}}^{0n}}{1 + H_{\text{A}}^{(n)}} \right) \quad (1.13)$$

with  $k_{\text{NA}}^{0n}$  as the corresponding diabatic rate for  $n=0 \rightarrow n$ . This rate is calculated by Equation 1.14.

$$k_{\text{NA}}^{0n} = A_{\text{NA}} \left| \langle 0|n \rangle \right|^2 \exp \left[ - \frac{(\Delta G_n - \lambda_o)^2}{4\lambda_o k_{\text{B}} T} \right] \quad (1.14)$$

with  $\left| \langle 0|n \rangle \right|^2$  being the nuclear Franck-Condon factor. The diabatic frequency factor  $A_{\text{NA}}$  is defined as follows

$$A_{\text{NA}} = \frac{2\pi^{1.5} hc^2 V^2}{\sqrt{hc\lambda_o k_{\text{B}} T}} \quad (1.15)$$

$H_{\text{A}}^{(n)}$  is the adiabaticity parameter for the  $n=0 \rightarrow n$  channel and is given by

$$H_A^{(n)} = H_A \left| \langle 0|n \rangle \right|^2 \quad (1.16)$$

where the adiabatic factor  $H_A$  is<sup>[24]</sup>

$$H_A = \frac{4\pi V^2 \tau_L}{\hbar \lambda_0} \quad (1.17)$$

By means of the adiabatic factor  $H_A$  (see Equation 1.17) it is possible to distinguish whether an electron transfer is of diabatic or solvent controlled adiabatic nature. A adiabatic transfer is present if the adiabatic factor is about unity, whereas a  $H_A$  near zero indicates a transfer located in the diabatic regime.<sup>[24]</sup>

The rate constant  $k_{ET}$  for the ET process depends on the electronic coupling  $V$  and the Franck-Condon weighted density of states  $F_{FC}$  at the intersecting point of the two parabolas and is given by the Fermi's Golden rule.<sup>[6]</sup>

$$k_{ET} = 4\pi^2 \hbar c^2 V^2 F_{FC} \quad (1.18)$$

The Franck-Condon weighted density of states  $F_{FC}$  corresponds to the overlap integral of all vibrational modes of the ground and the excited states.<sup>[6]</sup> In the diabatic regime  $k_{ET}$  is expected to depend exponentially on the distance of donor and acceptor subunit.

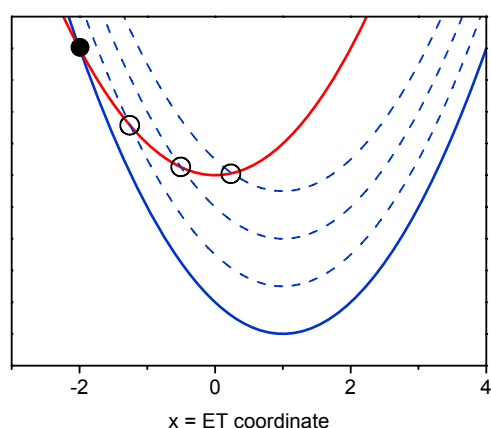


**Figure 1.5** Potentials of reactants and products as a function of the reaction coordinate for a diabatic ET transfer. Additional transition channels (dashed) arising from high energy vibrations of the product state (○) on the basis of the Bixon-Jortner theory are plotted as well as the only transition state in classical Marcus theory (●).

A major achievement of Jortner's work was to simplify the nuclear Franck-Condon factor by an expression including the Huang-Rhys factor. The nuclear Franck-Condon factor for the vibration between the  $n=0$  ground vibrational state of the reactant and the  $n^{\text{th}}$  vibrational state of the product is given by Equation 1.19.<sup>[24]</sup>

$$|\langle 0|n\rangle|^2 = \left(\frac{S^n}{n!}\right) \exp(-S) \quad (1.19)$$

The Huang-Rhys factor  $S$  is a coupling constant and is defined as follows

$$S = \frac{\lambda_i}{\tilde{\nu}_v} \quad (1.20)$$

with the inner reorganisation energy  $\lambda_i$  and the high temperature averaged molecular vibration mode  $\tilde{\nu}_v$ . The Bixon-Jortner theory can be applied accurately in case of a small Huang-Rhys factor  $S$ .

Theoretical calculations revealed that there is only little difference in rate constants for the normal region between classical Marcus expressions and semiclassical expressions according to Bixon and Jortner. In contrast, striking differences are obvious in the inverted region. If large energy quantum intramolecular vibrations are a significant contribution to the inner reorganisation, Bixon-Jortner theory predicts in the inverted region that  $\log k_{\text{ET}}$  depends more or less linearly on  $-\Delta G^0$  rather than quadratic.<sup>[6]</sup>

On the basis of the Bixon-Jortner theory it is possible to obtain molecular properties which influence the rate constant for electron transfer from analysing absorption or emission bands.<sup>[27]</sup> Fitting of the corresponding spectra in various solvents yields an estimation of the inner  $\lambda_i$  and outer  $\lambda_o$  reorganisation energy, the averaged molecular vibration mode  $\tilde{\nu}_v$  and the difference in Gibb's free energy  $-\Delta G^0$  of the diabatic ground and excited state. Jortner fits are restricted to asymmetrical bands because otherwise the fitting results for the four parameters are not unambiguously. As small Huang-Rhys factors indicate asymmetric absorption or emission bands Jortner fits can be applied successfully in case of a small inner reorganisation energy  $\lambda_i$  and a large high temperature averaged molecular vibration mode  $\tilde{\nu}_v$ .

A further extension of the ET theory was given by Marcus and Sumi.<sup>[28]</sup> Additional transition channels are possible if the curvature of the energy surface is small near the transition barrier or motions along the reaction coordinate differ significantly compared to perpendicular motions. In such a case the system can favour a transition channel which has a higher activation barrier but which facilitates the ET process dynamically. This approach is based on fluctuations of the solvent and on an intramolecular nuclear vibration with low energy. Consequently, the energy surface is a two-dimensional function of an intramolecular coordinate and a solvent coordinate. The fluctuations of the solvent are regarded as completely diffusive. A crucial quantity is the relation  $r$  of the intramolecular nuclear vibration with low energy  $\lambda_{nv}$  and the reorganisation energy of the solvent  $\lambda_o$ .

$$r = \frac{\lambda_{nv}}{\lambda_o} \quad (1.21)$$

A value of  $r > 1$  indicates a broad transition regime, where the transition barrier can be crossed. However, in the case of  $r < 1$  the Gibb's free energy increases strongly with distance from the barrier and a transition is only possible in a quite narrow regime.

Qualitatively, the dynamics of the ET transfer are determined by two processes. The system crosses the activation barrier along the low-energy nuclear vibration and reaches the product minima on the energy surface. Motion along the solvent coordinate repopulates the depopulated positions.<sup>[7]</sup>



## 1.2.4 Electron Transfer Mechanisms

Generally, two important electron transfer mechanisms concerning the active participation of bridge units connecting donor and acceptor are distinguished, the superexchange and the hopping mechanism.<sup>[29, 30]</sup> The total rate constant  $k_{\text{ET}}$  is the sum of both mechanisms but in certain  $\Delta G^0$  regimes one mechanism might dominate.

### 1.2.4.1 Superexchange Mechanism

Electrons are transferred according to the superexchange mechanism if bridge localised states are energetically higher than either donor or acceptor (see Figure 1.6a). The charge is transferred in one single step and is never localised onto the bridging unit because the superexchange mechanism is a nuclear tunnelling process. The Marcus-Jortner-Levich equation illustrates the dependence of the rate constant  $k_{\text{ET}}$  on the distance  $R$ .

$$k_{\text{ET}} = k_0 \cdot \exp(-\beta \cdot R) \quad (1.22)$$

The rate constant  $k_{\text{ET}}$  depends exponentially on the distance  $R$  between donor and acceptor. The influence of the distance on the rate constant is usually described by the  $\beta$ -factor which has the dimension of a reciprocal distance. Consequently, a large  $\beta$ -factor indicates a strong dependence of the rate constant  $k_{\text{ET}}$  on the distance  $R$ .

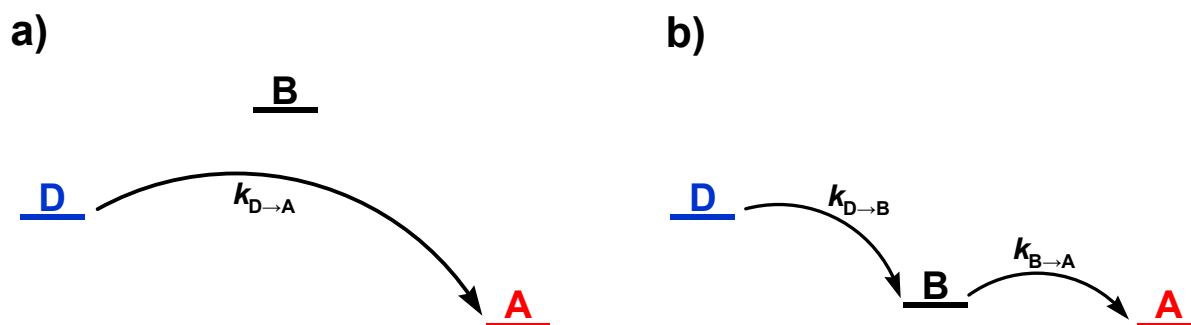


**Figure 1.6** State diagrams for an ET process from a **donor** to an **acceptor** in a donor-bridge-acceptor compound in case of a **a)** superexchange and **b)** hopping mechanism.

The Marcus equation has often been applied to calculate  $k_{\text{ET}}$  for the superexchange mechanism (see Equation 1.3). Although the charge is transferred in one coherent step, higher lying states of the bridging unit influence the electronic coupling  $V$  between donor and acceptor and consequently the rate constant. According to the McConnell model<sup>[31]</sup>  $V$  can be calculated as follows

$$V_{(\text{D} \rightarrow \text{A})} = \frac{V_{(\text{B} \leftarrow \text{D})} \cdot V_{(\text{B} \rightarrow \text{A})}}{\Delta G_{(\text{B} \leftarrow \text{D})}^0} \quad (1.23)$$

if one neglects direct  $\text{D} \rightarrow \text{A}$  interaction. In this equation  $V_{(\text{D} \rightarrow \text{A})}$ ,  $V_{(\text{B} \leftarrow \text{D})}$  and  $V_{(\text{B} \rightarrow \text{A})}$  are the electronic couplings between donor and acceptor, bridging unit and donor and bridging unit and acceptor, respectively.  $\Delta G_{(\text{B} \leftarrow \text{D})}^0$  is the free-energy change between the bridging unit and the donor.

#### 1.2.4.2 Hopping Mechanism

A second possibility of electron transfer is the hopping mechanism. The electron is transferred in several steps from one subunit to the other. After each step the charge is localised for a certain time onto the bridge and this state is principally detectable by means of appropriate spectroscopic methods. A precondition for this incoherent mechanism are low-lying states of the bridging unit (see Figure 1.6b). The rate constant  $k_{\text{ET}}$  of this mechanism depends on the number of electron transfer steps  $N$ .

$$k_{\text{ET}} \propto \frac{1}{N} \quad (1.24)$$

In the case of an incoherent hopping mechanism charge can also be transferred via two steps in which an energetically higher lying though still accessible excited state is involved (Figure 1.7). The total rate constant  $k_{\text{hop}}$  is then calculated by Equation 1.25 on the basis of the quasi-steady-state approximation (QSSA, Bodenstein principle)<sup>[32]</sup>, where each sequential rate constant ( $k_{(\text{B} \leftarrow \text{D})}$ ,  $k_{(\text{B} \rightarrow \text{D})}$  and  $k_{(\text{B} \rightarrow \text{A})}$ ) is given by the Marcus equation 1.22.

$$k_{\text{hop}} = \frac{k_{(\text{B} \leftarrow \text{D})} \cdot k_{(\text{B} \rightarrow \text{A})}}{k_{(\text{B} \rightarrow \text{D})} + k_{(\text{B} \rightarrow \text{A})}} \quad (1.25)$$

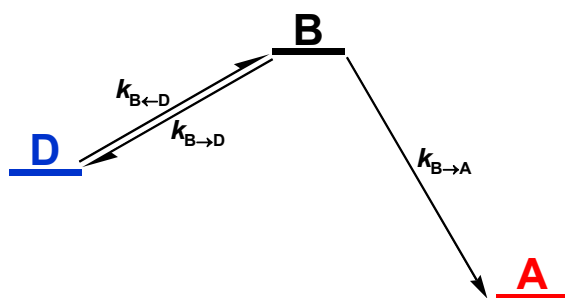


**Figure 1.7** State diagram for an ET process from a **donor** to an **acceptor** in a donor-bridge-acceptor via a high lying state which corresponds to the bridging unit.

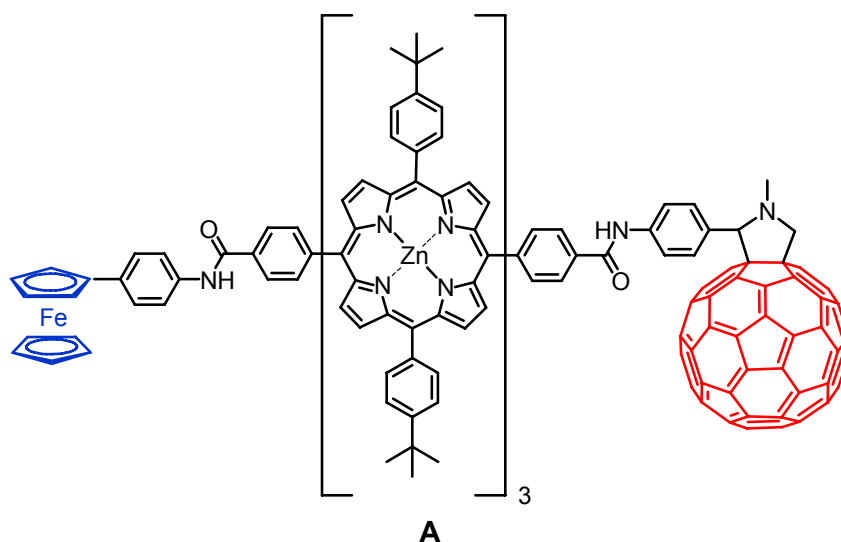
## 1.3 State of the Art

### 1.3.1 Application of Suitable Redox Centres

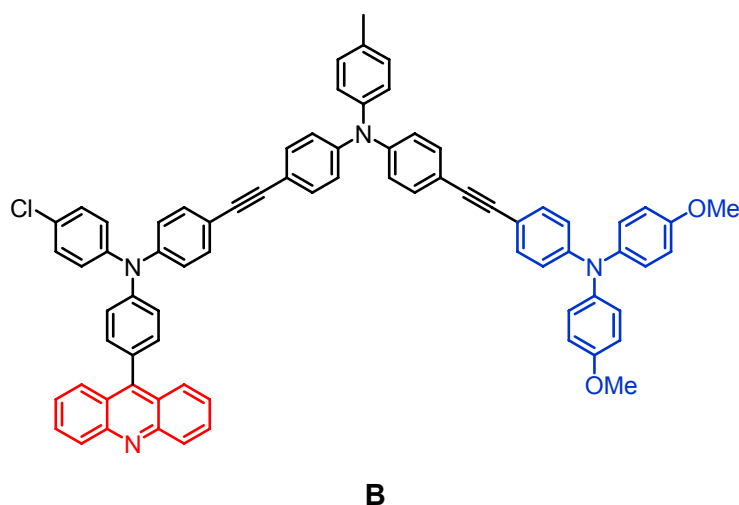
One important aspect in designing redox cascades is the use of suitable redox centres. A perfect subunit should combine several properties. Understandably, each redox centre has certain advantages and disadvantages. As a consequence, cascades with many different building blocks such as (metallo)porphyrines, triarylaminines, ferrocene, (sub)phthalocyanines, carotenoids, tetrathiafulvalenes, fullerenes and quinones have been synthesised and investigated. In the following, examples of cascades are shown which comprise these redox centres. At first, the donors' properties are discussed followed by those of the acceptors. For a better illustration the subunit which acts as electron acceptor is drawn in red and the subchromophore where the hole is located in the final CS state is given in blue.

Most systems comprise one or more (metallo)porphyrine subunits<sup>[33-44]</sup> (**A**, **G**, **J**) as electron donors in close analogy to nature although their synthesis is quite challenging. Porphyrins are chromophores which consist of four pyrrole subunits connected by methine groups. They are part of many natural complexes such as chlorophyll (with  $Mg^{2+}$  at the centre of the ring) or haemoglobin (with  $Fe^{2+}$ ). The redox potential of porphyrins can be tuned by substituents and by the nature of the metal in case of (metallo)porphyrines. The stability of the corresponding cations is sufficient that no degradation occurs while the hole is located in the subunit. In context of solar energy conversion absorption of light of the solar spectrum is favourable. (Metallo)porphyrines are often used because they exhibit a relative bathochromic ground state absorption whereas many other organic compounds absorb quite hypsochromically. Thus, (metallo)porphyrines absorb an additional part of the solar spectrum which is often lost. However, a handicap in solar energy conversion is the narrow-band absorption of (metallo)porphyrines even though the absorption is characterised by large

extinction coefficients. The small reorganisation energy of (metallo)porphyrins is another reason for their broad application in redox cascades. For example, the reorganisation energy of a Zn-porphyrin for radical cation formation was estimated to be ca.  $550 \text{ cm}^{-1}$ .<sup>[45]</sup>

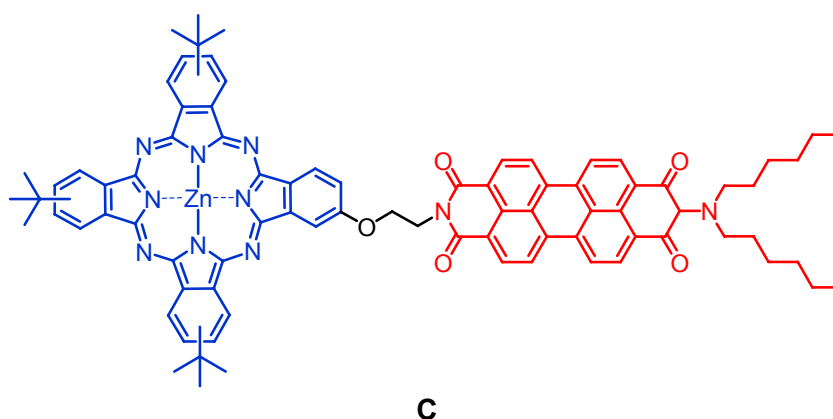


Cascade **B** was synthesised in order to study directed charge transfer processes along a redox potential gradient. Triarylamines were chosen as donor subunits because they combine several important advantages. In addition to their comparatively simple synthetic accessibility and their low reorganisation energy<sup>[16, 46, 47]</sup> ( $\sim 4100 \text{ cm}^{-1}$  of tri-*p*-tolylamine in acetonitrile)<sup>[48]</sup>, substituents in *para*-position of the phenyl ring increase the stability of the corresponding radical cations<sup>[49, 50]</sup> and allow a certain tuning within a broad range of the redox potential.<sup>[51, 52]</sup> By modulating the redox potential of each subunit a directed redox potential gradient can easily be ensured.



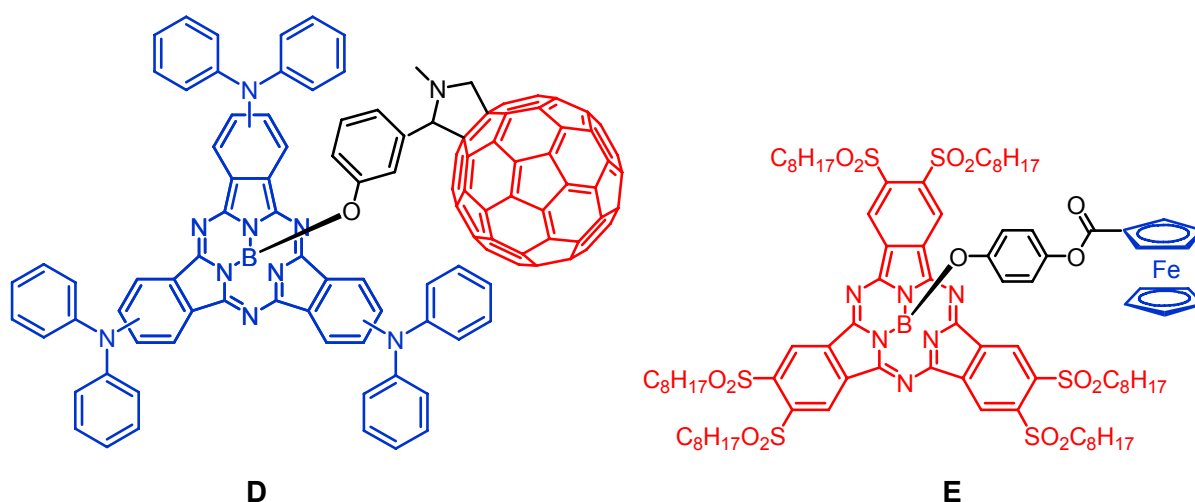
Ferrocene (**A**, **E**) is another donor which is used in many cascades.<sup>[33, 53-57]</sup> It has a low oxidation potential and, consequently, stabilises the corresponding charge separated state efficiently. Its relative low reorganisation energy ( $\sim 8100 \text{ cm}^{-1}$  in acetonitrile)<sup>[58]</sup> is one further aspect which explains its frequent utilisation as donor subunit. Additionally, due to the stability of the ferrocenium cation the ferrocene / ferrocenium redox couple is used as reference in electrochemical measurements.

The donor subunit in compound **C** is a phthalocyanine. Phthalocyanines are analogues of porphyrins which show some unique electronic characteristics as a result of the planar delocalised  $18\pi$ -system. They exhibit high chemical and thermal stability. Phthalocyanines are utilised as hole conductors in laser printers or as light absorbing dyes in recordable CDs. They are also used as model compounds in biological systems. Cobalt(II)- and copper(II)-phthalocyanines (CoPc, CuPc) are of commercial interest as pigments. Although their absorption properties are enhanced compared to those of porphyrins<sup>[59-63]</sup>, the low lying triplet state limits their utilisation when a long-lived charge separated state is required.<sup>[64-66]</sup> A low lying triplet state usually acts as an energy sink and quenches the charge separated state. The process of population of a locally excited triplet state corresponds to the charge recombination process. Consequently, the lifetime of the desired energy-rich state decreases. These consequences of a low lying triplet state on the lifetime of CS states are discussed in detail in Chapter 1.4.



Subphthalocyanines (**D**, **E**) which comprise three rather than four aromatic units are a relatively new class of molecular units for photoactive systems.<sup>[56, 67, 68]</sup> Their electron-donating properties are easily tuned by adequate peripheral substituents which is an important factor in designing cascades with a directed redox gradient. Subphthalocyanines are excellent antenna units because they absorb visible light in the region of 550 –

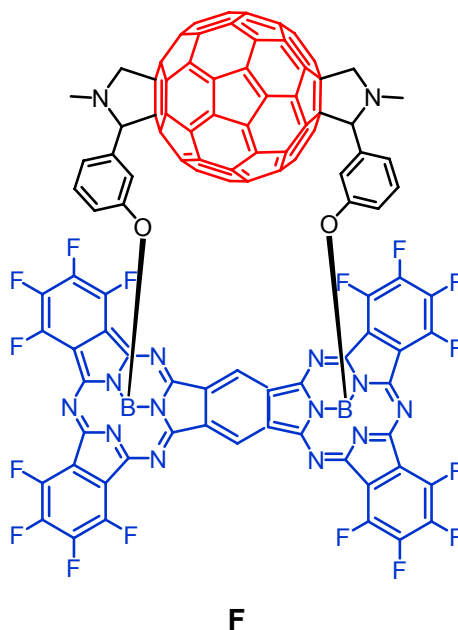
650 nm.<sup>[56]</sup> Moreover, they have low reorganisation energies ( $\sim 3200 \text{ cm}^{-1}$  in acetonitrile).<sup>[69]</sup> In a dyad consisting of a ferrocene subunit as donor subphthalocyanine has also been used as electron acceptor successfully (**E**).<sup>[56]</sup> The redox potential can be tuned by peripheral substituents and theoretical studies have shown that the corresponding radical anion is stabilised by partial delocalisation of the negative charge over the B-O bond.<sup>[70]</sup>



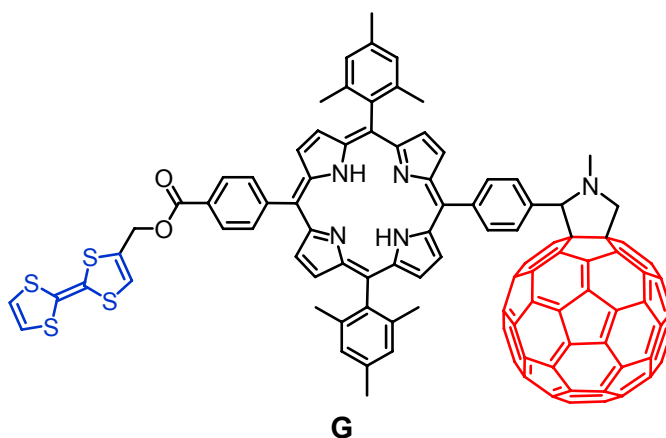
In close analogy a dyad consisting of a fused subphthalocyanine dimer (**F**) acting as electron donor has been presented.<sup>[67]</sup> The optical and magnetical properties differ significantly from those of the monomer. Significant red shifts of ground state absorption as well as of emission ( $\sim 3000 \text{ cm}^{-1}$ ) have been reported. The fluorescence quantum yield (0.24) decreases compared to a monomeric subphthalocyanine (0.4)<sup>[56]</sup> whereas the lifetime of the fluorescent state increases (2.5 ns compared to 1.8 ns). This class – monomers as well as fused dimers – presents promising properties to be used in future cascades.

Carotenoids are pigments which occur in plants, algae, fungi or bacteria. More than 600 types of carotenoids are known so far. They are an important class concerning the photosynthetic reaction centre. Carotenoids are involved in the energy-transfer process and moreover can protect the reaction centre from free radicals because carotenoids are efficient scavengers. Carotenoids (see cascade **J** in Scheme 1.1) are used as strong donors in various triads.<sup>[71]</sup> Thus, due to their excellent ability of stabilisation the resulting CS state a series of pentads<sup>[72]</sup> has been synthesised each consisting of one carotenoid. The lifetime of the CS state was at least 10000 times longer than in corresponding dyads without carotenoids. A major problem of carotenoids as subunits in multichromophore systems is the relative low energy level (0.9 eV) of the lowest excited triplet state.<sup>[73]</sup> The influence of the

energetic level on different deactivation pathways is outlined in Figure 1.7 and discussed in detail in Chapter 1.4.



Tetrathiafulvalenes (**G**) are one more group of established electron donors in dyads and triads.<sup>[74-82]</sup> Due to their excellent electron donating properties tetrathiafulvalenes are used as electrical conductors and superconductors.<sup>[83]</sup> They can be easily and reversibly oxidised to mono- and dications.<sup>[84]</sup> Thus, tetrathiafulvalenes stabilise the charge separated state efficiently.

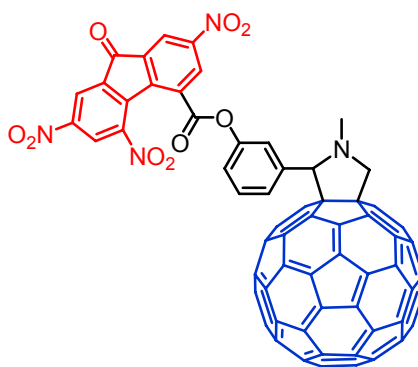


Many if not most of artificial systems comprise  $C_{60}$  (**A**, **D**, **F**, **G**) as electron acceptor<sup>[33, 37, 39, 41, 42, 85-101]</sup> because it can easily be reduced. Moreover, the total reorganisation energy of *t*-butyl substituted  $C_{60}$  is reported to be quite small ( $\sim 5200 \text{ cm}^{-1}$  in a benzonitrile / benzene solution)<sup>[102]</sup> or can even be neglected ( $\lambda_i < 1 \text{ cm}^{-1}$ ).<sup>[103]</sup> Although  $C_{60}$  has a quite weak

absorption in the region of visible light it is very popular as acceptor in cascades because  $C_{60}$  has a quite high lying excited triplet state (1.5 eV).<sup>[104]</sup>

Under certain conditions,  $C_{60}$  can also act as electron donor in redox cascades (**H**).<sup>[105]</sup> In this case, a stronger electron acceptor than  $C_{60}$  is required. Otherwise,  $C_{60}$  acts as electron acceptor again. In a fullerene-trinitrofluorenone linked dyad  $C_{60}$  can act as electron donor because trinitrofluorenone is the stronger acceptor. Trinitrofluorenone was part of the first commercial photoreceptor introduced by IBM. They were the first who used an organic charge-transfer complex based on trinitrofluorenone and polyvinylcarbazole as a single layer photoreceptor in laser printers.<sup>[106]</sup>

Some of the first dyads consisted of quinones (see **J** in Scheme 1.1)<sup>[107]</sup> as electron acceptors which are also part of various biological relevant compounds. Quinone and its derivatives are electron acceptors both in photosystem I and II as well as in aerobic respiration. Up to now, quinones are successfully used as acceptors in multichromophore systems up to pentads (**J**).<sup>[72]</sup> The primary step upon photoexcitation is an almost quantitative intersystem crossing from the locally excited singlet state to the triplet state. Chances and risks of a population of locally excited triplet states is discussed later. Electron transfer processes have also been reported originating from the short lived excited singlet state producing radical ion pairs with fast recombination rates.

**H**

Acridine was used as electron acceptor in a series of redox cascades such as **B**<sup>[16]</sup> because the fluorescence characteristics of donor substituted acridine have intensively been investigated by Kapturkiewicz *et. al.* and are well understood.<sup>[108-110]</sup> In addition, donor substituted acridine fluoresces with high quantum yields in a wide range of solvent polarity. This fact indicates a sufficient long-lived charge transfer (<sup>1</sup>CT) state which may be able to initiate hole transfer processes in adjacent subunits. Furthermore, it has been reported that

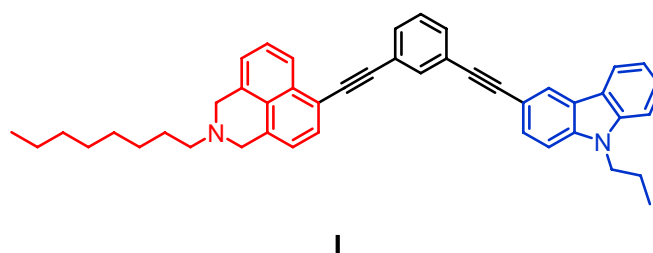


the conformational changes of 9-donor-substituted acridine accompanying the charge separation process in the excited state are only marginally.<sup>[108]</sup>

### 1.3.2 Possible Approaches to Realise a Long-lived CS State

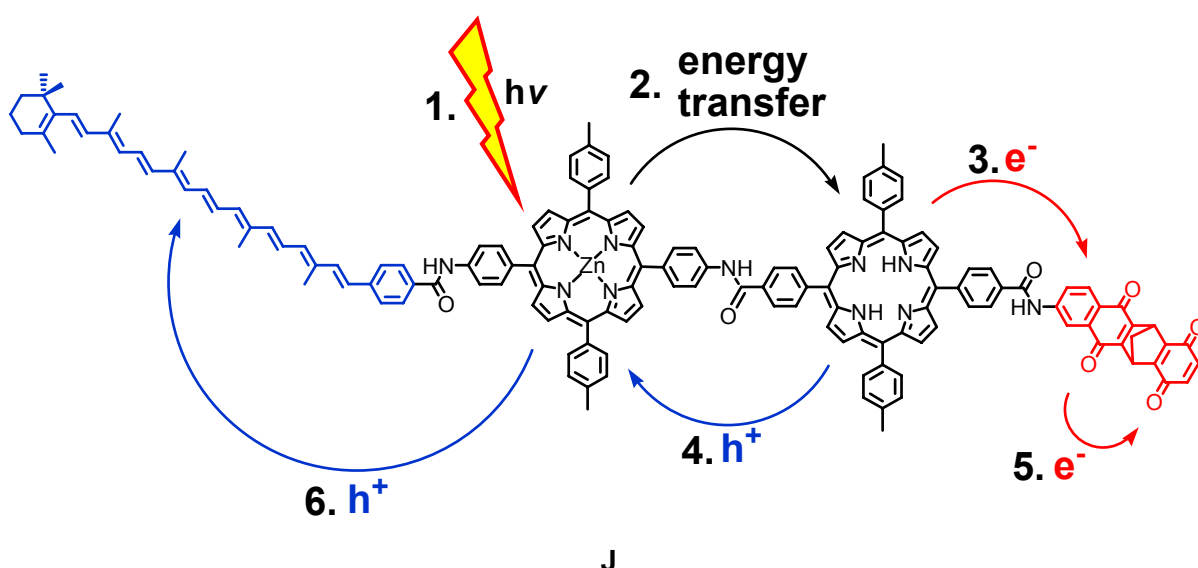
In biological systems charge separation occurs via several fast electron transfer steps. Natural redox cascades usually consist of several membrane-bound complexes which act as redox centres. In contrast, in most artificial systems which serve as model compounds intramolecular electron transport is studied i.e. electron transfer occurs within one single molecule. These electron transfer processes normally result in a CS state. For an application of such systems e.g. in optoelectronic devices a sufficient long-lived CS state is an utmost condition. Generally, various approaches are known to increase the lifetime of this energy-rich state.

As can be seen from Equations 1.3 and 1.23 the rate constant of ET processes depends on the square of the electronic coupling. Thus, one obvious attempt is to decrease the electronic coupling. However, a major problem is that charge separation is also impeded by a small electronic coupling and has to compete with other deactivation processes. A CS state with a long lifetime is useless if it is formed in low quantum yields. A quite elegant approach to ensure fast separation and slow recombination processes of charges was reported by Zimmt *et. al.*<sup>[111, 112]</sup> They designed compounds in which the electronic coupling for the charge separation process is much larger than that for the recombination process. Nevertheless, the increase of the lifetime was only little pronounced compared to the decrease of the electronic coupling for the recombination process. Thompson *et. al.* pursued the same strategy of fast charge separation and slow recombination. They reported on *para*- and *meta*-linked chromophores which showed quite similar forward ET rates. In case of the *meta*-conjugated compound (I) charge recombination is slower which was explained by a small electronic coupling concerning the process  $CS \rightarrow S_0$ .<sup>[113]</sup>



Another approach to increase the lifetime of the CS state is its stabilisation in the Marcus normal region. This can be achieved by comprising strong donor and acceptor subunits such as ferrocene and fullerene. Separation of the charges over wide distances also stabilises the CS state. Both approaches are combined in pentad **(A)** whose CS state has a lifetime of 0.53 s in DMF.<sup>[57]</sup> Furthermore, this CS state is prepared in a comparatively high quantum yield of 80 %.

Utilisation of complex compounds is restricted by time-consuming and expensive synthetic work. Thus, their synthesis is a big challenge in the field of basic research but it is impractical for use in commercial applications. As illustrated in cascade **J** several electron and hole transfer processes lead to the final CS state.<sup>[72]</sup> Competing deactivation pathways at each step reduce the quantum yield. Thus, the overall quantum yield for population of the CS state decreases with an increasing number of charge transfer processes.



**Scheme 1.1** Photoexcitation, energy, electron and hole transfer processes in pentad **J** resulting in the final charge separated (CS) state.

Consequently, it is desirable to design compact dyads which show fast and efficient charge separation but slow recombination processes. Generally, small donor-acceptor systems are easily accessible compared to large chromophores. It is noteworthy that in most dyads a charge transfer (CT) state forms the energy-rich state (instead of a charge separated (CS) state) in which the charges are almost completely separated. In small compounds the separated charges are in close vicinity to each other and consequently further approaches are required to impede the recombination process.

One promising attempt to slow down charge recombination is that of spin control.<sup>[8]</sup> In small molecules the excited singlet state is always energetically above the triplet state (see Figure 1.7). Assuming that the compound exhibits a CT band, the  $^1\text{CT}$  state can be populated by irradiation directly. Both fluorescence and nonradiative deactivation processes lead to the singlet ground state  $S_0$  by spin-allowed processes. If the  $^1\text{CT}$  state decays into the  $^3\text{CT}$  state, the lifetime of the energy-rich excited state dramatically increases. Assuming that the  $^3\text{CT}$  state is the lowest excited triplet state charge recombination is impeded due to spin restriction of the process  $^3\text{CT} \rightarrow S_0$ . The solvatochromism of CT states is usually more pronounced than that of locally excited states. Thus, in polar solvents dipolar CT states are stabilised and are consequently more likely to be below locally excited ones. Otherwise, the decay from the  $^3\text{CT}$  state into a locally excited triplet state is fast and is the dominant recombination process.

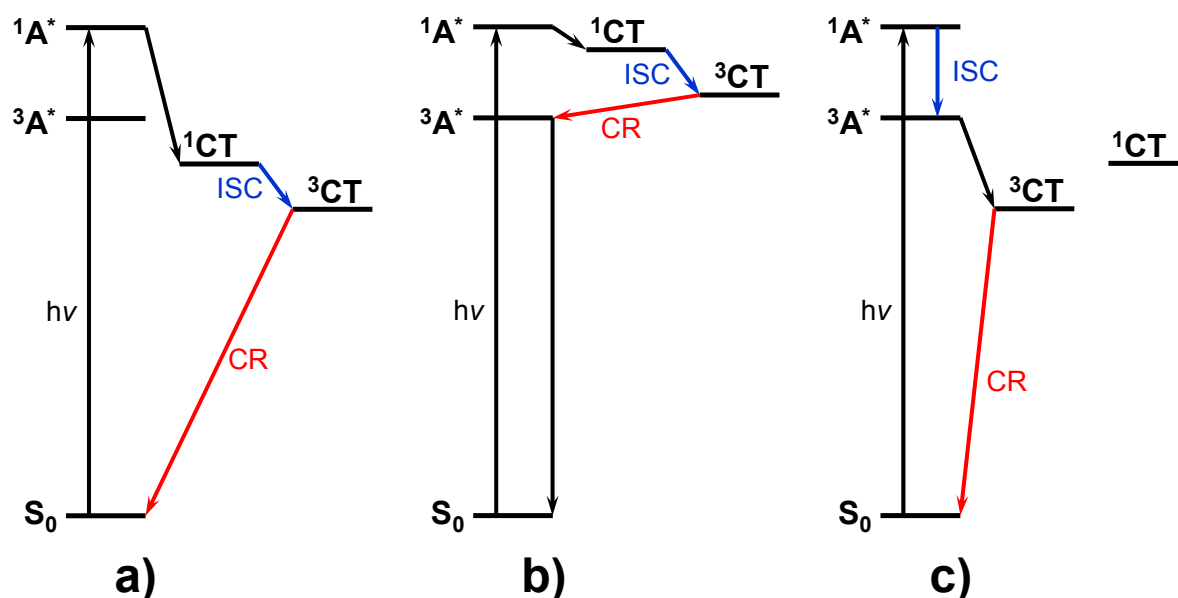
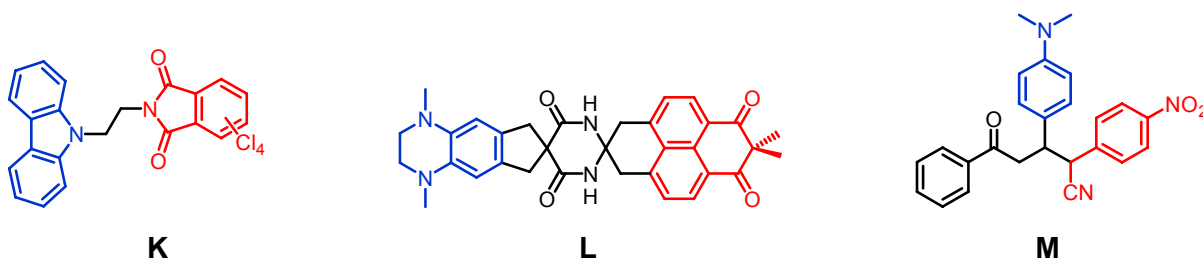


**Figure 1.7** Possible ISC pathways for population of the  $^3\text{CT}$  state and subsequent charge recombination (CR) processes. a) and c) polar solvent; b) nonpolar solvent.

It is not only the lifetime of excited CT states that is important but also that the CT state is formed in high quantum yields. A long-lived CT state is useless for applications if it is prepared only as a byproduct. If the  $^3\text{CT}$  state shall be the main product of  $^1\text{CT}$  state deactivation one has to optimise the process  $^1\text{CT} \rightarrow ^3\text{CT}$ . Due to the fact that this pathway is spin-forbidden and consequently quite slow, other competing processes might be faster. A rapid spin conversion is an important condition for a sufficient population of the  $^3\text{CT}$  state. Enhanced intersystem crossing (ISC) increases the rate of this process. ISC is the major process in metal-organic compounds due to the heavy-atom effect. In 1988 the first purely

organic compound (**K**) with a  $^3\text{CT}$  state has been reported that displays a long lifetime ( $0.7 \mu\text{s}$  in cyclohexane).<sup>[114]</sup> After excitation of a subchromophore the  $^1\text{CT}$  state is formed in high quantum yields.<sup>[115]</sup> The population of the  $^3\text{CT}$  state shows a pronounced solvatochromism and reaches its maximum (52 %) in case of cyclohexane as solvent. That the  $^3\text{CT}$  state is the lowest excited triplet state in nonpolar solvents is rather unique because normally a locally excited state is the lowest triplet state except for polar solvents (see Figure 1.7a and 1.7b).



Upon photoexcitation of the acceptor subunit of **L** fast ISC occurs within the locally excited states before charge separation in the singlet states can take place (see Figure 1.7c).<sup>[116]</sup> Then, the  $^3\text{CT}$  state can be almost quantitatively populated by a spin-allowed deactivation process from the locally excited triplet state. Only a few other compounds are known in which ISC occurs within locally excited states but in lower yields.<sup>[117, 118]</sup>

ISC is also increased by excitation of triplet-sensitisers and subsequent energy transfer to the chromophore. Whereas sensitiser added to the solution might have major disadvantages (e.g. quantum yield, energy transfer), compounds with intramolecular sensitisation avoid the problems caused by intermolecular interactions. System **M** is the first compound which shows a successful intramolecular sensitisation step producing a  $^3\text{CT}$  state by means of a carbonyl group acting as triplet sensitiser.<sup>[8]</sup> The  $^3\text{CT}$  state has a lifetime of  $0.33 \mu\text{s}$  in deoxygenated acetonitrile.

A general problem of impeding charge recombination by spin control is the energy which can be stored. As already explained above it is an utmost condition that the  $^3\text{CT}$  state is the lowest excited triplet state. However, with increasing stabilisation of the  $^3\text{CT}$  state the energy stored within in this state decreases.

In close analogy to extended cascades one possibility to prolong the lifetime of the CT state in a compact dyad is its stabilisation as far as charge recombination is located in the normal Marcus region. A quite new approach is the use of subphthalocyanines as electron acceptors (**E**).<sup>[56]</sup> The resulting negative charge in the CT state is stabilised by partial delocalisation along the B-O bond. The generated CT state possesses a remarkable stability with a lifetime of 0.2 ms in benzonitrile at  $25^\circ\text{C}$ . However, the absence of the spectral features of the ferrocenium cation in the transient spectra raises suspicion that a ionised

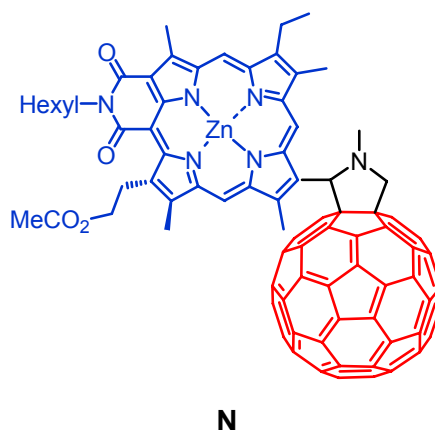
species has been generated and characterised. Additionally, a small reorganisation energy as it is typically for subphthalocyanines should lead to a short-lived CS state.

A quite similar attempt is the stabilisation of CT states by addition of appropriate salts.<sup>[54, 59, 105]</sup> In case of a dyad with fullerene as donor and trinitrofluorenone as acceptor (**H**) Sc(OTf)<sub>3</sub> forms a strong complex with the acceptor subunit and accepts part of the negative charge. Thus, the negative charge is more delocalised which results in an increase of the stability of the CT state. The lifetime of the CT state was determined to be 23 ms in benzonitrile at 25 °C.

An extraordinary increase of the lifetime of a CT state resulted from addition of Y(OTf)<sub>3</sub> to a ferrocene anthraquinone dyad.<sup>[54]</sup> The lifetime of 83 μs was explained by very strong bindings of Y(OTf)<sub>3</sub> with the anthraquinone subunit which causes major changes in reorganisation energy and driving force of electron transfer. This lifetime is all the more exceptional because back electron transfer is located in the Marcus normal region.

Stabilising the CT state has a further advantage. With increasing stability, that means with decreasing energy, it becomes more likely that this state is below the lowest locally excited triplet state (see Figure 1.7a).

A further approach to prolong the lifetime of excited states is to increase the energy gap between the energy-rich excited state and that state in which the charges are recombined. As already explained above charge separation should be fast in the Marcus normal region whereas charge recombination is impeded in the inverted region. The importance of a small reorganisation energy has already been outlined. In the inverted region the rate constant of charge recombination decreases with increasing  $\Delta G^0$ . This fact is a major advantage compared to the spin controlled approach. The more energy is stored in the excited state the more decelerated the excited state decays. The lifetime of the CT state of a dyad consisting of a fullerene acceptor and a zinc chlorine as donor (**N**) was reported to be 230 μs at 25 °C.<sup>[119]</sup> As a result of the charge recombination process being located in the Marcus inverted region, the lifetime increases with decreasing temperature. The published lifetime for this dyad at -150 °C is 120 s which would be a record for linked donor-acceptor compounds.



However, the CS state is only formed in 12 %. Due to this fact, Verhoeven *et. al.*<sup>[8]</sup> proposed that a long-lived <sup>3</sup>CT state is formed as it has outlined above. Then, the long lifetime can be explained by a spin-forbidden deactivation process (<sup>3</sup>CT → S<sub>0</sub>).

## 1.4 Project Aim

### 1.4.1 Design of the Cascades

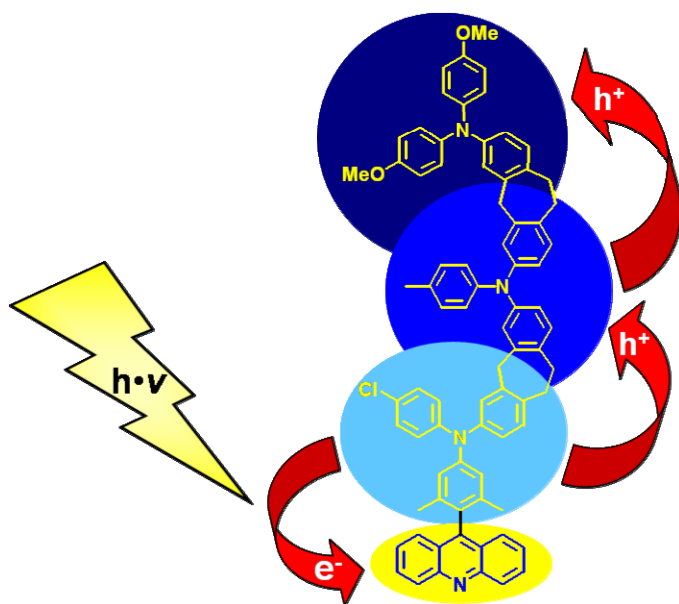
The aim of this project was the synthesis and the investigation of redox cascades concerning their photophysical properties. On the basis of a recent study in our group<sup>[16]</sup>, we retained the basic design of these redox cascades which is outlined in Scheme 1.2. These chromophores consist of an acceptor which is covalently linked to a donor chain, comprising up to three subunits.

As acceptor we used acridine due to reasons discussed in Chapter 1.3.1. Moreover, various synthetic approaches of donor substituted acridines have been reported.<sup>[120-128]</sup>

Triaryl amines are well-known hole transport components and are used in many commercial applications because they combine several important advantages (see Chapter 1.3.2). Triaryl amines are utilised as hole conductors in light emitting materials<sup>[129-138]</sup>, as photorefractive materials for optical data storage<sup>[139]</sup> and in electrochromic mirrors.<sup>[140]</sup> Moreover, their synthesis as well as their optical and electrochemical properties are well-established in the Lambert group. Tuning of the redox potential of the triarylamine subunits by adequate substituents in *para*-position of the phenyl ring ensures that the redox gradient is always correctly directed downhill to the terminal donor. Various terminal donors were used to study their influence on the kinetics of charge separation and recombination processes.

To continue the work which substantiated acridine and triarylamine as suitable compounds for redox cascades<sup>[16]</sup>, it was desired to prolong the lifetime of the finally prepared charge separated state. Different approaches are discussed in Chapter 1.3.2. We preferred to decrease the electronic coupling between the redox centres. This was done by saturated bridges separating the donor subunits. In order to suppress conformational flexibility as much as possible, we chose a methylene and ethylene bridging unit. Furthermore, the electronic coupling between the acridine acceptor and the adjacent donor subunit is decreased by an orthogonal orientation of the phenyl group attached to the acceptor. This orientation which is enforced by two methyl groups reduces  $\pi$ -overlap and results in a more pronounced charge transfer state.

With the aforementioned molecular properties in mind we anticipate the following scenario of photoinduced charge transfer processes in the cascades (see Scheme 1.2): upon photoexcitation of the moiety consisting of the acceptor and the adjacent donor either a locally excited acridine state followed by rapid internal conversion into a  $^1\text{CT}$  state is prepared or directly the  $^1\text{CT}$  state. This  $^1\text{CT}$  state injects a hole onto the next donor which, in cases of chromophores with three donor moieties, then migrates to the periphery of the cascade forming a charge separated (CS) state.



**Scheme 1.2** Principle of photoinduced electron transfer processes. The redox gradient is indicated as follows: the darker the blue background the stronger the donor subunit.

Characterisation of the cascades includes various optical and electrochemical techniques. The redox potentials are determined by cyclic voltammetry to check if the redox gradient is directed correctly. The redox potentials can be further used to check if the potential depends mainly on the substituents of the triarylamines as a consequence of a very

small electronic coupling between them or if they depend on the nature of adjacent redox centres. The dynamics of various charge transfer processes is investigated by means of stationary and time-resolved absorption and fluorescence spectroscopy. These techniques are further used to identify the deactivation pathways in the cascades.

### 1.4.2 Characterisation of CS States

An indispensable precondition for the use of redox cascades in commercial applications is an intense investigation of basic optical and electrochemical properties. As already mentioned above the lifetime of the CS state is a key feature. A common method to investigate the kinetics of the excited states is transient absorption spectroscopy. The laser flash photolysis technique has become a powerful method to gain insight into the kinetics and the energy of excited states in chemical as well as in biological systems upon irradiation.<sup>[141-143]</sup> In the ns time domain, transient absorption spectra are often interfered by fluorescence which limits the time resolution decisively. Consequently, transient absorption spectra can either be measured only for compounds which show virtually no fluorescence or in the time domain longer than fluorescence decays. As most organic chromophores fluoresce and it is not tolerable to lose kinetic information in the ns time domain, a new fluorescence correction method is required which no longer limits the time resolution of transient absorption spectroscopy by means of the laser flash photolysis technique.

It should be mentioned that CS states must be characterised carefully. It is an utmost condition that the spectral features of the originated radical cation *and* the radical anion as well must be evident from the corresponding transient absorption spectra. One further condition to confirm a CS state is the same monoexponential decay of the transient absorption bands both of donor and acceptor subunits. It appears suspect if spectral features of one part are missing or the spectral characteristics exhibit complex decays. Ionisation is a likely process that causes incomplete transient spectra or multiexponential decays. With increasing lifetimes of the CS state and decreasing complexity of the compounds a serious investigation becomes more and more important to allay any suspicion of ionisation.



## 2 Transient Absorption Spectroscopy of Fluorescent Compounds in the ns Time Domain

### 2.1 Introduction

Laser flash photolysis (LFP) technique has become a powerful method to study transient species in gaseous, liquid or solid phase<sup>[143]</sup> since its introduction by Kosonocky *et. al.*<sup>[141]</sup> in 1965 and Lindqvist<sup>[142]</sup> in 1966. The technique of LFP is used to gain insight into the kinetics and the energy of excited states in chemical as well as in biological systems upon laser excitation. The temporally changing absorption characteristics can be attributed to chemical or physical processes of the excited state species.

Generally, the recorded transient absorption signal consists of transient absorption, fluorescence and ground state bleaching. Thus, for fluorescent chromophores a correction is indispensable in order to obtain undisturbed absorption decay curves as well as accurate transient absorption spectra. While ground state bleaching cannot be corrected, it is essential to correct at least emission as this signal is likely to appear in spectral regions where transient absorption signals are expected. Without any fluorescence correction no transient absorption spectra of short living (ns domain) excited singlet states of fluorescent compounds can be recorded. Consequently, LFP is mainly restricted to the investigation of long living species such as triplet states. In order to circumvent these problems, different approaches to eliminate or minimise fluorescence contributions have been reported.

One recent approach by Scaiano *et. al.*<sup>[144]</sup> to solve the above mentioned problem is the use of a lens system which focuses the probe light beam through the sample onto a fibre which conducts the signal to a monochromator-photomultiplier (PMT) assembly. The fibre which collects the beam discriminates between the attenuated probe light and unwanted fluorescence under solid angle conditions. Thus, most of the fluorescence which is emitted from the excited probe into all directions is excluded. It is reported that the interfering fluorescence signal is tolerably minimised by this technique.

A further method to solve the problem of interfering fluorescence is to measure the emission separately. In this case the sample is excited by the laser while the probe light is blocked.<sup>[145]</sup> The change in optical density is then calculated by Equation 2.1.

$$\Delta OD(t) = \log \frac{I^p}{I_T^p(t) - I_F(t)} \quad (2.1)$$

In Equation 2.1  $I^p$  stands for the background level caused by the white probe light which is assumed to be constant with time,  $I_T^p(t)$  is the time dependent probe light intensity transmitted through the sample and  $I_F(t)$  is the fluorescence decay which is separately recorded while the probe light is switched off.

However, this correction proved to be applicable only in cases in which the fluorescence quantum yield is below ca. 1 %. This is due to the photon flux dependent response characteristics of the PMT which yields distorted transient signals if the white light background is switched on compared to the same signal with white light being switched off. As many organic chromophores fluoresce with quantum yields  $> 1 \%$  and have lifetimes in the lower ns time domain it is highly desirable to develop a reliable method which accounts for those fluorescence contributions in transient absorption spectroscopy.

## 2.2 Results and Discussion

First, we demonstrate that simple subtraction of emission signals using Equation 2.1 does not yield correct transient absorption spectra. With our setup the calculation of the transient absorption according to Equation 2.1 failed because the rise time<sup>[146]</sup> and additionally the intensity of the instrument response function depend on the initial photon flux level which shines on the PMT as it is shown in Figure 2.1.

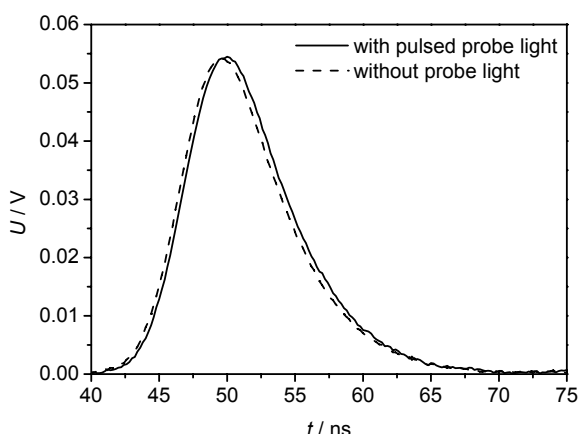


**Figure 2.1** Instrument response function with high intensity (pulsed) probe light (solid) and without probe light (dashed). The offset caused by the probe white light in the solid curve is eliminated for better illustration.

The instrument response curves shown in Figure 2.1 differ in three crucial points: first, the solid curve is shifted by  $\sim 0.3$  ns, second, the solid curve is  $\sim 1 \%$  more intense, and

third, the rise times of both curves differ by  $\sim 0.06$  ns. Although these differences on their own are superficially not dramatic, subtraction of both curves results in an absolutely unsuitable fluorescence correction compared to the weak transient absorption signal. To illustrate this behaviour we used the chromophore Hoechst 33258 (**H**) which is widely used as a DNA stain. The absorption and emission spectra of **H** in DMF are shown in Figure 2.2. The two corresponding transient traces at 490 nm of a solution of **H** with a fluorescence quantum yield of 35 % in DMF are shown in Figure 2.3a. It should be noted that transient absorption appears as a negative signal if it is plotted versus time. Consequently, ground state bleaching and fluorescence appear as a positive signal. In contrast, transient absorption is illustrated as a positive signal in the spectral plots and analogously ground state bleaching and fluorescence as negative signals.

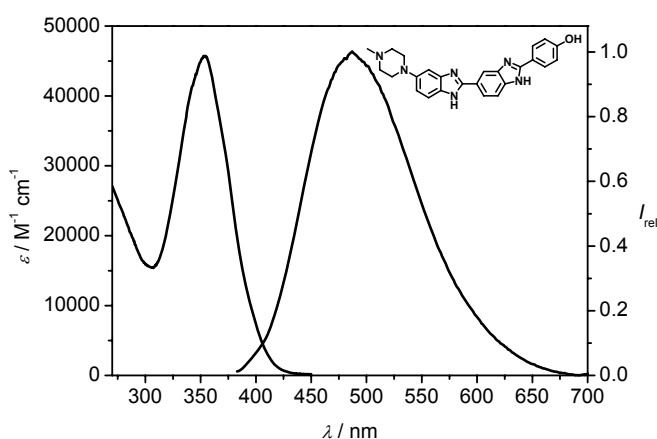


**Figure 2.2** Absorption and emission spectra of **H** in DMF.

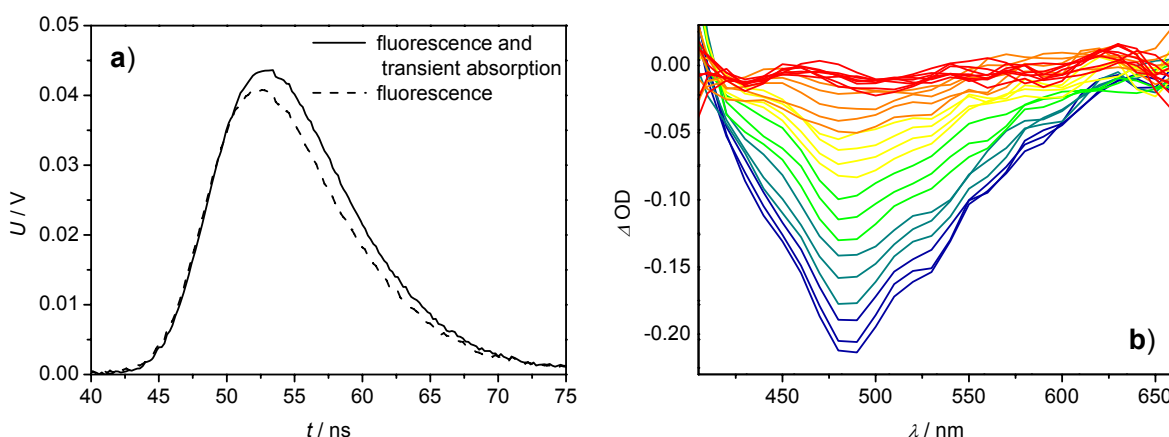


**Figure 2.3** Photoexcitation of **H** in DMF at 355 nm; **a**) time dependent measurements at 490 nm: fluorescence and transient absorption (solid) and fluorescence correction (dashed); **b**) transient absorption spectra recorded at 10 nm steps with standard fluorescence correction using Equation 2.1. Fluorescence appears as a negative signal in this representation.

Figure 2.3a illustrates the failure of the standard fluorescence correction. Apart from the slight time-shift of both curves one can easily see that the fluorescence correction curve is less intense than the curve consisting of transient absorption *and* fluorescence. It is obvious that a less intense fluorescence curve makes no physical sense and is the consequence of the response characteristics of the PMT. The effect of this kind of fluorescence correction on transient absorption spectra is shown in Figure 2.3b. These transient spectra are very similar to those obtained without any correction. Thus, for an adequate fluorescence correction measurement it is an outmost condition that the time response characteristics of the instrument response for the  $I_T(t)$  trace match closely that of the fluorescence correction trace. Although it is not completely understood yet, we observed that differences in time response characteristics are less pronounced if two transient signals are measured while in both experiments probe light of even very different intensity is shining onto the PMT. Obviously, the PMT response differs if *no* probe light is shining onto the PMT from if probe light of *any* intensity is shining. Thus, instead of correcting the transient signal (transient absorption & fluorescence) at a given probe light intensity by a separately measured fluorescence trace (with probe light blocked) we correct the transient signal by recording a second transient signal measured with a probe light at lower intensity. In our set-up this can easily be done by using the Xe flash lamp in pulsed mode (probe light with high intensity) and in CW mode (probe light with low intensity, ca. 10 % of pulsed mode). In practice, this intensity ratio of pulsed to CW light (10:1) turned out to be optimal to measure many different fluorescent compounds with our setup but it might be necessary to modify the ratio when using a different transient absorption equipment. Figure 2.4a displays two curves of **H** in DMF which were recorded under the same conditions as those of Figure 2.3a but with different probe light intensities. It can be clearly seen that the signal recorded with pulsed probe light is less intense because the transient absorption contribution reduces the signal compared to the measurement with weak CW probe light. In contrast to the two curves shown in Figure 2.3a both signals show the same rise times which is a further improvement.

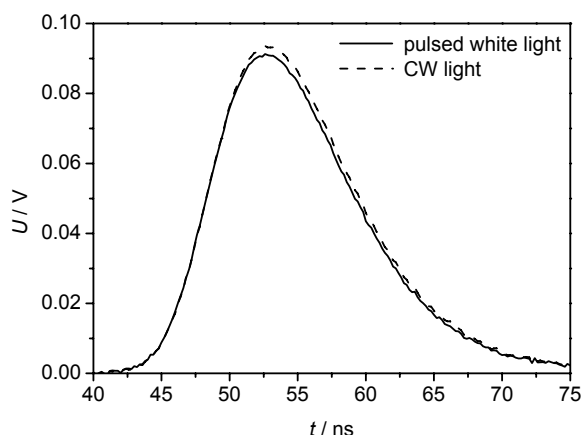


**Figure 2.4** Time dependent measurements of **H** in DMF at 490 nm upon photoexcitation at 355 nm: traces with intense pulsed white light (solid) and with low intensity CW light (dashed). The constant offset caused by the probe light is eliminated in both curves.

As fluorescence depends on the intensity of the pulsed and not on the probe light, it is considered to be identical in both transient signals. In contrast, the amount of transient absorption varies linearly with the intensity of the probe light. Taking these two facts into account, we derived Equation 2.2 to calculate the changes of optical density where  $I_T^{CW}(t)$  is the transient signal with weak probe light (CW Xe lamp with background  $I^{CW}$ ).

$$\Delta OD(t) = \log \left( \frac{I^p - I^{CW}}{I_T^p(t) - I_T^{CW}(t)} \right) \quad (2.2)$$

Applying the new approach, we are able to obtain undisturbed transient absorption spectra of fluorescent compounds. For illustration, we derived transient absorption spectra of **H** in DMF (see Figure 2.5) from fluorescence corrected time dependent measurements using Equation 2.2, although fluorescence and transient absorption of this sample occur in the same spectral region.

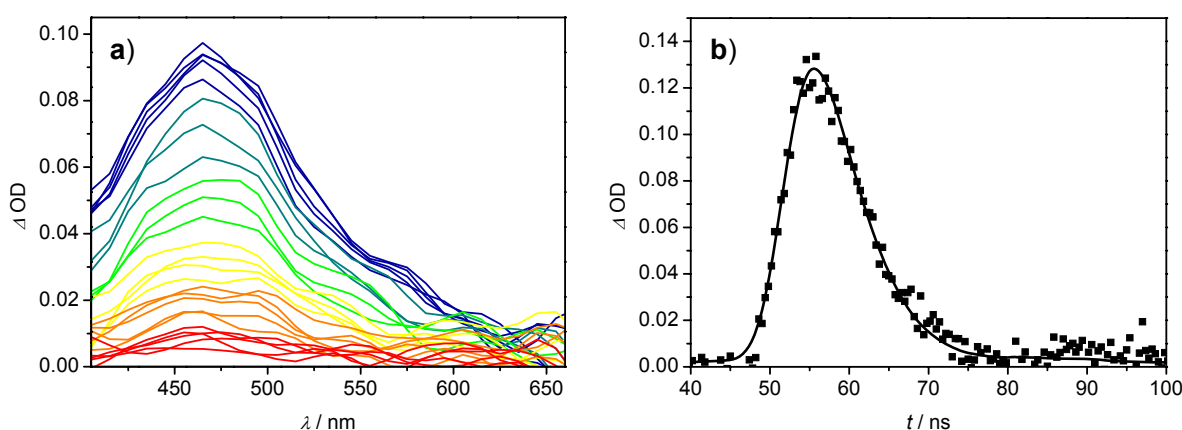


**Figure 2.5** a) Transient absorption spectra of **H** in DMF (photoexcitation at 355 nm). Early spectra are shown in blue/green and late spectra are shown in orange/red colours; b) Time dependent absorption measurements (data points) of **H** and of fit (line) at 465 nm.

From transient absorption measurements the lifetime of the first excited state was determined to be 3.4 ns. This value is in quite good agreement with the fluorescence lifetime (3.6 ns) which was determined from fluorescence decay measurements. This decay was recorded with a fluorescence-lifetime spectrometer with a nanosecond flash lamp. The agreement of both decays proves beyond doubt that the new fluorescence correction according to Equation 2.2 works very well.

## 2.3 Conclusion

Measuring two transient absorption signals with different intensities of the probe light allows us to investigate compounds with quantum yields up to  $\sim 35\%$ . This procedure is a distinct improvement because we are not aware of any method which allow fluorescent states of compounds with such high quantum yields to be investigated by laser flash photolysis technique. For samples with quantum yields  $> 40\%$  it is still very difficult to obtain accurate transient spectra, because the fluorescence signal increases compared to that of the transient absorption. Consequently, the very small difference of two comparatively large signals results in a major error in the denominator of Equation 2.2.

## 3 Photoinduced Charge Separation and Recombination in Acridine-Triarylamine Based Redox Cascades

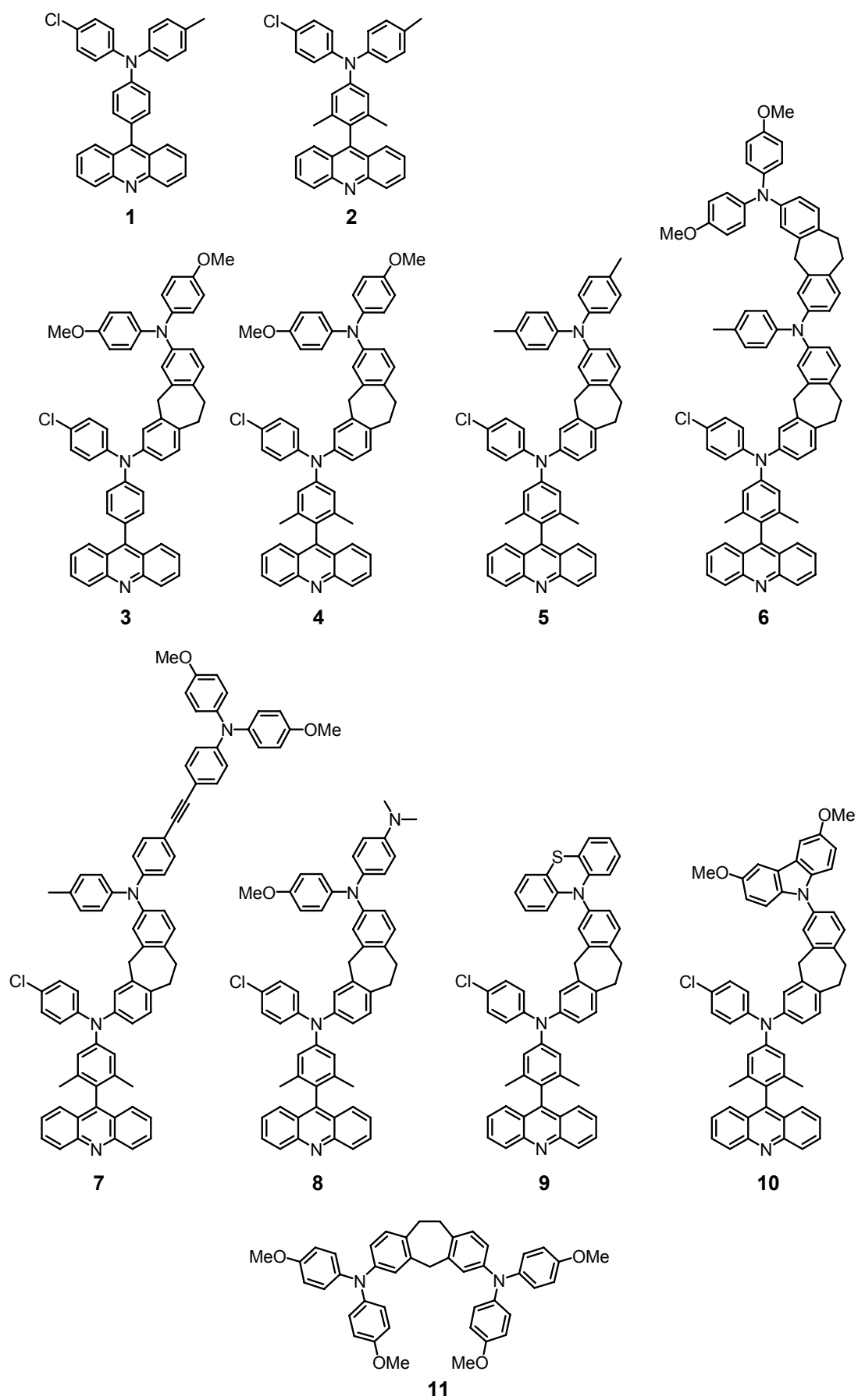
### 3.1 Introduction

Photoinduced electron transfer (PET) processes along redox cascades are of fundamental relevance in biology (e.g. photosynthesis)<sup>[107, 147-149]</sup> and in artificial devices such as dye sensitised (in)organic solar cells (DSSC)<sup>[150-160]</sup> or solar cells based on semiconducting organic polymers.<sup>[161-163]</sup> In order to study electron and hole transfer processes many systems close to nature (biomimetic)<sup>[89, 164, 165]</sup> as well as many completely artificial ones<sup>[56, 166-175]</sup> have been synthesised. Many if not most of these artificial systems comprise either C<sub>60</sub><sup>[33, 37, 39, 41, 42, 85-101]</sup> as the electron acceptor (because it can easily be reduced and has a low reorganisation energy) or (metallo)porphyrine subunits<sup>[33-44]</sup> as electron donors because they mimic the naturally occurring chlorophyll properties so nicely.

In this chapter we report about fully artificial redox cascades which might be a further step towards efficient light driven systems by photoinducing a long-lived charge separated state in cascades consisting of up to three donor subunits with decreasing redox potential. Chart 3.1 shows the cascades **3 – 10** and the two reference compounds **1** and **2** which were synthesised. All chromophores comprise acridine (Ac) as the electron acceptor moiety, one triarylamine donor subunit in the case of the reference compounds, and up to three donor subunits within the cascades. Acridine was used because the fluorescence characteristics of donor substituted acridine have intensively been investigated by Kapturkiewicz *et. al.* and are well understood.<sup>[108-110]</sup> In addition, donor substituted acridine fluoresces with high quantum yields in a wide range of solvent polarity. This fact indicates a sufficiently long-lived charge transfer (<sup>1</sup>CT) state which may be able to inject a hole into the cascade. The internal reorganisation energy of donor substituted acridine derivatives is relatively small<sup>[108]</sup> as is that of triarylamine in general.<sup>[16, 46, 47]</sup> Consequently, as in photoinduced electron transfer processes charge separation is expected to be in the Marcus normal region and charge recombination in the inverted region, a small internal reorganisation energy will promote fast hole transfer and slow recombination rates.

In all cascades we used triarylamine as the electron donors. Owing to their excellent stability as radical cations<sup>[49, 50]</sup> triarylamine have already been used in many charge transfer systems like arrays<sup>[16, 176-179]</sup>, dendrimers<sup>[180-189]</sup> or polymers<sup>[190, 191]</sup> as hole transport components. Moreover, their redox potential can easily be tuned within a broad range by adequate substituents of the phenyl ring.<sup>[51, 52]</sup> Substituents in *para*-position also serve to increase the stability of the triarylamine upon oxidation.

Chart 3.1



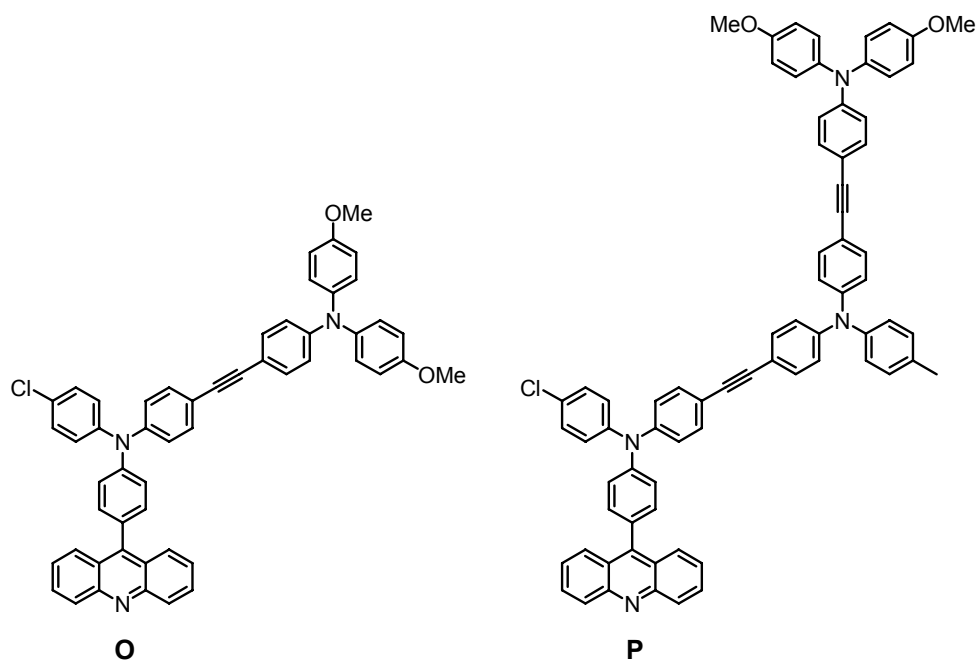


To simplify the discussion below, we make the following assignments to the redox centres in the chromophores: the acridine moiety (Ac) is connected to the adjacent donor subunit (D1) which is in all cases a triarylamine, followed by a second (D2) and, in **6** and **7**, by a third (D3) donor subunit. The terminal redox centre (either D2 or D3) has in all chromophores the lowest oxidation potential. This terminal redox centre is in most cases a triarylamine but in some cases D2 is replaced by carbazole<sup>[192, 193]</sup> or phenothiazine<sup>[194]</sup> in order to study the influence of different donor subunits within the redox cascades.

In a recent study<sup>[16]</sup> we investigated the photoinduced electron transfer dynamics in cascades comprising acridine as the electron acceptor and a donor array of two or three triarylaminines connected by conjugated triple bonds (see Chart 3.2). Because of the conjugated bridge in between the triarylaminines and between the acridine and the first triarylamine photoinduced charge separation was fast (2 ps to 5 ns depending on the solvent) but also charge recombination (20 ps to > 2 ns).

In order to increase the lifetime of the charge separated (CS) state compared to the cascades **O** and **P** already studied in our group (see Chart 3.2), the electronic coupling between the acridine acceptor (Ac) and the donor subunit D1 is decreased by the perpendicular orientation of the phenyl group attached to Ac (cf **1** vs **2** and **3** vs **4**). This orientation which reduces  $\pi$ -overlap considerably is enforced by two methyl groups. Furthermore, the electronic communication between the amine redox centres is decreased by saturated spacers. We chose a methylene and ethylene bridging unit in order to minimize conformational flexibility of the donor chain as much as possible. One exception is cascade **7** where the second and third triarylamine is bridged by a conjugated rigid triple bond. We can estimate the electronic coupling between the triarylamine redox centres by analysing the intervalence charge transfer (IVCT) band in the mixed valence radical cation of the reference bis-triarylamine **11**. The IVCT band of **11**<sup>•+</sup> was obtained by chemical oxidation of **11** with SbCl<sub>5</sub> in CH<sub>2</sub>Cl<sub>2</sub> (see Experimental Section). A Mulliken-Hush analysis<sup>[195]</sup> of **11**<sup>•+</sup> gave an electronic coupling  $V$  between the two redox centres of 90 cm<sup>-1</sup> compared to 1200 cm<sup>-1</sup> in the case of an acetylene spacer.<sup>[195, 196]</sup>

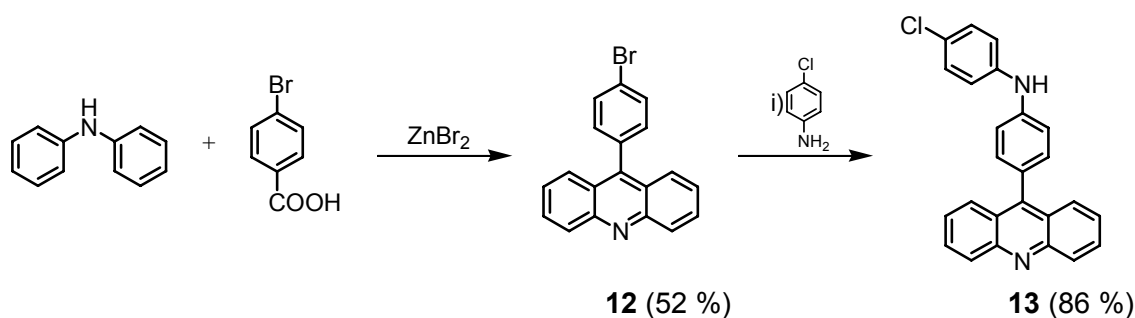
Chart 3.2



## 3.2 Results and Discussion

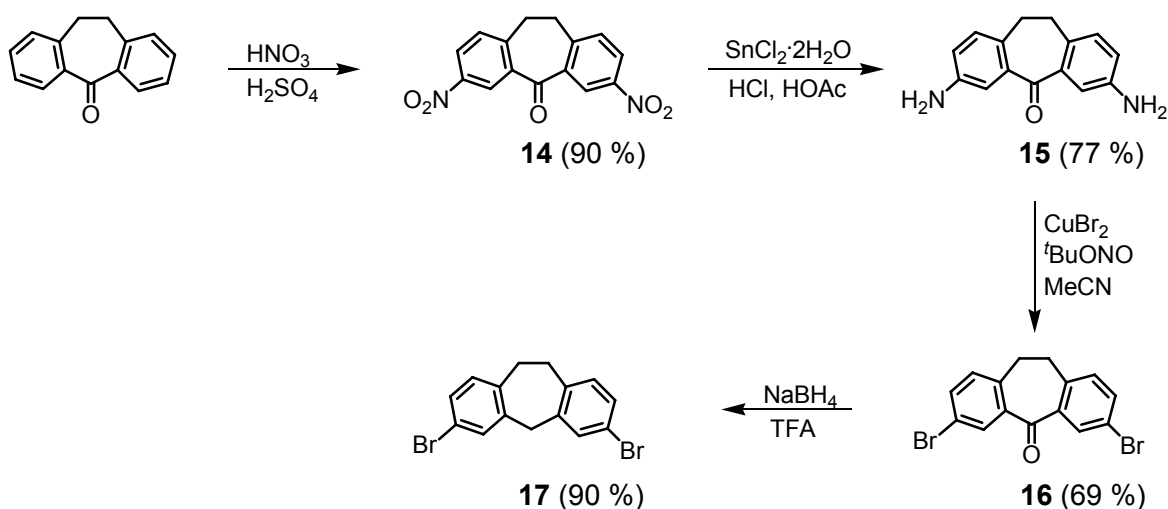
### 3.2.1 Synthesis

The synthesis of compound **13** is shown in Scheme 3.1. 9-(4-Bromophenyl)acridine **12** was synthesised by a Berntsen reaction of diphenylamine and 4-bromobenzoic acid in a microwave assisted reaction. The diarylamine **13** was prepared by a palladium catalysed Buchwald-Hartwig amination<sup>[197-201]</sup> of **12** and 4-chloroaniline.



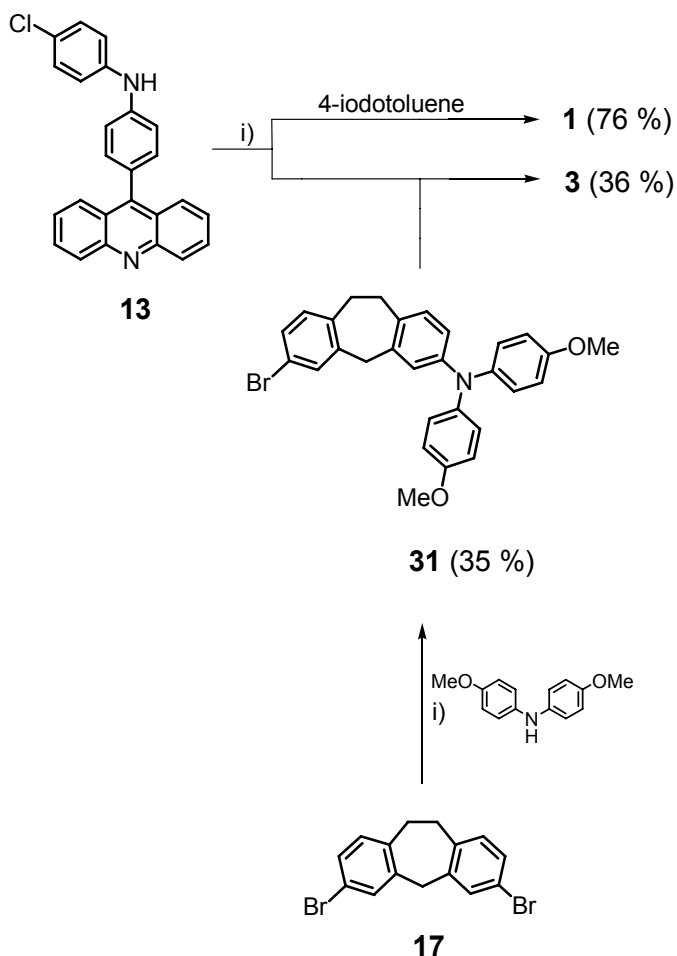
**Scheme 3.1** Synthesis of precursor **13**. i)  $\text{Pd}_2(\text{dba})_3 \cdot \text{CHCl}_3$ ,  $\text{P}^t\text{Bu}_3$ ,  $\text{NaO}^t\text{Bu}$ , toluene.

The synthetic approach to the bridge unit **17** is outlined in Scheme 3.2. 2,9-Diaminodibenzosuberone was synthesised in two steps according to literature.<sup>[202]</sup> First, dibenzosuberone was treated with a nitric acid / sulphuric acid mixture to yield 2,9-dinitrodibenzosuberone. Then, reduction of both nitro groups was accomplished by tin(II)chloride in a mixture of hydrochloric and acetic acid. Conversion of both amino groups into bromo substituents by a modified Sandmeyer reaction using copper(II)bromide and *tert*-butylnitrite in acetonitrile<sup>[203]</sup> was followed by the reduction of the carbonyl group with NaBH<sub>4</sub> in trifluoroacetic acid<sup>[204]</sup> to yield compound **17**.<sup>[205]</sup>



**Scheme 3.2** Synthesis of bridge unit **17**.

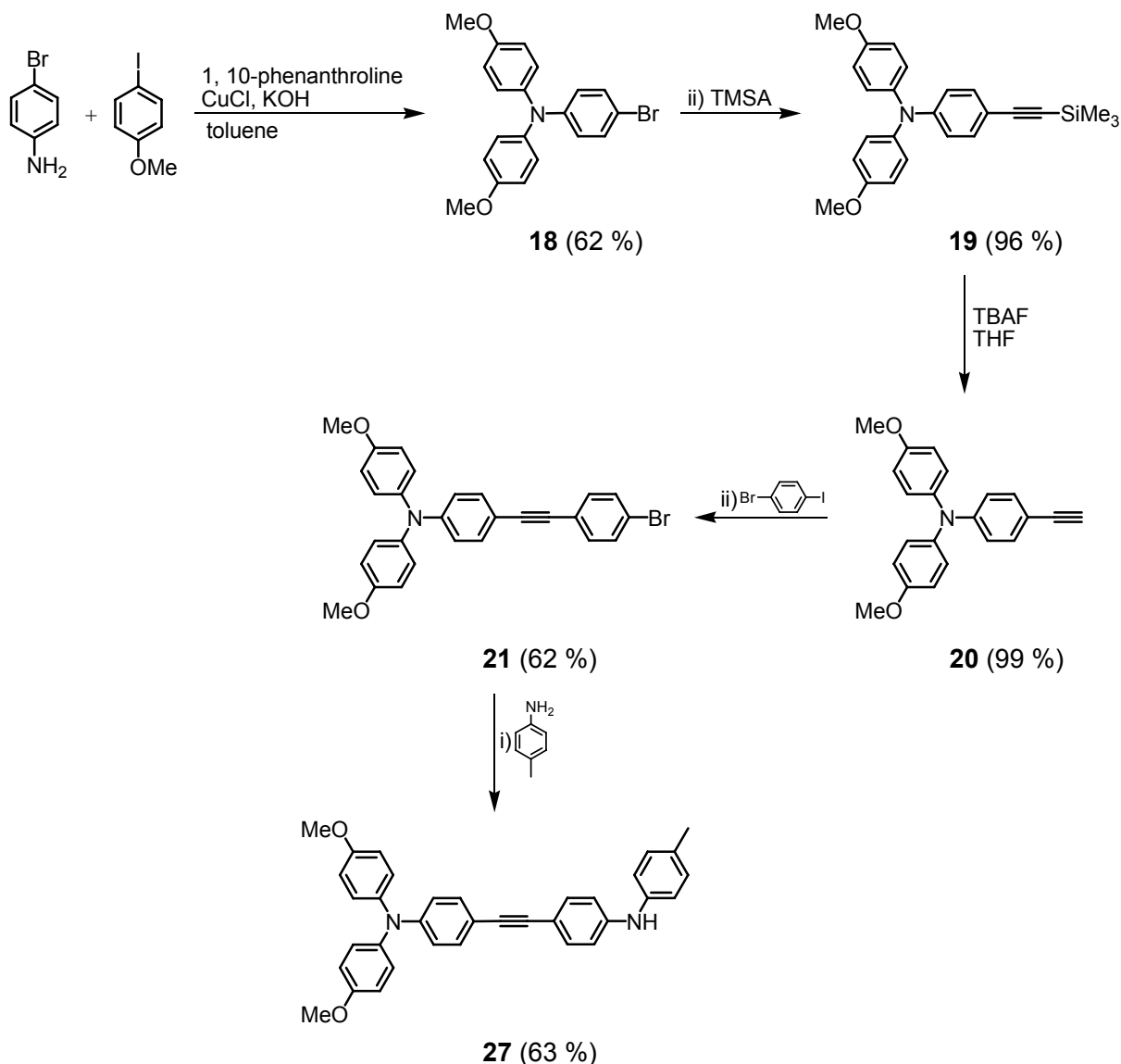
The synthesis of reference chromophore **1** and its extension **3** is illustrated in Scheme 3.3. Compound **31** was prepared by a palladium catalysed amination of **17** and di-*p*-anisylamine (**24**). Target compounds **1** and **3** were prepared under the same conditions by reaction of **13** with 4-iodotoluene or **31**, respectively.



**Scheme 3.3** Synthesis of compounds **1** and **3**. i)  $\text{Pd}_2(\text{dba})_3 \cdot \text{CHCl}_3$ ,  $\text{P}^t\text{Bu}_3$ ,  $\text{NaO}^t\text{Bu}$ , toluene.

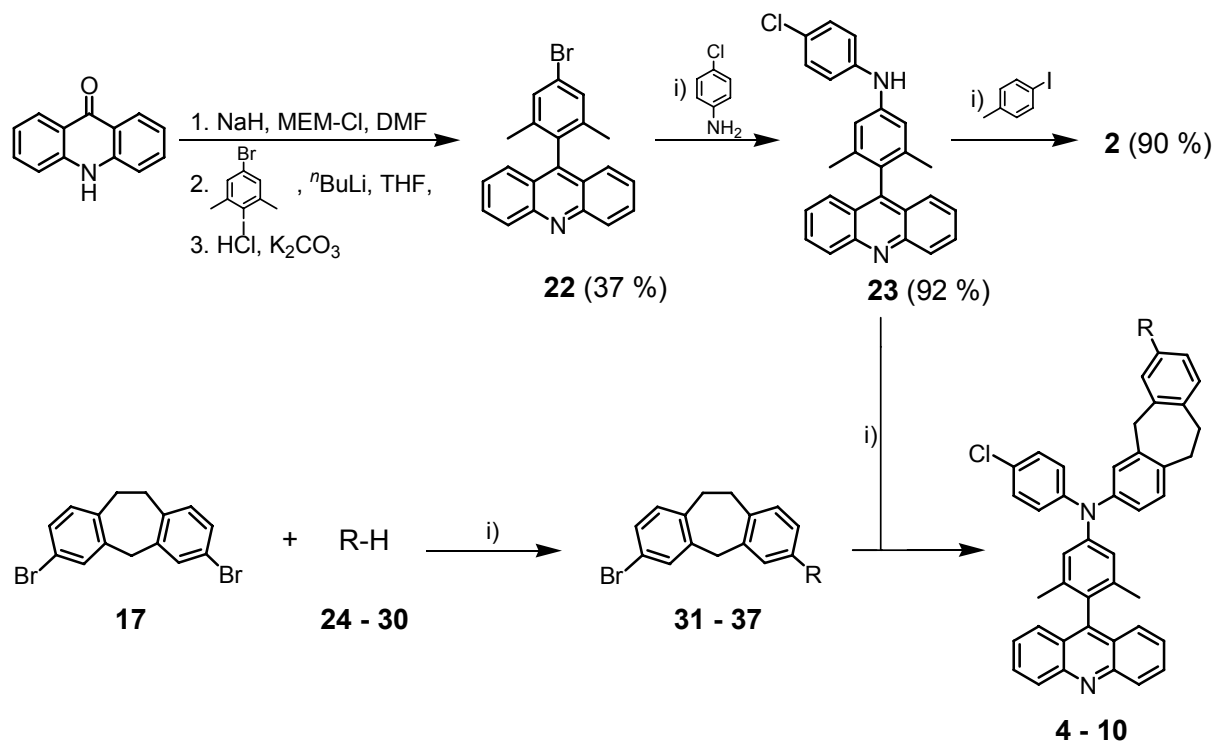
The synthesis of the donor chain **27** is shown in Scheme 3.4. The triarylamine **18** was prepared by a copper catalysed Ullmann condensation of 4-bromoaniline and 4-iodoanisole. The terminal alkyne **20** is accessible by a palladium catalysed Hagihara coupling of **18** with TMSA.<sup>[206-208]</sup> The protecting TMS group was removed by TBAF in THF.<sup>[209]</sup> We used the above mentioned Hagihara coupling to obtain compound **21** by reaction of **20** with 1-bromo-4-iodobenzene. The required precursor **27** was prepared by a palladium catalysed aryl-*N*-coupling of **21** and 4-iodoaniline.

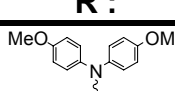
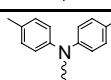
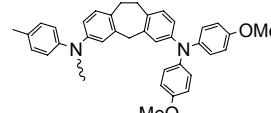
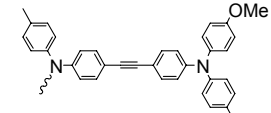
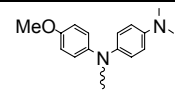
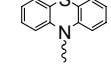
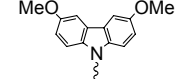
The syntheses developed for compounds **4** – **10** are given in Scheme 3.5. First, the starting compound 9(10*H*)-acridone was protected by MEM chloride.<sup>[210]</sup> After addition of 5-bromo-2-lithio-1,3-dimethylbenzene the protecting group was removed by sequential addition of HCl and  $\text{K}_2\text{CO}_3$  to yield the aromatic compound **22** in acceptable yields (42 %) compared to similar reactions reported in literature.<sup>[125-127, 211]</sup> The diarylamine **23** was synthesised by a palladium catalysed aryl-*N*-coupling of **22** and 4-chloroaniline. Formation of compound **2** was finally accomplished in the same way as chromophore **1**.



**Scheme 3.4** Synthesis of donor chain **27**. i)  $\text{Pd}_2(\text{dba})_3 \cdot \text{CHCl}_3$ ,  $\text{P}^t\text{Bu}_3$ ,  $\text{NaO}^t\text{Bu}$ , toluene. ii)  $\text{Pd}(\text{C}_6\text{H}_5\text{CN})_2\text{Cl}_2$ ,  $\text{P}^t\text{Bu}_3$ ,  $\text{CuI}$ ,  $\text{HN}^i\text{Pr}_2$ , dioxane.

Compounds **24**, **25** and **29** are commercially available and were used without further purification. The precursor **26** is accessible by a palladium catalysed amination of **31** and 4-methylaniline. Using this palladium catalysed Buchwald-Hartwig amination, compound **28** was obtained by reaction of (4-bromophenyl)dimethylaniline with *p*-anisidine. Following a procedure published by Kikugawa *et. al.*<sup>[212]</sup> we synthesised **30** in an one-step-reaction using commercially available 3,6-dibromo-9*H*-carbazole as the starting material. A direct methoxide displacement of bromo was achieved by using  $\text{MeONa}$  and  $\text{CuI}$  in  $\text{DMF}$ . All intermediates **31** – **37** were prepared by palladium catalysed aminations of **17** and the corresponding donor fragments **24** – **30**. Finally, these key precursors were again coupled by Pd catalysis with **23** to obtain the desired target compounds **4** – **10**.



R :			
	<b>24</b>	<b>31</b> (35 %)	<b>4</b> (69 %)
	<b>25</b>	<b>32</b> (17 %)	<b>5</b> (64 %)
	<b>26</b> (78 %)	<b>33</b> (29 %)	<b>6</b> (38 %)
	<b>27</b> (63 %)	<b>34</b> (31 %)	<b>7</b> (68 %)
	<b>28</b> (36 %)	<b>35</b> (46 %)	<b>8</b> (52 %)
	<b>29</b>	<b>36</b> (34 %)	<b>9</b> (86 %)
	<b>30</b> (89 %)	<b>37</b> (32 %)	<b>10</b> (68 %)

**Scheme 3.5** Synthesis of compounds **2** and **4 - 10**. i)  $Pd_2(dba)_3 \cdot CHCl_3$ ,  $P^tBu_3$ ,  $NaO^tBu$ , toluene.

### 3.2.2 Redox Properties

For a discussion of photoinduced electron and hole transfer processes in **1 – 10** it is essential to know the local redox potentials of all redox centres. Therefore we determined the redox potentials of all chromophores **1 – 10** by cyclic voltammetry (CV). The measurements were performed in benzonitrile for all compounds using TBAH (0.2 M) as supporting electrolyte. The redox potentials are referenced against the ferrocene/ferrocenium redox couple as internal standard. The half wave potentials obtained from measurements in benzonitrile are summarised in Table 3.1 and the CV of cascade **4** in benzonitrile is given in Figure 3.1 as a representative CV for all chromophores.

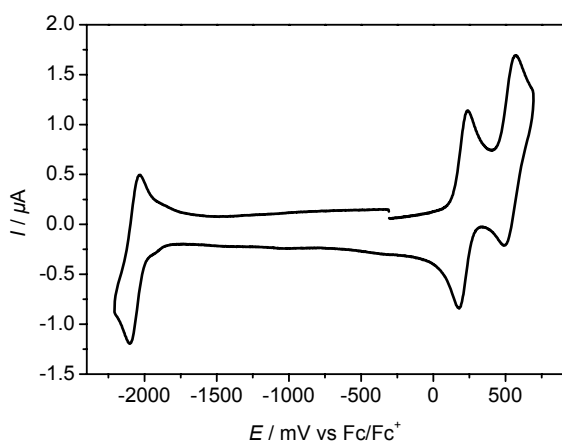


**Figure 3.1** CV of **4** in benzonitrile / 0.2 M TBAH,  $\nu = 100$  mV/s.

The redox process at about -2070 mV is nearly constant for all chromophores and is associated with the reduction of the acridine acceptor. As already reported by Steckhan *et al.*<sup>[51, 52]</sup> the oxidation potentials of triaryl amines can be tuned by substituents. The values of compounds **1 – 10** (see Table 3.1) indicate that the oxidation potentials depend mainly on the substituents attached to the triaryl amines. This implies that the electronic coupling between the redox centres is negligible compared to the influence of their substituents. In all chromophores **1 – 10** the redox centre D1 is structurally the same and is most difficult to oxidise. The redox potentials of the donor subunits D2 and – if present – D3 are shifted to lower values than D1 owing to the methoxy (at D2 in **3** and **4** and at D3 in **6** and **7**) or methyl (at D2 in **5 – 7**) groups or to a combination of dimethylamino and methoxy substituents (at D2 in **8**) or owing to the phenothiazine redox centre (D2 in **9**). Although cascades **4** and **10** differ only in one bond (triarylamine vs. carbazole subunit) the oxidation potential of the bis-methoxy substituted carbazole moiety in **10** is shifted to such a high potential that its redox

wave is superposed by the signal of the redox centre D1. Thus, the carbazole subunit in **10** is only somewhat easier to oxidise than D1 and cannot be compared at all with the redox properties of bis-methoxy substituted triarylaminines.

All further redox processes are chemically irreversible as they are related to the second oxidation of one donor subunit and could only be observed in a few compounds due to the limited accessible potential window of the solvent.

**Table 3.1** Redox potentials ( $E_{1/2}$  vs. Fc/Fc<sup>+</sup>) of **1** – **10** in benzonitrile / 0.2 M TBAH determined by cyclic voltammetry.

	$E_{1/2}^{\text{red}}(\text{Ac})/\text{mV}$	$E_{1/2}^{\text{ox}}(\text{D1})/\text{mV}$	$E_{1/2}^{\text{ox}}(\text{D2})/\text{mV}$	$E_{1/2}^{\text{ox}}(\text{D3})/\text{mV}$
<b>1</b>	-2060	570 <sup>[a]</sup>		
<b>2</b>	-2070	520 <sup>[a]</sup>		
<b>3</b>	-2050	570 <sup>[a]</sup>	210	
<b>4</b>	-2070	530 <sup>[a]</sup>	210	
<b>5</b>	-2070	540 <sup>[a]</sup>	370	
<b>6</b>	-2070	540 <sup>[a]</sup>	390	210
<b>7</b>	-2070	540 <sup>[a]</sup>	450	260
<b>8</b>	-2070	560 <sup>[a]</sup>	-130 / 420 <sup>[b]</sup>	
<b>9</b>	-2070	530 <sup>[a]</sup>	270	
<b>10</b>	-2070	530 <sup>[a]</sup>	470	

<sup>[a]</sup> chemically irreversible, <sup>[b]</sup> second oxidation of the same subunit

The results of the CV measurements (see Table 3.1) illustrate that the redox gradient in cascades **3** – **10** for hole migration is always correctly directed downhill from D1 to D2 and in **6** and **7** further to D3. Furthermore, it is confirmed that the redox potentials of the redox centres can be tuned by adequate substituents and that electronic interaction between the redox centres is very weak. This is an important condition for the proper design of redox cascades with a directed hole transfer gradient.



### 3.2.3 Stationary Spectroscopy

#### 3.2.3.1 Steady State Absorption Spectroscopy

The steady state absorption spectra of the two reference compounds **1** and **2** are shown in Figure 3.2.

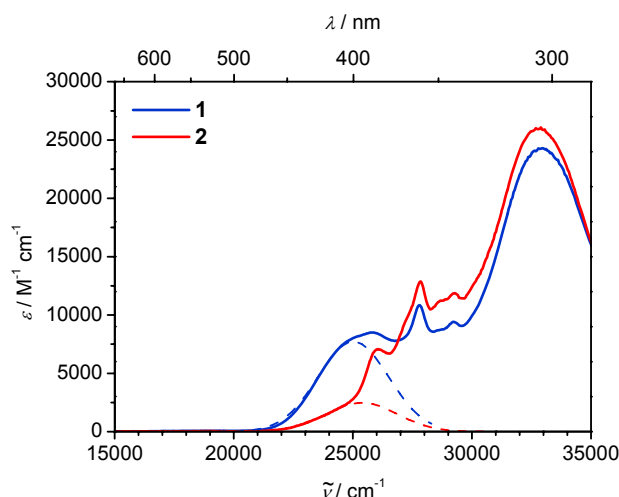


**Figure 3.2** Steady state absorption spectra of **1** and **2** in  $\text{CH}_2\text{Cl}_2$ . The dotted lines show a Gaussian deconvolution of the spectra to yield the corresponding CT bands.

The broad band in both spectra at ca.  $32800\text{ cm}^{-1}$  is characteristic for triaryl amines and can be attributed to localised transitions within this donor subunit. The peaks at ca.  $26100$ ,  $27800$  and  $29200\text{ cm}^{-1}$  arise from  $\pi$ - $\pi$ -transitions of the phenylacridine subunit. Both in **1** and in **2** the fine structure of the acceptor is superposed by a very broad band which can be attributed to a charge transfer (CT) from the triarylamine to the acridine redox centre. A Gaussian deconvolution of the absorption spectra yields the CT bands at ca.  $25000\text{ cm}^{-1}$ . This band is about three times more intense in **1** than in **2** which is due to the orthogonal orientation of the 2,6-dimethylphenylene group in **2**. These different intensities of the CT-bands indicate that the charge transfer character is more pronounced in **2** than in **1**, i.e. **2** has a higher degree of charge separation. Further evidence for and consequences of this important difference will be discussed in detail below. Both the localised absorption bands of the donor and the acceptor subunits do not show any solvatochromic behaviour at all. In contrast, the CT band of **1** is bathochromically shifted in polar solvents because the dipolar CT state is better stabilised. Owing to the weak CT band being superposed by the acridine absorption band no solvatochromic effect is visible in **2**.

The steady state absorption spectra of **3**, **4**, **5** and **8** are given in Figure 3.3a. These spectra do not deviate much owing to the similarity of the subunits. Compared to their

corresponding reference compounds **1** and **2**, respectively, the intensity of the localised triarylamine bands in the cascades **3**, **4**, **5**, and **8** is about twice as high because of the doubled number of triarylamine moieties being present. As in **1** and **2**, the CT-band in **3** is much stronger than in **4**, **5** and **8**.

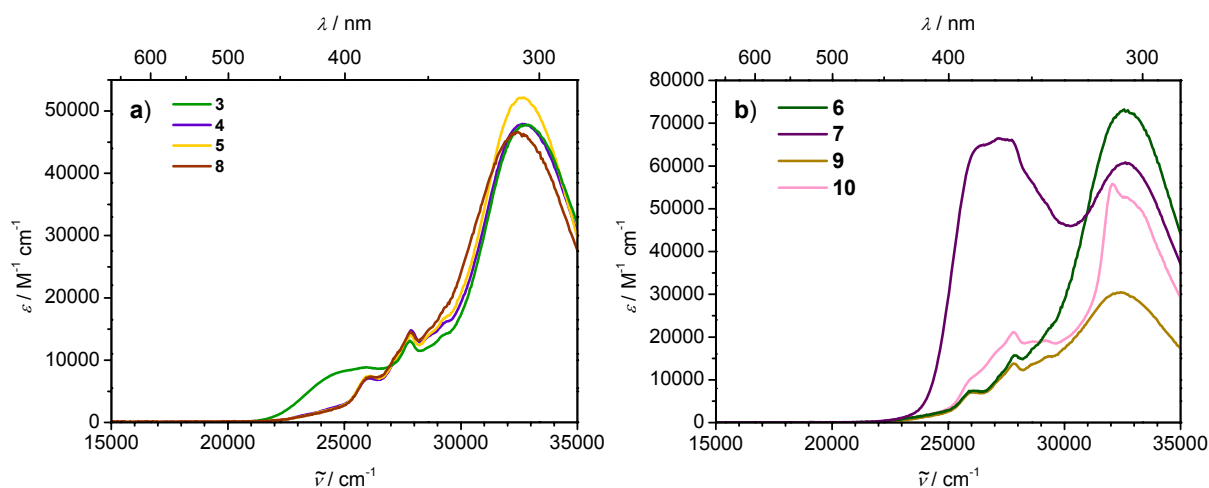


**Figure 3.3** Steady state absorption spectra in  $\text{CH}_2\text{Cl}_2$  **a)** of **3**, **4**, **5** and **8**; **b)** of **6**, **7**, **9** and **10**.

The absorption spectra of cascades **6** and **7** – which are the ones with four redox centres – and of **9** and **10** are shown in Figure 3.3b. The spectrum of compound **6** continues the trend observed for **2** and **4**: a weak CT band shoulder, a fine structure of the acridine subunit at 26100, 27800 and 29200  $\text{cm}^{-1}$  and a broad and intense band arising from the triarylamine at ca. 32600  $\text{cm}^{-1}$  with an intensity being three times that of **2** as a result of three triarylamine groups in **6** instead of one in **2**. In contrast, the absorption spectrum of **7** is quite different. The absorption band of the acridine subunit is strongly superposed by an intense band at about 27000  $\text{cm}^{-1}$  which is due to a  $\pi$ - $\pi$ -transitions within the tolandiamine.<sup>[16]</sup>

The absorption spectrum of **9** is similar to that of **2** because the absorption band of localised  $\pi$ - $\pi$ -transitions at ca. 31000  $\text{cm}^{-1}$  within the phenothiazine donor is very weak and, moreover, is superposed by transitions of D1. Much in contrast, the steady state absorption spectrum of cascade **10** exhibits a sharp peak at about 32100  $\text{cm}^{-1}$  with a shoulder at higher energy which can be attributed to a superposition of local transitions of the triarylamine and the bis-methoxy substituted carbazole subunits, respectively. Weak transitions of the carbazole around 27000  $\text{cm}^{-1}$  result in a more intense absorption of **9** compared to **10** in this region.

## 3.2.3.2 Steady State Emission Spectroscopy

Fluorescence spectra of compounds **1** – **6** and **8** – **10** were measured in a series of solvents with different polarity, ranging from nonpolar cyclohexane to highly polar acetonitrile. The chromophores were excited at the low energy tail of their absorption spectra ( $26300\text{ cm}^{-1}$ ), that is, at a superposition of  $^1\text{CT}$  and localised acridine band. The fluorescence properties of compounds **1** – **6** and **8** – **10** are collected in Table 3.3.

Both compounds **1** and **2** show strong fluorescence with high quantum yields. They exhibit a broad solvatochromic emission band with large Stokes shift in polar media. Only in solvents of very low polarity a fine structure of this emission band is observed. The emission band of compounds **1** and **2** displays a pronounced positive solvatochromism. As an example, the normalised fluorescence spectra of **2** in different solvents are shown in Figure 3.4.

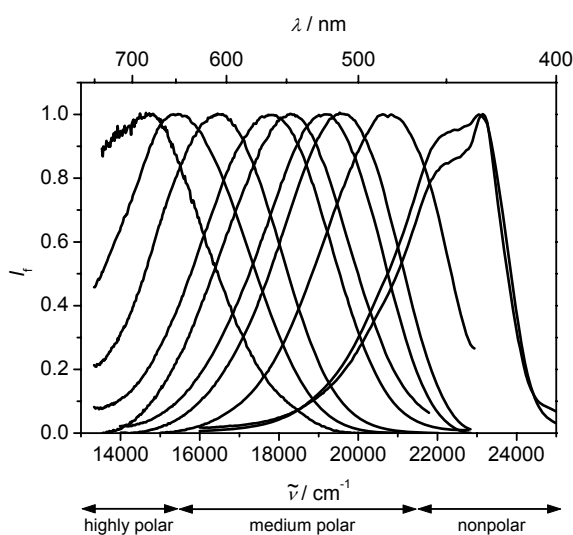


**Figure 3.4** Normalised fluorescence spectra of **2**. The solvents are from left to right: MeCN, *n*-PrCN,  $\text{CH}_2\text{Cl}_2$ , THF,  $\text{Et}_2\text{O}$ , 1,4-dioxane, MTBE, *n*-Bu $_2\text{O}$ ,  $\text{C}_6\text{H}_{12}$ , Me- $\text{C}_6\text{H}_{11}$ .

A large Stokes-shift in combination with a pronounced positive solvatochromism indicates an emission from a highly dipolar excited state. The solvatochromic behaviour of the fluorescence spectra can be used to estimate the change of dipole moments upon photoexcitation from the ground to the first excited state using Equation 3.1<sup>[213]</sup>:

$$\tilde{\nu}_f = \tilde{\nu}_f^{\text{vac}} - \frac{2\mu_e(\mu_e - \mu_g)}{4\pi\epsilon_0 h c a^3} (f(\epsilon)) \quad \text{with } f(\epsilon) = \frac{\epsilon - 1}{2\epsilon + 1} \quad (3.1)$$

where  $\tilde{\nu}_f$  is the fluorescence energy maximum in  $\text{cm}^{-1}$ ,  $\tilde{\nu}_f^{\text{vac}}$  is the energy maximum of the fluorescence in vacuo in  $\text{cm}^{-1}$ ,  $\mu_g$  and  $\mu_e$  are the ground state and excited-state dipole moments in Cm, which are assumed to be parallel,  $a_0$  is the effective radius of the solute and  $\epsilon$  is the permittivity of the solvent.

If the emission maximum is plotted against the Onsager solvent parameter  $f(\epsilon)$  the product of the excited states dipole moment and the difference dipole moment upon excitation is obtained from the slope of the linear fit. The intercept corresponds to the emission maximum in vacuo. The data of the linear fits for **1 – 6**, **8 – 10** are given in Table 3.2. Because we cannot evaluate either  $\mu_e$  or  $\mu_g$  without knowing the other we only discuss the product  $\mu_e(\mu_e - \mu_g)$ .

**Table 3.2** Fitted parameters from the plots of Equation 3.1.

	$\tilde{\nu}_f^{\text{vac}} / \text{cm}^{-1}$	$\frac{2\mu_e(\mu_e - \mu_g)}{4\pi\epsilon_0 hca_0^3} / \text{cm}^{-1}$
<b>1</b>	28000	-25700
<b>2</b>	28600	-28400
<b>3</b>	27300	-22800
<b>4</b>	28300	-27800
<b>5</b>	28500	-28100
<b>6</b>	28600	-28500
<b>8</b>	28200	-27400
<b>9</b>	28400	-28000
<b>10</b>	28600	-28300

The linear fits for **1** and **2** are shown in Figure 3.5. Both fits yield almost the same intercept which is expected because both compounds consist of the same donor and acceptor moieties. If one assumes a similar and solvent independent ground state polarisation  $\mu_g$  for both **1** and **2** the slopes of the linear fits depend on the change of dipole moment upon excitation. Thus, the larger slope of **2** indicates a more dipolar excited state compared to **1**. This observation can be understood by a more orthogonal orientation of acridine acceptor and amine donor in **2** which is induced by the ortho-methyl groups. This orthogonal arrangement leads to a stronger decoupling of negative and positive charge, and thus, to a higher dipole moment in the excited state of **2**.

This explanation is in accordance with results obtained from absorption measurements already discussed above. The data of all compounds **1 – 6**, **8 – 10** can be linearly fitted very well with only slightly varying parameters which suggests that the fluorescence always originates from the same dipolar excited state.

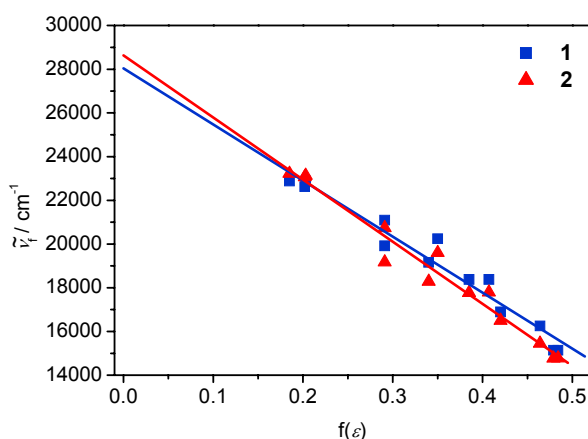


**Figure 3.5** Plots of  $\tilde{\nu}_f$  for **1** and **2** vs  $f(\epsilon) = (\epsilon - 1)/(2\epsilon + 1)$  and linear fits. The solvents are from left to right:  $C_6H_{14}$ ,  $C_6H_{12}$ , 1,4-dioxane,  $n$ -Bu $_2$ O, Et $_2$ O, MTBE, EtOAc, THF,  $CH_2Cl_2$ ,  $n$ -PrCN, DMSO, MeCN.

In all solvents the excitation spectra of **1** and **2** match very well with the corresponding absorption spectra. This signifies a complete energy transfer from higher excited states to the fluorescent first excited state.

The quantum yields of compounds **1** and **2** are summarised in Table 3.3. As reported earlier, donor substituted acridine fluoresces with high quantum yields in a wide range of solvent polarity with a maximum in moderately polar solvents.<sup>[108]</sup> These results are in good agreement with the fluorescent nature of **1**. In contrast, except for very nonpolar solvents the quantum yields of **2** are throughout smaller than those of **1**. As we will see in the next section this effect is due to the lower fluorescence rate constant  $k_f$  because of the perpendicular geometry of donor and acceptor in **2**.

Like **1** and **2** cascades **3 – 6** and **8 – 10** exhibit one emission band which shows a strong positive solvatochromism. The fluorescence spectra of **3 – 6** and **8 – 10** are qualitatively very similar to those of **1** and **2**, respectively. The Lippert-Mataga fits (see Table 3.2) show that the intercept and the slope of **4 – 6** and **8 – 10** are similar to that of **2** while the slope of **3** – without methyl groups at the phenylene spacer – is significantly smaller, but in good agreement with reference compound **1**.

The excitation spectra of chromophores **3 – 6** and **8 – 10** match very well with the corresponding absorption spectra in nonpolar up to moderately polar solvents. In very polar solvents the bands associated with the second and, if being present, the third donor subunit at ca.  $32800\text{ cm}^{-1}$  is marginally smaller in the excitation spectra than in the absorption spectra. This incomplete energy transfer from higher excited triarylamine localised states to the first excited  $^1CT$  state results in a local fluorescence of the triarylamine donor at ca.  $27100\text{ cm}^{-1}$ . This energy transfer is even more incomplete in **7** for which a strong

fluorescence at  $22100\text{ cm}^{-1}$  is visible in  $\text{CH}_2\text{Cl}_2$  from localised tolandiamine states. This emission is much stronger than that from the  $^1\text{CT}$  state.

We suppose that due to large distances and saturated spacers energy transfer within the cascades **3 – 10** proceeds primarily by a Förster mechanism.<sup>[214]</sup> Because of only small spectral overlap of tolandiamine fluorescence with the  $^1\text{CT}$  absorption the rate constant for energy transfer in **7** is much smaller than in **3 – 6** and **8 – 10**. Thus, deactivation by fluorescence from the tolandiamine excited state is a competitive process to Förster energy transfer from higher locally excited states to the  $^1\text{CT}$  state.

Considering the fluorescence quantum yields  $\phi_f$  of **3 – 6** and **8 – 10** (see Table 3.3) relative to those of **1** and **2**, respectively, a dramatic decrease is observed in solvents of moderate or high polarity. Generally, the stronger the electron donor D2 the less polar the solvent needs to be to allow fluorescence quenching. This trend is due to an additional deactivation process which depends to a certain degree on the solvent polarity. The obvious explanation is a hole transfer from the redox centre D1 to D2. The resulting charge separated (CS) state ( $\text{Ac}^- - \text{D1} - \text{D2}^+$ ) is more stabilised in polar solvents which leads to a stronger fluorescence quenching. However, in nonpolar solvents, this CS state is higher in energy than the initially populated  $^1\text{CT}$  state and, thus, no fluorescence quenching occurs. In a given solvent, the fluorescence quantum yield decreases in the series **5 > 4 > 8** which follows the donor strength of D2. From this behaviour we conclude that the forward hole transfer is within the Marcus normal region.

#### 3.2.4 Time Resolved Spectroscopy

##### 3.2.4.1 Time Resolved Fluorescence Spectroscopy

In order to quantify the dynamics of the hole transfer from the  $^1\text{CT}$  to the  $^1\text{CS}$  state we measured the temporal decay of fluorescence signals of **1 – 6** and **8 – 10** by a time gated technique. The chromophores were excited at  $26200\text{ cm}^{-1}$  which ensures that only the  $^1\text{CT}$  state and local acridine states are populated. The fluorescence lifetimes  $\tau_f$  were measured in the same solvents as the stationary emission experiments (solvent polarity ranging from cyclohexane to acetonitrile). The decays were monoexponentially fitted in the nanosecond regime unless otherwise indicated. The  $\chi^2$  test (about 1.0), Durbin Watson ( $> 1.7$ ), residuals and autocorrelation function (without any significant structure) served as the main criteria in the evaluation of the fit. The rate constants for radiative  $k_f$  and all nonradiative  $k_{nr}$

deactivation processes of the excited state, respectively, are derived by Equations 3.2 and 3.3:

$$k_f = \frac{\Phi_f}{\tau_f} \quad (3.2)$$

$$k_{nr} = \frac{1 - \Phi_f}{\tau_f} \quad (3.3)$$

The decay times and rate constants for chromophores **1** – **6** and **8** – **10** are given in Table 3.3. The rate constants for the radiative deactivation  $k_f$  of both **1** and **2** plotted versus the emission maximum exhibit a similar trend (see Figure 3.6). Generally, in this paper we use plots vs energy because we will show that the photophysical processes in the compounds studied here are mainly governed by the energy of the involved states. The rate constant  $k_f$  increases with increasing fluorescence energy which is in qualitative agreement with the Strickler-Berg equation<sup>[215]</sup> which predicts a cubic dependence on the energy, see Equation 3.4.

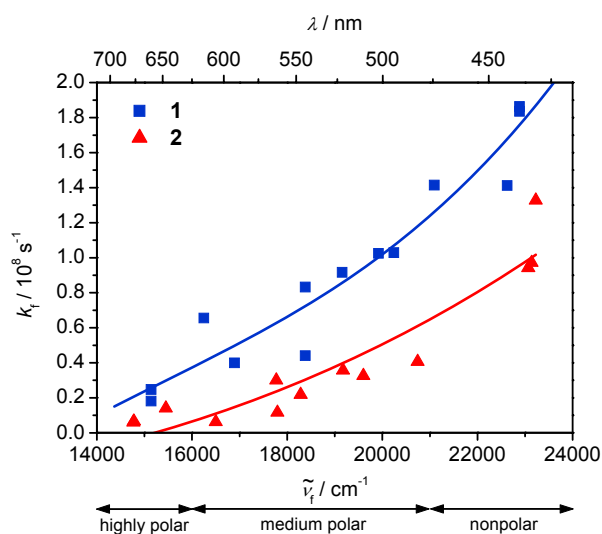


**Figure 3.6** Rate constant of the radiative process  $k_f$  vs fluorescence energy  $\tilde{\nu}_f$  for **1** and **2** in different solvents. The lines may serve as a guide to the eye and are 3<sup>rd</sup> order polynomials.

The radiative deactivation of compound **1** is consistently faster in any solvent than that of compound **2**. This is due to the higher squared fluorescence transition moment  $\mu_f^2$  in **1** which varies linearly with  $k_f$  (Equation 3.4):

$$k_f = \frac{16 \cdot 10^6 \pi^3}{3h\epsilon_0} \frac{n(n^2 + 2)^2}{9} \frac{g_g}{g_e} \langle \tilde{\nu}_f^{-3} \rangle_{av}^{-1} \mu_f^2 \quad (3.4)$$

where  $\langle \tilde{\nu}_f^{-3} \rangle^{-1} = \int I_f d\tilde{\nu} / \int \tilde{\nu}^{-3} I_f d\tilde{\nu}$  is the average cubic fluorescence energy in  $\text{cm}^{-1}$ ,  $\mu_f$  is the fluorescence transition moment in Cm,  $g_g$  and  $g_e$  are the degree of degeneracy of ground and excited state (which is 1 for both states) and  $n$  is the refractive index of the solvent.

Because the  $S_1$  state of **1** has a pronounced CT character and a relatively large transition moment, fluorescence is quite fast and is the most important deactivation pathway. In contrast, due to the perpendicular orientation of the subunits in compound **2**, its first excited state has an almost purely charge separated character and, consequently, its transition moment  $\mu_f$  is significantly smaller than that of **1**. Thus, the lower transition moment between the first excited and the ground state of **2** results in a decreased rate of fluorescence. Another possible reason for reduced fluorescence quantum yields might be enhanced nonradiative deactivation mechanisms such as intersystem crossing (ISC). As we will show below we indeed observed triplet formation for both **1** and **2** with  $k_{nr} = k_{ISC}$ . However, in contrast to what has been discussed in literature for other donor-acceptor dyads with orthogonal orientation<sup>[109, 216-218]</sup> the rate constant for nonradiative deactivation  $k_{nr}$  is larger in **1** than in **2** although the latter has the more orthogonal geometry. Thus, it appears that in **2** the perpendicular geometry does not enhance spin-orbit coupling as a source of ISC.

The sum of all nonradiative deactivation processes for **1** and **2** exhibit qualitatively the same dependence on the fluorescence energy (see Figure 3.7). While  $k_{nr}$  is more or less constant at low energies (this corresponds to polar to moderately polar solvents) it rises at higher energy (with decreasing solvent polarity). This effect is more pronounced in the case of compound **1** than in **2**. For similar acridine-donor compounds Kapturkiewicz *et. al.* found an increase of nonradiative rate constants with increasing fluorescence energy. This effect was attributed to intersystem crossing.<sup>[108]</sup> Much in contrast, for a compound similar to **1** in which the chloro and methyl groups were replaced by methoxy groups we did not observe any triplet formation.<sup>[16]</sup>



### 3 Photoinduced Charge Separation and Recombination in Redox Cascades

**Table 3.3** Emission maximum  $\tilde{\nu}_f$ , fluorescence quantum yields  $\phi_f$ , fluorescence lifetimes  $\tau_f$ , and rate constants for the fluorescent  $k_f$  and nonradiative deactivation process  $k_{nr}$  of compounds **1 – 6** and **8 – 10**.

	$\tilde{\nu}_f / \text{cm}^{-1}$	$\phi_f$	$\tau_f/\text{ns}$	$k_f/10^8 \text{ s}^{-1}$	$k_{nr}/10^8 \text{ s}^{-1}$		$\tilde{\nu}_f / \text{cm}^{-1}$	$\phi_f$	$\tau_f/\text{ns}$	$k_f/10^8 \text{ s}^{-1}$	$k_{nr}/10^8 \text{ s}^{-1}$
<b>1</b>						<b>2</b>					
C <sub>6</sub> C <sub>12</sub>	22600	0.11	0.77	1.4	12	C <sub>6</sub> C <sub>12</sub>	23100	0.28	3.0	0.94	2.4
<i>n</i> -hexane	22900	0.12	0.63	1.8	14	<i>n</i> -hexane	23200	0.28	2.1	1.3	3.4
Me-C <sub>6</sub> H <sub>11</sub>	22900	0.12	0.64	1.9	14	Me-C <sub>6</sub> H <sub>11</sub>	23100	0.27	2.8	0.97	2.7
<i>n</i> -Bu <sub>2</sub> O	21100	0.23	1.6	1.4	4.8	<i>n</i> -Bu <sub>2</sub> O	20700	0.19	4.7	0.41	1.7
MTBE	20200	0.34	3.3	1.0	2.0	MTBE	19600	0.21	6.3	0.33	1.3
1,4-dioxane	19900	0.51	5.0	1.0	0.97	1,4-dioxane	19200	0.33	9.3	0.36	0.72
Et <sub>2</sub> O	19200	0.48	5.3	0.92	0.98	Et <sub>2</sub> O	18300	0.14	6.6	0.22	1.3
EtOAc	18400	0.63	7.5	0.83	0.50	EtOAc	17800	0.31	10	0.30	0.68
THF	18400	0.49	11	0.44	0.46	THF	17800	0.25	21	0.12	0.36
CH <sub>2</sub> Cl <sub>2</sub>	16900	0.53	13	0.40	0.35	CH <sub>2</sub> Cl <sub>2</sub>	16500	0.13	21	0.06	0.42
butyronitrile	16300	0.66	10	0.66	0.34	butyronitrile	15500	0.20	14	0.14	0.56
acetonitrile	15100	0.11	4.6	0.25	1.9	acetonitrile	14800	0.05	7.8	0.06	1.2
DMSO	15100	0.13	7.4	0.18	1.2	DMSO	14800	0.08	12	0.07	0.75
<b>3</b>						<b>4</b>					
C <sub>6</sub> C <sub>12</sub>	22600	0.19	0.96	2.0	8.4	C <sub>6</sub> C <sub>12</sub>	23100	0.28	3.1	0.91	2.4
<i>n</i> -hexane	22700	0.15	0.68	2.2	13	<i>n</i> -hexane	23100	0.17	2.1	0.80	3.9
Me-C <sub>6</sub> H <sub>11</sub>	22600	0.15	0.81	1.9	11	Me-C <sub>6</sub> H <sub>11</sub>	23000	0.19	2.6	0.72	3.1
<i>n</i> -Bu <sub>2</sub> O	21200	0.23	1.6	1.5	4.9	<i>n</i> -Bu <sub>2</sub> O	20700	0.14	2.8	0.50	3.1
MTBE	20000	0.11	1.6	0.65	5.5	MTBE	19300	0.07	4.0	0.16	2.3
1,4-dioxane	19800	0.33	5.0	0.66	1.4	1,4-dioxane	19000	0.21	8.1	0.26	0.97
Et <sub>2</sub> O <sup>[a]</sup>	19600	0.03	6.0	0.28	1.4	Et <sub>2</sub> O	18900	0.02	7.6	0.03	1.3
EtOAc <sup>[a]</sup>	18500	0.06	6.1	0.68	0.98	EtOAc <sup>[a]</sup>	17400	0.03	3.9	0.08	2.5
THF	18700	0.06	5.0	0.12	1.9	THF <sup>[a]</sup>	16900	0.03	5.1	0.06	1.9
CH <sub>2</sub> Cl <sub>2</sub>	18100	0.04	7.4	0.05	1.3	CH <sub>2</sub> Cl <sub>2</sub> <sup>[a]</sup>	16300	0.02	2.5	0.09	4.0
butyronitrile	17000	0.02	5.7	0.03	1.7	butyronitrile <sup>[a]</sup>	15900	< 0.01	1.7	0.01	5.9
acetonitrile	15800	< 0.01	1.5	0.05	6.8	acetonitrile <sup>[a]</sup>	15000	< 0.01	1.2	0.01	8.1
DMSO	15400	< 0.01	1.9	0.01	5.3	DMSO <sup>[a]</sup>	15000	< 0.01	1.0	0.01	9.6
<b>5</b>						<b>6</b>					
C <sub>6</sub> C <sub>12</sub>	22800	0.26	3.6	0.74	2.1	C <sub>6</sub> C <sub>12</sub>	23100	0.23	3.9	0.60	2.0
<i>n</i> -hexane	23000	0.23	2.4	0.93	3.2	<i>n</i> -hexane	23200	0.11	2.1	0.54	4.2
Me-C <sub>6</sub> H <sub>11</sub>	23000	0.23	3.4	0.68	2.3	Me-C <sub>6</sub> H <sub>11</sub>	23200	0.15	2.9	0.52	3.0
<i>n</i> -Bu <sub>2</sub> O	20600	0.21	4.4	0.49	1.8	<i>n</i> -Bu <sub>2</sub> O	20500	0.07	3.8	0.19	2.5
MTBE	20000	0.23	8.2	0.28	0.95	MTBE	19300	0.07	4.3	0.16	2.2
1,4-dioxane	18900	0.34	14	0.24	0.47	1,4-dioxane	19090	0.17	7.4	0.23	1.1
Et <sub>2</sub> O	19200	0.14	4.7	0.30	1.8	Et <sub>2</sub> O	18400	0.03	2.5	0.14	3.9
EtOAc	17200	0.24	10	0.24	0.76	EtOAc	17700	0.06	5.4	0.11	1.7
THF	17600	0.35	20	0.18	0.33	THF	17700	0.04	2.5	0.16	3.8
CH <sub>2</sub> Cl <sub>2</sub>	16300	0.33	13	0.25	0.50	CH <sub>2</sub> Cl <sub>2</sub>	16500	0.01	1.4	0.06	7.1
butyronitrile	15600	0.12	7.4	0.16	1.2	butyronitrile	15800	0.01	1.6	0.05	6.1
acetonitrile	14600	0.02	3.5	0.05	2.8	acetonitrile	14500	< 0.01	0.66	0.04	15
DMSO	14600	0.02	2.5	0.07	4.0	DMSO	14700	< 0.01	1.5	0.03	6.8

### 3 Photoinduced Charge Separation and Recombination in Redox Cascades

	$\tilde{\nu}_f / \text{cm}^{-1}$	$\phi_f$	$\tau_f/\text{ns}$	$k_f/10^8 \text{ s}^{-1}$	$k_{nr}/10^8 \text{ s}^{-1}$		$\tilde{\nu}_f / \text{cm}^{-1}$	$\phi_f$	$\tau_f/\text{ns}$	$k_f/10^8 \text{ s}^{-1}$	$k_{nr}/10^8 \text{ s}^{-1}$
<b>8</b>						<b>9</b>					
C <sub>6</sub> C <sub>12</sub>	22900	0.03	3.1	0.09	3.2	C <sub>6</sub> C <sub>12</sub>	23100	0.21	2.7	0.78	2.9
<i>n</i> -hexane <sup>[a]</sup>	23000	0.02	2.1	0.08	4.6	<i>n</i> -hexane	23100	0.17	2.0	0.84	4.2
Me-C <sub>6</sub> H <sub>11</sub>	23100	0.01	1.8	0.08	5.6	Me-C <sub>6</sub> H <sub>11</sub>	23000	0.20	2.7	0.73	3.0
<i>n</i> -Bu <sub>2</sub> O <sup>[a]</sup>	20300	0.01	1.3	0.09	7.4	<i>n</i> -Bu <sub>2</sub> O	20700	0.23	4.0	0.58	1.9
MTBE <sup>[a]</sup>	19400	< 0.01	1.2	0.01	8.7	MTBE	19400	0.17	6.5	0.27	1.3
1,4-dioxane <sup>[a]</sup>	19000	< 0.01	2.2	0.01	4.5	1,4-dioxane	19100	0.25	9.1	0.27	0.83
Et <sub>2</sub> O	18800	< 0.01	2.4	<0.01	4.1	Et <sub>2</sub> O	18400	0.13	6.5	0.21	1.3
EtOAc	17600	< 0.01	1.9	0.02	5.2	EtOAc	17700	0.23	12	0.19	0.64
THF	17900	< 0.01	1.7	<0.01	6.0	THF	17700	0.23	11	0.21	0.70
CH <sub>2</sub> Cl <sub>2</sub>	16100	< 0.01	1.4	0.02	7.0	CH <sub>2</sub> Cl <sub>2</sub>	16400	0.08	4.1	0.19	2.3
butyronitrile						butyronitrile	15600	0.08	8.7	0.10	1.1
acetonitrile						acetonitrile	14800	0.04	6.5	0.05	1.5
DMSO						DMSO	14800	0.06	6.4	0.09	1.5
<b>10</b>											
C <sub>6</sub> C <sub>12</sub>	23200	0.21	3.2	0.65	2.5						
<i>n</i> -hexane	23200	0.13	2.1	0.61	4.2						
Me-C <sub>6</sub> H <sub>11</sub>	23200	0.20	2.9	0.70	2.7						
<i>n</i> -Bu <sub>2</sub> O	20700	0.17	5.2	0.33	1.6						
MTBE	19300	0.19	7.2	0.26	1.1						
1,4-dioxane	19200	0.21	8.1	0.26	0.97						
Et <sub>2</sub> O	18400	0.17	9.4	0.18	0.88						
EtOAc	17800	0.24	16	0.16	0.49						
THF	17800	0.27	15	0.19	0.50						
CH <sub>2</sub> Cl <sub>2</sub>	16400	0.22	17	0.13	0.47						
butyronitrile	15700	0.12	12	0.10	0.73						
acetonitrile	14800	0.04	7.0	0.06	1.4						
DMSO	14800	0.06	7.6	0.08	1.3						

<sup>[a]</sup> biexponentially fitted; quoted values refer to the lifetime with the dominating preexponential factor.

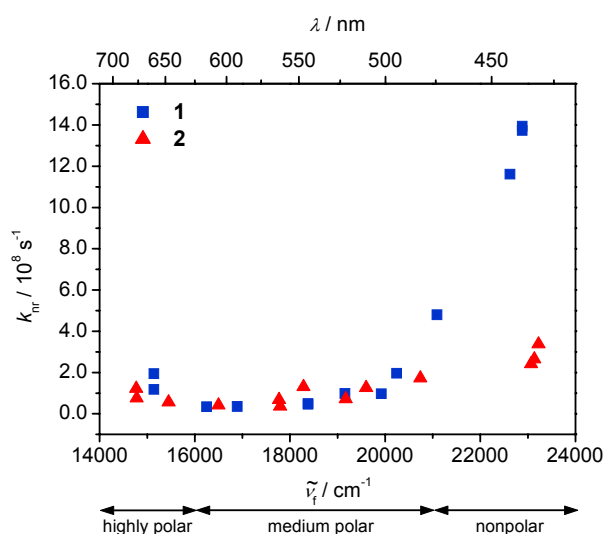


**Figure 3.7** Rate constant of the nonradiative process  $k_{nr}$  vs fluorescence energy  $\tilde{\nu}_f$  for **1** and **2** in different solvents.

The rate constants for radiative deactivation  $k_f$  of cascades **3 – 6** and **8 – 10** exhibit the same trends as the two reference compounds **1** and **2**, respectively (see Figure 3.8a). Again, the cascade **3** without methyl groups attached to the 9-phenylacridine shows a stronger increase of  $k_f$  with fluorescence energy than all other cascades. Due to very strong fluorescence quenching in cascade **8** the rate constants for radiative deactivation  $k_f$  are rather inaccurate. This fact might explain the lower values for  $k_f$  of **8** compared to **4 – 6**, **9**, **10**. As a result of the identical fluorescent subunits in **4 – 6** and **8 – 10** the rate constants for radiative deactivation are expected to be almost constant in a given solvent.

The rate constants for nonradiative deactivation  $k_{nr}$  for cascades **3 – 6** and **8 – 10** in nonpolar up to moderately polar solvents are qualitatively in good agreement with those of their corresponding reference compounds **1** and **2**, respectively. However, in polar solvents a significant increase of  $k_{nr}$  is observed which indicates an additional deactivation pathway. The extent of solvent polarity at which a strong increase of  $k_{nr}$  is observed depends on the donor strength of D2. Cascades **3**, **4**, **6**, and **8** with strong donors show an additional deactivation pathway at fluorescence energies  $\leq 17000 \text{ cm}^{-1}$ . Because of the donors D2 in the cascades **5** and **10** being weaker,  $k_{nr}$  increases at fluorescence energies below  $15000 \text{ cm}^{-1}$ . This means the stronger the donor the less stabilisation by the solvent is necessary in order to promote the additional nonradiative deactivation pathway. This fact confirms our hypothesis that the additional nonradiative deactivation process is a hole transfer from the first excited  $^1\text{CT}$  state to a charge separated (CS) state with the hole

located at the redox centre being farthest away from the acridine. This redox centre is always that with the lowest redox potential. This CS state is strongly stabilised in polar solvents.

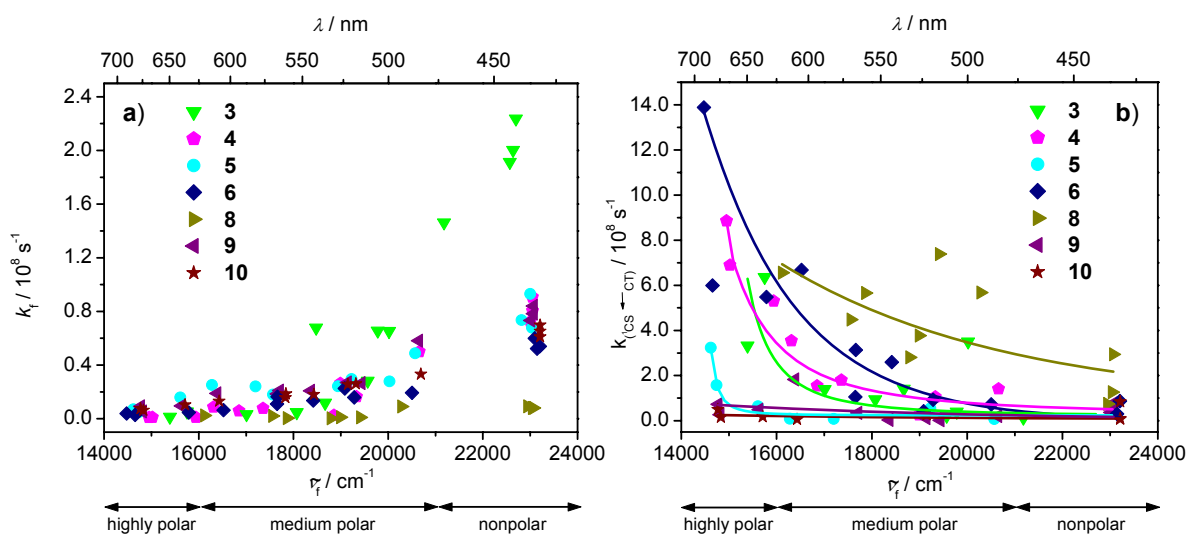


**Figure 3.8** Rate constants vs fluorescence energy  $\tilde{\nu}_f$  of **3 – 6** and **8 – 10** in different solvents: **a)** radiative process  $k_f$ ; **b)** rate constants of the hole transfer process  $k_{(1CT \rightarrow 1CS)}$ . The lines may be used as a rough guide to the eye.

To check the energetics of the additional nonradiative deactivation process we applied the Rehm-Weller equation.<sup>[219]</sup> Although this equation may only serve as a rough estimation for calculating the driving force  $\Delta G_{(1CT \rightarrow 1CS)}^0$  for photoinduced intramolecular hole transfer processes, it substantiates our results. The overall change of the free energy for HT from an excited state generated by photoexcitation with the energy  $\Delta G^{00}$  to a charge separated state can be derived by Equation 3.5 which yields  $\Delta G_{(1CT \rightarrow 1CS)}^0$  in  $\text{kJ} \cdot \text{mol}^{-1}$ .

$$\Delta G_{(1CT \rightarrow 1CS)}^0 = \frac{N_A}{1000} \cdot z \cdot e \cdot (E_{\text{ox}}(D/D^+) - E_{\text{red}}(A/A^-)) - \Delta G_{(S_1 \leftarrow S_0)}^{00} - \frac{N_A \cdot e^2}{1000 \cdot 4\pi\epsilon_0} \left[ \left( \frac{1}{2r_D} + \frac{1}{2r_A} \right) \left( \frac{1}{\epsilon_r} - \frac{1}{\epsilon_s} \right) + \frac{1}{\epsilon_s \cdot d_{DA}} \right] \quad (3.5)$$

The  $\Delta G^{00}$  free energy of the  $S_1 \leftarrow S_0$  transition was determined from the intersection point of the low-energy flank of the absorption band with the high energy flank of the fluorescence band. Because of the same fluorescent subunits we determined the  $\Delta G^{00}$  values for the reference compounds **1** and **2** and used them for the cascades **3** and **4 – 6**, **8 – 10**. The energy gap of the final charge separated state and the ground state corresponds to the redox potential difference of the donor and the acceptor (in Volt). Their potentials were determined by cyclic voltammetry and are given in Table 3.1. Equation 3.5 includes a

Coulomb term which takes into account that the separated charges are extra stabilised by Coulomb attraction. In this term  $r_D$ ,  $r_A$  and  $r_{DA}$  are the radii of the donor and acceptor and the centre to centre distance between them (in Meter), respectively. The Coloumb term also corrects for the difference of solvation energy if cyclic voltammetry is performed in another solvent with permittivity  $\epsilon_s$  than the photophysical excitation ( $\epsilon_r$ ). The values calculated by Equation 3.5 are collected in Table 3.4.

**Table 3.4** Free-energy changes  $\Delta G_{(1CT \rightarrow 1CS)}^0$  of charge separation processes of cascades **3 – 6**, **8** and **9**.

	C <sub>6</sub> H <sub>12</sub>		THF		PhCN		MeCN	
	kJ mol <sup>-1</sup>	eV	kJ mol <sup>-1</sup>	eV	kJ mol <sup>-1</sup>	eV	kJ mol <sup>-1</sup>	eV
<b>3</b>	+ 35	+ 0.36	- 24	- 0.25	- 35	- 0.36	- 33	- 0.34
<b>4</b>	+ 33	+ 0.34	- 21	- 0.22	- 30	- 0.31	- 25	- 0.26
<b>5</b>	+ 43	+ 0.44	- 7.2	- 0.07	- 15	- 0.15	- 9.1	- 0.09
<b>6</b>	+ 50	+ 0.52	- 17	- 0.17	- 29	- 0.30	- 24	- 0.25
<b>8</b>	+ 13	+ 0.14	- 51	- 0.53	- 62	- 0.65	- 57	- 0.59
<b>9</b>	+ 52	+ 0.54	- 13	- 0.13	- 24	- 0.25	- 19	- 0.20
<b>10</b>	+ 53	+ 0.55	+ 2.6	+ 0.03	- 4.9	- 0.05	+ 0.64	+ 0.01

The free-energy changes  $\Delta G_{(1CT \rightarrow 1CS)}^0$  calculated by the Rehm-Weller equation indicate a moderately to strongly exergonic HT process in polar solvents while it is unfavourable in nonpolar solvents.

The rate constant  $k_{(1CT \rightarrow 1CS)}$  for hole transfer from D1 to D2 in cascades **3 – 6** and **8 – 10** (see Table 3.5 and Figure 3.8b) can be estimated from data derived by time resolved fluorescence spectroscopy. The rate constant  $k_{(1CT \rightarrow 1CS)}$  is calculated by the difference between the nonradiative rate constants  $k_{nr}$  of cascades **3 – 10** and their reference compounds:  $k_{(1CT \rightarrow 1CS)} = k_{nr}(\mathbf{3-10}) - k_{nr}(\mathbf{1,2})$ . Compound **1** was used as the reference for cascade **3** and chromophore **2** for cascades **4 – 10**, respectively, in order to match the subunit forming the fluorescent unit as close as possible. In Table 3.5 the missing value for **5** in THF as well as for all other compounds in nonpolar solvents (not shown in Table 3.5) indicate that hole transfer is an unfavourable process because the polarity of the solvent and the donor strength of D2 are too weak to lower the energy of the CS state sufficiently below the energy of the first excited state. Hole migration is a favourable process at a certain degree of solvent polarity and donor strength which is in excellent agreement with foregoing results and interpretations. In Figure 3.8b we plotted  $k_{(1CT \rightarrow 1CS)}$  for each compound in different solvents vs. the fluorescence energy. The rapid increase of  $k_{(1CT \rightarrow 1CS)}$  at low fluorescence

energies for **3** – **6** illustrates the onset of hole transfer. For **9** and **10** there is hardly any HT even at very low energies (polar solvents).

Cascade **5** with a weak donor shows no hole transfer in THF but it does in acetonitrile where  $k_{(1CT \rightarrow 1CS)}$  is about one order of magnitude smaller than that of **6** in the same solvent. The influence of a very strong donor subunit D2 can be studied in **8**. Even in very nonpolar solvents there is a significant HT which increases with increasing solvent polarity to such an extent that fluorescence cannot be detected any more in solvents more polar than dichloromethane. If we were able to determine the corresponding data in polar solvents we would expect the fastest hole transfer reactions for **8** in that regime of polarity.

**Table 3.5** Hole transfer rates  $k_{(1CT \rightarrow 1CS)}$  for compounds **3** – **6** and **8** – **10** from fluorescence lifetime measurements.

	$k_{(1CT \rightarrow 1CS)} = k_{nr}(\text{cascade}) - k_{nr}(\text{reference}) / 10^8 \text{ s}^{-1}$			
	THF	butyronitrile	acetonitrile	DMSO
<b>3</b>	1.41	1.40	6.36	3.32
<b>4</b>	1.54	5.31	6.90	8.86
<b>5</b>	-	0.64	1.58	3.23
<b>6</b>	3.14	5.48	13.9	5.99
<b>8<sup>a)</sup></b>	5.66			
<b>9</b>	0.35	0.49	0.27	0.73
<b>10</b>	0.14	0.17	0.15	0.49

<sup>a)</sup> For compound **8** we were unable to determine  $k_{(1CT \rightarrow 1CS)}$  in solvents more polar than THF because of the fluorescence being too weak.

### 3.2.4.2 Transient Absorption Spectroscopy

The spectra of the charge separated states (CS) of **3** – **10** are expected to show characteristic features of both the spectra of the acridine radical anion and of the radical cation of the strongest donor moiety. Hence, we superposed the spectra of the radical cations of D2 and D3, respectively, obtained by chemical oxidation in  $\text{CH}_2\text{Cl}_2$  with  $\text{SbCl}_5$  with the spectra of the acridine radical anion (see Figure 3.9). The latter spectrum was generated by reduction of 9-(2,6-dimethylphenyl)acridine in THF by spectroelectrochemistry (SEC).

Before discussing the photophysical properties of the cascades it is helpful to have a closer look at the two compounds **1** and **2** serving as reference systems. The transient spectra of these reference systems in benzonitrile are shown in Figure 3.10. The bands of both compounds rise immediately upon photoexcitation within the pulse duration of our experimental setup. Thus, energy transfer processes are not resolved in our experiments. Consequently, we ascribe the changes in the transient spectra to hole transfer processes.

The spectra of **1** are characterised by two bands at about  $15300\text{ cm}^{-1}$  and  $17100\text{ cm}^{-1}$ . The band at higher energy is attributed to the acridine where a negative partial charge is localised. The broad and almost structureless band at lower energy arises from the triarylamine subunit which serves as the donor and, thus, has radical cation character. The transient absorption spectra of chromophore **2** are somewhat different. The two bands are more separated and shifted to lower energy ( $13800\text{ cm}^{-1}$  and  $16300\text{ cm}^{-1}$ ) and the band at higher energy is broader compared to that of **1**. These transient spectra are those of the  $S_1$  states because they decay with the same time constant as the fluorescent states (compare data in Table 3.6 and Table 3.3). Comparison of these two bands in **1** and **2** with those of  $\text{Ac}^-$  (see Figure 9a) and substituted triarylamine radical cations ( $\tilde{\nu}_{\text{max}}$  is typically  $13000\text{ cm}^{-1}$ )<sup>[49]</sup> shows that the  $^1\text{CT}$  character of the  $S_1$  state is much more pronounced in **2** than in **1** due to the orthogonal decoupled arrangement of acceptor and donor in the former chromophore.

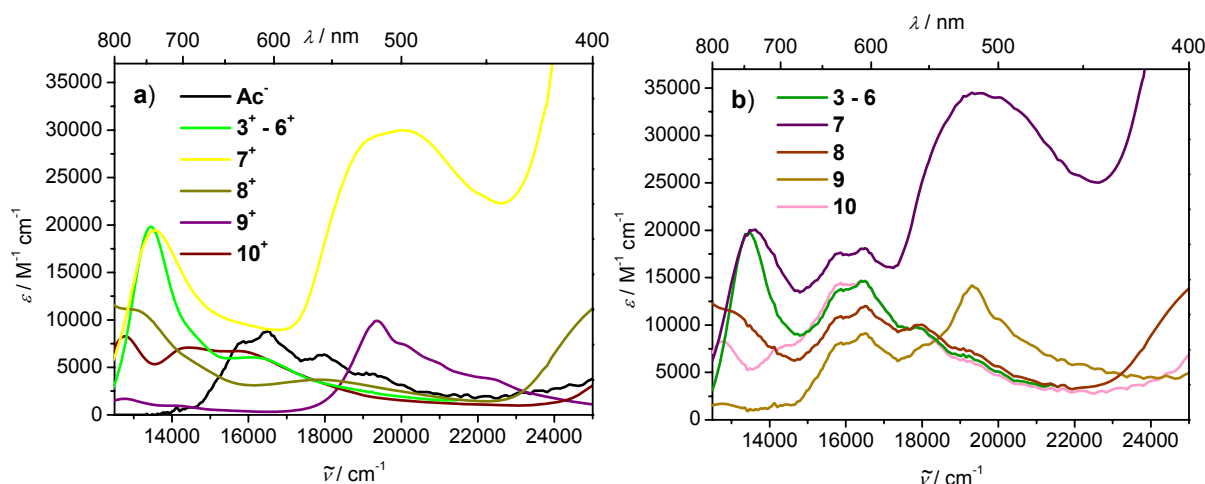


**Figure 3.9** a) Absorption spectra of the acridine radical anion obtained by SEC in THF and of the spectra of the radical cations of different donor moieties obtained by chemical oxidation. b) Superposition of the stationary absorption spectra of  $\text{Ac}^-$  radical anion and the radical cations of the corresponding donor subunits. For  $3^+ - 6^+$  the spectra are so similar that we display that of  $4^+$  only.

Besides the above mentioned transient absorptions there is a second absorption at  $\sim 22000\text{ cm}^{-1}$  for **1** (the maximum of this absorption is shifted to lower energy because of overlap with a negative signal due to ground state bleaching at ca.  $25000\text{ cm}^{-1}$ ) and at  $\sim 22500\text{ cm}^{-1}$  for **2**. These signals at  $\sim 22000 / 22500\text{ cm}^{-1}$  decay with time constants of ca.  $3 - 40\ \mu\text{s}$  depending on the solvent. In agreement with literature values these absorptions are ascribed to an acridine localised  $^3(\pi, \pi^*)$  triplet state which is the lowest triplet state in donor substituted acridines.<sup>[109]</sup> Isosbestic points at  $21900\text{ cm}^{-1}$  in **1** and  $21000\text{ cm}^{-1}$  in **2** indicate that the triplet states are directly formed from the  $^3\text{CT}$  states in **1** and **2**. One can safely assume that **1** and **2** have both similar excited  $^3\text{CT}$  state and triplet state absorption

coefficients. If one takes into account that the triplet-triplet absorption signal of **1** at ca.  $22000\text{ cm}^{-1}$  is more weakened by the overlap with ground state bleaching from the  $^1\text{CT}$  state than it is in **2** (the  $^1\text{CT}$  band at ca.  $25000\text{ cm}^{-1}$  in **1** is ca. three times more intense than that of **2**, see Figure 3.2) one can follow from the ratio of the triplet state absorption signals of **1** : **2** ( $\sim 1 : 3$ ) that the ISC rate are similar for both **1** and **2**. This is in agreement with the conclusions drawn from the fluorescence lifetime measurements but contrasts the findings that orthogonal structures should enhance ISC due to spin-orbit coupling.<sup>[109, 216]</sup>

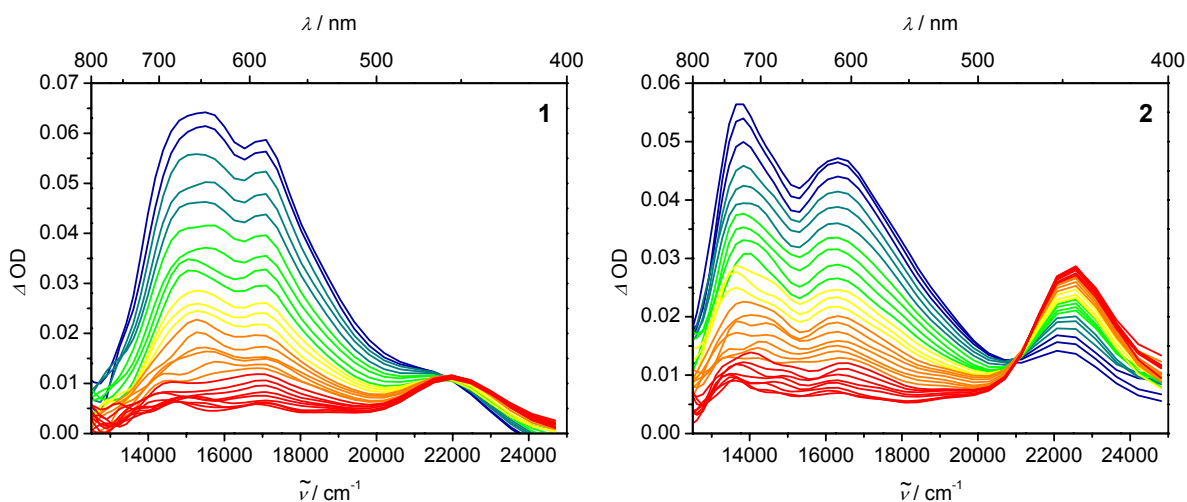


**Figure 3.10** Transient absorption spectra of compounds **1** and **2** in benzonitrile after photoexcitation at  $24000\text{ cm}^{-1}$ . Early spectra are shown in blue/green and late spectra are shown in orange/red colours.

Photoexcitation of cascades **3** – **6** leads within the rise time of our experimental setup to the spectra of the charge separated states (see Figure 3.11). As we expected from the superposition of the spectra of radical cations and anion, respectively (see Figure 3.9b), the spectra of the CS states consist of a broad and intense band at  $13500\text{ cm}^{-1}$  for compounds **3**, **4** and **6** arising from the radical cation of the triarylamine donor D2 (D3 in **6**). For compound **5** this band is somewhat broader and shifted to higher energies at  $16400\text{ cm}^{-1}$  because of the small variation of triarylamine substituents (OMe  $\rightarrow$  Me). Although the transient spectra of cascade **5** resemble qualitatively those of **2**, they represent the CS and not the  $^1\text{CT}$  state. This fact is substantiated by fluorescence quenching measurements and a significant hypsochromic shift of the absorption band referring to the radical cation in the transient spectra of compound **5**. In addition, for **3** – **6** there is a structured band at  $16400\text{ cm}^{-1}$  with more or less pronounced shoulders at  $17800\text{ cm}^{-1}$  and  $19100\text{ cm}^{-1}$ . These bands are associated with the radical anion of the acridine acceptor. Both bands at ca.  $14000\text{ cm}^{-1}$  and  $16000 - 20000\text{ cm}^{-1}$  decline with the same time constant which indicates that they originate from the same state.



### 3 Photoinduced Charge Separation and Recombination in Redox Cascades

**Table 3.6** Lifetime ( $\tau_{\text{CS}\rightarrow\text{T}}$ ) and rate constants ( $k_{\text{CS}\rightarrow\text{T}}$ ) of the charge separated state and of the triplet state ( $\tau_{\text{T}\rightarrow\text{S}_0}$ ,  $k_{\text{T}\rightarrow\text{S}_0}$ )

	THF		benzonitrile		acetonitrile	
	$\tau_{\text{CS}\rightarrow\text{T}}/\text{ns}$ ( $k_{\text{CS}\rightarrow\text{T}}/10^7 \text{ s}^{-1}$ )	$\tau_{\text{T}\rightarrow\text{S}_0}/\mu\text{s}$ ( $k_{\text{T}\rightarrow\text{S}_0}/10^4 \text{ s}^{-1}$ )	$\tau_{\text{CS}\rightarrow\text{T}}/\text{ns}$ ( $k_{\text{CS}\rightarrow\text{T}}/10^7 \text{ s}^{-1}$ )	$\tau_{\text{T}\rightarrow\text{S}_0}/\mu\text{s}$ ( $k_{\text{T}\rightarrow\text{S}_0}/10^4 \text{ s}^{-1}$ )	$\tau_{\text{CS}\rightarrow\text{T}}/\text{ns}$ ( $k_{\text{CS}\rightarrow\text{T}}/10^7 \text{ s}^{-1}$ )	$\tau_{\text{T}\rightarrow\text{S}_0}/\mu\text{s}$ ( $k_{\text{T}\rightarrow\text{S}_0}/10^4 \text{ s}^{-1}$ )
<b>1</b>	11 <sup>1)</sup> (4.4) <sup>2)</sup>	3.2 (32)	17 <sup>1)</sup>	38 (2.7)	5.0 <sup>1)</sup> (2.5) <sup>2)</sup>	9.3 (11)
<b>2</b>	21 <sup>1)</sup> (3.6) <sup>2)</sup>	3.9 (25)	26 <sup>1)</sup>	20 (5.0)	4.6 <sup>1)</sup> (12) <sup>2)</sup>	9.7 (10)
<b>3</b>	9.8 (10)	10 (9.6)	11 (9.3)	– <sup>3)</sup>	< 1.00 (> 100)	1.1 (88)
<b>4</b>	13 (7.8)	3.0 (34)	12 (8.6)	22 (4.5)	2.2 (47)	0.52 (190)
<b>5</b>	21 <sup>1)</sup>	13 (7.8)	43 (2.3)	16 (6.1)	9.0 (11)	1.6 (63)
<b>6</b>	8.2 (12)	5.0 (20)	13 (7.6)	16 (6.3)	5.1 (20)	3.0 (34)
<b>7</b>	13 (7.6)	11 (9.0)	22 (4.5)	28 (3.6)	5.3 (19)	9.6 (10)
<b>8</b>	17 (5.9)	6.9 (15)	21 (4.8)	6.7 (15)	2.6 (38)	– <sup>4)</sup>
<b>9</b>	11 <sup>1)</sup>	6.2 (16)	23 (4.3)	56 (1.8)	6.5 <sup>1)</sup>	38 (2.6)
<b>10</b>	22 (4.7)	11 (8.9)	27 (3.7)	26 (3.8)	6.2 <sup>1)</sup>	7.5 (13)

<sup>1)</sup> Lifetime of <sup>1</sup>CT state <sup>2)</sup> rate constant for <sup>3</sup>CT → T process from time resolved fluorescence measurements if one assumes that  $k_{\text{nr}} = k_{\text{CS}\rightarrow\text{T}}$ ; <sup>3)</sup> formation of triplet was observed, but intensity was too low to be measured; <sup>4)</sup> owing to low solubility the signal to noise ratio was not sufficient to measure the lifetime of the triplet state.

The transient absorption spectra of compounds **7** – **10** are shown in Figure 3.12. Chromophore **7** is a cascade which comprises three donor subunits similar to compound **6**. However, the two terminal redox centres D2 and D3 are connected by a rigid triple bond. As we have reported recently this type of bridge also influences the spectral characteristics of the CS state: the corresponding spectra consists of an additional intense band at about 20000 cm<sup>-1</sup> which is assigned to the positively charged tolandiamine bridge.<sup>[16]</sup>

The terminal donor D2 of cascade **8** is the strongest one used in this series of compounds reported in this paper. Based on structural similarity of this donor subunit to those of chromophores **3** – **7**, its spectral response is also very similar. The band assigned to the radical cation of D2 is shifted to lower energy (13300 cm<sup>-1</sup>) whereas the band of the acridine radical anion remains nearly constant.

Both in acetonitrile and THF the spectra of chromophore **9** correspond to the first excited <sup>1</sup>CT state. In contrast to results derived from fluorescence measurements no hole transfer was detectable in these solvents. In fact the rate constants for hole transfer  $k_{\text{CT}\rightarrow\text{CS}}$  (see Table 3.5) are relatively small. From fluorescence measurements the fastest hole transfer process is seen in benzonitrile and in fact, this is the only solvent for which a CS state could be monitored. Thus, in different solvents other deactivation processes might be faster than HT from the <sup>1</sup>CT to the <sup>1</sup>CS state and compete quite successfully with HT. Slow HT is also confirmed by transient absorption spectroscopy. In benzonitrile the CS as well as the <sup>1</sup>CT state were observed. Time decays in PhCN at characteristic energies are illustrated in Figure 3.13. It is obvious that the band attributed to the <sup>1</sup>CT state at 13500 cm<sup>-1</sup> decays rapidly whereas the band at 19100 cm<sup>-1</sup> which is ascribed to the phenothiazine radical cation (see Figure 3.9a) rises with some delay. The absorption band assigned to the acridine

radical anion (at  $16300\text{ cm}^{-1}$ ) shows a biexponential decay with decay times of both the first excited (12 ns) and the CS state (23 ns), because its anion character is part of both states.

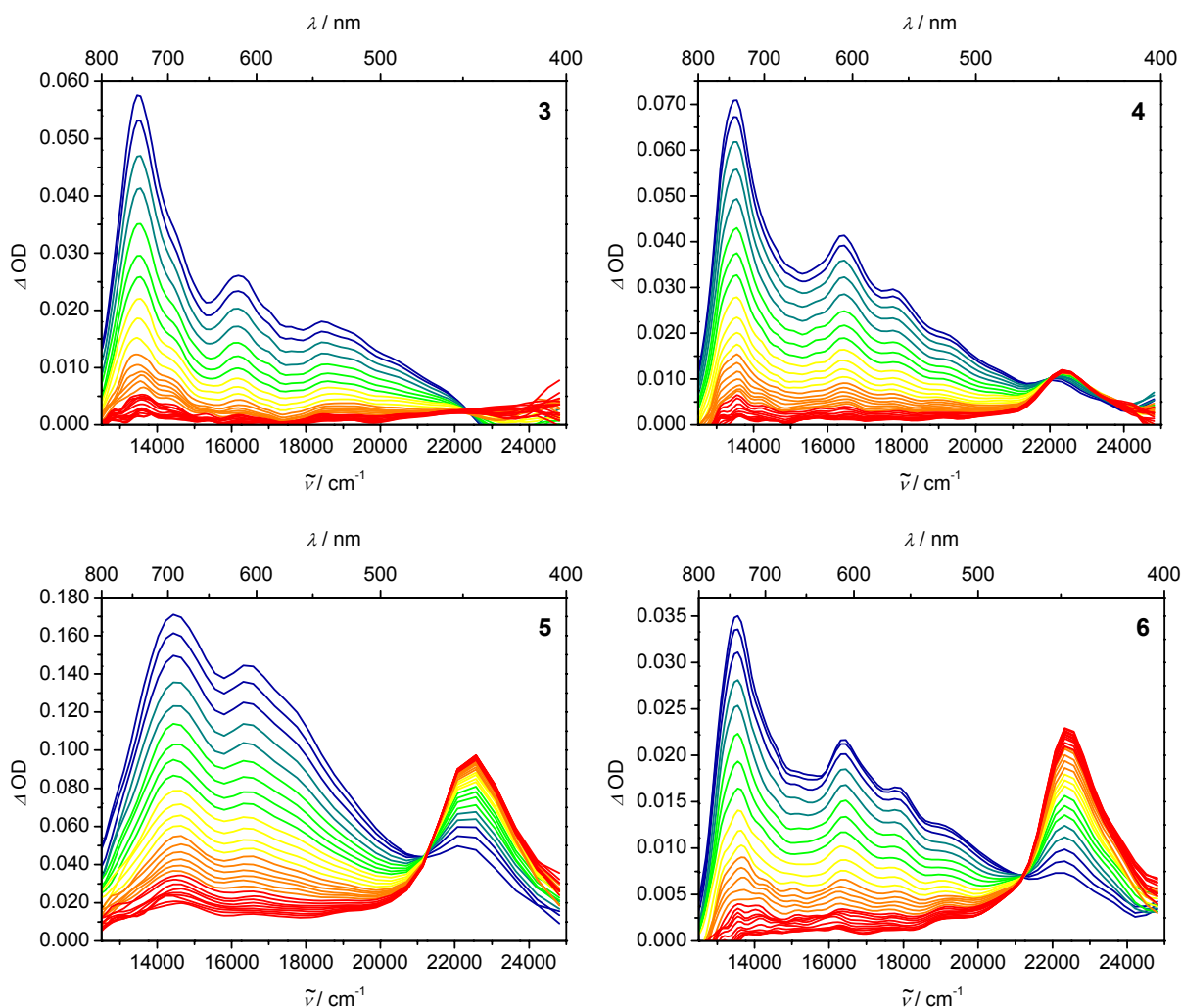


**Figure 3.11** Transient absorption spectra of compounds **3** – **6** in benzonitrile (photoexcitation:  $24000\text{ cm}^{-1}$ ). Early spectra are shown in blue/green and late spectra are shown in orange/red colours.

According to Figure 3.9b the CS state of cascade **10** should show two absorption bands at ca.  $12800\text{ cm}^{-1}$  and  $16000\text{ cm}^{-1}$ . In acetonitrile no CS state was monitored but only the  $^1\text{CT}$  state which matches those of the reference compound **2** very well. In addition this  $^1\text{CT}$  state has the same decay time as the fluorescent state. The transient absorption spectra in benzonitrile are spectrally similar to the ones in acetonitrile. However, the decay times in benzonitrile do not match those of the fluorescence lifetime. The oxidation potentials derived from cyclic voltammetry (see Table 3.1) indicate that the donor D2 is only slightly stronger than D1. Thus, the CT and the CS states have almost the same energy so that an equilibration of these excited states has to be taken into account. This might result in a spectral superposition of both states with various contributions which could not be resolved

because the decay profiles could be fitted by a single exponent. In THF however, the spectral features agree very well with those of Figure 3.9b which points towards the formation of a CS state whose decay time is somewhat longer than the fluorescence lifetime of the  $^1\text{CT}$  state. The fact that the CS state was observed in THF and not in the more polar solvent acetonitrile is unexpected. However, the free-energy changes  $\Delta G_{(1\text{CT} \rightarrow 1\text{CS})}^0$  (see Table 3.4) are very small and slightly endergonic in both solvents. This fact indicates that the CT and the CS state are energetically quite similar. Considering the rate constants  $k_{(1\text{CT} \rightarrow 1\text{CS})}$  for the hole transfer process (see Table 3.5) it is obvious that for cascade **10** the population of the  $^1\text{CS}$  state is relatively slow. Thus, other competitive deactivation processes have to be taken into account which might prevent the formation of the  $^1\text{CS}$  state although this is a thermodynamically favourable process in PhCN.

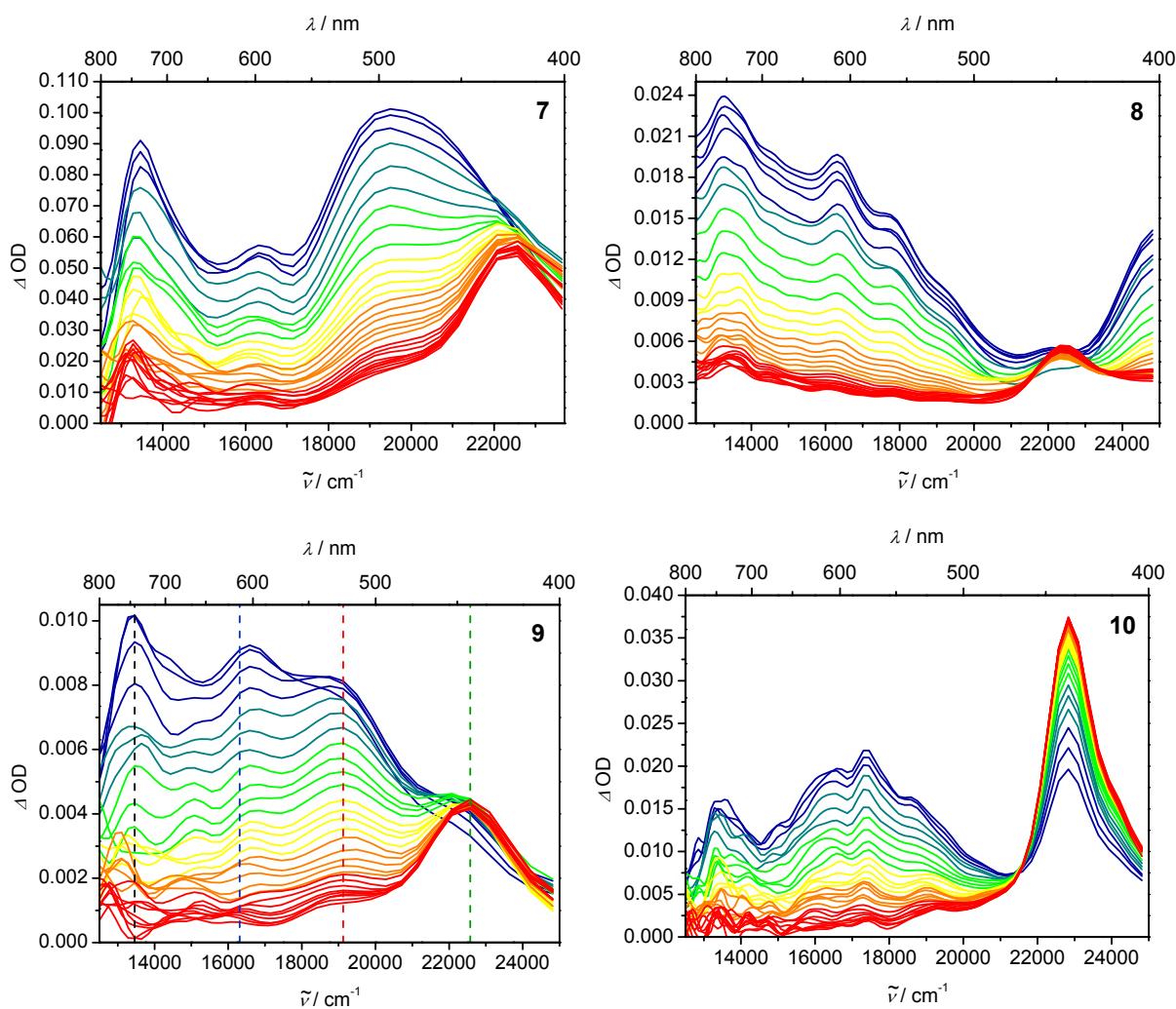


**Figure 3.12** Transient absorption spectra of compounds **7** – **9** in benzonitrile (photoexcitation: **7**, **8**:  $24000\text{ cm}^{-1}$ , **9**:  $28200\text{ cm}^{-1}$ ) and of **10** in THF (photoexcitation:  $24000\text{ cm}^{-1}$ ). Early spectra are shown in blue/green and late spectra are shown in orange/red colours.

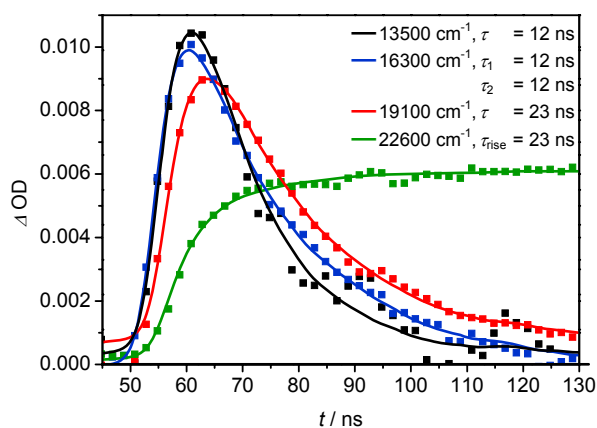


**Figure 3.13** Time dependent absorption measurements (data points) of **9** and fits (line) at characteristic energies: triarylamine cation, acridine anion, phenothiazine cation and triplet of acridine.

The decay times of all CS states of cascades **3** – **10** match very well with the corresponding rise times of a new state, which is characterised by a sharp band at about  $22700\text{ cm}^{-1}$ . In **3** this band overlaps with strong ground state bleaching. As in **1** and **2** this band is attributed to a locally excited  $^3(\pi, \pi^*)$  triplet state of the acridine moiety. Its triplet character is proved by quenching experiments with oxygen and  $\beta$ -carotene and a lifetime of several  $\mu\text{s}$  which is typical of excited triplet states. The identity of the decay time of the CS state with the rise time of the triplet state in addition to an isosbestic point at ca.  $21500\text{ cm}^{-1}$  suggests that the CS state is quenched by population of the triplet state, possibly via a  $^3\text{CS}$  state (see Figure 3.16) which cannot be distinguished spectroscopically from a  $^1\text{CS}$  state with our methods. In the CS state the charges are well separated due to large distances. Conversion of the  $^1\text{CS}$  into the  $^3\text{CS}$  state should be extremely fast because singlet-triplet splitting decreases exponentially with increasing distance of the radical centres. Consequently, these two excited states are expected to be almost degenerated. Due to the small  $S_1$ - $T_1$  splitting the hyperfine interaction of the unpaired electrons with the nuclear magnetic spins (a local effect independent of the distance of the radical centres) becomes the dominant mechanism for the ISC process  $^1\text{CS} \rightarrow ^3\text{CS}$ .<sup>[220]</sup> The alternative direct ISC from  $^1\text{CS}$  to T would be promoted by spin-orbit coupling induced by the orthogonal orientation of spin bearing donor and acceptor groups. However, this process is unlikely because of the large distance of the spin bearing units which prevents spin-orbit coupling.

The energy of the locally excited  $^3(\pi, \pi^*)$  triplet state of 4-(9-acridyl)-*N,N*-dimethylaniline is reported to be  $E_T = 1.91\text{ eV}$ .<sup>[109]</sup> The energies of all the CS states can be estimated by the Rehm-Weller equation (Eq. 3.5:  $\Delta G_{^1\text{CS}}^0 = \Delta G_{(^1\text{CT} \rightarrow ^1\text{CS})}^0 + \Delta G_{(S_1 \leftarrow S_0)}^{00} - \Delta G_T^0$ ) which yields values between 1.9 and 2.6 eV depending on the cascade and the solvent. Thus, triplet formation from the  $^3\text{CS}$  state is thermodynamically favourable in all cases which

is additionally substantiated by observing the characteristic absorption band in all transient absorption spectra. In contrast, the triarylamine triplet state is too high to be populated ( $E_T = 3.01$  eV).<sup>[221]</sup> Conversion of a CS into a low-lying triplet state is a well-known deactivation pathway<sup>[91, 222]</sup>, although in some cases it seems possible to generate long-lived excited singlet states without the population of the corresponding lower lying triplet states.<sup>[223-225]</sup> In the following we discuss the charge transfer mechanisms in the triplet manifold because we assume that  ${}^3\text{CS} \rightleftharpoons {}^1\text{CS}$  ISC is fast and that back hole transfer to the acridine localised triplet state proceeds rapidly via other triplet states.

The driving force dependence of the hole transfer rate constants  $k_{({}^3\text{CS} \rightarrow \text{T})}$  of cascades **3**, **4**, **5** and **8** for the process  ${}^3\text{CS} \rightarrow \text{T}$  in different solvents is shown in Figure 3.14. The total reorganisation energies of the cascades are between 1.0 and 1.5 eV depending on the solvent and the cascade. The reorganisation energy was calculated by summing up the inner ( $\lambda_i$ ) and outer ( $\lambda_o$ ) reorganisation energies.  $\lambda_i$  was determined by Jortner fits of the fluorescence bands of compound **2** in different solvents.<sup>[16]</sup>  $\lambda_i$  was considered to be almost constant for all chromophores. The outer reorganisation energy was calculated by the Born equation.<sup>[17]</sup> The driving force for the formation of the acridine triplet state ( $< 0.6$  eV) is smaller than the total reorganisation energy and that for the deactivation from the acridine triplet to the ground state (1.91 eV). Hence, the back hole transfer from the  ${}^3\text{CS}$  to the triplet state is located in the Marcus normal region or, at best, at top of a Marcus parabola.

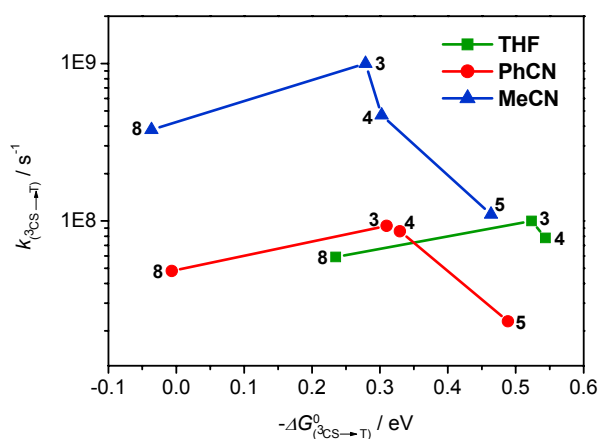


**Figure 3.14** Driving force ( $-\Delta G_{({}^3\text{CS} \rightarrow \text{T})}^0$ ) dependence of intramolecular back hole transfer rate constants ( $k_{({}^3\text{CS} \rightarrow \text{T})}$ ) for the process  ${}^3\text{CS} \rightarrow \text{T}$  in different solvents.

The data shown in Figure 3.14 obviously do not follow a simple Marcus parabola. While this might be due to the limited range of free energy and to possibly large data errors the trends for different solvents are so similar that it appears unlikely that the data are

erroneous. Therefore we consider two independent charge recombination mechanisms: a superexchange and a hopping mechanism.<sup>[226-231]</sup> Generally, the total rate constant  $k_{(^3\text{CS} \rightarrow \text{T})}$  is the sum of both mechanisms but in certain  $\Delta G_{(^3\text{CS} \rightarrow \text{T})}^0$  regimes one mechanism might be dominant (see Figure 3.15). In the case of an incoherent hopping mechanism charge recombination proceeds via two steps in which the energetically higher  $^3\text{CT}$  state is involved. The total rate constant  $k_{\text{hop}}$  is calculated by Equation 3.6 where each sequential rate constant ( $k_{(^3\text{CT} \leftarrow ^3\text{CS})}$ ,  $k_{(^3\text{CT} \rightarrow ^3\text{CS})}$  and  $k_{(^3\text{CT} \rightarrow \text{T})}$ ) is given by the Marcus equation 3.7:

$$k_{\text{hop}} = \frac{k_{(^3\text{CT} \leftarrow ^3\text{CS})} \cdot k_{(^3\text{CT} \rightarrow \text{T})}}{k_{(^3\text{CT} \rightarrow ^3\text{CS})} + k_{(^3\text{CT} \rightarrow \text{T})}} \quad (3.6)$$

$$k = 4\pi^2 hc^2 V^2 \sqrt{\frac{1}{4\pi\hbar c \lambda_o kT}} \exp\left[-\frac{\hbar c (\lambda_o + \lambda_i + \Delta G^0)^2}{4\lambda_o kT}\right] \quad (3.7)$$

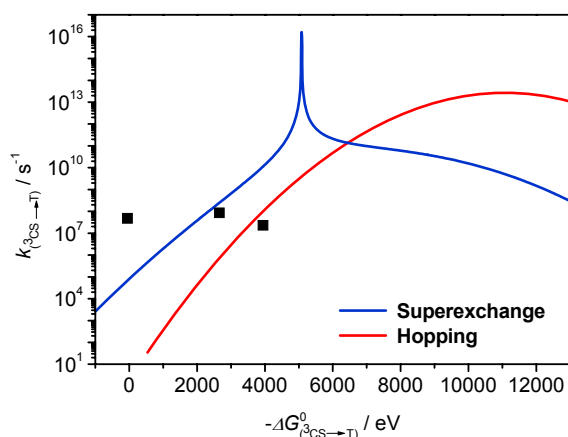
Hereafter, all calculated values refer to PhCN as the solvent. The estimated electronic couplings are  $V_{(^3\text{CT} \rightarrow ^3\text{CS})} = V_{(^3\text{CT} \leftarrow ^3\text{CS})} \approx 90 \text{ cm}^{-1}$  (see Introduction) and  $V_{(^3\text{CT} \rightarrow \text{T})} = 480 \text{ cm}^{-1}$ .<sup>[108]</sup> The free energy change  $\Delta G_{(^3\text{CS} \rightarrow \text{T})}^0$  is the difference between the energy of the  $\Delta G^{00}$  transition (see Equation 3.5) and of the localised excited triplet state and was calculated to be  $5080 \text{ cm}^{-1}$ . The inner reorganisation energy ( $\lambda_i$ ) for the process  $^3\text{CT} \rightarrow \text{T}$  is approximated by that of  $^1\text{CT} \rightarrow \text{S}_0$  process which was determined by Jortner fits of the fluorescence bands which yields  $1350 \text{ cm}^{-1}$ . The  $\lambda_i$  value for  $^3\text{CT} \leftarrow ^3\text{CS}$  and  $^3\text{CT} \rightarrow ^3\text{CS}$  should be slightly smaller than that for the charge recombination process  $^3\text{CT} \rightarrow \text{T}$  and was estimated to be  $1000 \text{ cm}^{-1}$ . The outer reorganisation energy for  $^3\text{CT} \leftarrow ^3\text{CS}$  and  $^3\text{CT} \rightarrow ^3\text{CS}$  is the difference between the total reorganisation energy (which corresponds to the energy at the IVCT band maximum<sup>[195]</sup> of  $\mathbf{11}^*$ ) and the inner reorganisation energy (see above) which yields  $5000 \text{ cm}^{-1}$ . The outer reorganisation energy for the charge recombination process  $^3\text{CT} \rightarrow \text{T}$  was estimated to be  $4700 \text{ cm}^{-1}$  by the help of Jortner fits of the fluorescence bands (see above).

The rate constant  $k_{(^3\text{CS} \rightarrow \text{T})}$  for the superexchange mechanism was also calculated by Equation 3.7. Although in this case hole transfer proceeds in one coherent step from the  $^3\text{CS}$  to the acridine localised triplet state, the higher lying  $^3\text{CT}$  state influences the electronic coupling  $V_{(^3\text{CS} \rightarrow \text{T})}$  according to the McConnell model, Equation 3.8:<sup>[31]</sup>

$$V_{({}^3\text{CS}\rightarrow\text{T})} = \frac{V_{({}^3\text{CT}\leftarrow{}^3\text{CS})} \cdot V_{({}^3\text{CT}\rightarrow\text{T})}}{\Delta G_{({}^3\text{CT}\leftarrow{}^3\text{CS})}^0} \quad \text{with} \quad \Delta G_{({}^3\text{CT}\leftarrow{}^3\text{CS})}^0 = \Delta G_{{}^3\text{CT}}^0 - \Delta G_{\text{T}}^0 - \Delta G_{({}^3\text{CS}\rightarrow\text{T})}^0 \quad (3.8)$$

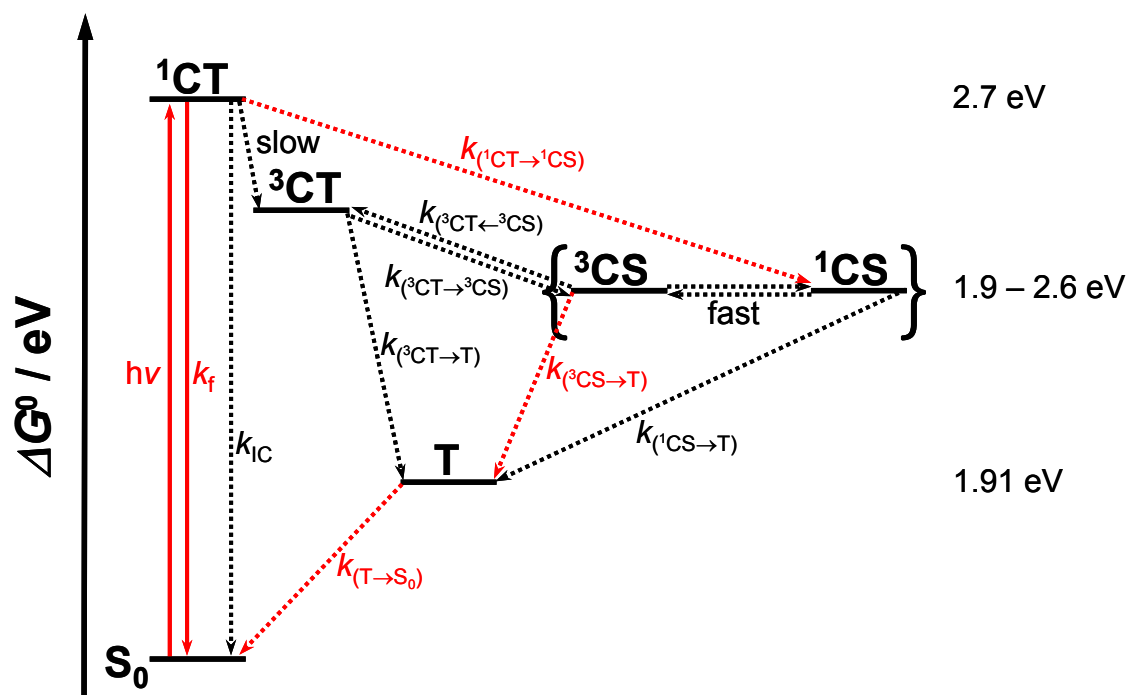
The values for the electronic couplings and the free energy change are the same as in case of the hopping mechanism. The inner reorganisation energy was estimated to be  $1350 \text{ cm}^{-1}$  as it is for  ${}^3\text{CT} \rightarrow \text{T}$  because in both mechanisms charges recombine. The outer reorganisation energy was estimated by the Born equation which yields  $7200 \text{ cm}^{-1}$ .

Figure 3.15 shows the hopping and the superexchange rates vs  $\Delta G_{({}^3\text{CS}\rightarrow\text{T})}^0$  calculated with the values given above together with the experimental rate constants  $k_{({}^3\text{CS}\rightarrow\text{T})}$  for **4**, **5** and **8** in PhCN. While the rate constants are relatively accurate the  $\Delta G_{({}^3\text{CS}\rightarrow\text{T})}^0$  free energies involve major errors so that the position of the experimental data points on the x-axis is quite vague. From Figure 3.15 it is obvious that both the superexchange and the hopping rate constants display a parabola behaviour. While the hopping mechanism dominates in the inverted region, superexchange prevails in the normal region where the experimental data points are located. For the superexchange there is a peak at  $\Delta G_{({}^3\text{CS}\rightarrow\text{T})}^0 = \Delta G_{{}^3\text{CT}}^0 - \Delta G_{\text{T}}^0$  where resonance with the  ${}^3\text{CT}$  state occurs (see Equations 3.7 and 3.8). Taking this peak into account and the fact that the horizontal position of the experimental data points might be erroneous a correlation quite different from a simple Marcus parabola is well possible. Although we have no definite proof, Figure 3.15 suggests that charge recombination in the cascades is located in the Marcus normal region and proceeds via a superexchange mechanism near to the energy where resonance with the intermediate virtual  ${}^3\text{CT}$  state occurs.



**Figure 3.15** Plot of calculated **superexchange** and **hopping** rate constants for charge recombination of cascades **4**, **5** and **8** in PhCN and the corresponding experimental data points.

Extension of the cascades up to three donor subunits in **6** and **7** results only in a moderately longer lifetime of the CS states in the polar solvents PhCN and MeCN compared to cascade **4**. The lifetimes of the CS states of **7** are slightly extended compared to **6** in all solvents. In **7** D2 and D3 are connected by a conjugated rigid triple bond whereas these subunits are separated by a saturated bridge in cascade **6**. Despite the larger donor acceptor separation the lifetimes of the  $^3\text{CS}$  state of **6** are quite similar to those of **4**. Transient spectra of **6** (cf Figure 3.11, **6** vs **4**) unequivocally prove that it is the terminal triarylamine donor D3 which is oxidised and not possibly D2. Because hopping mechanism generally prevails over superexchange at long charge transfer distances this might be the reason for the similar charge recombination in **6** compared to **4**. Another explanation, however, is the increased conformational flexibility of **6** which might lead to a conformer in which the terminal triarylamine is bent back to the acridine. This leads to a shorter through space charge transfer distance which might become the dominating mechanism if assisted by solvent molecules bridging donor and acceptor.<sup>[232, 233]</sup>



**Figure 3.16** State diagram for cascades **3 – 5** and **8 – 10** with two donor subunits. The processes which are manifested by experimental data are given in red.



**Table 3.7** Comparison of rate constants  $k_{(1CT \rightarrow 1CS)}$  and lifetimes of charge separated states  $\tau_{CR}$  of **3** with **O** and **P** in different solvents.

	$k_{(1CT \rightarrow 1CS)} / 10^8 \text{ s}^{-1}$			$\tau_{CR} / \text{ns}$	
	THF	benzonitrile	acetonitrile	benzonitrile	acetonitrile
<b>3</b>	1.41		6.36	11	< 1.0
<b>O</b>	1.7	330	3100	0.18	0.022
<b>P</b>	0.71	40	500	> 2	0.41

It is noteworthy that the lifetimes of the  $^3\text{CS}$  states of cascades **4** (in THF and PhCN), **6** (in THF and PhCN), **7** (in THF) and **8** (in MeCN) are significantly shorter than the lifetime of the  $^1\text{CT}$  state of their reference compound **2**. In these cascades hole transfer from the  $^1\text{CT}$  to the  $^1\text{CS}$  states is generally very efficient concerning rate and quantum yield. The primarily formed  $^1\text{CS}$  state transforms rapidly into a  $^3\text{CS}$  state promoted by hyperfine interactions (see above). The latter relaxes by a spin-allowed back hole transfer to the T state which we assume is the rate determining step. Obviously, this sequence of processes is faster than direct spin-orbit induced ISC from the  $^1\text{CT}$  to the energetically lowered  $^3\text{CT}$  state and subsequent spin-allowed deactivation to the locally excited triplet state<sup>[109]</sup> which is the predominant nonradiative deactivation pathway in **1** and **2**. E.g. for **4** in THF (MeCN) the rate constant  $k_{(3CS \rightarrow T)}$  is  $7.8 \cdot 10^7 \text{ s}^{-1}$  ( $47 \cdot 10^7 \text{ s}^{-1}$ ) whereas for **2** the rate constant  $k_{(1CS \rightarrow T)}$  is significantly smaller  $3.6 \cdot 10^7 \text{ s}^{-1}$  ( $12 \cdot 10^7 \text{ s}^{-1}$ ). Hence, the population of the localised excited triplet state T via the  $^1\text{CS}$  and the  $^3\text{CS}$  states is accelerated compared to its direct formation via the spin-forbidden ISC process of in **1** and **2**.

A comparison of cascade **3** with cascade **O** who have both two triarylamine donors with identical substituents demonstrates the consequences of different spacers separating the donor subunits: in case of **O** HT ( $k_{(1CT \rightarrow 1CS)}$ ) from D1 to D2 is consistently faster particularly in MeCN because its redox centres are connected by conjugated triple bond (see Table 3.7). In MeCN the saturated bridge in **3** slows down the HT by a factor of almost 500 because of a smaller electronic coupling  $V$  between the two states in which the hole is localised at either triarylamine. In standard diabatic ET theory the ET rate depends on  $V^2$  (see Equation 3.7). From the electronic couplings for a bis-triarylamine radical cation connected by a triple bond ( $V = 1200 \text{ cm}^{-1}$ )<sup>[195, 196]</sup> or a methylene/ethylene bridge ( $V = 90 \text{ cm}^{-1}$ ) (see Introduction) one can estimate a rate acceleration by  $1200^2 / 90^2 = 178$  which is in reasonable agreement with the factor of 500 mentioned above.

As already explained above charge recombination in **3** takes place in the normal Marcus region and is ascribed to the formation of a localised excited triplet state via  $^3\text{CS} \rightarrow \text{T}$ . Although charge recombination in **O** is located in the Marcus inverted region because it is attributed to the process  $^1\text{CS} \rightarrow \text{S}_0$  the lifetime of the CS state of **3** is prolonged up to a factor of 60 due to the weaker electronic coupling between CS and T state provided by the

saturated spacers. Owing to the twisted donor acceptor geometry in **4** compared to **3** an even weaker electronic coupling in **4** leads to slightly increased  $^3\text{CS}$  lifetimes. Unlike cascade **P** whose back hole transfer in e.g. MeCN is by a factor of 20 slower than that of **O** due to the larger donor acceptor separation, the CS lifetime of cascade **6** is only twice as long as that of **4** in MeCN and is even slightly shorter in THF.

From the fact that we do not observe any  $^1\text{CS} \rightarrow \text{S}_0$  process in our transient absorption experiments in all cascades we conclude that these processes are at least 10 fold slower than the rate constants for the process  $^3\text{CS} \rightarrow \text{T}$ . Thus, if the  $^3\text{CS}$  state of our cascades were below the acridine localised excited triplet state, and consequently, the triplet state no longer could act as an energy sink we expect the lifetimes of the  $^3\text{CS}$  states to be in the order of 100 ns up to several  $\mu\text{s}$ .

### 3.3 Conclusion

In this paper we investigated the photophysical properties of a series of redox cascades. The data derived by stationary and time resolved fluorescence measurements (see Table 3.3) show that the influence of perpendicular orientation of the donor and acceptor on the electronic nature of the first excited state in the reference chromophores **1** and **2** is pronounced. Because the corresponding subunits are much stronger twisted in **2**, the transition moments for absorption and fluorescence processes are much smaller. On the other hand, the degree of charge separation is higher in **2** compared to **1**.

Fluorescence and transient absorption measurements of the cascades **3 – 10** substantiated that HT ( $^1\text{CT} \rightarrow ^1\text{CS}$ ) depends strongly on solvent polarity as well as on oxidation potentials of the donor moieties. The corresponding CS state is stabilised by strong donors and highly polar solvents, respectively. HT was only observed in cases where the  $^1\text{CS}$  state is below the first excited  $^1\text{CT}$  state. HT is a nonradiative deactivation pathway which leads to fluorescence quenching and to the formation of the corresponding CS state as was verified by transient absorption measurements. No HT is observed if the terminal donor is too weak or the solvent is not polar enough. Our transient absorption experiments revealed that all CS states are quenched into a low lying localised  $^3(\pi, \pi^*)$  triplet state of the acridine subunit. Even in case of chromophore **8** whose CS state is energetically lowered owing to the very strong donor D2, the localised triplet state of the acceptor is still below and acts as an energy trap. The process  $^3\text{CS} \rightarrow \text{T}$  refers to a back hole transfer from acridine to D2 (D3). Due to hyperfine interaction conversion of the  $^1\text{CS}$  into the  $^3\text{CS}$  state and subsequent

deactivation into the triplet state is very fast. This deactivation pathway “catalyses” the formation of the acridine localised triplet state which results in a shorter lifetime of the  $^3\text{CS}$  states of the cascades **4**, **6**, **7** and **8** (in the solvents mentioned above) compared to the lifetime of the  $^1\text{CT}$  states of their reference compounds **1** and **2**.

The decoupling of acceptor and donor subunits on the one hand and between the different donors on the other hand results in an extended lifetime of the  $^3\text{CS}$  states. Comparing the decay kinetics of compounds **0** and **3**, and **3** and **4**, respectively, it is obvious that the main contribution of the longer lifetime of the CS state originates from the electronic decoupling of the donor subunits on the basis of saturated spacers (**0** vs **3**). The twisting of acceptor and donor subunits has only relatively small influence on the lifetimes (**3** vs **4**). Combining both approaches as outlined in the Introduction the lifetime of the CS state is prolonged by two orders of magnitude (**0** vs **4**). This significant increase of the lifetimes of the CS states is noteworthy because charge recombination of **3** – **10** is located in the Marcus normal region whereas this process of **0** takes place in the Marcus inverted region.

However, if we compare these results with CS lifetimes of similarly large systems reported in literature<sup>[34, 56, 90, 167, 234]</sup> the cascades **3** – **10** decay quite fast. We anticipate that the lifetimes would increase dramatically if the energy of the CS state were below that of the localised acridine triplet state of an incorporated subunit which then cannot act as an energy trap furthermore. Consequently, the lifetime of the CS states should increase dramatically because of two facts: First, formation of a  $^3\text{CS}$  state does not result in a “catalysed” deactivation mechanism of the charge separated state to the now higher lying localised triplet state. Second, the energy gap between the  $^1\text{CS}$  and the  $S_0$  state is large enough that charge recombination ( $^1\text{CS} \rightarrow S_0$ ) is located deeply in the Marcus inverted region.

Our findings are important for designing chromophores based on triarylamine cascades with CS lifetimes being sufficiently long to be used as photosensitisers in organic solar cells, for generation of photocurrent or for use in other optoelectronic devices. A next step will be to find a more suitable electron acceptor whose reduction is completely reversible, whose reorganisation energy is low and whose locally excited triplet state is higher in energy than the corresponding CS states.

## 4 Experimental Section

### 4.1 Analytical Methods

#### 4.1.1 General Analytical Methods

##### *NMR spectroscopy*

- Bruker Avance 400 FT-Spectrometer ( $^1\text{H}$ : 400.1 MHz,  $^{13}\text{C}$ : 100.6 MHz)
- Bruker Avance DMX 600 FT-Spectrometer ( $^1\text{H}$ : 600.13 MHz,  $^{13}\text{C}$ : 150.92 MHz)

All  $^1\text{H}$ - and  $^{13}\text{C}$ -NMR spectra were recorded at 295 K. The signal of the respective solvent was used as the internal reference and the chemical shifts are given in ppm ( $\delta$ -scale) versus TMS. Multiplicities were denoted as *s* (singlet), *d* (doublet), *dd* (doublet of doublets), *ddd* (doublet of doublets of doublets) and *m* (multiplet). Coupling constants are given in Hz. NMR-Spectroscopy data are quoted as follows: chemical shift (multiplicity, coupling constants, number of protons).

##### *Mass spectroscopy*

- Finnigan MAT 90
- Bruker Daltonik microTOF focus

Mass spectra were recorded at the Institute of Organic Chemistry, University of Würzburg. For ESI-spectra 10  $\mu\text{M}$  solutions of the sample in acetone, chloroform or acetonitrile were prepared.

##### *Melting points*

All melting points were measured with a Tottoli melting-point apparatus from Büchi and are not corrected.

#### 4.1.2 Cyclic Voltammetry

- Electrochemical Workstation BAS CV-50 W including software version 2.0

Cyclic voltammograms were measured under an argon atmosphere (argon dried with Sicapent<sup>®</sup> from Merck, traces of oxygen removed with copper oxide catalyst R3-11 from BASF) in dry and oxygen-free solvents with 0.2 M tetrabutylammonium hexafluorophosphate

(TBAH) as supporting electrolyte. The concentration of the solute was about 0.5 mM. A conventional three electrode setup consisting of a platinum disc working electrode ( $\varnothing$  2 mm), a Ag/AgCl pseudoreference electrode and a platinum wire counter electrode was used. The redox potentials were referenced against the ferrocene/ferrocenium redox couple as an internal standard. For measurements under thin-layer conditions the working electrode was placed onto a mobile glass hemisphere.<sup>[235]</sup> Digital simulation of CVs was done with DigiSim 3.03.

### 4.1.3 Spectroelectrochemistry

- JASCO V-570 UV/Vis/NIR spectrometer
- EG & G potentiostat/galvanostat model 363

Spectroelectrochemical experiments were performed in reflection mode at a platinum disc electrode ( $\varnothing$  6 mm) through the planar quartz bottom of a cylindrical vessel. A gold/nickel covered metal (V2A) plate served as the counter electrode and a Ag/AgCl electrode as the pseudoreference electrode. The optical path length of 20  $\mu$ m between the working electrode and the quartz bottom was adjusted by a micrometer screw.<sup>[236]</sup> The potential applied to the electrolyte was varied in steps of 10 – 100 mV and a UV/Vis/NIR spectrum was recorded ca. one minute after each potential change.

### 4.1.4 UV/Vis/NIR Spectroscopy

- JASCO V-570 UV/Vis/NIR spectrometer

All solvents were of spectroscopic grade and were used without any further purification. Absorption spectra were recorded in 1 cm quartz cuvettes (Hellma). For chemical oxidation a  $\text{SbCl}_5$  solution in dichloromethane ( $5 \cdot 10^{-3}$  M) was added drop by drop to a  $10^{-5}$  M solution of the compound. After each drop a spectrum was recorded over the whole range (200 – 2500 nm) with a scan rate of  $1000 \text{ nm min}^{-1}$ .

### 4.1.5 Fluorescence Spectroscopy

- Photon Technology International QuantaMaster™ Model QM-2000-4 including a cooled photomultiplier (R928P) and a 75 W xenon short arc lamp (UXL-75XE, Ushio)
- Photon Technology International TimeMaster™ Model TM-2/2003 fluorescence lifetime spectrometer including a nanosecond flash-lamp operating at 18-20 kHz charged with H<sub>2</sub>/N<sub>2</sub> (1:1).

Stationary fluorescence spectra were recorded in 1 cm quartz cells (Hellma). All solvents were of spectroscopic grade and were used as received. The concentration was ca. 10<sup>-5</sup> – 10<sup>-6</sup> M and oxygen was removed by bubbling inert gas through the solutions for about 5 minutes before each measurement. The fluorescence quantum yields were determined by Equation 4.1, in which  $I_f$ ,  $OD$ , and  $n$  are the intensity of the fluorescence, the optical density of the solution at the excitation energy and the refractive index of the solvent.

$$\Phi_f = \Phi_{\text{ref}} \frac{\int I_f(\tilde{\nu}) \frac{OD_{\text{ref}}}{OD} \frac{n^2}{n_{\text{ref}}^2}}{\int I_f(\tilde{\nu})_{\text{ref}} \frac{OD_{\text{ref}}}{OD} \frac{n^2}{n_{\text{ref}}^2}} \quad (4.1)$$

As reference a solution of rhodamin 101 in EtOH was used due to its constant quantum yield of 1.0 over a wide range of temperature.<sup>[237]</sup>

For time-dependent fluorescence decay measurements 1000 data points were collected for each scan. The signal to noise ratio was improved by an integration time (time over which the signal will be averaged for each point of each scan) of 0.2 – 0.5 ns depending on fluorescence intensity of the sample and the final decay curve was averaged by 2 – 4 complete scans. The instrument response of the nanosecond flash lamp was determined by using Ludox® AS-30 colloidal silica in de-ionised water as a scatterer. The fluorescence decay curves were deconvoluted with the signal of the flash lamp using the corresponding spectrometer software. The decays were monoexponentially fitted in the nanosecond regime unless otherwise indicated. The  $\chi^2$  test (about 1.0), Durbin Watson (> 1.7), residuals and autocorrelation function (without any significant structure) served as the main criteria in the evaluation of the fit. The analysis of the fluorescence decay of compound **1** in cyclohexane is given as example in Figure 4.1. Oxygen was removed as outlined above.

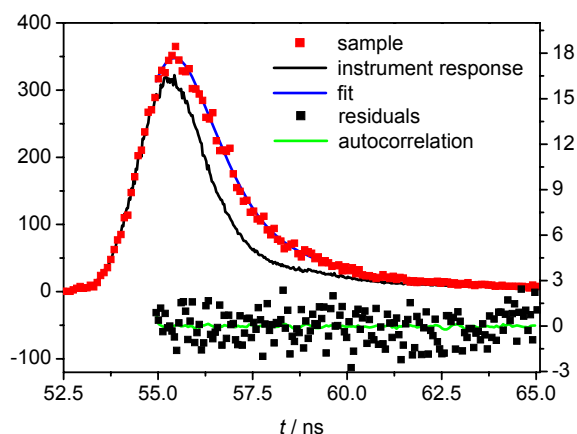


**Figure 4.1** Instrument response function, fluorescence decay of **1** in cyclohexane (■) and **monoexponential fit** (left axis) as well as residuals (■) and **autocorrelation function** (right axis);  $\tau = 0.77$  ns,  $\chi^2 = 1.11$ , Durbin Watson = 2.2.

#### 4.1.6 Transient Absorption Spectroscopy

- Edinburgh LP 920 laser flash spectrometer with a 300 W ozone-free Xe arc lamp including a photomultiplier (Hamamatsu R955) and a digital storage oscilloscope (Tektronix TDS3012B)
- Continuum Minilite II Nd:YAG laser operating at 10 Hz, 8 ns pulse duration, ca. 57 mW average power at  $28200\text{ cm}^{-1}$

Nanosecond transient absorption spectra were acquired on a laser flash spectrometer. All solvents were of spectroscopic grade and were used as received. Measurements were carried out in 1 cm quartz cells (Hellma) with an optical density between 0.1 – 1.0 at the excitation energy. Oxygen was removed by bubbling inert gas through the solutions until a constant decay time was monitored. Samples were excited with a 8 ns duration laser pulse at  $24000\text{ cm}^{-1}$  (416 nm) and  $28200\text{ cm}^{-1}$  (355 nm), respectively. The excitation pulse was produced by a the Nd:YAG laser operating at 10 Hz and the probe pulse was provided by a pulsed Xe flash lamp.

In general the recorded transient signal consists of transient absorption, fluorescence and ground state bleaching. We eliminated fluorescence contributions by measuring two different transient signals, one signal  $I_T(t)$  with a high intensity of the probe light (pulsed Xe flash lamp with background  $I_{100}$ ) and a second signal  $I_T^{CW}(t)$  with low intensity of the probe light (CW Xe lamp with background  $I_{100}^{CW}$ ). Assuming that the fluorescence in both transient

signals is identical, and the amount of transient absorption varies with intensity of the probe light, we derived Equation 4.2 as follows:

$$\text{high intensity of the probe light:} \quad \Delta OD^{\text{high}}(t) = \log\left(\frac{I_{100}}{I_T - I_F}\right) \quad (4.2a)$$

$$\text{low intensity of the probe light:} \quad \Delta OD^{\text{low}}(t) = \log\left(\frac{I_{100}^{\text{CW}}}{I_T^{\text{CW}} - I_F}\right) \quad (4.2b)$$

$$\text{assuming that } \Delta OD^{\text{high}}(t) = \Delta OD^{\text{low}}(t) \Rightarrow \log\left(\frac{I_{100}}{I_T - I_F}\right) = \log\left(\frac{I_{100}^{\text{CW}}}{I_T^{\text{CW}} - I_F}\right) \quad (4.2c)$$

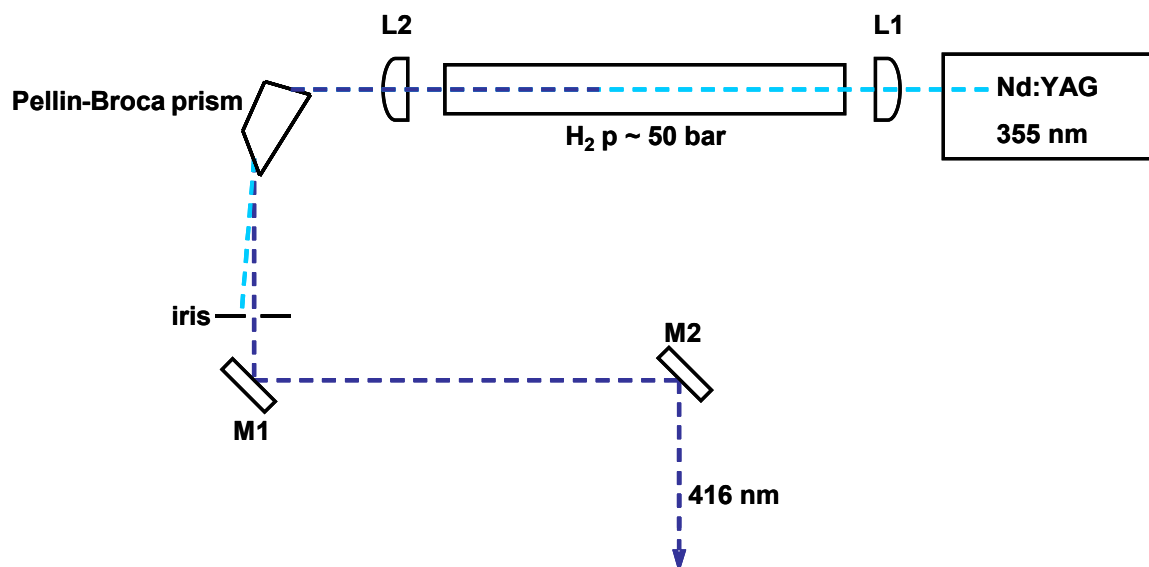
$$\Rightarrow I_F = \frac{I_T^{\text{CW}} \cdot I_{100} - I_T \cdot I_{100}^{\text{CW}}}{I_{100} - I_{100}^{\text{CW}}} \quad (4.2d)$$

$$\text{substitution of 4.2d in 4.2b} \Rightarrow \Delta OD(t) = \log\left(\frac{I_{100} - I_{100}^{\text{CW}}}{I_T(t) - I_T^{\text{CW}}(t)}\right) \quad (4.2)$$

The instrument response of the Nd:YAG laser was determined by using Ludox<sup>®</sup> AS-30 colloidal silica in de-ionised water as a scatterer. The decay curves were deconvoluted with the signal of the laser using the corresponding spectrometer software. Residuals and autocorrelation function (without any significant structure) served as the main criteria in the evaluation of the fit.

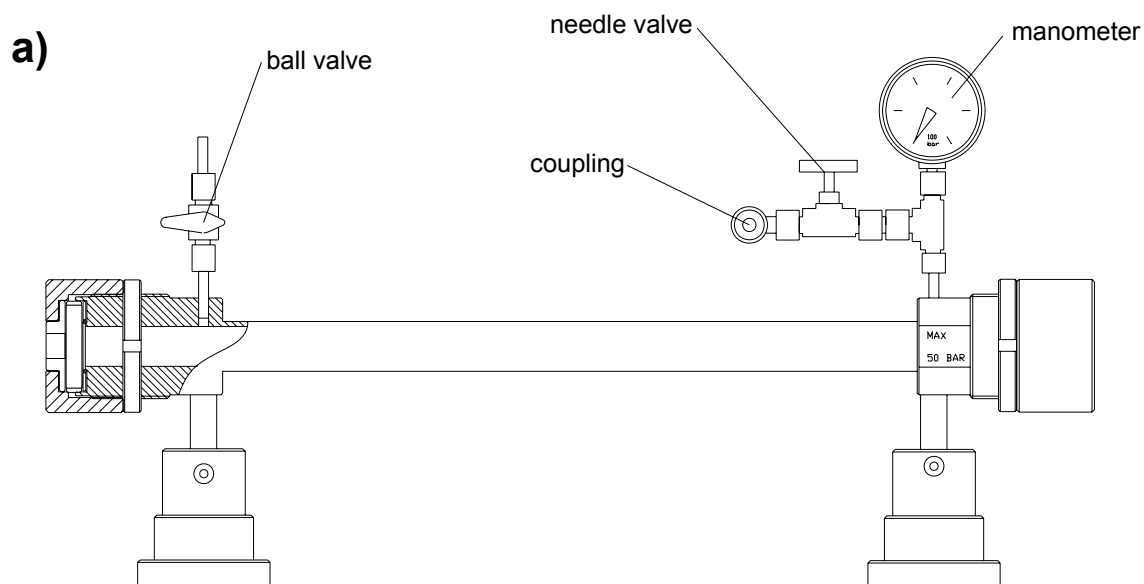
To avoid photoionisation, the solute was excited either with low power at 28200 cm<sup>-1</sup> (< 5 mW) or with high power at 24000 cm<sup>-1</sup> (> 50 mW) where the triarylamine part of the compounds does not absorb. To increase the signal to noise ratio the compounds were excited at 24000 cm<sup>-1</sup>. The THG of the fundamental of 9400 cm<sup>-1</sup> (1064 nm) was shifted to 24000 cm<sup>-1</sup> by means of a 50 cm Raman shifter which was charged with hydrogen (50 bar). The corresponding energy was selected by a Pellin-Broca prism. The setup to generate the excitation energy of 24000 cm<sup>-1</sup> is outlined in Figure 4.1.





**Figure 4.1** Experimental setup for Raman shifting. L1 and L2 are fused silica plano-convex lenses. M1 and M2 are dielectric coated plane mirrors LBSM-UV.

A blueprint of the Raman shifter is given in Figure 4.2. The main components of the Raman shifter are made of brass. The mountings are made of stainless steel, the plastics used in the gasket are POM and the material of the O-ring seal is viton.



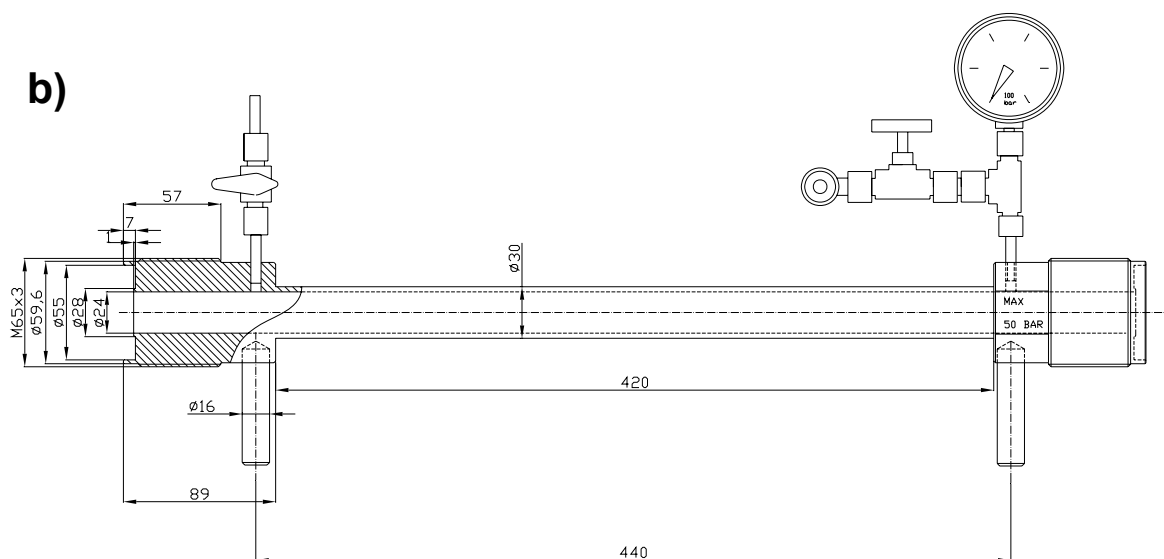


**Figure 4.2** a) General plan of the Raman shifter; b) Plan of the Raman shifter including dimensioning.

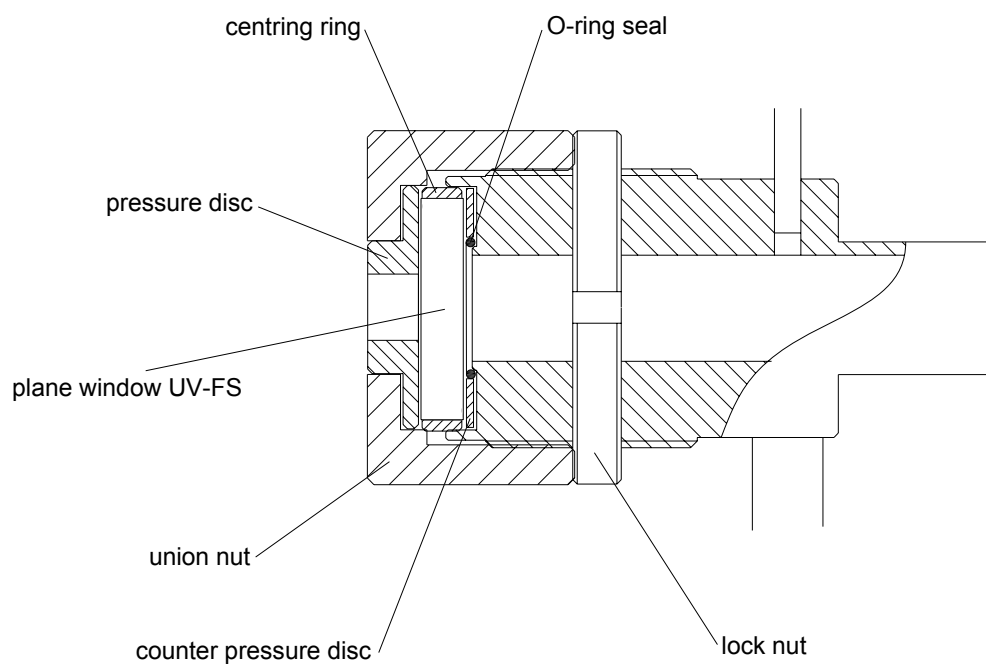


**Figure 4.3** Detailed drawing of the Raman shifter's gasket.

In order to estimate the performance of the Raman shifter we measured the power output at  $24000\text{ cm}^{-1}$  at different pressures within the cell (see Figure 4.4). The energy of the 8 ns laser pulse of the first Stokes emission at  $24000\text{ cm}^{-1}$  increases with increasing pressure in the Raman shifter until it attains a maximum of ca. 23 % conversion efficiency (ca. 57 mW power input at  $28200\text{ cm}^{-1}$ ) at about 35 bar. The variation in intensity of 16 averaged 8 ns

laser pulses each was also plotted as a function of the pressure (see Figure 4.5) to estimate the pressure which provides the most constant power output. The energy of the laser pulse becomes more constant with higher pressure. The variation in intensity is reduced below 3 % at a pressure > 45 bar. Consequently, high pressure (ca. 50 bar) within the cell is required to get a constant energy of the laser pulse although the maximum energy is already obtained at lower pressures (35 bar).

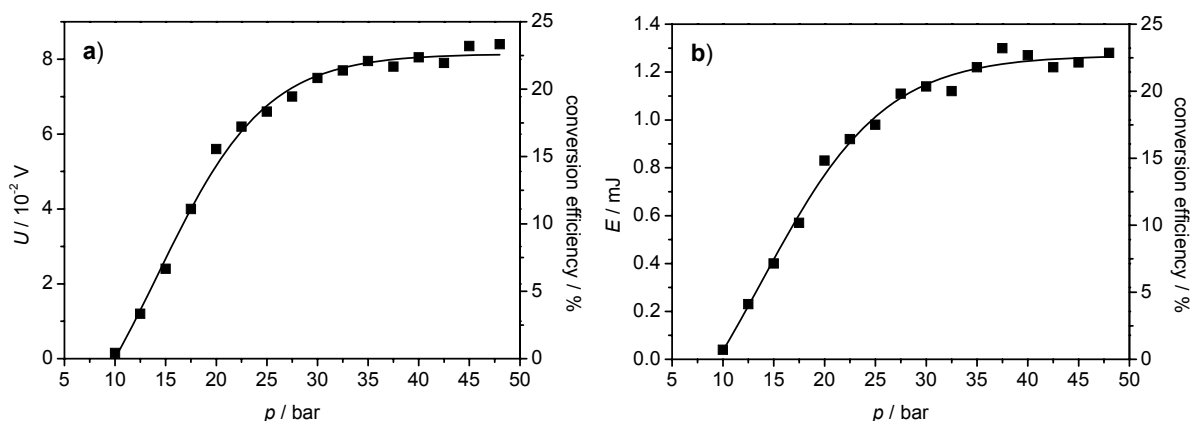


**Figure 4.4** Energy of a 8 ns laser pulse of the first Stokes emission as a function of the  $\text{H}_2$ -pressure in the Raman shifter. The energy was determined by **a)** the voltage given by the PMT and **b)** by means of a laser power meter. The conversion efficiency ( $E_{24000 \text{ cm}^{-1}}$  output /  $E_{28200 \text{ cm}^{-1}}$  input) is given at the right axis and is not corrected for reflexion losses in the case of the  $24000 \text{ cm}^{-1}$  pulses. Thus, the actual conversion efficiency might be somewhat higher.

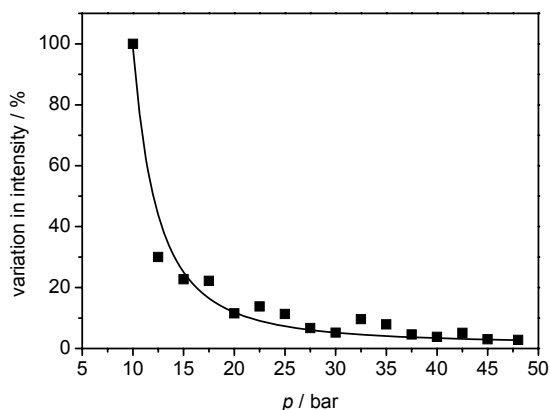


**Figure 4.5** Variation in intensity of 16 averaged 8 ns laser pulses each of the first Stokes emission as a function of the pressure.

### 4.1.7 Synthesis

All chemicals were of standard quality and were used without further purification. All reactions under inert-gas conditions (nitrogen, dried with Sicapent<sup>®</sup> from Merck, oxygen was removed by copper oxide catalyst R3-11 from BASF) were performed in flame-dried Schlenk tubes. If necessary, the solvents were purified and dried by standard procedures and kept under an inert-gas atmosphere. Flash-column chromatography was carried out using silica gel (32 – 63  $\mu\text{m}$ ) from MP Biomedicals. For column chromatography neutral alumina with activity V (63 – 200  $\mu\text{m}$ ) from Macherey-Nagel was used.

Microwave reactions were carried out in a MLS Microwave  $\mu\text{CHEMIST}$  using a 50 ml 3-necked round-bottom flask (open system). The temperature of the reaction was measured directly with a fibre optic sensor.

## 4.2 Synthesis

### 4.2.1 General Experimental Procedures

#### 4.2.1.1 General Procedure for the Palladium Catalysed Amination of Aryl Halides (GP1)

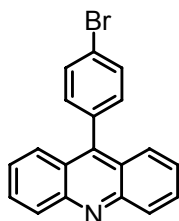
A solution of the aryl halide, the aryl amine,  $\text{Pd}_2(\text{dba})_3\text{-CHCl}_3$ , sodium *tert*-butoxide,  $\text{P}^t\text{Bu}_3$  (0.33 M solution in hexane) in dry toluene was stirred under a nitrogen atmosphere at the given temperature for the given time. The mixture was diluted with dichloromethane and washed twice with a saturated  $\text{Na}_2\text{S}_2\text{O}_3$  solution in water. The solvent was removed under reduced pressure and the crude product was purified by (flash-)column chromatography.

#### 4.2.1.2 General Procedure for the Hagihara-Coupling (GP2)

The aryl halide, the alkyne,  $\text{Pd}(\text{C}_6\text{H}_5\text{CN})_2\text{Cl}_2$  and  $\text{CuI}$  were dissolved under a nitrogen atmosphere in dry dioxane. After the addition of  $\text{P}^t\text{Bu}_3$  (0.33 M solution in hexane) and  $\text{HN}^i\text{Pr}_2$  the mixture was stirred at room temperature for the given time. The mixture was diluted with dichloromethane and washed twice with a saturated  $\text{Na}_2\text{S}_2\text{O}_3$  solution in water. The solvent was removed under reduced pressure and the crude product was purified by flash-column chromatography.

## 4.2.2 Synthesis of Precursors

### 9-(4-Bromophenyl)acridine (12)



CA: [94255-63-7]

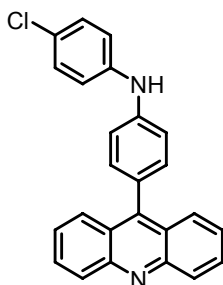
Diphenylamine (1.50 g; 8.86 mmol), 4-bromobenzoic acid (2.67 g; 13.3 mmol) and zinc bromide (4.98 g; 22.1 mmol) were mixed in a 3-necked round-bottom flask and heated in a microwave oven (gradient of heating: 10 min RT to 170 °C; holding time: 2 h at 170 °C). The glassy residue is dissolved in boiling ethanol (60 ml) and poured into water (100 ml). After the addition of conc. ammonia (40 ml) the resulting brown precipitation was filtered off and was washed with methanol (5 ml). The crude product was dissolved in dichloromethane and the insoluble benzoic acid was removed by filtration. The solvent was removed under reduced pressure and the crude material was purified by flash-column chromatography (CH<sub>2</sub>Cl<sub>2</sub> : EtOAc = 20:1). The crude product was dissolved in methanol (15 ml) and was heated for 5 min under reflux. After the suspension was cooled down the product was filtered off and dried in vacuo.

**Formula:** C<sub>19</sub>H<sub>12</sub>BrN [334.21]

**Yield:** 1.53 g (4.58 mmol; 52 %) yellow solid

**Melting point:** 242 °C (Lit.: 234 °C)<sup>[120]</sup>

**<sup>1</sup>H-NMR** (400.1 MHz; [D<sub>1</sub>]chloroform):  $\delta$  = 8.42 - 8.28 (m, 2H); 7.81 (ddd, <sup>3</sup>J<sub>HH</sub> = 8.6 Hz, <sup>4</sup>J<sub>HH</sub> = 6.8 Hz, <sup>5</sup>J<sub>HH</sub> = 1.6 Hz, 2H); 7.77 (AA', 2H); 7.71 - 7.66 (m, 2H); 7.47 (ddd, <sup>3</sup>J<sub>HH</sub> = 8.8 Hz, <sup>4</sup>J<sub>HH</sub> = 6.8 Hz, <sup>5</sup>J<sub>HH</sub> = 1.0 Hz, 2H); 7.34 (BB', 2H).

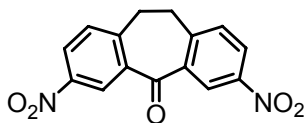
**Compound 13**

CA: [863678-21-1]

Following GP1: Compound **12** (1.00 g; 3.00 mmol), 4-chloroaniline (477 mg; 3.74 mmol), Pd<sub>2</sub>(dba)<sub>3</sub>·CHCl<sub>3</sub> (39.0 mg; 37.7 μmol), P<sup>t</sup>Bu<sub>3</sub> (20.0 μl; 66.0 μmol), sodium *tert*-butoxide (359 mg; 3.74 mmol), toluene (15 ml); 2.5 d at 45 °C, flash-column chromatography (CH<sub>2</sub>Cl<sub>2</sub> : EtOAc = 40:1).

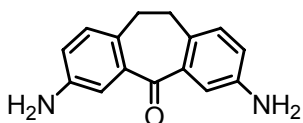
**Formula:** C<sub>25</sub>H<sub>17</sub>ClN [380.88]**Yield:** 980 mg (4.58 mmol; 86 %) yellow solid**Melting point:** 191 °C (Lit.: 189 – 191 °C)<sup>[16]</sup>

<sup>1</sup>H-NMR (400.1 MHz; [D<sub>2</sub>]dichloromethane): δ = 8.22 (ddd, <sup>3</sup>J<sub>HH</sub> = 8.7 Hz, <sup>4</sup>J<sub>HH</sub> = 1.2 Hz, <sup>5</sup>J<sub>HH</sub> = 0.8 Hz, 2H); 7.85 (ddd, <sup>3</sup>J<sub>HH</sub> = 8.7 Hz, <sup>4</sup>J<sub>HH</sub> = 1.4 Hz, <sup>5</sup>J<sub>HH</sub> = 0.8 Hz, 2H); 7.77 (ddd, <sup>3</sup>J<sub>HH</sub> = 8.8 Hz, <sup>4</sup>J<sub>HH</sub> = 6.5 Hz, <sup>5</sup>J<sub>HH</sub> = 1.4 Hz, 2H); 7.46 (ddd, <sup>3</sup>J<sub>HH</sub> = 8.7 Hz, <sup>4</sup>J<sub>HH</sub> = 6.6 Hz, <sup>5</sup>J<sub>HH</sub> = 1.3 Hz, 2H); 7.36 (AA', 2H); 7.33 - 7.27 (-, 4H); 7.19 (BB', 2H); 6.09 (s, 1H).

**2,9-Dinitrodibenzosuberone (14)**

CA: [96886-98-5]

Dibenzosuberone (25.0 g; 120 mmol) was dissolved in sulphuric acid (120 ml) and at 0 °C a mixture of sulphuric acid (30.6 ml; 573 mmol) and nitric acid (13.1 ml; 316 mmol) was added slowly. The mixture was heated to 75 °C for 30 min. After the mixture was cooled down, it was poured into icecold water. The resulting precipitation was filtered off and suspended in ethanol. The mixture heated for 5 min under reflux. After the suspension was cooled down the crude product was filtered off and recrystallised from nitromethane. The product was filtered off and dried in vacuo.

**Formula:** C<sub>15</sub>H<sub>10</sub>N<sub>2</sub>O<sub>5</sub> [298.25]**Yield:** 32.2 g (108 mmol; 90 %) colourless solid**Melting point:** 212 °C**<sup>1</sup>H-NMR** (400.1 MHz; [D<sub>6</sub>]DMSO):  $\delta$  = 8.24 (d, <sup>4</sup>J<sub>HH</sub> = 2.5 Hz, 2H); 7.94 (dd, <sup>3</sup>J<sub>HH</sub> = 8.4 Hz, <sup>4</sup>J<sub>HH</sub> = 2.6 Hz, 2H); 7.27 (d, <sup>3</sup>J<sub>HH</sub> = 8.5 Hz, 2H); 2.92 (s, 4H).**2,9-Diaminodibenzosuberone (15)**

CA: [96886-97-4]

Conc. hydrochloric acid (130 ml) was added slowly to tin(II)chloride dehydrate (126 g; 558 mmol) at 0 °C. Then, conc. acetic acid (183 ml) was also carefully added at 0 °C. After 2,9-dinitrodibenzosuberone (**14**) (20.2 g; 67.7 mmol) was added under vigorous stirring the solution was heated for 1 h under reflux. The mixture was diluted with water (950 ml) and was basified with a sodium hydroxide solution (10 %). After the resulting precipitation was

filtered off and washed with water the dried crude product was recrystallised from ethanol and dried in vacuo.

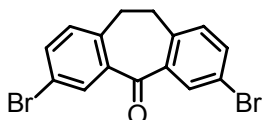
**Formula:** C<sub>15</sub>H<sub>14</sub>N<sub>2</sub>O [238.11]

**Yield:** 12.4 g (52.1 mmol; 77 %) yellow solid

**Melting point:** 170 °C (Lit.: 171 – 171.5 °C)<sup>[202]</sup>

**<sup>1</sup>H-NMR** (400.1 MHz; [D<sub>2</sub>]dichloromethane):  $\delta$  = 7.24 (d, <sup>4</sup>J<sub>HH</sub> = 2.5 Hz, 2H); 7.01 (d, <sup>3</sup>J<sub>HH</sub> = 8.1 Hz, 2H); 6.77 (dd, <sup>3</sup>J<sub>HH</sub> = 8.1 Hz, <sup>4</sup>J<sub>HH</sub> = 2.7 Hz, 2H); 3.73 (s, 4H); 3.03 (s, 4H).

### 2,9-Dibromodibenzosuberone (16)



CA: [226946-20-9]

2,9-Diaminodibenzosuberone (**15**) (1.85 g; 7.77 mmol) in dry acetonitrile (34 ml) was added to a solution of copper-(II)-bromide (4.55 g; 19.5 mmol) and *tert*-butylnitrite (2.48 ml; 20.9 mmol) in dry acetonitrile (26 ml). The resulting suspension was stirred for 10 h at RT and subsequently heated for 2 h under reflux. After the addition of hydrochloric acid (40 ml of a 20 % solution) the solution was extracted with diethyl ether (4 x 40 ml). The combined organic layers were washed with hydrochloric acid and dried over magnesium sulphate. The solvent was removed in vacuo. The residue was purified by flash-column chromatography (CH<sub>2</sub>Cl<sub>2</sub> : PE = 1:4) and dried in vacuo.

**Formula:** C<sub>15</sub>H<sub>10</sub>Br<sub>2</sub>O [366.05]

**Yield:** 1.96 g (5.35 mmol; 69 %) colourless solid

**Melting point:** 143 °C

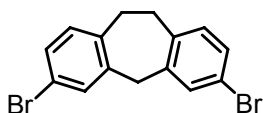
**<sup>1</sup>H-NMR** (400.1 MHz; [D<sub>1</sub>]chloroform):  $\delta$  = 8.13 (d, <sup>4</sup>J<sub>HH</sub> = 2.3 Hz, 2H); 7.56 (dd, <sup>3</sup>J<sub>HH</sub> = 8.2 Hz, <sup>4</sup>J<sub>HH</sub> = 2.2 Hz, 2H); 7.12 (d, <sup>3</sup>J<sub>HH</sub> = 8.1 Hz, 2H); 3.14 (s, 4H).

**<sup>13</sup>C-NMR** (100.6 MHz; [D<sub>1</sub>]chloroform):  $\delta$  = 192.5 (quart.); 140.8 (quart.); 139.6 (quart.); 135.6 (tert.); 133.6 (tert.); 131.3 (tert.); 120.9 (quart.); 34.4 (sec.).



**HRMS** (70 eV, EI):  $m/z$  calcd for  $[M^+] = C_{15}H_{10}Br_2O^+$ : 363.90929; found: 363.90926 ( $\Delta = 0.08$  ppm).

### Compound 17



Sodium borohydride (9.26 g; 245 mmol) was suspended under an inert gas atmosphere at 0 °C in trifluoroacetic acid (292 ml). A solution of 2,9-dibromodibenzosuberone (**16**) (6.36 g; 17.4 mmol) in dichloromethane (130 ml) was added carefully at RT and was stirred for 12 h. An additional amount of sodium borohydride (4.49 g; 119 mmol) was added and the solution was stirred for further 2 h. The solution was hydrolysed with water (100 ml) and extracted with dichloromethane (3 x 80 ml). The combined organic layers were washed with water and dried over magnesium sulphate. The crude product was purified by flash-column chromatography (PE).

**Formula:**  $C_{15}H_{12}Br_2$  [352.06]

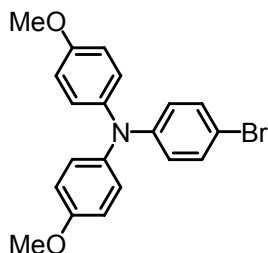
**Yield:** 5.50 g (15.6 mmol; 90 %) colourless solid

**Melting point:** 90 – 91 °C

**$^1H$ -NMR** (400.1 MHz;  $[D_6]$ acetone):  $\delta = 7.44$  (d,  $^4J_{HH} = 2.1$  Hz, 2H); 7.29 (dd,  $^3J_{HH} = 8.2$  Hz,  $^4J_{HH} = 2.1$  Hz, 2H); 7.09 (d,  $^3J_{HH} = 8.2$  Hz, 2H); 4.15 (s, 2H); 3.14 (s, 4H).

**$\{^1H\}^{13}C$ -NMR** (100.6 MHz;  $[D_6]$ acetone):  $\delta = 142.2$  (quart.); 139.5 (quart.); 132.6 (tert.); 132.5 (tert.); 130.6 (tert.); 120.0 (quart.); 40.0 (sec.); 32.3 (sec.).

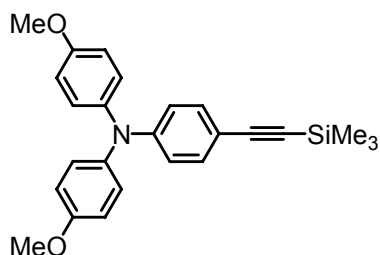
**HRMS** (70 eV, EI):  $m/z$  calcd for  $[M^+] = C_{15}H_{12}Br_2^+$ : 349.93002; found: 349.93015 ( $\Delta = 0.37$  ppm).

**Compound 18**

CA: [194416-45-0]

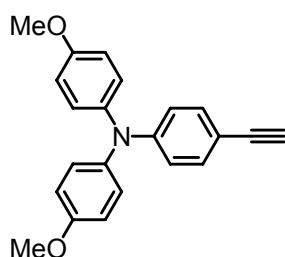
4-Iodoanisole (28.6 g; 122 mmol), 4-bromoaniline (10.0 g; 58.1 mmol), 1,10-phenanthroline (418 mg; 2.32 mmol), CuI (230 mg; 2.32 mmol) and powdered potassium hydroxide (25.4 g; 453 mmol) were dissolved in dry toluene (40 ml) and heated under reflux for 2 days. Dichloromethane (300 ml) was added and the suspension was washed with water (3 x 250 ml). The organic layer was dried over magnesium sulfate and the solvent was removed under reduced pressure. The crude product was purified by flash-column chromatography (CH<sub>2</sub>Cl<sub>2</sub> : PE = 3:5).

**Formula:** C<sub>20</sub>H<sub>18</sub>BrNO<sub>2</sub> [384.27]**Yield:** 13.8 g (35.9 mmol; 62 %) beige solid**Melting point:** 97 °C (Lit.: 91 – 92 °C)<sup>[238]</sup>**<sup>1</sup>H-NMR** (400.1 MHz; [D<sub>6</sub>]acetone): δ = 7.29 (AA', 2H); 7.06 (AA', 4H); 6.91 (BB', 4H); 6.75 (BB', 2H); 3.79 (s, 6H).

**Compound 19**

CA: [218608-72-1]

Following GP2: Compound **18** (5.00 g; 13.0 mmol), trimethylsilylacetylene (2.24 ml; 15.7 mmol), Pd(PhCN)<sub>2</sub>Cl<sub>2</sub> (156 mg; 407 μmol), CuI (24.8 mg; 130 μmol), P<sup>t</sup>Bu<sub>3</sub> (2.40 ml; 792 μmol), HN<sup>i</sup>Pr<sub>2</sub> (2.19 ml; 15.6 mmol), dioxane (20 ml); 1 d, flash-column chromatography (CH<sub>2</sub>Cl<sub>2</sub> : PE = 1:3).

**Formula:** C<sub>25</sub>H<sub>27</sub>NO<sub>2</sub>Si [401.57]**Yield:** 5.01 g (12.5 mmol; 96 %) yellow oil**<sup>1</sup>H-NMR** (400.1 MHz; [D<sub>6</sub>]acetone): δ = 7.23 (AA', 2H); 7.09 (AA', 4H); 6.93 (BB', 4H); 6.72 (BB', 2H); 3.80 (s, 6H); 0.20 (s, 9H).**Compound 20**

CA: [218608-73-2]

Compound **19** (5.01 g; 12.5 mmol) was dissolved in THF (35 ml) and TBAF (12.5 ml of 1 M solution in THF; 12.5 mmol) was added. The solution was stirred at room temperature for 1 h. Then, the solvent was removed under reduced pressure and the residue was dissolved in dichloromethane (200 ml). The solution was washed with water (3 x 100 ml) and the

organic layer was dried over magnesium sulfate. Finally, the solvent was removed under reduced pressure and the product was dried in vacuo.

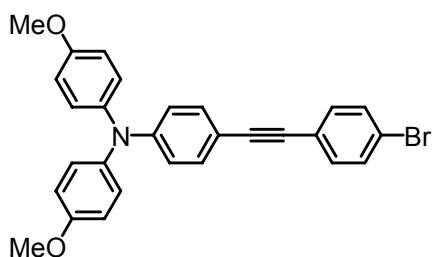
**Formula:**  $C_{22}H_{19}NO_2$  [329.39]

**Yield:** 4.10 g (12.4 mmol; 99 %) red solid

**Melting point:** 85 – 88 °C

**$^1H$ -NMR** (400.1 MHz;  $[D_6]$ acetone):  $\delta$  = 7.26 (AA', 2H); 7.09 (AA', 4H); 6.93 (BB', 4H); 6.74 (BB', 2H); 3.80 (s, 6H); 3.44 (s, 1H).

### Compound 21



CA: [863678-33-5]

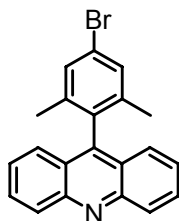
Following GP2: Compound **20** (4.10 g; 12.4 mmol), 1-bromo-4-iodobenzene (4.60 g; 16.3 mmol),  $Pd(PhCN)_2Cl_2$  (149 mg; 388  $\mu$ mol),  $CuI$  (23.7 mg; 124  $\mu$ mol),  $P^tBu_3$  (2.29 ml; 756  $\mu$ mol),  $HN^iPr_2$  (2.09 ml; 14.9 mmol), dioxane (19 ml); 1 d, flash-column chromatography ( $CH_2Cl_2$  : PE = 1:3).

**Formula:**  $C_{28}H_{22}BrNO_2$  [484.38]

**Yield:** 3.72 g (7.68 mmol; 62 %) yellow solid

**Melting point:** 104 – 105 °C

**$^1H$ -NMR** (400.1 MHz;  $[D_6]$ acetone):  $\delta$  = 7.57 (AA', 2H); 7.43 (BB', 2H); 7.32 (AA', 2H); 7.11 (AA', 4H); 6.95 (BB', 4H); 6.78 (BB', 2H); 3.81 (s, 6H).

**Compound 22**

Sodium hydride (1.10 g of a 60% suspension in an oil; 27.5 mmol) was added under an inert gas atmosphere to a solution of 9(10*H*)-acridone (2.00 g; 10.2 mmol) in DMF (200 ml) which was stirred for 30 minutes at RT. The solution was cooled to 0 °C and 2-methoxyethoxymethyl chloride (1.50 ml; 13.1 mmol) was added carefully. The mixture was stirred for 30 minutes at 0 °C and for 2 h at RT. The solvent was removed in vacuo and the residue was dissolved in dichloromethane (400 ml). The mixture was washed with a saturated NaCl solution (3 x 250 ml) and dried over magnesium sulphate. Subsequently the solvent was removed under reduced pressure. The crude product was purified by column chromatography (CH<sub>2</sub>Cl<sub>2</sub> : PE = 1:1) to obtain *N*-(2-methoxyethoxymethyl)-9-acridone.

**Formula:** C<sub>17</sub>H<sub>17</sub>NO<sub>3</sub> [283.32]

**Yield:** 2.54 g (8.97 mmol; 88 %) light yellow solid.

**Melting point:** 181 °C

**<sup>1</sup>H-NMR** (400.1 MHz; [D<sub>1</sub>]chloroform): δ = 8.52 (m, 2H); 7.75 – 7.68 (-, 4H); 7.32 (m, 2H); 5.81 (s, 2H); 3.86 (m, 2H); 3.64 (m, 2H); 3.44 (s, 3H).

A solution of *n*-BuLi (3.10 ml of a 1.55 M solution in hexane; 4.81 mmol) was added drop by drop to a solution of 4-bromo-1-iodo-2,6-dimethylbenzene (1.50 g; 4.82 mmol) in THF (40 ml) at -78 °C which was then stirred for 3 h. This solution was transferred via cannula to a solution of *N*-(2-methoxyethoxymethyl)-9-acridone (845 mg; 2.98 mmol) in THF (50 ml), which was cooled down to -78 °C and stirred for further 2 h. The solution was stirred for 10 h at RT, diluted hydrochloric acid was added, followed by the addition of a solution of potassium carbonate in water. The solution was extracted with dichloromethane (3 x 200 ml) and the combined organic layers were dried over magnesium sulphate. The solvent was removed under reduced pressure. Purification of the crude product was achieved by flash-column chromatography (CH<sub>2</sub>Cl<sub>2</sub>).

**Formula:** C<sub>21</sub>H<sub>16</sub>BrN [362.26]

**Yield:** 732 mg (2.02 mmol; 42 %) yellow solid

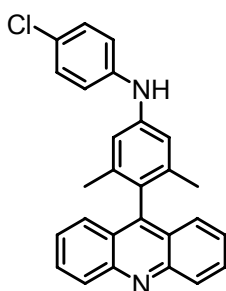
**Melting point:** 194 °C

**<sup>1</sup>H-NMR** (400.1 MHz; [D<sub>6</sub>]acetone): δ = 8.26 (ddd, <sup>3</sup>J<sub>HH</sub> = 8.8 Hz, <sup>4</sup>J<sub>HH</sub> = 0.9 Hz, <sup>5</sup>J<sub>HH</sub> = 0.9 Hz, 2H); 7.79 (ddd, <sup>3</sup>J<sub>HH</sub> = 8.8 Hz, <sup>3</sup>J<sub>HH</sub> = 5.6 Hz, <sup>4</sup>J<sub>HH</sub> = 2.3 Hz, 2H); 7.41 – 7.34 (-, 6H); 1.72 (s, 6H).

**{<sup>1</sup>H}<sup>13</sup>C-NMR** (100.6 MHz; [D<sub>6</sub>]acetone): δ = 149.4 (quart.); 145.2 (quart.); 139.7 (quart.); 134.6 (quart.); 130.8 (tert.); 130.5 (tert.); 130.4 (tert.); 126.6 (tert.); 125.9 (tert.); 125.0 (quart.); 122.5 (quart.); 19.9 (prim.).

**HRMS** (70 eV, EI): *m/z* calcd for [M<sup>+</sup>] = C<sub>21</sub>H<sub>16</sub>BrN<sup>+</sup>: 361.04606; found: 361.04619 (Δ = 0.36 ppm).

### Compound 23



Following GP1: Compound **22** (120 mg; 331 μmol), 4-chloroaniline (57.2 mg; 448 μmol), Pd<sub>2</sub>(dba)<sub>3</sub>·CHCl<sub>3</sub> (4.68 mg; 4.52 μmol), P<sup>*t*</sup>Bu<sub>3</sub> (24.0 μl; 7.92 μmol), sodium *tert*-butoxide (43.1 mg; 448 μmol), toluene (2 ml); 20 h at 100 °C, flash-column chromatography (CH<sub>2</sub>Cl<sub>2</sub> → CH<sub>2</sub>Cl<sub>2</sub> : EtOAc = 40:1).

**Formula:** C<sub>27</sub>H<sub>21</sub>ClN<sub>2</sub> [408.92]

**Yield:** 124 mg (303 μmol; 92 %) yellow solid

**Melting point:** 267 °C

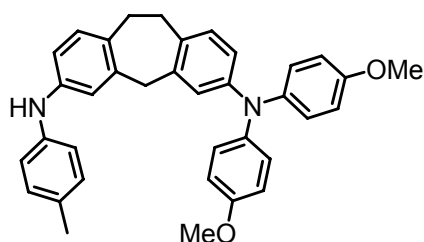
**<sup>1</sup>H-NMR** (400.1 MHz; [D<sub>6</sub>]acetone): δ = 8.25 (m, 2H); 7.78 (ddd, <sup>3</sup>J<sub>HH</sub> = 8.8 Hz; <sup>3</sup>J<sub>HH</sub> = 6.5 Hz, <sup>4</sup>J<sub>HH</sub> = 1.5 Hz, 2H); 7.59 (ddd, <sup>3</sup>J<sub>HH</sub> = 8.7 Hz, <sup>4</sup>J<sub>HH</sub> = 1.1 Hz, <sup>5</sup>J<sub>HH</sub> = 0.5 Hz, 2H); 7.45 (ddd, <sup>3</sup>J<sub>HH</sub> = 8.7 Hz, <sup>3</sup>J<sub>HH</sub> = 6.5 Hz, <sup>4</sup>J<sub>HH</sub> = 1.2 Hz, 2H); 7.29 (AA', 2H); 7.17 (BB', 2H); 7.00 (s, 2H); 5.95 (s, 1H); 1.70 (s, 6H).

**{<sup>1</sup>H}<sup>13</sup>C-NMR** (100.6 MHz; [D<sub>6</sub>]acetone): δ = 149.5 (quart.); 146.9 (quart.); 143.2 (quart.); 142.3 (quart.); 142.3 (quart.); 138.5 (quart.); 130.4 (tert.); 130.2 (tert.);

129.6 (tert.); 128.3 (quart.); 126.5 (tert.); 126.2 (tert.); 125.8 (quart.);  
119.6 (tert.); 117.0 (tert.); 20.3 (prim.).

**HRMS** (70 eV, EI):  $m/z$  calcd for  $[M^+] = C_{27}H_{21}ClN_2^+$ : 408.13878; found: 408.13889 ( $\Delta = 0.27$  ppm).

### Compound 26



Following GP1: Compound **24** (280 mg; 560  $\mu$ mol), *p*-toluidine, (120 mg; 1.12 mmol),  $Pd_2(dba)_3 \cdot CHCl_3$  (5.91 mg; 5.71  $\mu$ mol),  $P^tBu_3$  (30.4  $\mu$ l; 10.0  $\mu$ mol), sodium *tert*-butoxide (67.2 mg; 699  $\mu$ mol), toluene (10 ml); heated in a microwave oven (gradient of heating: 10 min RT to 75  $^\circ$ C; holding time: 30 min at 75  $^\circ$ C); flash-column chromatography ( $CH_2Cl_2$  : PE = 2:1).

**Formula:**  $C_{36}H_{34}N_2O_2$  [526.67]

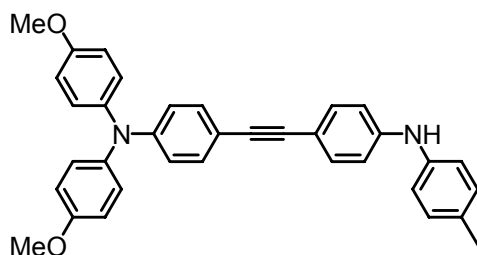
**Yield:** 230 mg (437  $\mu$ mol; 78 %) colourless solid

**Melting point:** 70  $^\circ$ C

**$^1H$ -NMR** (400.1 MHz;  $[D_6]$ acetone):  $\delta = 7.40 - 6.93$  (-, 11H); 6.88 - 6.83 (-, 6H); 6.77 (d,  $^4J_{HH} = 2.3$  Hz, 1H); 6.66 (dd,  $^3J_{HH} = 8.2$  Hz,  $^4J_{HH} = 2.5$  Hz, 1H); 3.90 (s, 2H); 3.77 (s, 6H); 3.06 (-, 4H); 2.23 (s, 3H).

**$\{^1H\}^{13}C$ -NMR** (150.9 MHz;  $[D_6]$ acetone):  $\delta = 156.6$  (quart.); 147.7 (quart.); 143.1 (quart.); 142.5 (quart.); 142.3 (quart.); 140.8 (quart.); 140.7 (quart.); 133.0 (quart.); 131.4 (quart.); 131.08 (tert.); 131.06 (tert.); 130.4 (tert.); 129.8 (quart.); 126.8 (tert.); 122.8 (tert.); 120.6 (tert.); 118.4 (tert.); 115.95 (tert.); 115.89 (tert.); 115.5 (tert.); 55.7 (prim.); 41.6 (sec.); 32.8 (sec.); 32.6 (sec.); 20.6 (prim.).

**ESI pos.** (high resolution): calcd for  $[M^+] = C_{36}H_{34}N_2O_2^+$ : 526.26148; found: 526.26053 ( $\Delta = 1.80$  ppm).

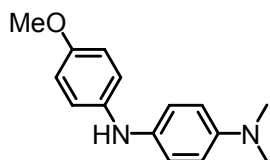
**Compound 27**

CA: [863678-32-4]

Following GP1: Compound **21** (2.80 g; 5.78 mmol), *p*-toluidine (739 mg; 6.90 mmol), Pd<sub>2</sub>(dba)<sub>3</sub>·CHCl<sub>3</sub> (61.0 mg; 58.9 μmol), P<sup>*t*</sup>Bu<sub>3</sub> (314 μl; 104 μmol), sodium *tert*-butoxide (694 mg; 7.22 mmol), toluene (20 ml); 2 d at 45 °C; flash-column chromatography (CH<sub>2</sub>Cl<sub>2</sub> : PE = 1:1 → CH<sub>2</sub>Cl<sub>2</sub>).

**Formula:** C<sub>35</sub>H<sub>30</sub>N<sub>2</sub>O<sub>2</sub> [510.62]**Yield:** 1.87 g (3.66 mmol; 63 %) yellow solid**Melting point:** 123 – 125 °C (Lit.: 123 – 125 °C)<sup>[16]</sup>

<sup>1</sup>H-NMR (400.1 MHz; [D<sub>6</sub>]acetone): δ = 7.34 (AA', 2H); 7.27 (AA', 2H); 7.12 (AA', 2H); 7.07 (AA', 4H); 7.04 (BB', 2H); 6.94 (BB', 2H); 6.86 (BB', 4H); 6.81 (BB', 2H); 5.84 (s, 1H); 3.79 (s, 6H); 2.31 (s, 3H).

**Compound 28**

[54480-44-3]

Following GP1: 4-bromo-*N,N*-dimethylaniline (2.00 g; 10.0 mmol), *p*-anisidine (1.60 g; 13.0 mmol), Pd<sub>2</sub>(dba)<sub>3</sub>·CHCl<sub>3</sub> (275 mg; 266 μmol), P(*t*-Bu)<sub>3</sub> (1.42 ml; 469 μmol), sodium *tert*-butoxide (1.38 g; 14.4 mmol), toluene (60 ml); 3 d at 80 °C; column chromatography (PE → PE : CH<sub>2</sub>Cl<sub>2</sub> = 20:1).

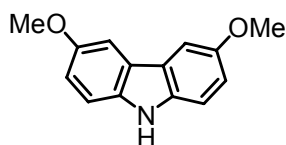


**Formula:** C<sub>15</sub>H<sub>18</sub>N<sub>2</sub>O [242.32]

**Yield:** 881 mg (3.64 mmol; 36 %) dark yellow oil

**<sup>1</sup>H-NMR** (400.1 MHz; [D<sub>6</sub>]acetone):  $\delta$  = 6.95 (AA', 2H); 6.90 (AA', 2H); 6.78 (BB', 2H); 6.72 (BB', 2H); 3.72 (s, 3H); 2.85 (s, 6H).

### Compound 30



[57103-01-2]

Sodium (1.70 g; 73.9 mmol) was dissolved in dry methanol (20 ml) and 3,6-dibromocarbazole (1.20 g; 3.69 mmol), copper-(I)-iodide (2.96 g; 15.5 mmol) and dry DMF (40 ml) were added and heated under reflux for 3 h. After ethyl acetate (160 ml) was added, the mixture was filtered over celite and washed with brine (3 x 75 ml). The solvent was removed under reduced pressure. The crude product was purified by flash-column chromatography (CH<sub>2</sub>Cl<sub>2</sub> : PE = 1:1).

**Formula:** C<sub>14</sub>H<sub>13</sub>NO<sub>2</sub> [227.26]

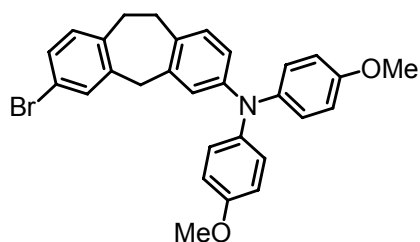
**Yield:** 750 mg (3.30 mmol; 89 %) colourless solid

**Melting point:** 113 – 114 °C

**<sup>1</sup>H-NMR** (400.1 MHz; [D<sub>6</sub>]acetone):  $\delta$  = 9.89 (s, 1H); 7.64 (d, <sup>4</sup>J<sub>HH</sub> = 2.4 Hz; 2H); 7.37 (m, 2H); 7.00 (dd, <sup>3</sup>J<sub>HH</sub> = 8.7 Hz, <sup>4</sup>J<sub>HH</sub> = 2.5 Hz, 2H); 3.87 (s, 6H).

**{<sup>1</sup>H}<sup>13</sup>C-NMR** (100.6 MHz; [D<sub>6</sub>]acetone):  $\delta$  = 154.4 (quart.); 136.6 (quart.); 124.4 (quart.); 115.9 (tert.); 112.5 (tert.); 103.5 (tert.); 56.1 (prim.).

**HRMS** (70 eV, EI): *m/z* calcd for [M<sup>+</sup>] = C<sub>14</sub>H<sub>13</sub>NO<sub>2</sub><sup>+</sup>: 227.09408; found: 227.09399 ( $\Delta$  = 0.40 ppm).

**Compound 31**

Following GP1: Compound **17** (312 mg; 886  $\mu\text{mol}$ ), di(4-methoxyphenyl)amine (204 mg; 890  $\mu\text{mol}$ ),  $\text{Pd}_2(\text{dba})_3 \cdot \text{CHCl}_3$  (11.5 mg; 11.1  $\mu\text{mol}$ ),  $\text{P}^t\text{Bu}_3$  (50.0  $\mu\text{l}$ ; 16.5  $\mu\text{mol}$ ), sodium *tert*-butoxide (106 mg; 1.10 mmol), toluene (7 ml); 60 h at 35  $^\circ\text{C}$ ; column chromatography (PE :  $\text{CH}_2\text{Cl}_2$  = 9:1).

**Formula:**  $\text{C}_{29}\text{H}_{26}\text{BrNO}_2$  [500.43]

**Yield:** 156 mg (312  $\mu\text{mol}$ ; 35 %) colourless solid

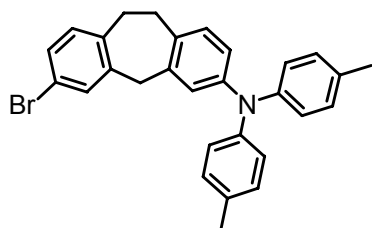
**Melting point:** 112  $^\circ\text{C}$

**$^1\text{H-NMR}$**  (400.1 MHz;  $[\text{D}_6]\text{acetone}$ ):  $\delta$  = 7.38 (d,  $^4J_{\text{HH}} = 2.1$  Hz, 1H); 7.28 (dd,  $^3J_{\text{HH}} = 8.1$  Hz,  $^4J_{\text{HH}} = 2.1$  Hz, 1H); 7.09 (d,  $^3J_{\text{HH}} = 8.2$  Hz, 1H); 6.96 (AA', 4H); 6.95 (d,  $^3J_{\text{HH}} = 5.7$  Hz, 1H); 6.86 (BB', 4H); 6.80 (d,  $^4J_{\text{HH}} = 2.4$  Hz); 6.66 (dd,  $^3J_{\text{HH}} = 8.2$  Hz,  $^4J_{\text{HH}} = 2.5$  Hz, 1H); 4.00 (s, 2H); 3.78 (s, 6H); 3.15 – 3.05 (–, 4H).

**$\{^1\text{H}\}^{13}\text{C-NMR}$**  (100.6 MHz;  $[\text{D}_6]\text{acetone}$ ):  $\delta$  = 156.8 (quart.); 147.9 (quart.); 142.7 (quart.); 142.2 (quart.); 140.0 (quart.); 139.8 (quart.); 132.4 (quart.); 132.4 (tert.); 132.3 (tert.); 131.2 (tert.); 130.2 (tert.); 127.0 (tert.); 122.7 (tert.); 120.7 (tert.); 119.7 (quart.); 115.5 (tert.); 55.7 (prim.); 40.7 (sec.); 32.7 (sec.); 32.1 (sec.).

**HRMS** (70 eV, EI):  $m/z$  calcd for  $[\text{M}^+]$  =  $\text{C}_{29}\text{H}_{26}\text{BrNO}_2^+$ : 499.11414; found: 499.11399 ( $\Delta$  = 0.26 ppm).

## Compound 32



Following GP1: Compound **17** (300 mg; 852  $\mu\text{mol}$ ), di-(4-methylphenyl)amine (168 mg; 852  $\mu\text{mol}$ ),  $\text{Pd}_2(\text{dba})_3 \cdot \text{CHCl}_3$  (11.0 mg; 10.6  $\mu\text{mol}$ ),  $\text{P}^t\text{Bu}_3$  (47.9  $\mu\text{l}$ ; 15.8  $\mu\text{mol}$ ), sodium *tert*-butoxide (102 mg; 1.06 mmol), toluene (4 ml); 20 h at 100  $^\circ\text{C}$ ; column chromatography (PE :  $\text{CH}_2\text{Cl}_2$  = 5:1).

**Formula:**  $\text{C}_{29}\text{H}_{26}\text{BrN}$  [468.43]

**Yield:** 68.0 mg (145  $\mu\text{mol}$ ; 17 %) colourless solid

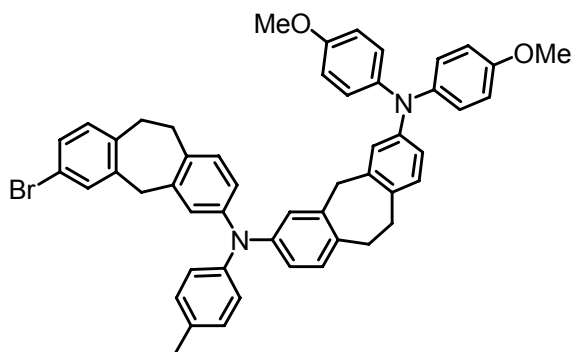
**Melting point:** 67  $^\circ\text{C}$

**$^1\text{H-NMR}$**  (400.1 MHz;  $[\text{D}_6]\text{acetone}$ ):  $\delta$  = 7.39 (d,  $^4J_{\text{HH}} = 2.0$  Hz, 1H); 7.29 (dd,  $^3J_{\text{HH}} = 8.0$  Hz,  $^4J_{\text{HH}} = 2.1$  Hz, 1H); 7.09 (d,  $^3J_{\text{HH}} = 8.2$  Hz, 1H); 7.06 (AA', 4H); 7.00 (d,  $^3J_{\text{HH}} = 8.2$  Hz, 1H); 6.90 (d,  $^4J_{\text{HH}} = 2.3$  Hz, 1H); 6.88 (BB', 4H); 6.76 (dd,  $^3J_{\text{HH}} = 8.2$  Hz,  $^4J_{\text{HH}} = 2.4$  Hz, 1H); 4.02 (s, 2H); 3.19 – 3.07 (-, 4H); 2.27 (s, 6H).

**$\{^1\text{H}\}^{13}\text{C-NMR}$**  (100.6 MHz;  $[\text{D}_6]\text{acetone}$ ):  $\delta$  = 147.2 (quart.); 146.6 (quart.); 142.7 (quart.); 140.2 (quart.); 139.7 (quart.); 133.9 (quart.); 132.8 (quart.); 132.4 (tert.); 132.3 (tert.); 131.4 (tert.); 130.7 (tert.); 130.2 (tert.); 124.9 (tert.) 124.8 (tert.); 122.8 (tert.); 119.7 (quart.); 40.5 (sec.); 32.6 (sec.); 32.2 (sec.); 20.8 (prim.).

**HRMS** (70 eV, EI):  $m/z$  calcd for  $[\text{M}^+] = \text{C}_{29}\text{H}_{26}\text{BrN}^+$ : 467.12431; found: 467.12224 ( $\Delta$  = 2.07 ppm).

## Compound 33



Following GP1: Compound **26** (480 mg; 911  $\mu\text{mol}$ ), **17** (3.00 g; 8.52 mmol),  $\text{Pd}_2(\text{dba})_3 \cdot \text{CHCl}_3$  (9.61 mg; 9.28  $\mu\text{mol}$ ),  $\text{P}^t\text{Bu}_3$  (49.5  $\mu\text{l}$ ; 16.3  $\mu\text{mol}$ ), sodium *tert*-butoxide (109 mg; 1.13 mmol), toluene (10 ml); heated in a microwave oven (gradient of heating: 10 min RT to 75  $^\circ\text{C}$ ; holding time: 30 min at 75  $^\circ\text{C}$ ); flash-column chromatography ( $\text{CH}_2\text{Cl}_2$  : PE = 1:2).

**Formula:**  $\text{C}_{51}\text{H}_{46}\text{BrN}_2\text{O}_2$  [797.82]

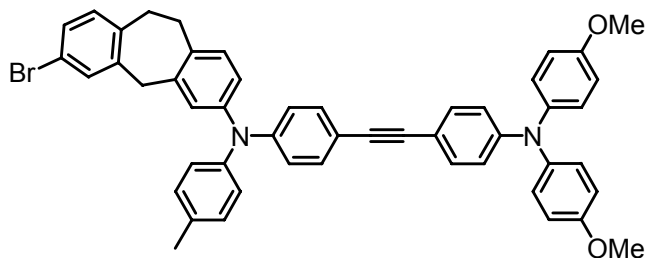
**Yield:** 210 mg (263  $\mu\text{mol}$ ; 29 %) colourless solid

**Melting point:** 138 – 140  $^\circ\text{C}$

**$^1\text{H-NMR}$**  (400.1 MHz;  $[\text{D}_6]\text{acetone}$ ):  $\delta$  = 7.37 (d,  $^4J_{\text{HH}} = 2.0$  Hz, 1H); 7.28 (dd,  $^3J_{\text{HH}} = 8.1$  Hz,  $^4J_{\text{HH}} = 2.0$  Hz, 1H); 7.15 – 6.89 (-, 11H); 6.88 – 6.77 (-, 7H); 6.75 – 6.68 (-, 3H); 6.66 (dd,  $^3J_{\text{HH}} = 8.2$  Hz,  $^4J_{\text{HH}} = 2.4$  Hz, 1H); 3.97 (s, 2H); 3.82 (s, 2H); 3.75 (s, 6H); 3.18 – 3.04 (-, 8H); 2.26 (s, 3H).

**$\{^1\text{H}\}^{13}\text{C-NMR}$**  (150.9 MHz;  $[\text{D}_6]\text{acetone}$ ):  $\delta$  = 156.6 (quart.); 147.8 (quart.); 147.0 (quart.); 146.8 (quart.); 146.4 (quart.); 142.7 (quart.); 142.2 (quart.); 140.9 (quart.); 140.7 (quart.); 140.1 (quart.); 139.8 (quart.); 134.4 (quart.); 133.8 (quart.); 132.8 (quart.); 132.31 (quart.); 132.28 (tert.); 131.4 (tert.); 131.3 (tert.); 131.0 (tert.); 130.7 (tert.); 130.6 (tert.); 130.2 (tert.); 126.9 (tert.); 126.8 (tert.); 125.0 (tert.); 123.0 (tert.); 122.8 (tert.); 122.7 (tert.); 122.6 (tert.); 120.4 (tert.); 119.7 (quart.); 115.4 (tert.); 55.7 (prim.); 41.2 (sec.); 40.4 (sec.); 32.8 (sec.); 32.53 (sec.); 52.49 (sec.); 32.2 (sec.); 20.8 (prim.).

**ESI pos.** (high resolution): calcd for  $[\text{M}+\text{H}^+] = \text{C}_{51}\text{H}_{46}\text{BrN}_2\text{O}_2^+$ : 797.27372; found: 797.27368 ( $\Delta = 0.04$  ppm).

**Compound 34**

Following GP1: Compound **27** (218 mg, 427  $\mu\text{mol}$ ), **17** (300 mg, 852  $\mu\text{mol}$ ),  $\text{Pd}_2(\text{dba})_3 \cdot \text{CHCl}_3$  (6.00 mg; 5.80  $\mu\text{mol}$ ),  $\text{P}^t\text{Bu}_3$  (24.0  $\mu\text{l}$ ; 7.92  $\mu\text{mol}$ ), sodium tert-butoxide (51.0 mg; 531  $\mu\text{mol}$ ), toluene (10 ml); heated in a microwave oven (gradient of heating: 10 min RT to 75  $^\circ\text{C}$ ; holding time: 20 min at 75  $^\circ\text{C}$ ); flash-column chromatography ( $\text{CH}_2\text{Cl}_2$  : PE = 1:1).

**Formula:**  $\text{C}_{50}\text{H}_{41}\text{BrN}_2\text{O}_2$  [781.78]

**Yield:** 103 mg (132  $\mu\text{mol}$ ; 31 %) yellow solid

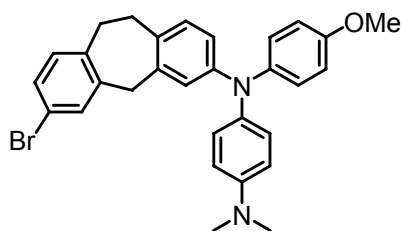
**Melting point:** 139 – 141  $^\circ\text{C}$

**$^1\text{H-NMR}$**  (400.1 MHz;  $[\text{D}_6]\text{acetone}$ ):  $\delta$  = 7.41 (m, 1H); 7.33 – 7.26 (-, 5H); 7.16 – 7.06 (-, 8H); 7.02 – 6.91 (-, 7H); 6.90 – 6.84 (-, 3H); 6.78 (BB', 2H); 4.07 (s, 2H); 3.80 (s, 6H); 3.17 – 3.13 (-, 4H); 2.31 (s, 3H).

**$\{^1\text{H}\}^{13}\text{C-NMR}$**  (150.9 MHz;  $[\text{D}_6]\text{acetone}$ ):  $\delta$  = 157.7 (quart.); 149.8 (quart.); 148.9 (quart.); 146.1 (quart.); 145.5 (quart.); 142.6 (quart.); 140.9 (quart.); 140.6 (quart.); 139.7 (quart.); 135.4 (quart.); 134.3 (quart.); 133.0 (tert.); 133.0 (tert.); 132.4 (tert.); 132.3 (tert.); 131.7 (tert.); 131.0 (tert.); 130.2 (tert.); 128.3 (tert.); 126.4 (tert.); 126.2 (tert.); 124.3 (tert.); 122.0 (tert.); 119.7 (quart.); 119.4 (tert.); 116.7 (quart.); 115.8 (tert.); 114.9 (quart.); 89.7 (quart.); 89.0 (quart.); 55.7 (prim.); 40.3 (sec.); 32.5 (sec.); 32.3 (sec.); 20.8 (prim.).

**ESI pos.** (high resolution): calcd for  $[\text{M}^+] = \text{C}_{50}\text{H}_{41}\text{BrN}_2\text{O}_2^+$ : 780.23459; found: 780.23283 ( $\Delta$  = 2.26 ppm).

## Compound 35



Following GP1: Compound **28** (250 mg; 1.03 mmol), **17** (1.20 g; 3.41 mmol), Pd<sub>2</sub>(dba)<sub>3</sub>·CHCl<sub>3</sub> (14.5 mg; 14.0 μmol), P<sup>t</sup>Bu<sub>3</sub> (57.9 μl; 19.1 μmol), sodium *tert*-butoxide (123 mg; 1.28 mmol), toluene (10 ml); heated in a microwave oven (gradient of heating: 10 min RT to 100 °C; holding time: 1 h at 100 °C); flash-column chromatography (CH<sub>2</sub>Cl<sub>2</sub>).

**Formula:** C<sub>30</sub>H<sub>29</sub>BrN<sub>2</sub>O [513.47]

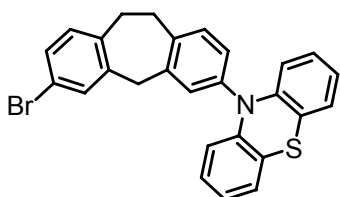
**Yield:** 244 mg (475 μmol; 46 %) yellow oil

**<sup>1</sup>H-NMR** (400.1 MHz; [D<sub>6</sub>]acetone): δ = 7.38 (d, <sup>4</sup>J<sub>HH</sub> = 2.0 Hz, 1H); 7.28 (dd, <sup>3</sup>J<sub>HH</sub> = 8.1 Hz, <sup>4</sup>J<sub>HH</sub> = 2.1 Hz, 1H); 7.08 (d, <sup>3</sup>J<sub>HH</sub> = 8.1 Hz, 1H); 6.99 – 6.88 (-, 5H); 6.84 (BB', 2H); 6.79 – 6.60 (-, 4H); 3.98 (s, 2H); 3.77 (s, 3H); 3.16 – 3.01 (-, 4H); 2.91 (s, 6H).

**{<sup>1</sup>H}<sup>13</sup>C-NMR** (150.9 MHz; [D<sub>6</sub>]acetone): δ = 156.3 (quart.); 148.42 (quart.); 148.40 (quart.); 148.1 (quart.); 142.7 (quart.); 142.3 (quart.); 139.7 (quart.); 138.3 (quart.); 132.3 (tert.); 132.2 (tert.); 131.5 (quart.); 130.9 (tert.); 130.0 (tert.); 127.4 (tert.); 126.4 (tert.); 121.7 (tert.); 119.8 (tert.); 119.6 (quart.); 115.3 (tert.); 114.4 (tert.); 55.6 (prim.); 40.9 (prim.); 40.6 (sec.); 32.7 (sec.); 32.0 (sec.).

**HRMS** (70 eV, EI): *m/z* calcd for [M<sup>+</sup>] = C<sub>30</sub>H<sub>29</sub>BrN<sub>2</sub>O<sup>+</sup>: 512.14578; found: 512.14527 (Δ = 1.00 ppm).

## Compound 36



Following GP1: Compound **17** (200 mg; 568  $\mu\text{mol}$ ), phenothiazine (102 mg; 512  $\mu\text{mol}$ ),  $\text{Pd}_2(\text{dba})_3 \cdot \text{CHCl}_3$  (16.7 mg; 16.1  $\mu\text{mol}$ ),  $\text{P}^t\text{Bu}_3$  (71.0  $\mu\text{l}$ ; 23.4  $\mu\text{mol}$ ), sodium *tert*-butoxide (136 mg; 1.42 mmol), toluene (10 ml); heated in a microwave oven (gradient of heating: 10 min RT to 45  $^\circ\text{C}$ ; holding time: 40 min at 45  $^\circ\text{C}$ ); flash-column chromatography ( $\text{CH}_2\text{Cl}_2$  : PE = 1:7).

**Formula:**  $\text{C}_{27}\text{H}_{20}\text{BrNS}$  [470.42]

**Yield:** 81.0 mg (172  $\mu\text{mol}$ ; 34 %) colourless solid

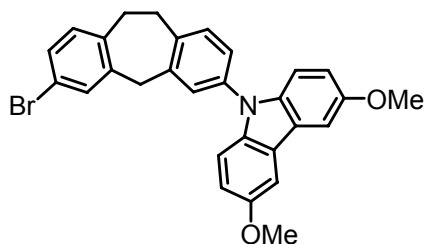
**Melting point:** 218 – 220 $^\circ\text{C}$

**$^1\text{H-NMR}$**  (400.1 MHz;  $[\text{D}_6]\text{acetone}$ ):  $\delta$  = 7.47 (d,  $^4\text{J}_{\text{HH}} = 2.0$  Hz, 1H); 7.44 (d,  $^3\text{J}_{\text{HH}} = 8.0$  Hz, 1H); 7.33 (dd,  $^3\text{J}_{\text{HH}} = 8.1$  Hz,  $^4\text{J}_{\text{HH}} = 2.1$  Hz, 1H); 7.30 (d,  $^4\text{J}_{\text{HH}} = 2.3$  Hz, 1H); 7.22 (dd,  $^3\text{J}_{\text{HH}} = 8.0$  Hz,  $^4\text{J}_{\text{HH}} = 2.3$  Hz, 1H); 7.16 (d,  $^3\text{J}_{\text{HH}} = 8.2$  Hz, 1H); 7.02 (dd,  $^3\text{J}_{\text{HH}} = 7.3$  Hz,  $^4\text{J}_{\text{HH}} = 1.83$  Hz, 2H); 6.90 – 6.78 (-, 4H); 6.22 (dd,  $^3\text{J}_{\text{HH}} = 8.1$  Hz,  $^4\text{J}_{\text{HH}} = 1.3$  Hz, 2H); 4.26 (s, 2H); 3.34 – 3.20 (-, 4H).

**$\{^1\text{H}\}^{13}\text{C-NMR}$**  (100.6 MHz;  $[\text{D}_6]\text{acetone}$ ):  $\delta$  = 145.3 (quart.); 142.5 (quart.); 142.3 (quart.); 140.4 (quart.); 139.7 (quart.); 139.5 (quart.); 133.0 (tert.); 132.4 (tert.); 132.3 (tert.); 132.0 (tert.); 130.5 (tert.); 130.0 (tert.); 127.9 (tert.); 127.4 (tert.); 123.4 (tert.); 120.8 (quart.); 120.0 (quart.); 117.0 (tert.); 40.3 (sec.); 32.7 (sec.); 32.2 (sec.).

**ESI pos.** (high resolution): calcd for  $[\text{M}^+] = \text{C}_{27}\text{H}_{20}\text{BrNS}^+$ : 469.04943; found: 469.04998 ( $\Delta = 1.17$  ppm).

## Compound 37



Following GP1: Compound **30** (675 mg; 2.97 mmol), **17** (4.96 g; 14.1 mmol), Pd<sub>2</sub>(dba)<sub>3</sub>·CHCl<sub>3</sub> (34.8 mg; 33.6 μmol), P<sup>t</sup>Bu<sub>3</sub> (179 μl; 59.1 μmol), sodium *tert*-butoxide (395 mg; 4.11 mmol), toluene (20 ml); heated in a microwave oven (gradient of heating: 10 min RT to 80 °C; holding time: 1 h at 80 °C); flash-column chromatography (CH<sub>2</sub>Cl<sub>2</sub> : PE = 1:2).

**Formula:** C<sub>29</sub>H<sub>24</sub>BrNO<sub>2</sub> [498.41]

**Yield:** 478 mg (959 μmol; 32 %) light yellow solid

**Melting point:** 99 °C

**<sup>1</sup>H-NMR** (400.1 MHz; [D<sub>6</sub>]acetone): δ = 7.74 (d, <sup>4</sup>J<sub>HH</sub> = 2.5 Hz; 2H); 7.49 – 7.36 (-, 3H); 7.36 – 7.31 (-, 2H); 7.29 (d, <sup>3</sup>J<sub>HH</sub> = 9.0 Hz, 2H); 7.15 (d, <sup>3</sup>J<sub>HH</sub> = 8.1 Hz, 1H); 7.02 (dd, <sup>3</sup>J<sub>HH</sub> = 9.0 Hz, <sup>4</sup>J<sub>HH</sub> = 2.5 Hz, 2H); 4.28 (s, 2H); 3.90 (s, 6H); 3.34 – 3.20 (-, 4H).

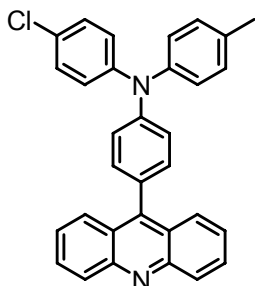
**{<sup>1</sup>H}<sup>13</sup>C-NMR** (150.9 MHz; [D<sub>6</sub>]acetone): δ = 155.2 (quart.); 141.9 (quart.); 140.2 (quart.); 139.9 (quart.); 139.1 (quart.); 137.1 (quart.); 136.7 (quart.); 132.1 (tert.); 130.3 (tert.); 129.8 (tert.); 127.61 (tert.); 127.59 (tert.); 127.0 (tert.); 125.3 (quart.); 124.6 (quart.); 116.0 (tert.); 111.5 (tert.); 103.8 (tert.); 56.2 (prim.); 40.9 (sec.); 32.9 (sec.); 32.8 (sec.).

**ESI pos.** (high resolution): calcd for [M<sup>+</sup>] = C<sub>29</sub>H<sub>24</sub>BrNO<sub>2</sub><sup>+</sup>: 497.09849; found: 497.09897 (Δ = 0.95 ppm).



### 4.2.3 Synthesis of Reference Chromophores

#### Chromophore 1



Following GP1: Compound **12** (152 mg; 399  $\mu\text{mol}$ ), 4-iodotoluene (176 mg; 807  $\mu\text{mol}$ ),  $\text{Pd}_2(\text{dba})_3 \cdot \text{CHCl}_3$  (22.4 mg; 21.6  $\mu\text{mol}$ ),  $\text{P}^t\text{Bu}_3$  (102  $\mu\text{l}$ ; 33.7  $\mu\text{mol}$ ), sodium *tert*-butoxide (97.0 mg; 1.01 mmol), toluene (5 ml); 24 h at 45 °C; flash-column chromatography ( $\text{CH}_2\text{Cl}_2$  : EtOAc = 30:1).

**Formula:**  $\text{C}_{32}\text{H}_{23}\text{ClN}_2$  [470.99]

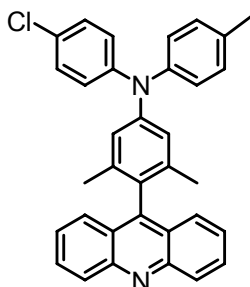
**Yield:** 143 mg (304  $\mu\text{mol}$ ; 76 %) yellow solid

**Melting point:** 247 °C

**$^1\text{H-NMR}$**  (400.1 MHz;  $[\text{D}_6]\text{acetone}$ ):  $\delta$  = 8.22 (ddd,  $^3J_{\text{HH}} = 8.6$  Hz,  $^4J_{\text{HH}} = 1.0$  Hz,  $^5J_{\text{HH}} = 1.0$  Hz, 2H); 7.86 (ddd,  $^3J_{\text{HH}} = 8.6$  Hz,  $^4J_{\text{HH}} = 1.3$  Hz,  $^5J_{\text{HH}} = 0.7$  Hz, 2H); 7.83 (ddd,  $^3J_{\text{HH}} = 8.7$  Hz,  $^3J_{\text{HH}} = 6.6$  Hz,  $^4J_{\text{HH}} = 1.4$  Hz, 2H); 7.54 (ddd,  $^3J_{\text{HH}} = 8.7$  Hz,  $^3J_{\text{HH}} = 6.6$  Hz,  $^4J_{\text{HH}} = 1.2$  Hz, 2H); 7.41 (AA', 2H); 7.36 (AA', 2H); 7.30 (BB', 2H); 7.26 (AA', 2H); 7.22 (BB', 2H); 7.19 (BB', 2H); 2.36 (s, 3H).

**$\{^1\text{H}\}^{13}\text{C-NMR}$**  (100.6 MHz;  $[\text{D}_6]\text{acetone}$ ):  $\delta$  = 149.3 (quart.); 148.2 (quart.); 147.4 (quart.); 146.9 (quart.); 144.9 (quart.); 134.6 (quart.); 131.9 (tert.); 130.7 (tert.); 130.2 (tert.); 130.0 (tert.); 129.7 (tert.); 129.6 (quart.); 127.9 (quart.); 127.3 (tert.); 126.0 (tert.); 125.8 (tert.); 125.7 (quart.); 125.5 (tert.); 122.7 (tert.); 21.0 (prim.).

**HRMS** (70 eV, EI):  $m/z$  calcd for  $[\text{M}^+] = \text{C}_{32}\text{H}_{23}\text{ClN}_2^+$ : 470.15443; found: 470.15489 ( $\Delta = 0.98$  ppm).

**Chromophore 2**

Following GP1: Compound **22** (100 mg; 245  $\mu\text{mol}$ ), 4-iodotoluene (65.4 mg; 300  $\mu\text{mol}$ ),  $\text{Pd}_2(\text{dba})_3 \cdot \text{CHCl}_3$  (3.47 mg; 3.35  $\mu\text{mol}$ ),  $\text{P}^t\text{Bu}_3$  (17.8  $\mu\text{l}$ ; 5.87  $\mu\text{mol}$ ), sodium *tert*-butoxide (31.9 mg; 332  $\mu\text{mol}$ ), toluene (4 ml); 18 h at 95  $^\circ\text{C}$ ; flash-column chromatography ( $\text{CH}_2\text{Cl}_2$  : EtOAc = 40:1).

**Formula:**  $\text{C}_{34}\text{H}_{27}\text{ClN}_2$  [499.04]

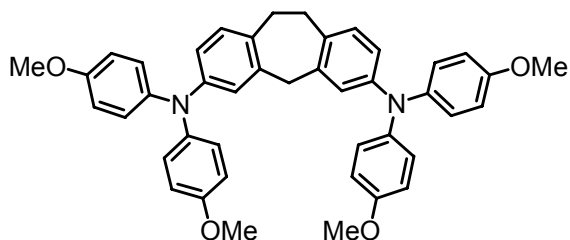
**Yield:** 110 mg (220  $\mu\text{mol}$ ; 90 %) yellow solid

**Melting point:** 252 $^\circ\text{C}$

**$^1\text{H-NMR}$**  (400.1 MHz;  $[\text{D}_6]\text{acetone}$ ):  $\delta$  = 8.25 (m, 2H); 7.85 (ddd,  $^3\text{J}_{\text{HH}} = 8.8$  Hz,  $^3\text{J}_{\text{HH}} = 6.4$  Hz,  $^4\text{J}_{\text{HH}} = 1.6$  Hz, 2H); 7.61 (ddd,  $^3\text{J}_{\text{HH}} = 8.7$  Hz,  $^4\text{J}_{\text{HH}} = 1.5$  Hz,  $^5\text{J}_{\text{HH}} = 0.7$  Hz, 2H); 7.55 (ddd,  $^3\text{J}_{\text{HH}} = 8.7$  Hz,  $^3\text{J}_{\text{HH}} = 6.4$  Hz,  $^4\text{J}_{\text{HH}} = 1.2$  Hz, 2H); 7.33 (AA', 2H); 7.23 (AA', 2H); 7.19 – 7.13 (-, 4H); 7.03 (s, 2H); 2.35 (s, 3H); 1.65 (s, 6H).

**$\{^1\text{H}\}^{13}\text{C-NMR}$**  (100.6 MHz;  $[\text{D}_2]\text{dichloromethane}$ ):  $\delta$  = 149.5 (quart.); 148.0 (quart.); 147.3 (quart.); 146.8 (quart.); 145.2 (quart.); 138.3 (quart.); 134.0 (quart.); 130.5 (tert.); 130.4 (tert.); 130.3 (tert.); 129.7 (quart.); 129.5 (tert.); 127.2 (quart.); 126.4 (tert.); 126.3 (tert.); 125.7 (tert.); 125.6 (quart.); 125.0 (tert.); 122.8 (tert.); 21.0 (prim.); 20.2 (prim.).

**HRMS** (70 eV, EI):  $m/z$  calcd for  $[\text{M}^+] = \text{C}_{34}\text{H}_{27}\text{ClN}_2^+$ : 498.18577; found: 498.18580 ( $\Delta = 0.08$  ppm).

**Chromophore 11**

Chromophore **11** was obtained as a secondary product within the synthesis of **31**.

**Formula:**  $C_{43}H_{40}N_2O_4$  [648.79]

**Yield:** 134 mg (207  $\mu$ mol; 47 %) colourless solid

**Melting point:** 124 °C

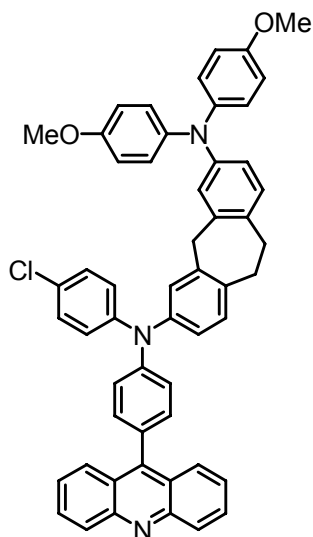
**$^1\text{H-NMR}$**  (400.1 MHz;  $[\text{D}_6]\text{acetone}$ ):  $\delta$  = 6.97 – 6.92 (–, 10H); 6.84 (BB', 8H); 6.72 (d,  $^4J_{\text{HH}}$  = 2.4 Hz, 2H); 6.66 (dd,  $^3J_{\text{HH}}$  = 8.2 Hz,  $^4J_{\text{HH}}$  = 2.5 Hz, 2H); 3.83 (s, 2H); 3.77 (s, 12H); 3.06 (s, 4H).

**$\{^1\text{H}\}^{13}\text{C-NMR}$**  (100.6 MHz;  $[\text{D}_6]\text{acetone}$ ):  $\delta$  = 156.7 (quart.); 147.7 (quart.); 142.2 (quart.); 140.7 (quart.); 132.8 (quart.); 131.1 (tert.); 126.9 (tert.); 122.7 (tert.); 120.4 (tert.); 115.5 (tert.); 55.7 (prim.); 41.5 (sec.); 32.7 (sec.).

**HRMS** (70 eV, EI):  $m/z$  calcd for  $[\text{M}^+] = C_{43}H_{40}N_2O_4^{+}$ : 648.29826; found: 648.29844 ( $\Delta$  = 0.28 ppm).

## 4.2.4 Synthesis of Cascades

## Cascade 3



Following GP1: Compound **12** (95.2 mg; 250  $\mu\text{mol}$ ), **23** (123 mg; 246  $\mu\text{mol}$ ),  $\text{Pd}_2(\text{dba})_3 \cdot \text{CHCl}_3$  (3.91 mg; 3.78  $\mu\text{mol}$ ),  $\text{P}^t\text{Bu}_3$  (17.8  $\mu\text{l}$ ; 5.87  $\mu\text{mol}$ ), sodium *tert*-butoxide (32.1 mg; 334  $\mu\text{mol}$ ), toluene (4 ml); 16 h at 100  $^\circ\text{C}$ ; column chromatography (PE  $\rightarrow$  PE :  $\text{CH}_2\text{Cl}_2$  = 2:1  $\rightarrow$  PE :  $\text{CH}_2\text{Cl}_2$  = 1:1  $\rightarrow$  PE :  $\text{CH}_2\text{Cl}_2$  = 1:2).

**Formula:**  $\text{C}_{54}\text{H}_{42}\text{ClN}_3\text{O}_2$  [800.38]

**Yield:** 73.0 mg (91.2  $\mu\text{mol}$ ; 36 %) yellow solid

**Melting point:** 142 – 145  $^\circ\text{C}$

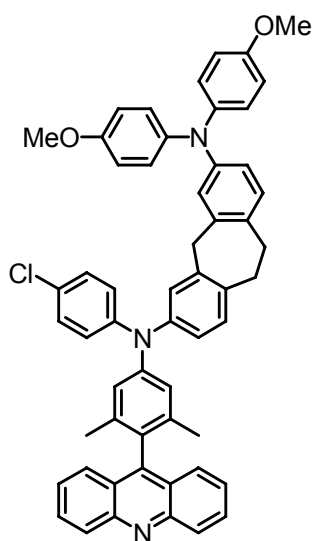
**$^1\text{H-NMR}$**  (600.1 MHz;  $[\text{D}_2]$ dichloromethane):  $\delta$  = 8.22 (m, 2H); 7.87 (m, 2H); 7.78 (ddd,  $^3J_{\text{HH}}$  = 8.7 Hz,  $^3J_{\text{HH}}$  = 6.6 Hz,  $^4J_{\text{HH}}$  = 1.3 Hz, 2H); 7.47 (ddd,  $^3J_{\text{HH}}$  = 8.7 Hz,  $^3J_{\text{HH}}$  = 6.6 Hz,  $^4J_{\text{HH}}$  = 1.2 Hz, 2H); 7.34 – 7.20 (-, 7H); 7.15 (AA', 2H); 7.05 – 6.94 (-, 7H); 6.79 (BB', 4H); 6.75 (d,  $^4J_{\text{HH}}$  = 2.4 Hz, 1H); 6.70 (dd,  $^3J_{\text{HH}}$  = 8.2 Hz,  $^4J_{\text{HH}}$  = 2.4 Hz, 1H); 3.91 (s, 2H); 3.73 (s, 6H); 3.18 - 3.08 (-, 4H).

**$\{^1\text{H}\}^{13}\text{C-NMR}$**  (150.9 MHz;  $[\text{D}_2]$ dichloromethane):  $\delta$  = 156.0 (quart.); 149.3 (quart.); 148.1 (quart.); 147.2 (quart.); 146.8 (quart.); 145.2 (quart.); 141.6 (quart.); 140.9 (quart.); 139.8 (quart.); 135.9 (quart.); 132.2 (quart.); 131.9 (tert.); 131.2 (tert.); 130.5 (tert.); 130.1 (tert.); 130.0 (tert.); 129.7 (tert.); 129.6 (quart.); 128.0 (quart.); 127.3 (tert.); 126.5 (tert.); 126.4 (tert.); 126.1 (tert.); 125.8 (tert.); 125.7 (tert.); 125.6 (quart.); 124.0 (tert.); 122.7 (tert.); 122.0 (tert.);

120.0 (tert.); 114.9 (quart.); 55.8 (prim.); 41.3 (sec.); 32.6 (sec.); 32.1 (sec.).

**HRMS** (70 eV, EI):  $m/z$  calcd for  $[M^+] = C_{54}H_{42}ClN_3O_2^+$ : 799.29601; found: 799.29713 ( $\Delta = 1.40$  ppm).

#### Cascade 4



Following GP1: Compound **22** (95.0 mg; 232  $\mu$ mol), **30** (115 mg; 230  $\mu$ mol),  $Pd_2(dba)_3 \cdot CHCl_3$  (3.26 mg; 3.15  $\mu$ mol),  $P^tBu_3$  (16.7  $\mu$ l; 5.51  $\mu$ mol), sodium *tert*-butoxide (30.0 mg; 312  $\mu$ mol), toluene (4 ml); 17 h at 100 °C; column chromatography ( $CH_2Cl_2$  : PE = 1:1).

**Formula:**  $C_{56}H_{46}ClN_3O_2$  [828.44]

**Yield:** 131 mg (158  $\mu$ mol; 69 %) yellow solid

**Melting point:** 191 °C

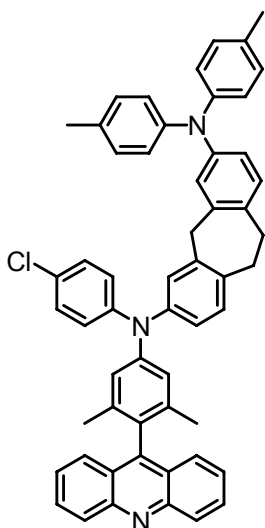
**$^1H$ -NMR** (400.1 MHz;  $[D_2]$ dichloromethane):  $\delta$  = 8.25 (m, 2H); 7.79 (ddd,  $^3J_{HH} = 8.7$  Hz;  $^3J_{HH} = 6.6$  Hz,  $^4J_{HH} = 1.5$  Hz, 2H); 7.61 (ddd,  $^3J_{HH} = 8.8$  Hz,  $^4J_{HH} = 1.2$  Hz,  $^5J_{HH} = 0.5$  Hz, 2H); 7.47 (ddd,  $^3J_{HH} = 8.7$  Hz,  $^3J_{HH} = 6.5$  Hz,  $^4J_{HH} = 1.2$  Hz, 2H); 7.25 (AA', 2H); 7.14 – 7.07 (-, 3H); 7.03 – 6.92 (-, 9H); 6.79 (BB', 4H); 6.75 (d,  $^4J_{HH} = 2.2$  Hz, 1H); 6.71 (dd,  $^3J_{HH} = 8.1$  Hz,  $^4J_{HH} = 2.2$  Hz, 1H); 3.91 (s, 2H); 3.75 (s, 6H); 3.19 – 3.08 (-, 4H); 1.62 (s, 6H).

**$\{^1H\}^{13}C$ -NMR** (100.6 MHz;  $[D_2]$ dichloromethane):  $\delta$  = 156.1 (quart.); 149.5 (quart.); 147.8 (quart.); 147.3 (quart.); 147.2 (quart.); 145.5 (quart.); 141.7 (quart.); 140.7 (quart.); 140.0 (quart.); 138.4 (quart.); 135.4 (quart.); 132.2 (quart.); 131.1

(tert.); 130.5 (tert.); 130.4 (tert.); 130.3 (tert.); 129.8 (tert.); 129.5 (tert.); 127.3 (quart.); 126.5 (quart.); 126.4 (tert.); 126.3 (tert.); 125.8 (tert.); 125.6 (quart.); 125.3 (tert.); 123.7 (quart.); 123.6 (tert.); 122.9 (tert.); 122.0 (tert.); 120.0 (tert.); 114.9 (tert.); 55.8 (prim.); 41.4 (sec.); 32.6 (sec.); 32.1 (sec.); 20.2 (prim.).

**HRMS** (70 eV, EI):  $m/z$  calcd for  $[M^+] = C_{56}H_{46}ClN_3O_2^{++}$ : 827.32731; found: 827.32697 ( $\Delta = 0.41$  ppm).

### Cascade 5



Following GP1: Compound **22** (60.0 mg; 147  $\mu$ mol), **31** (68.0 mg; 145  $\mu$ mol),  $Pd_2(dba)_3 \cdot CHCl_3$  (2.06 mg; 1.99  $\mu$ mol),  $P^tBu_3$  (10.5  $\mu$ l; 3.47  $\mu$ mol), sodium *tert*-butoxide (18.9 mg; 197  $\mu$ mol), toluene (3 ml); 20 h at 100 °C; flash-column chromatography ( $CH_2Cl_2 \rightarrow CH_2Cl_2 : EtOAc = 40:1$ ).

**Formula:**  $C_{56}H_{46}ClN_3$  [796.44]

**Yield:** 74.3 mg (93.3  $\mu$ mol; 64 %) yellow solid

**Melting point:** 192 °C

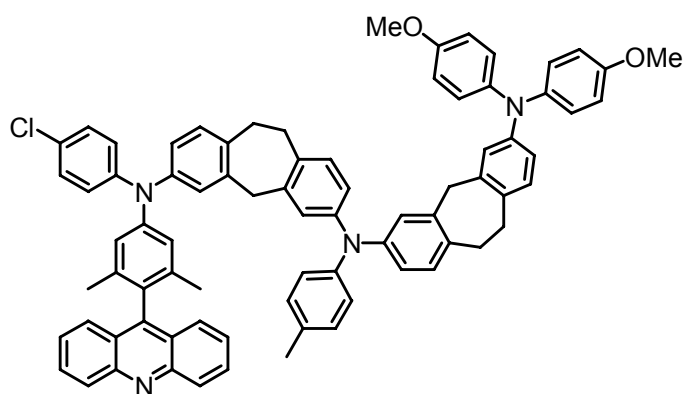
**$^1H$ -NMR** (400.1 MHz;  $[D_2]$ dichloromethane):  $\delta$  = 8.25 (m, 2H); 7.79 (ddd,  $^3J_{HH} = 8.7$  Hz,  $^3J_{HH} = 6.5$  Hz,  $^4J_{HH} = 1.4$  Hz, 2H); 7.60 (m, 2H); 7.46 (ddd,  $^3J_{HH} = 8.6$  Hz,  $^3J_{HH} = 6.5$  Hz,  $^4J_{HH} = 1.2$  Hz, 2H); 7.25 (AA', 2H); 7.15 – 7.08 (-, 3H); 7.03 (AA', 4H); 7.01 – 6.97 (-, 3H); 6.95 (s, 2H); 6.91 (BB', 4H); 6.84 (d,  $^4J_{HH} =$

2.3 Hz, 1H); 6.79 (dd,  $^3J_{\text{HH}} = 8.1$  Hz,  $^4J_{\text{HH}} = 2.5$  Hz, 1H); 3.93 (s, 2H); 3.15 (s, 4H); 2.27 (s, 6H); 1.63 (s, 6H).

$\{^1\text{H}\}^{13}\text{C-NMR}$  (150.9 MHz;  $[\text{D}_2]$ dichloromethane):  $\delta = 149.5$  (quart.); 147.8 (quart.); 147.1 (quart.); 146.7 (quart.); 146.6 (quart.); 145.9 (quart.); 145.5 (quart.); 140.6 (quart.); 140.1 (quart.); 138.3 (quart.); 135.3 (quart.); 133.5 (quart.); 132.5 (quart.); 131.1 (tert.); 130.6 (tert.); 130.4 (tert.); 130.3 (tert.); 130.1 (tert.); 129.8 (quart.); 129.5 (tert.); 127.3 (quart.); 126.4 (tert.); 126.3 (tert.); 125.7 (quart.); 125.6 (tert.); 125.3 (tert.); 124.5 (tert.); 124.0 (tert.); 123.6 (tert.); 122.9 (tert.); 122.0 (tert.); 41.2 (sec.); 32.5 (sec.); 32.2 (sec.); 20.8 (prim.); 20.2 (prim.).

**HRMS** (70 eV, EI):  $m/z$  calcd for  $[\text{M}^+] = \text{C}_{56}\text{H}_{46}\text{ClN}_3$ : 795.33748; found: 795.33828 ( $\Delta = 1.40$  ppm).

### Cascade 6



Following GP1: Compound **22** (101 mg; 247  $\mu\text{mol}$ ), **32** (200 mg; 251  $\mu\text{mol}$ ),  $\text{Pd}_2(\text{dba})_3 \cdot \text{CHCl}_3$  (3.56 mg; 3.44  $\mu\text{mol}$ ),  $\text{P}^t\text{Bu}_3$  (18.3  $\mu\text{l}$ ; 6.04  $\mu\text{mol}$ ), sodium *tert*-butoxide (32.8 mg; 341  $\mu\text{mol}$ ), toluene (10 ml); heated in a microwave oven (gradient of heating: 10 min RT to 90  $^\circ\text{C}$ ; holding time: 30 min at 90  $^\circ\text{C}$ ); column chromatography ( $\text{CH}_2\text{Cl}_2$  : PE = 1:2).

**Formula:**  $\text{C}_{78}\text{H}_{65}\text{ClN}_4\text{O}_2$  [1125.83]

**Yield:** 106 mg (94.2  $\mu\text{mol}$ ; 38 %) yellow solid

**Melting point:** 187 – 188  $^\circ\text{C}$

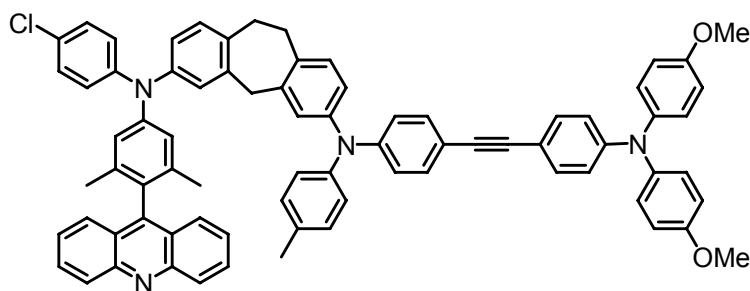
$^1\text{H-NMR}$  (400.1 MHz;  $[\text{D}_2]$ dichloromethane):  $\delta = 8.25$  (AA', 2H); 7.78 (ddd,  $^3J_{\text{HH}} = 8.68$  Hz,  $^3J_{\text{HH}} = 6.60$  Hz,  $^4J_{\text{HH}} = 1.48$  Hz, 2H); 7.60 (AA', 2H); 7.46 (ddd,  $^3J_{\text{HH}} = 8.62$  Hz,  $^3J_{\text{HH}} = 6.54$  Hz,  $^4J_{\text{HH}} = 1.17$  Hz, 2H); 7.24 (AA', 2H); 7.14 – 7.08

(-, 3H); 7.05 – 6.88 (-, 15H); 6.84 (d,  $^4J_{\text{HH}} = 2.27$  Hz, 1H); 6.80 – 6.73 (-, 7H); 6.71 – 6.65 (-, 2H); 3.92 (s, 2H); 3.80 (s, 2H); 3.74 (s, 6H); 3.18 – 3.08 (-, 4H); 3.07 – 3.00 (-, 4H); 2.27 (s, 3H); 1.62 (s, 6).

**$\{^1\text{H}\}^{13}\text{C-NMR}$**  (150.9 MHz;  $[\text{D}_2]$ dichloromethane):  $\delta = 156.0$  (quart.); 147.8 (quart.); 147.13 (quart.); 147.11 (quart.); 146.4 (quart.); 146.2 (quart.); 145.7 (quart.); 145.5 (quart.); 141.6 (quart.); 140.6 (quart.); 140.2 (quart.); 140.05 (quart.); 139.99 (quart.); 138.3 (quart.); 135.3 (quart.); 133.8 (quart.); 133.6 (quart.); 132.7 (quart.); 132.2 (quart.); 131.1 (tert.); 130.70 (tert.); 130.67 (tert.); 130.4 (tert.); 130.31 (quart.); 130.29 (quart.); 130.1 (tert.); 129.5 (tert.); 127.3 (quart.); 126.45 (tert.); 126.40 (tert.); 126.30 (tert.); 126.29 (tert.); 126.28 (tert.); 126.27 (tert.); 125.7 (tert.); 125.59 (quart.); 125.57 (quart.); 125.3 (tert.); 124.7 (tert.); 124.34 (tert.); 124.25 (tert.); 123.6 (tert.); 122.9 (tert.); 122.2 (tert.); 121.9 (tert.); 119.8 (tert.); 114.9 (tert.); 55.7 (prim.); 41.3 (sec.); 41.2 (sec.); 32.5 (sec.); 32.4 (sec.); 32.25 (sec.); 32.17 (sec.); 20.8 (prim.); 20.2 (prim.).

**ESI pos.** (high resolution): calcd for  $[\text{M}^+] = \text{C}_{78}\text{H}_{65}\text{ClN}_4\text{O}_2^{+}$ : 1124.47906; found: 1124.47791 ( $\Delta = 1.02$  ppm).

### Cascade 7



Following GP1: Compound **22** (52.0 mg; 127  $\mu\text{mol}$ ), **33** (100 mg; 128  $\mu\text{mol}$ ),  $\text{Pd}_2(\text{dba})_3\cdot\text{CHCl}_3$  (3.47 mg; 3.35  $\mu\text{mol}$ ),  $\text{P}^t\text{Bu}_3$  (17.9  $\mu\text{l}$ ; 5.91  $\mu\text{mol}$ ), sodium *tert*-butoxide (16.7 mg; 174  $\mu\text{mol}$ ), toluene (10 ml); heated in a microwave oven (gradient of heating: 10 min RT to 90  $^\circ\text{C}$ ; holding time: 1 h at 90  $^\circ\text{C}$ ); column chromatography ( $\text{CH}_2\text{Cl}_2$  : PE = 1:2).

**Formula:**  $\text{C}_{77}\text{H}_{61}\text{ClN}_4\text{O}_2$  [1109.79]

**Yield:** 96.0 mg (86.5  $\mu\text{mol}$ ; 68 %) yellow solid

**Melting point:** 188 – 190  $^\circ\text{C}$

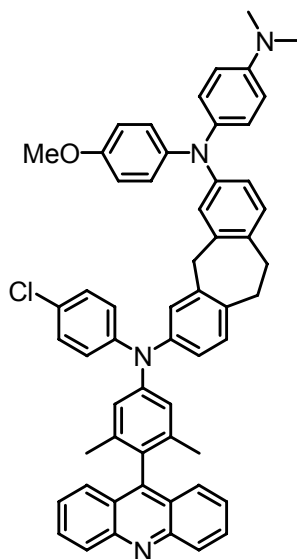


**<sup>1</sup>H-NMR** (400.1 MHz; [D<sub>2</sub>]dichloromethane):  $\delta$  = 8.24 (AA', 2H); 7.77 (ddd, <sup>3</sup>J<sub>HH</sub> = 8.7 Hz, <sup>3</sup>J<sub>HH</sub> = 6.5 Hz, <sup>4</sup>J<sub>HH</sub> = 1.4 Hz, 2H); 7.60 (ddd, <sup>3</sup>J<sub>HH</sub> = 8.7 Hz, <sup>4</sup>J<sub>HH</sub> = 1.4 Hz, <sup>5</sup>J<sub>HH</sub> = 0.7 Hz, 2H); 7.46 (ddd, <sup>3</sup>J<sub>HH</sub> = 8.7 Hz, <sup>3</sup>J<sub>HH</sub> = 6.5 Hz, <sup>4</sup>J<sub>HH</sub> = 1.2 Hz, 2H); 7.29 – 7.21 (-, 6H); 7.13 – 7.04 (-, 10H); 7.04 – 6.94 (-, 6H); 6.93 – 6.83 (-, 8H); 6.79 (BB', 2H); 3.96 (s, 2H); 3.79 (s, 6H); 3.20 – 3.14 (-, 4H); 2.29 (s, 3H); 1.62 (s, 6H).

**{<sup>1</sup>H}<sup>13</sup>C-NMR** (150.9 MHz; [D<sub>2</sub>]dichloromethane):  $\delta$  = 156.9 (quart.); 149.5 (quart.); 149.0 (quart.); 148.2 (quart.); 147.8 (quart.); 147.1 (quart.); 146.6 (quart.); 145.55 (quart.); 145.54 (quart.); 144.9 (quart.); 140.50 (quart.); 140.48 (quart.); 140.4 (quart.); 138.4 (quart.); 135.2 (quart.); 135.0 (quart.); 133.9 (quart.); 132.39 (tert.); 132.36 (tert.); 131.1 (tert.); 130.9 (tert.); 130.4 (tert.); 130.32 (tert.); 130.27 (tert.); 129.9 (quart.); 129.5 (tert.); 127.5 (tert.); 127.3 (quart.); 126.4 (tert.); 126.3 (tert.); 125.70 (tert.); 125.68 (tert.); 125.54 (tert.); 125.47 (quart.); 125.3 (tert.); 123.6 (tert.); 123.5 (tert.); 122.9 (tert.); 121.7 (tert.); 119.3 (tert.); 116.1 (quart.); 115.1 (tert.); 114.4 (quart.); 89.2 (quart.); 88.5 (quart.); 55.8 (prim.); 41.2 (sec.); 32.4 (sec.); 32.3 (sec.); 20.9 (prim.); 20.2 (prim.).

**ESI pos.** (high resolution): calcd for [M<sup>+</sup>] = C<sub>77</sub>H<sub>61</sub>ClN<sub>4</sub>O<sub>2</sub><sup>+</sup>: 1108.44776; found: 1108.44606 ( $\Delta$  = 1.53 ppm).

## Cascade 8



Following GP1: Compound **22** (95.7 mg; 234  $\mu\text{mol}$ ), **34** (120 mg; 234  $\mu\text{mol}$ ),  $\text{Pd}_2(\text{dba})_3 \cdot \text{CHCl}_3$  (6.39 mg; 6.17  $\mu\text{mol}$ ),  $\text{P}^t\text{Bu}_3$  (33.0  $\mu\text{l}$ ; 10.9  $\mu\text{mol}$ ), sodium *tert*-butoxide (30.8 mg; 320  $\mu\text{mol}$ ), toluene (10 ml); heated in a microwave oven (gradient of heating: 10 min RT to 90  $^\circ\text{C}$ ; holding time: 1 h at 90  $^\circ\text{C}$ ); flash-column chromatography ( $\text{CH}_2\text{Cl}_2$  : EtOAc = 40:1).

**Formula:**  $\text{C}_{57}\text{H}_{49}\text{ClN}_4\text{O}$  [841.48]

**Yield:** 103 mg (122  $\mu\text{mol}$ ; 52 %) orange solid

**Melting point:** 193  $^\circ\text{C}$

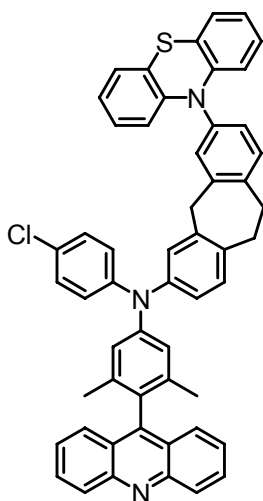
**$^1\text{H-NMR}$**  (400.1 MHz;  $[\text{D}_6]\text{acetone}$ ):  $\delta$  = 8.25 (m, 2H); 7.85 (ddd,  $^3J_{\text{HH}} = 8.7$  Hz,  $^3J_{\text{HH}} = 6.4$  Hz;  $^4J_{\text{HH}} = 1.6$  Hz, 2H); 7.62 – 7.56 (-, 2H); 7.53 (ddd,  $^3J_{\text{HH}} = 8.6$  Hz,  $^3J_{\text{HH}} = 6.4$  Hz,  $^4J_{\text{HH}} = 1.2$  Hz, 2H); 7.31 (AA', 2H); 7.18 – 7.08 (-, 4H); 7.05 – 6.89 (-, 8H); 6.82 (BB', 2H); 6.76 (m, 1H); 6.69 (BB', 2H); 6.65 (dd,  $^3J_{\text{HH}} = 8.1$  Hz,  $^4J_{\text{HH}} = 2.5$  Hz, 1H); 3.96 (s, 2H); 3.74 (s, 3H); 3.20 – 3.08 (-, 4H); 2.88 (s, 6H); 1.64 (s, 6H).

**$\{^1\text{H}\}^{13}\text{C-NMR}$**  (150.9 MHz;  $[\text{D}_6]\text{acetone}$ ):  $\delta$  = 156.3 (quart.); 150.0 (quart.); 148.48 (quart.); 148.45 (quart.); 148.1 (quart.); 147.8 (quart.); 146.6 (quart.); 145.8 (quart.); 142.4 (quart.); 141.5 (quart.); 140.4 (quart.); 138.6 (quart.); 138.4 (quart.); 136.2 (quart.); 132.0 (quart.); 131.8 (tert.); 131.1 (tert.); 130.93 (tert.); 130.87 (tert.); 130.2 (quart.); 130.1 (tert.); 127.5 (tert.); 127.4 (quart.); 127.2 (tert.); 126.7 (tert.); 126.6 (tert.); 126.4 (tert.); 125.8 (quart.); 125.6 (tert.); 124.4 (tert.); 123.2 (tert.); 121.7 (tert.); 119.6 (tert.);

115.2 (tert.); 114.4 (tert.); 55.6 (prim.); 41.3 (sec.); 40.9 (prim.); 33.0 (sec.); 32.2 (sec.); 20.2 (prim.).

**HRMS** (70 eV, EI):  $m/z$  calcd for  $[M^{2+}] = C_{57}H_{49}ClN_4O^{2+}$ : 420.17920; found: 420.17906 ( $\Delta = 0.33$  ppm).

### Cascade 9



Following GP1: Compound **22** (200 mg, 489  $\mu$ mol), **35** (242 mg, 514  $\mu$ mol),  $Pd_2(dba)_3 \cdot CHCl_3$  (7.29 mg; 7.04  $\mu$ mol),  $P^tBu_3$  (37.5  $\mu$ l; 12.4  $\mu$ mol), sodium *tert*-butoxide (67.3 mg; 700  $\mu$ mol), toluene (10 ml); heated in a microwave oven (gradient of heating: 10 min RT to 110  $^{\circ}C$ ; holding time: 1 h at 110  $^{\circ}C$ ); flash-column chromatography ( $CH_2Cl_2$  : EtOAc = 60 : 1).

**Formula:**  $C_{54}H_{40}ClN_3S$  [798.43]

**Yield:** 335 mg (420  $\mu$ mol; 86 %) yellow solid

**Melting point:** 212  $^{\circ}C$

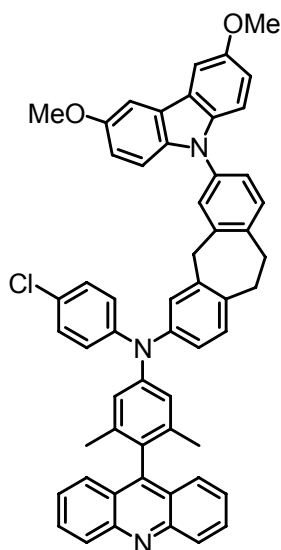
**$^1H$ -NMR** (400.1 MHz;  $[D_6]acetone$ ):  $\delta$  = 8.24 (m, 2H); 7.78 (ddd,  $^3J_{HH} = 8.7$  Hz,  $^3J_{HH} = 6.6$  Hz,  $^4J_{HH} = 1.5$  Hz, 2H); 7.60 (m, 2H); 7.46 (ddd,  $^3J_{HH} = 8.7$  Hz,  $^3J_{HH} = 6.5$  Hz,  $^4J_{HH} = 1.2$  Hz, 2H); 7.39 (m, 1H); 7.24 (AA', 2H); 7.21 – 7.15 (-, 3H); 7.11 (BB', 2H); 7.08 – 7.02 (-, 2H); 6.99 (dd,  $^3J_{HH} = 7.4$  Hz,  $^4J_{HH} = 1.7$  Hz, 2H); 6.95 (s, 2H); 6.85 – 6.74 (-, 4H); 6.25 (dd,  $^3J_{HH} = 8.0$  Hz,  $^4J_{HH} = 1.3$  Hz, 2H); 4.12 (s, 2H); 3.34 – 3.22 (-, 4H); 1.62 (s, 6H).

**$\{^1H\}^{13}C$ -NMR** (100.6 MHz;  $[D_6]acetone$ ):  $\delta$  = 149.8 (quart.); 147.8 (quart.); 147.1 (quart.); 146.6 (quart.); 145.7 (quart.); 144.8 (quart.); 142.0 (quart.); 140.3 (quart.); 140.2 (quart.); 138.9 (quart.); 138.4 (quart.); 135.1 (quart.); 132.2 (tert.);

131.3 (tert.); 131.1 (tert.); 130.3 (tert.); 130.3 (tert.); 129.9 (quart.); 129.6 (tert.); 129.3 (tert.); 127.4 (quart.); 127.2 (tert.); 126.9 (tert.); 126.4 (tert.); 126.3 (tert.); 125.8 (tert.); 125.5 (quart.); 125.3 (tert.); 123.8 (tert.); 123.0 (tert.); 122.7 (tert.); 120.5 (quart.); 116.4 (tert.); 41.2 (sec.); 32.8 (sec.); 32.2 (sec.); 20.2 (prim.).

ESI pos. (high resolution): calcd for  $[M^+] = C_{54}H_{40}ClN_3S^+$ : 797.26260; found: 797.26366 ( $\Delta = 1.33$  ppm).

### Cascade 10



Following GP1: Compound **22** (114 mg; 279  $\mu$ mol), **36** (155 mg; 311  $\mu$ mol),  $Pd_2(dba)_3 \cdot CHCl_3$  (4.41 mg; 4.26  $\mu$ mol),  $P^tBu_3$  (22.7  $\mu$ l; 7.49  $\mu$ mol), sodium *tert*-butoxide (40.6 mg; 422  $\mu$ mol), toluene (4 ml); 18 h at 100  $^\circ$ C; flash-column chromatography ( $CH_2Cl_2$  : EtOAc = 40:1).

**Formula:**  $C_{56}H_{44}ClN_3O_2$  [826.42]

**Yield:** 157 mg (190  $\mu$ mol; 68 %) yellow solid

**Melting point:** 187  $^\circ$ C

**$^1H$ -NMR** (400.1 MHz;  $[D_2]$ dichloromethane):  $\delta = 8.23$  (d,  $^3J_{HH} = 8.7$  Hz, 2H); 7.77 (ddd,  $^3J_{HH} = 8.6$  Hz,  $^3J_{HH} = 6.7$  Hz,  $^4J_{HH} = 1.5$  Hz, 2H); 7.61 – 7.57 (-, 2H); 7.55 (d,  $^4J_{HH} = 2.5$  Hz, 2H); 7.43 (ddd,  $^3J_{HH} = 8.7$  Hz,  $^3J_{HH} = 6.6$  Hz,  $^4J_{HH} = 1.2$  Hz, 2H); 7.40 – 7.33 (-, 3H); 7.31 (d,  $^3J_{HH} = 8.8$  Hz, 2H); 7.25 (AA', 2H); 7.17 (d,  $^3J_{HH} = 8.2$  Hz, 1H); 7.13 (BB', 2H); 7.09 – 7.03 (-, 2H); 7.00 (dd,  $^3J_{HH} =$

8.8 Hz,  ${}^4J_{\text{HH}} = 2.5$  Hz, 2H); 6.97 – 6.95 (-, 2H); 4.16 (s, 2H); 3.91 (s, 6H);  
3.35 – 3.24 (-, 4H); 1.62 (s, 6H).

**$\{^1\text{H}\}^{13}\text{C-NMR}$**  (100.6 MHz;  $[\text{D}_2]$ dichloromethane):  $\delta = 154.4$  (quart.); 149.5 (quart.); 147.8 (quart.); 147.17 (quart.); 147.15 (quart.); 146.6 (quart.); 145.7 (quart.); 141.1 (quart.); 140.2 (quart.); 138.8 (quart.); 138.4 (quart.); 136.7 (quart.); 136.3 (quart.); 135.0 (quart.); 131.3 (tert.); 131.2 (tert.); 130.34 (tert.); 130.33 (tert.); 129.6 (tert.); 129.5 (tert.); 127.4 (quart.); 127.1 (tert.); 126.4 (tert.); 126.3 (tert.); 125.9 (tert.); 125.6 (quart.); 125.3 (tert.); 125.0 (quart.); 123.8 (tert.); 123.0 (tert.); 115.4 (tert.); 111.0 (tert.); 103.1 (tert.); 56.3 (prim.); 41.2 (sec.); 32.7 (sec.); 32.3 (sec.); 20.2 (prim.).

**ESI pos.** (high resolution): calcd for  $[\text{M}^+] = \text{C}_{56}\text{H}_{44}\text{ClN}_3\text{O}_2^+$ : 825.31166; found: 825.31102 ( $\Delta = 0.78$  ppm).

## 5 Literature

- [1] D. Voet, J. G. Voet, *Biochemie*, VCH, Weinheim (Germany), **1992**, 586-618.
- [2] J. M. Berg, J. L. Tymoczko, L. Stryer, *Biochemistry*, W. H. Freeman and Company, New York (USA), **2006**, 541-591.
- [3] B. Alberts, D. Bray, K. Hopkin, A. Johnson, J. Lewis, M. Raft, K. Roberts, P. Walter, *Lehrbuch der Molekularen Zellbiologie*, Wiley-VCH, Weinheim (Germany), **2005**, 453-489.
- [4] D. Voet, J. G. Voet, *Biochemie*, VCH, Weinheim (Germany), **1992**, 527-560.
- [5] J. M. Berg, J. L. Tymoczko, L. Stryer, *Biochemistry*, W. H. Freeman and Company, New York (USA), **2006**, 409-519.
- [6] J. R. Bolton, M. D. Archer, *Adv. Chem. Ser.* **1991**, 228, 7-23.
- [7] H. Heitele, *Angew. Chem., Int. Ed. Engl.* **1993**, 32, 359-377.
- [8] J. W. Verhoeven, H. J. van Ramesdonk, M. M. Groeneveld, A. C. Benniston, A. Harriman, *ChemPhysChem* **2005**, 6, 2251-2260.
- [9] M. J. Weaver, *Chem. Rev.* **1992**, 92, 463-480.
- [10] N. Sutin, *J. Phys. Chem.* **1986**, 90, 3465-3466.
- [11] R. A. Marcus, *Pure Appl. Chem.* **1997**, 69, 13-29.
- [12] R. A. Marcus, *J. Chem. Phys.* **1956**, 24, 966-978.
- [13] R. A. Marcus, *Faraday Discuss. Chem. Soc.* **1960**, 29, 21-31.
- [14] R. A. Marcus, H. Eyring, *Ann. Rev. Phys. Chem.* **1964**, 15, 155-196.
- [15] R. A. Marcus, *J. Chem. Phys.* **1965**, 43, 679-701.
- [16] C. Lambert, J. Schelter, T. Fiebig, D. Mank, A. Trifonov, *J. Am. Chem. Soc.* **2005**, 127, 10600-10610.
- [17] T. B. Truong, *J. Phys. Chem.* **1984**, 88, 3906-3913.
- [18] A. Harriman, *Angew. Chem., Int. Ed. Engl.* **2004**, 43, 4985-4987.
- [19] J. Kroon, H. Oevering, J. W. Verhoeven, J. M. Warman, A. M. Oliver, M. N. Paddon-Row, *J. Phys. Chem.* **1993**, 97, 5065-5069.
- [20] J. R. Miller, L. T. Calcaterra, G. L. Closs, *J. Am. Chem. Soc.* **1984**, 106, 3047-3049.
- [21] V. G. Levich, *Adv. Electrochem. Electrochem. Eng.* **1966**, 4, 249-371.
- [22] V. G. Levich, R. R. Dogonadze, *Dokl. Akad. Nauk SSSR* **1959**, 124, 123-126.
- [23] J. Kommandeur, W. L. Meerts, *Isr. J. Chem.* **1990**, 30, 131-134.
- [24] J. Jortner, M. Bixon, *J. Chem. Phys.* **1988**, 88, 167-170.
- [25] J. Jortner, *J. Chem. Phys.* **1976**, 64, 4860-4867.
- [26] M. Bixon, J. Jortner, *Faraday Discuss. Chem. Soc.* **1982**, 74, 17-29.
- [27] I. R. Gould, D. Noukakis, L. Gomez-Jahn, R. H. Young, J. L. Goodman, S. Farid, *Chem. Phys.* **1993**, 176, 439-456.
- [28] H. Sumi, R. A. Marcus, *J. Phys. Chem.* **1986**, 84, 4894-4914.
- [29] H.-A. Wagenknecht, *Chem. Unserer Zeit* **2002**, 5, 318-330.
- [30] W. B. Davis, M. R. Wasielewski, M. A. Ratner, V. Mujica, A. Nitzan, *J. Phys. Chem. A* **1997**, 101, 6158-6164.
- [31] M. D. Newton, *Chem. Rev.* **1991**, 91, 767-792.
- [32] Z. G. Szabo, *Naturwissenschaftliche Rundschau* **1969**, 22, 69-72.
- [33] M. Fujitsuka, O. Ito, H. Imahori, K. Yamada, H. Yamada, Y. Sakata, *Chem. Lett.* **1999**, 28, 721-722.
- [34] Y.-Z. Hu, S. Tsukiji, S. Shinkai, S. Oishi, I. Hamachi, *J. Am. Chem. Soc.* **2000**, 122, 241-253.
- [35] H. Imahori, D. M. Guldi, K. Tamaki, Y. Yoshida, C. Luo, Y. Sakata, S. Fukuzumi, *J. Am. Chem. Soc.* **2001**, 123, 6617-6628.
- [36] H. Inoue, S. Funyu, Y. Shimada, S. Takagi, *Pure Appl. Chem.* **2005**, 77, 1019-1033.
- [37] Y. Kashiwagi, K. Ohkubo, J. A. McDonald, I. M. Blake, M. J. Crossley, Y. Araki, O. Ito, H. Imahori, S. Fukuzumi, *Org. Lett.* **2003**, 5, 2719-2721.

- [38] Y. Kobuke, K. Ogawa, *Bull. Chem. Soc. Jpn.* **2003**, *76*, 689-708.
- [39] C. Luo, D. M. Guldi, H. Imahori, K. Tamaki, Y. Sakata, *J. Am. Chem. Soc.* **2000**, *122*, 6535-6551.
- [40] P. Piotrowiak, *Chem. Soc. Rev.* **1999**, *28*, 143-150.
- [41] M. Regehly, E. A. Ermilov, M. Helmreich, A. Hirsch, N. Jux, B. Röder, *J. Phys. Chem. B* **2007**, *111*, 998-1006.
- [42] L. Sánchez, I. Pérez, N. Martín, D. M. Guldi, *Chem. Eur. J.* **2003**, *9*, 2457-2468.
- [43] J. Springer, G. Kodis, L. de la Garza, A. L. Moore, T. A. Moore, D. Gust, *J. Phys. Chem. A* **2003**, *107*, 3567-3575.
- [44] H. Tsue, H. Imahori, T. Kaneda, Y. Tanaka, T. Okada, K. Tamaki, Y. Sakata, *J. Am. Chem. Soc.* **2000**, *122*, 2279-2288.
- [45] X. Amashukeli, N. E. Gruhn, D. L. Lichtenberger, J. R. Winkler, H. B. Gray, *J. Am. Chem. Soc.* **2004**, *126*, 15566-15571.
- [46] L. Eberson, *Electron-Transfer Reactions in Organic Chemistry*, Springer, Berlin (Germany), **1987**.
- [47] B. C. Lin, C. P. Cheng, Z. P. M. Lao, *J. Phys. Chem. A* **2003**, *107*, 5241-5251.
- [48] S. P. Sorensen, W. H. Bruning, *J. Am. Chem. Soc.* **1973**, *95*, 2445-2451.
- [49] S. Amthor, B. Noller, C. Lambert, *Chem. Phys.* **2005**, *316*, 141-152.
- [50] H. Zhao, C. Tanjutco, S. Thayumanavan, *Tetrahedron Lett.* **2001**, *42*, 4421-4424.
- [51] S. Dapperheld, E. Steckhan, K.-H. Grosse Brinkhaus, T. Esch, *Chem. Ber.* **1991**, *124*, 2557-2567.
- [52] W. Schmidt, E. Steckhan, *Chem. Ber.* **1980**, *113*, 577-585.
- [53] H. Imahori, H. Norieda, H. Yamada, Y. Nishimura, I. Yamazaki, Y. Sakata, S. Fukuzumi, *J. Am. Chem. Soc.* **2001**, *123*, 100-110.
- [54] K. Okamoto, Y. Araki, O. Ito, S. Fukuzumi, *J. Am. Chem. Soc.* **2004**, *126*, 56-57.
- [55] D. M. Guldi, M. Maggini, G. Scorrano, M. Prato, *J. Am. Chem. Soc.* **1997**, *119*, 974-980.
- [56] D. González-Rodríguez, T. Torres, M. M. Olmstead, J. Rivera, M. Á. Herranz, L. Echegoyen, C. A. Castellanos, D. M. Guldi, *J. Am. Chem. Soc.* **2006**, *128*, 10680-10681.
- [57] H. Imahori, Y. Sekiguchi, Y. Kashiwagi, T. Sato, Y. Araki, O. Ito, H. Yamada, S. Fukuzumi, *Chem. Eur. J.* **2004**, *10*, 3184-3196.
- [58] E. S. Yang, M. S. Chan, A. C. Wahl, *J. Phys. Chem.* **1975**, *79*, 2049-2052.
- [59] S. Fukuzumi, K. Ohkubo, J. Ortiz, A. M. Gutiérrez, F. Fernández-Lázaro, Á. Sastre-Santos, *Chem. Commun.* **2005**, 3814-3816.
- [60] M. Hanack, M. Lang, *Adv. Mater.* **1994**, *6*, 819-833.
- [61] G. de la Torre, P. Vázquez, F. Agulló-López, T. Torres, *Chem. Rev.* **2004**, *104*, 3723-3750.
- [62] D. Dini, M. Hanack, *J. Porphyrins Phthalocyanines* **2004**, *8*, 915-933.
- [63] Á. Sastre, A. Gouloumis, P. Vázquez, T. Torres, V. Doan, B. J. Schwartz, F. Wudl, L. Echegoyen, J. Rivera, *Org. Lett.* **1999**, *1*, 1807-1810.
- [64] X. Li, L. E. Sinks, B. Rybtchinski, M. R. Wasielewski, *J. Am. Chem. Soc.* **2004**, *126*, 10810-10811.
- [65] A. de la Escosura, M. V. Martínez-Díaz, P. Thordarson, A. E. Rowan, M. Nolte, T. Torres, *J. Am. Chem. Soc.* **2003**, *125*, 12300-12308.
- [66] A. González-Cabello, P. Vázquez, T. Torres, D. M. Guldi, *J. Org. Chem.* **2003**, *68*, 8635-8642.
- [67] R. S. Iglesias, C. G. Claessens, T. Torres, G. M. A. Rahman, D. M. Guldi, *Chem. Commun.* **2005**, 2113-2115.
- [68] D. González-Rodríguez, T. Torres, D. M. Guldi, J. Rivera, M. A. Herranz, L. Echegoyen, *J. Am. Chem. Soc.* **2004**, *126*, 6301-6313.
- [69] R. A. Kipp, J. A. Simon, M. Beggs, H. E. Ensley, R. H. Schmechl, *J. Phys. Chem. A* **1998**, *102*, 5659-5664.

- [70] V. R. Ferro, L. A. Poveda, C. G. Claessens, R. H. González-Jonte, J. M. García de la Vega, *Int. J. Quantum Chem.* **2003**, *91*, 369-375.
- [71] T. A. Moore, D. Gust, P. Mathis, J. C. Mialocq, C. Chachaty, R. V. Bensasson, E. J. Land, D. Doizi, P. A. Liddell, W. R. Lehman, G. A. Nemeth, A. L. Moore, *Nature (London)* **1984**, *307*, 630-632.
- [72] D. Gust, T. A. Moore, A. L. Moore, A. N. Macpherson, A. Lopez, J. M. DeGraziano, I. Gouni, E. Bittersmann, G. R. Seely, F. Gao, A. Nieman, X. C. Ma, L. J. Demanche, S.-C. Hung, D. K. Luttrull, S.-J. Lee, P. K. Kerrigan, *J. Am. Chem. Soc.* **1993**, *115*, 11141-11152.
- [73] A. P. Losev, N. D. Lyal'kova, E. I. Sagun, *Zh. Prikl. Spektrosk.* **1981**, *35*, 671-677.
- [74] M. Prato, M. Maggini, C. Giacometti, G. Scorrano, G. Sandonà, G. Farnia, *Tetrahedron* **1996**, *52*, 5221-5234.
- [75] C. Boule, J. M. Rabreau, P. Hudhomme, M. Cariou, M. Juhault, A. Gorgues, J. Orduna, J. Garín, *Tetrahedron Lett.* **1997**, *38*, 3909-3910.
- [76] J. Llacay, J. Veciana, J. Vidal-Gancedo, J. L. Bourdelande, R. Gonzalez-Moreno, C. Rovira, *J. Org. Chem.* **1998**, *63*, 5201-5210.
- [77] M. R. Bryce, *Adv. Mater.* **1999**, *11*, 11-23.
- [78] D. M. Guldi, S. González, N. Martín, A. Antón, J. Garín, J. Orduna, *J. Org. Chem.* **2000**, *65*, 1978-1983.
- [79] N. Martín, L. Sánchez, M. A. Herranz, D. M. Guldi, *J. Phys. Chem. A* **2000**, *104*, 4648-4657.
- [80] E. Allard, J. Cousseau, J. Orduna, J. Garín, H. Luo, Y. Araki, O. Ito, *Phys. Chem. Chem. Phys.* **2002**, *4*, 5944-5951.
- [81] D. Kreher, P. Hudhomme, A. Gorgues, H. Luo, Y. Araki, O. Ito, *Phys. Chem. Chem. Phys.* **2003**, *5*, 4583-4592.
- [82] M. Segura, L. Sanchez, J. de Mendoza, N. Martin, D. M. Guldi, *J. Am. Chem. Soc.* **2003**, *125*, 15093-15100.
- [83] See the special issue on molecular conductors: *Chem. Rev.* **2004**, *104*, 4887-5781.
- [84] M. R. Bryce, *Adv. Mater.* **1999**, *11*, 11-23.
- [85] R. Berera, G. F. Moore, I. H. M. van Stokkum, G. Kodis, P. A. Liddell, M. Gervaldo, R. van Grondelle, J. T. M. Kennis, D. Gust, T. A. Moore, A. L. Moore, *Photochem. Photobiol. Sci.* **2006**, *5*, 1142-1149.
- [86] J. N. Clifford, T. Gu, J.-F. Nierengarten, N. Armaroli, *Photochem. Photobiol. Sci.* **2006**, *5*, 1165-1172.
- [87] M. E. El-Khouly, P. Padmawar, Y. Araki, S. Verma, L. Y. Chiang, O. Ito, *J. Phys. Chem. A* **2006**, *110*, 884-891.
- [88] D. M. Guldi, A. Swartz, C. Luo, R. Gómez, J. L. Segura, N. Martín, *J. Am. Chem. Soc.* **2002**, *124*, 10875-10886.
- [89] D. Gust, T. A. Moore, A. L. Moore, In *Electron Transfer in Chemistry*; V. Balzani, Ed.; Wiley-VCH, Weinheim (Germany), **2001**; Vol. 3; 272-336.
- [90] Y. Han, L. Dobeck, A. Gong, F. Meng, C. W. Spangler, L. H. Spangler, *Chem. Commun.* **2005**, 1067-1069.
- [91] H. Imahori, M. E. El-Khouly, M. Fujitsuka, O. Ito, Y. Sakata, S. Fukuzumi, *J. Phys. Chem. A* **2001**, *105*, 325-332.
- [92] S. Komamine, M. Fujitsuka, O. Ito, *Phys. Chem. Chem. Phys.* **1999**, *1*, 4745-4749.
- [93] H. Luo, M. Fujitsuka, Y. Araki, O. Ito, P. Padmawar, L. Y. Chiang, *J. Phys. Chem. B* **2003**, *107*, 9312-9318.
- [94] T. Ohno, K. Moriwaki, T. Miyata, *J. Org. Chem.* **2001**, *66*, 3397-3401.
- [95] G. A. Rajkumar, A. S. D. Sandanayaka, K. Ikeshita, M. Itou, Y. Araki, Y. Furusho, N. Kihara, O. Ito, T. Takata, *J. Phys. Chem. A* **2005**, *109*, 2428-2435.
- [96] A. M. Ramos, S. C. J. Meskers, P. A. van Hal, J. Knol, J. C. Hummelen, R. A. J. Janssen, *J. Phys. Chem. A* **2003**, *107*, 9269-9283.
- [97] A. S. D. Sandanayaka, K. Ikeshita, G. A. Rajkumar, Y. Furusho, Y. Araki, T. Takata, O. Ito, *J. Phys. Chem. A* **2005**, *109*, 8088-8095.



- [98] A. S. D. Sandanayaka, K. Matsukawa, T. Ishi-i, S. Mataka, Y. Araki, O. Ito, *J. Phys. Chem. B* **2004**, *108*, 19995-20004.
- [99] A. S. D. Sandanayaka, Y. Taguri, Y. Araki, T. Ishi-i, S. Mataka, O. Ito, *J. Phys. Chem. B* **2005**, *109*, 22502-22512.
- [100] Y. A. Skryshevskii, *J. Appl. Spectrosc.* **2002**, *69*, 726-731.
- [101] H.-P. Zeng, T. Wang, A. S. D. Sandanayaka, Y. Araki, O. Ito, *J. Phys. Chem. A* **2005**, *109*, 4713-4720.
- [102] S. Fukuzumi, I. Nakanishi, T. Suenobu, K. M. Kadish, *J. Am. Chem. Soc.* **1999**, *121*, 3468-3474.
- [103] D. M. Guldi, *Pure Appl. Chem.* **2003**, *75*, 1069-1075.
- [104] R. M. Williams, J. M. Zwier, J. W. Verhoeven, *J. Am. Chem. Soc.* **1995**, *117*, 4093-4099.
- [105] K. Ohkubo, J. Ortíz, L. Martín-Gomis, F. Fernández-Lázaro, Á. Sastre-Santos, S. Fukuzumi, *Chem. Commun.* **2007**, 589-591.
- [106] R. O. Loutfy, A.-M. Hor, C.-K. Hsiao, G. Baranyi, P. Kazmaier, *Pure Appl. Chem.* **1988**, *60*, 1047-1054.
- [107] M. R. Wasielewski, *Chem. Rev.* **1992**, *92*, 435-461.
- [108] J. Herbich, A. Kapturkiewicz, *J. Am. Chem. Soc.* **1998**, *120*, 1014-1029.
- [109] J. Herbich, A. Kapturkiewicz, *Chem. Phys.* **1991**, *158*, 143-153.
- [110] J. Herbich, A. Kapturkiewicz, *Chem. Phys. Lett.* **1997**, *273*, 8-17.
- [111] Y. Zeng, M. B. Zimmt, *J. Am. Chem. Soc.* **1991**, *113*, 5107-5109.
- [112] Y. Zeng, M. B. Zimmt, *J. Phys. Chem.* **1992**, *96*, 8395-8403.
- [113] A. L. Thompson, T.-S. Ahn, K. R. J. Thomas, S. Thayumanavan, T. J. Martínez, C. J. Bardeen, *J. Am. Chem. Soc.* **2005**, *127*, 16348-16349.
- [114] K. J. Smit, J. M. Warman, *J. Lumin.* **1988**, *42*, 149-154.
- [115] J. H. Borkent, A. W. J. de Jong, J. W. Verhoeven, T. J. de Boer, *Chem. Phys. Lett.* **1978**, *57*, 530-534.
- [116] D. Anglos, V. Bindra, A. Kuki, *J. Chem. Soc., Chem. Commun.* **1994**, *2*, 213-215.
- [117] J. Karpiuk, *Phys. Chem. Chem. Phys.* **2003**, *5*, 1078-1090.
- [118] S. I. van Dijk, C. P. Groen, F. Hartl, A. M. Brouwer, J. W. Verhoeven, *J. Am. Chem. Soc.* **1996**, *118*, 8425-8432.
- [119] K. Ohkubo, H. Kotani, J. Shao, Z. Ou, K. M. Kadish, G. Li, R. K. Pandey, M. Fujitsuka, O. Ito, H. Imahori, S. Fukuzumi, *Angew. Chem., Int. Ed. Engl.* **2004**, *43*, 853-856.
- [120] A. E. Dunstan, J. A. Stubbs, *Chem. Ber.* **1906**, *39*, 2402.
- [121] S. C. Zimmerman, C. M. VanZyl, G. S. Hamilton, *J. Am. Chem. Soc.* **1989**, *111*, 1373-1381.
- [122] J. A. Seijas, M. P. Vázquez-Tato, M. M. Martínez, J. Rodríguez-Parga, *Green Chem.* **2002**, *4*, 390-391.
- [123] H. Koshima, K. Kutsunai, *Heterocycles* **2002**, *57*, 1299-1302.
- [124] Z. Zeng, S. C. Zimmerman, *Tetrahedron Lett.* **1988**, *29*, 5123-5124.
- [125] T. Hasobe, S. Hattori, H. Kotani, K. Ohkubo, K. Hosomizu, H. Imahori, P. V. Kamat, S. Fukuzumi, *Org. Lett.* **2004**, *6*, 3103-3106.
- [126] A. Bernthsen, *Chem. Ber.* **1883**, *16*, 767-769.
- [127] A. Bernthsen, *Liebigs Ann. Chem.* **1884**, *224*, 1-56.
- [128] R. Mosurkal, L. Hoke, S. A. Fossey, L. A. Samuelson, J. Kumar, D. Waller, R. A. Gaudiana, *J. Macromol. Sci., Part A: Pure Appl. Chem.* **2006**, *43*, 1907-1922.
- [129] P. M. Borsenberger, D. S. Weiss, *Organic Photoreceptors for Imaging Systems*, Marcel Dekker, New York (USA), **1993**.
- [130] M. Thelakkat, R. Fink, F. Haubner, H.-W. Schmidt, *Macromol. Symp.* **1998**, *125*, 157-164.
- [131] M. Thelakkat, *Macromol. Mater. Eng.* **2002**, *287*, 442-461.
- [132] C. W. Tang, *Appl. Phys. Lett.* **1986**, *48*, 183-185.
- [133] C. W. Tang, S. A. van Slyke, *Appl. Phys. Lett.* **1987**, *51*, 913-915.

- [134] E. S. Kolb, R. A. Gaudiana, P. G. Mehta, *Macromolecules* **1996**, *29*, 2359-2364.
- [135] H. Fujikawa, S. Tokito, Y. Taga, *Synth. Met.* **1997**, *91*, 161-162.
- [136] C. Giebeler, H. Antoniadis, D. D. C. Bradley, Y. Shirota, *Appl. Phys. Lett.* **1998**, *72*, 2448-2450.
- [137] M. Redecker, D. D. C. Bradley, M. Inbasekaran, W. W. Wu, E. P. Woo, *Adv. Mater.* **1999**, *11*, 241-246.
- [138] T. Braig, D. C. Müller, M. Groß, K. Meerholz, O. Nuyken, *Macromol. Rapid Commun.* **2000**, *21*, 583-589.
- [139] W. E. Moerner, S. M. Silence, *Chem. Rev.* **1994**, *94*, 127-155.
- [140] Y. Nishikitani, M. Kobayashi, S. Uchida, T. Kubo, *Electrochim. Acta* **2001**, *46*, 2035-2040.
- [141] W. F. Kosonocky, S. E. Harrison, R. Stander, *J. Chem. Phys.* **1965**, *43*, 831-833.
- [142] M. L. Lindqvist, *Hebd Seances Acad Sci, Ser. C* **1966**, *263*, 852-854.
- [143] J. C. Scaiano, In *Reactive Intermediate Chemistry*; A. M. Moss, M. S. Platz, M. Jones Jr., Eds.; Wiley, New York (USA), **2004**, 847-871.
- [144] J. C. Scaiano, G. Charette, A. Simard, in *Patent US 6741347*, **2004**.
- [145] L. M. Hadel, In *Handbook of Organic Photochemistry I*; J. C. Scaiano, Ed.; CRC Press, Boca Raton, Florida (USA), **1989**, 279-283.
- [146] The rise time refers to the time which is required for a signal to change from 10 % to 90 % of the peak amplitude.
- [147] W. Leibl, P. Mathis, *Series on Photoconversion of Solar Energy*, Vol. 2, Imperial College Press, London (UK), **2004**.
- [148] N. Nelson, A. Ben-Shem, *Nat. Rev. Mol. Cell Biol.* **2004**, *5*, 971-982.
- [149] W. Zinth, J. Wachtveitl, *ChemPhysChem* **2005**, *6*, 871-880.
- [150] R. Argazzi, C. A. Bignozzi, T. A. Heimer, F. N. Castellano, G. J. Meyer, *J. Phys. Chem. B* **1997**, *101*, 2591-2597.
- [151] A. Goetzberger, J. Luther, G. Willeke, *Sol. Energy Mater.* **2002**, *74*, 1-11.
- [152] M. Grätzel, *J. Photochem. Photobiol., C* **2003**, *4*, 145-153.
- [153] M. Grätzel, *Chem. Lett.* **2005**, *34*, 8-13.
- [154] M. Grätzel, *Inorg. Chem.* **2005**, *44*, 6841-6851.
- [155] N. Hirata, J.-J. Lagref, E. J. Palomares, J. R. Durrant, M. K. Nazeeruddin, M. Grätzel, D. Di Censo, *Chem. Eur. J.* **2004**, *10*, 595-602.
- [156] T. Horiuchi, H. Miura, K. Sumioka, S. Uchida, *J. Am. Chem. Soc.* **2004**, *126*, 12218-12219.
- [157] B. O'Regan, M. Grätzel, *Nature (London)* **1991**, *353*, 737-740.
- [158] L. Schmidt-Mende, U. Bach, R. Humphry-Baker, T. Horiuchi, H. Miura, S. Ito, S. Uchida, M. Grätzel, *Adv. Mater.* **2005**, *17*, 813-815.
- [159] A. V. Shah, R. Platz, H. Keppner, *Sol. Energy Mater.* **1995**, *38*, 501-520.
- [160] K. Westermark, S. Tingry, P. Persson, H. Rensmo, S. Lunell, A. Hagfeldt, H. Siegbahn, *J. Phys. Chem. B* **2001**, *105*, 7182-7187.
- [161] C. J. Brabec, N. S. Sariciftci, J. C. Hummelen, *Adv. Funct. Mater.* **2001**, *11*, 15-26.
- [162] K. M. Coakley, M. D. McGehee, *Chem. Mater.* **2004**, *16*, 4533-4542.
- [163] H. Spanggaard, F. C. Krebs, *Sol. Energy Mater.* **2004**, *83*, 125-146.
- [164] R. Lomoth, A. Magnuson, M. Sjoedin, P. Huang, S. Styring, L. Hammarstroem, *Photosynth. Res.* **2006**, *87*, 25-40.
- [165] J. A. Mercer-Smith, D. C. Mauzerall, *Photochem. Photobiol.* **1984**, *39*, 397-405.
- [166] T. D. M. Bell, A. Stefan, S. Masuo, T. Vosch, M. Lor, M. Cotlet, J. Hofkens, S. Bernhardt, K. Müllen, M. Van der Auweraer, J. W. Verhoeven, F. C. De Schryver, *ChemPhysChem* **2005**, *6*, 942-948.
- [167] M. Borgström, O. Johansson, R. Lomoth, H. Berglund Baudin, S. Wallin, L. Sun, B. Akermark, L. Hammarström, *Inorg. Chem.* **2003**, *42*, 5173-5184.
- [168] S. Chakraborty, T. J. Wadas, H. Hester, R. I. Schmehl, R. Eisenberg, *Inorg. Chem.* **2005**, *44*, 6865-6878.
- [169] C.-C. Chao, M. Leung, *J. Org. Chem.* **2005**, *70*, 4323-4331.

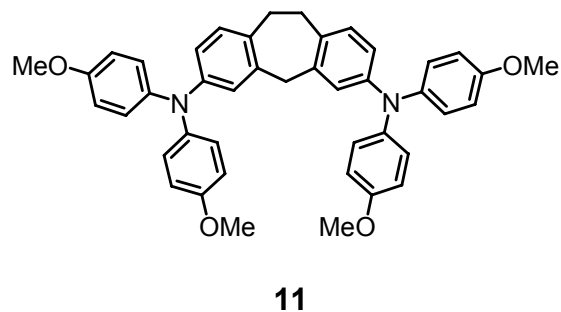
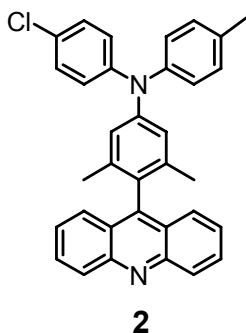
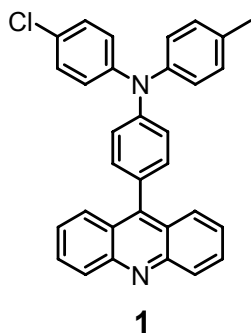
- [170] M. Cotlet, S. Masuo, G. Luo, J. Hofkens, M. Van der Auweraer, J. W. Verhoeven, K. Müllen, X. S. Xie, F. C. De Schryver, *Proc. Natl. Acad. Sci. U. S. A.* **2004**, *101*, 14343-14348.
- [171] T. Ganguly, S. K. Pal, *J. Chin. Chem. Soc. (Taipei)* **2006**, *53*, 219-226.
- [172] M. Lor, J. Thielemans, L. Viaene, M. Cotlet, J. Hofkens, T. Weil, C. Hampel, K. Müllen, J. W. Verhoeven, M. Van der Auweraer, F. C. De Schryver, *J. Am. Chem. Soc.* **2002**, *124*, 9918-9925.
- [173] M. Lor, L. Viaene, R. Pilot, E. Fron, S. Jordens, G. Schweitzer, T. Weil, K. Müllen, J. W. Verhoeven, M. Van der Auweraer, F. C. De Schryver, *J. Phys. Chem. B* **2004**, *108*, 10721-10731.
- [174] A. M. Ramos, E. H. A. Beckers, T. Offermans, S. C. J. Meskers, R. A. J. Janssen, *J. Phys. Chem. A* **2004**, *108*, 8201-8211.
- [175] A. Stockmann, J. Kurzawa, N. Fritz, N. Acar, S. Schneider, J. Daub, R. Engl, T. Clark, *J. Phys. Chem. A* **2002**, *106*, 7958-7970.
- [176] K.-Y. Kim, J. D. Hassenzahl, T. D. Selby, G. J. Szulczewski, S. C. Blackstock, *Chem. Mater.* **2002**, *14*, 1691-1694.
- [177] J. C. Li, K.-Y. Kim, S. C. Blackstock, G. J. Szulczewski, *Chem. Mater.* **2004**, *16*, 4711-4714.
- [178] M. J. Plater, T. Jackson, *Tetrahedron* **2003**, *59*, 4687-4692.
- [179] T. D. Selby, K.-Y. Kim, S. C. Blackstock, *Chem. Mater.* **2002**, *14*, 1685-1690.
- [180] K. Bronk, S. Thayumanavan, *J. Org. Chem.* **2003**, *68*, 5559-5567.
- [181] C. H. Chen, J. Shi, C. W. Tang, *Macromol. Symp.* **1997**, *125*, 1-48.
- [182] K. Katsuma, Y. Shirota, *Adv. Mater.* **1998**, *10*, 223-226.
- [183] J. Louie, J. F. Hartwig, A. J. Fry, *J. Am. Chem. Soc.* **1997**, *119*, 11695-11696.
- [184] J. Lu, P. F. Xia, P. K. Lo, Y. Tao, M. S. Wong, *Chem. Mater.* **2006**, *18*, 6194-6203.
- [185] N. Satoh, J.-S. Cho, M. Higuchi, K. Yamamoto, *J. Am. Chem. Soc.* **2003**, *125*, 8104-8105.
- [186] N. Satoh, J.-S. Cho, M. Higuchi, K. Yamamoto, *J. Photopolym. Sci. Technol.* **2005**, *18*, 55-58.
- [187] T. D. Selby, S. C. Blackstock, *J. Am. Chem. Soc.* **1998**, *120*, 12155-12156.
- [188] H.-J. Son, W.-S. Han, K. H. Lee, H. J. Jung, C. Lee, J. Ko, S. O. Kang, *Chem. Mater.* **2006**, *18*, 5811-5813.
- [189] I.-Y. Wu, J. T. Lin, Y.-T. Tao, E. Balasubramaniam, *Adv. Mater.* **2000**, *12*, 668-669.
- [190] C. Lambert, G. Nöll, *Synth. Met.* **2003**, *139*, 57-62.
- [191] Y. Ohsawa, M. Ishikawa, T. Miyamoto, Y. Murofushi, M. Kawai, *Synth. Met.* **1987**, *18*, 371-374.
- [192] A. Kapturkiewicz, J. Herbich, J. Karpiuk, J. Nowacki, *J. Phys. Chem. A* **1997**, *101*, 2332-2344.
- [193] A. Kapturkiewicz, J. Nowacki, *J. Phys. Chem. A* **1999**, *103*, 8145-8155.
- [194] P. Borowicz, J. Herbich, A. Kapturkiewicz, M. Opallo, J. Nowacki, *Chem. Phys.* **1999**, *249*, 49-62.
- [195] C. Lambert, G. Nöll, *J. Am. Chem. Soc.* **1999**, *121*, 8434-8442.
- [196] C. Lambert, G. Nöll, *Angew. Chem., Int. Ed. Engl.* **1998**, *37*, 2107-2110.
- [197] J. F. Hartwig, *Synlett* **1997**, *4*, 329-340.
- [198] J. F. Hartwig, *Angew. Chem., Int. Ed. Engl.* **1998**, *37*, 2046-2067.
- [199] M. Nishiyama, T. Yamamoto, Y. Koie, *Tetrahedron Lett.* **1998**, *39*, 617-620.
- [200] J. P. Wolfe, S. Wagaw, J.-F. Marcoux, S. L. Buchwald, *Acc. Chem. Res.* **1998**, *31*, 805-818.
- [201] T. Yamamoto, M. Nishiyama, Y. Koie, *Tetrahedron Lett.* **1998**, *39*, 2367-2370.
- [202] W. S. Trahanovsky, J. L. Tunkel, J. C. Thoen, Y. Wang, *J. Org. Chem.* **1995**, *60*, 8407-8409.
- [203] M. P. Doyle, B. Siegfried, J. F. Dellaria Jr., *J. Org. Chem.* **1977**, *42*, 2426-2431.
- [204] G. W. Gribble, W. J. Kelly, S. E. Emery, *Synthesis* **1978**, *10*, 763-765.

- [205] Because it turned out to be impossible to exchange selectively one bromine by one iodine atom in **17** we used **17** in a large excess in order to minimise the formation of symmetric substitution products.
- [206] S. Takahashi, Y. Kuroyama, K. Sonogashira, N. Hagihara, *Synthesis* **1980**, 627-630.
- [207] K. Sonogashira, Y. Tohda, N. Hagihara, *Tetrahedron Lett.* **1975**, 4467-4470.
- [208] T. Hundertmark, A. F. Littke, S. L. Buchwald, G. C. Fu, *Org. Lett.* **2000**, *2*, 1729-1731.
- [209] M. Holzapfel, C. Lambert, C. Selinka, D. Stalke, *J. Chem. Soc., Perkin Trans. 2* **2002**, 1553-1561.
- [210] T. Tanaka, T. Tasaki, Y. Aoyama, *J. Am. Chem. Soc.* **2002**, *124*, 12453-12462.
- [211] Although it is the common procedure to prepare phenylacridine derivatives by a Bernthsen reaction of diphenylamine and the adequately substituted benzoic acid, this reaction was not used to obtain compound **22** because this procedure gave low yields and involved time consuming purifications.
- [212] Y. Kikugawa, Y. Aoki, T. Sakamoto, *J. Org. Chem.* **2001**, *66*, 8612-8615.
- [213] P. Suppan, N. Ghoneim, *Solvatochromism*, The Royal Society of Chemistry, Cambridge (UK), **1997**.
- [214] J. B. Birks, *Photophysics of Aromatic Molecules*, Wiley-Interscience, London (UK), **1970**.
- [215] S. J. Strickler, R. A. Berg, *J. Chem. Phys.* **1962**, *37*, 814-822.
- [216] H. van Willigen, G. Jones II., M. S. Farahat, *J. Phys. Chem.* **1996**, *100*, 3312-3316.
- [217] Z. E. X. Dance, Q. Mi, D. W. McCamant, M. J. Ahrens, M. A. Ratner, M. R. Wasielewski, *J. Phys. Chem. B* **2006**, *110*, 25163-25173.
- [218] T. Okada, I. Karaki, E. Matsuzawa, N. Mataga, Y. Sakata, S. Misumi, *J. Phys. Chem.* **1981**, *85*, 3957-3960.
- [219] A. Weller, *Z. Phys. Chem. Neue Folge* **1982**, *133*, 93-98.
- [220] M. Klessinger, J. Michl, *Excited States and Photochemistry of Organic Molecules*, VCH, New York (USA), **1995**.
- [221] N. Chattopadhyay, C. Serpa, P. Purkayastha, L. G. Arnaut, S. J. Formosinho, *Phys. Chem. Chem. Phys.* **2001**, *3*, 70-73.
- [222] S. Fukuzumi, *Bull. Chem. Soc. Jpn.* **2006**, *79*, 177-195.
- [223] B. K. Kaletas, R. Dobrawa, A. Sautter, F. Würthner, M. Zimine, L. De Cola, R. M. Williams, *J. Phys. Chem. A* **2004**, *108*, 1900-1909.
- [224] A. Prodi, C. Chiorboli, F. Scandola, E. Iengo, E. Alessio, R. Dobrawa, F. Würthner, *J. Am. Chem. Soc.* **2005**, *127*, 1454-1462.
- [225] M. S. Rodríguez-Morgade, T. Torres, C. Atienza-Castellanos, D. M. Guldi, *J. Am. Chem. Soc.* **2006**, *128*, 15145-15154.
- [226] B. P. Paulson, J. R. Miller, W.-X. Gan, G. Closs, *J. Am. Chem. Soc.* **2005**, *127*, 4860-4868.
- [227] L. D. Zusman, D. N. Beratan, *J. Chem. Phys.* **1999**, *10*, 10468-10481.
- [228] G. Iversen, Y. I. Khartkats, A. M. Kuznetsov, J. Ulstrup, *Adv. Chem. Phys.* **1999**, *106*, 453-514.
- [229] E. G. Petrov, Y. V. Shevchenko, V. I. Teslenko, *J. Chem. Phys.* **2001**, *115*, 7107-7122.
- [230] H. Sumi, T. Kakitani, *J. Phys. Chem. B* **2001**, *105*, 9603-9622.
- [231] X.-Q. Li, Y. J. Yan, *J. Chem. Phys.* **2001**, *115*, 4169-4174.
- [232] A. M. Napper, N. J. Head, A. M. Oliver, M. J. Shepard, M. N. Paddon-Row, I. Read, D. H. Waldeck, *J. Am. Chem. Soc.* **2002**, *124*, 10171-10181.
- [233] R. W. Kaplan, A. M. Napper, D. H. Waldeck, M. B. Zimmt, *J. Am. Chem. Soc.* **2000**, *122*, 12039-12040.
- [234] G. C. Terry, V. E. Uffindell, F. W. Willets, *Nature (London)* **1969**, *223*, 1050-1051.
- [235] R. Carlier, J. Simonet, *Bull. Soc. Chim. Fr.* **1988**, *5*, 831-833.
- [236] J. Salbeck, *J. Electroanal. Chem.* **1992**, *340*, 1-2.
- [237] T. Karstens, K. Kobs, *J. Phys. Chem.* **1980**, *84*, 1871-1872.

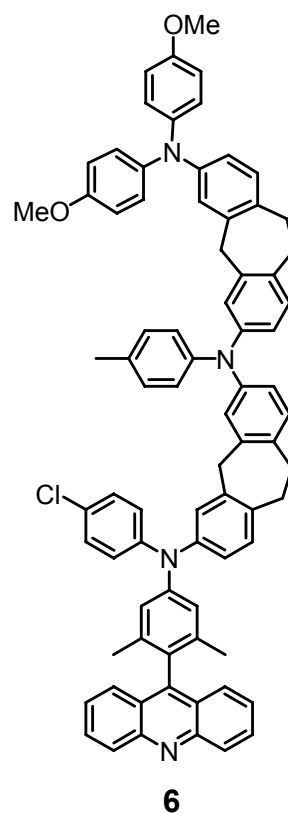
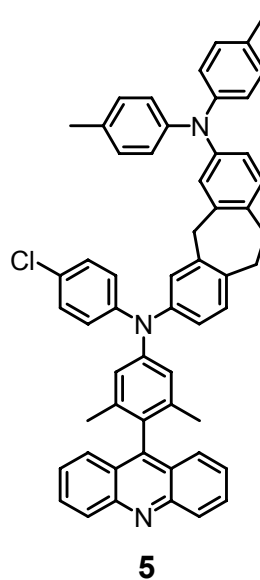
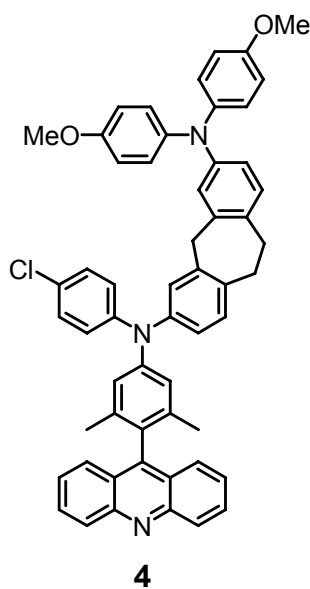
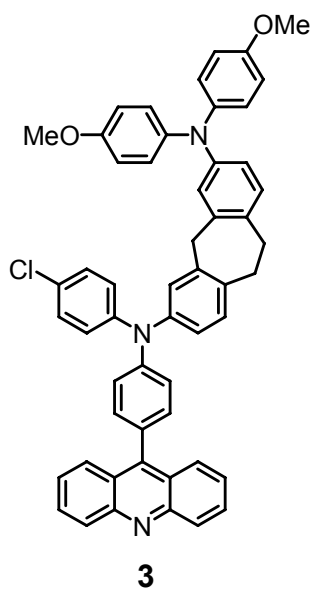
- [238] R. J. Bushby, D. R. McGill, K. M. Ng, N. Taylor, *J. Chem. Soc., Perkin Trans. 2* **1997**, 1405-1414.

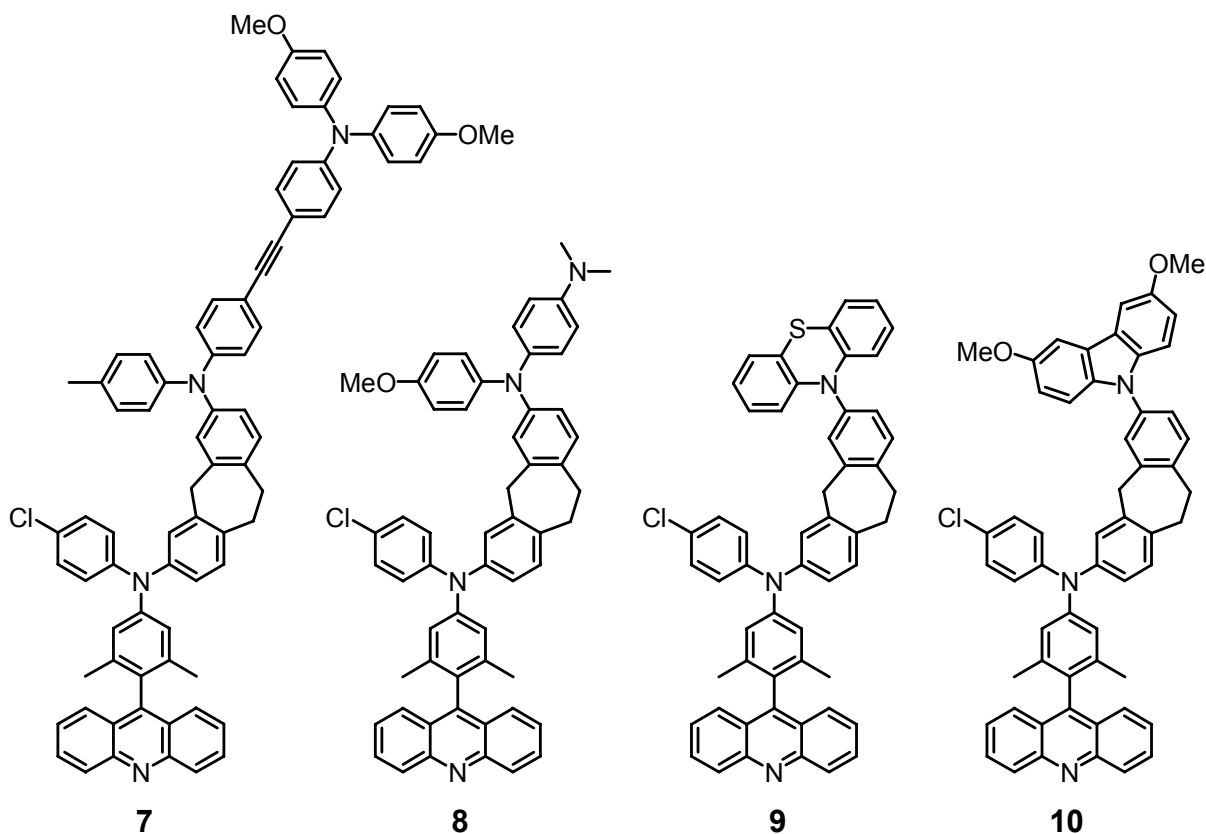
## 6 Table of Formulas

### 6.1 Reference Chromophores

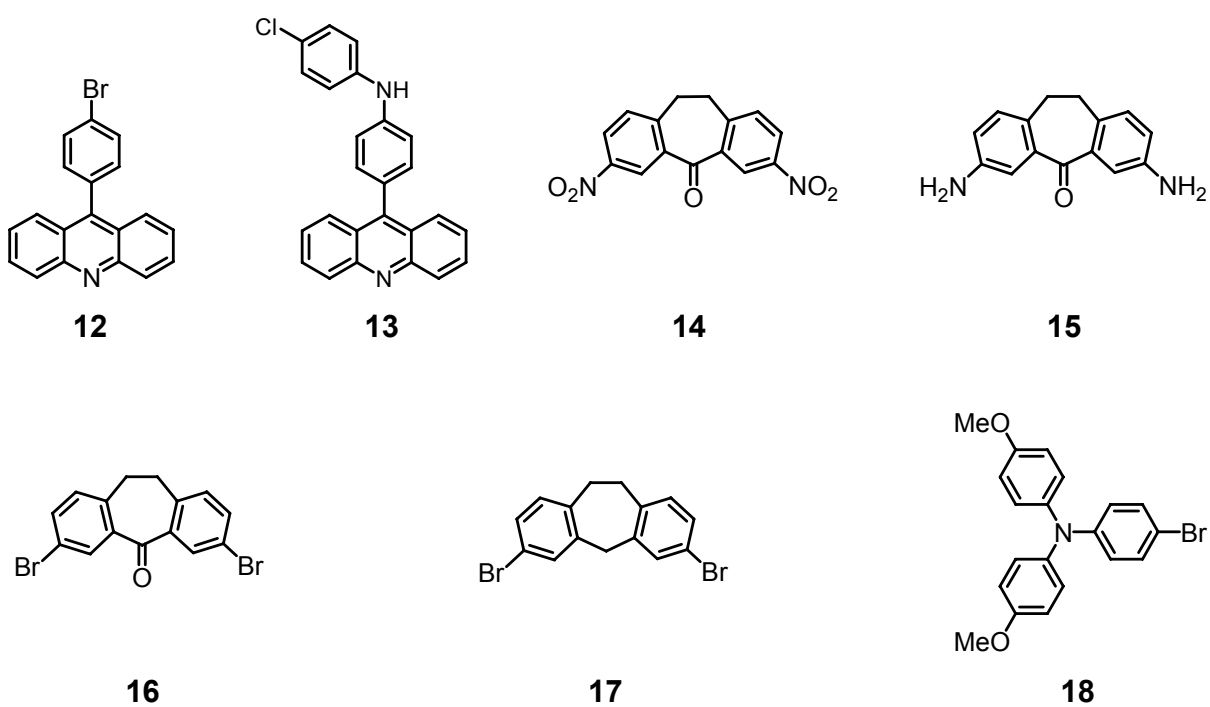


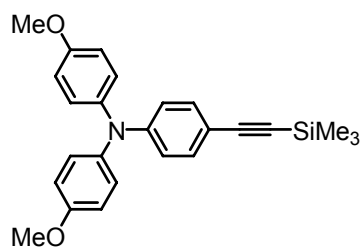
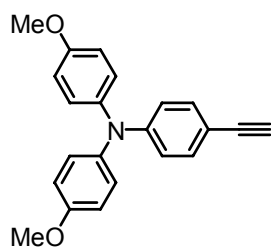
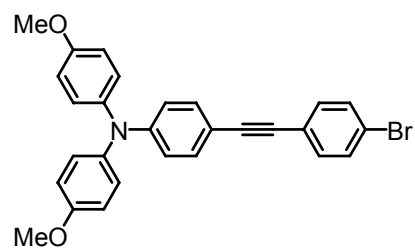
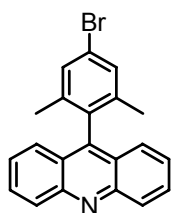
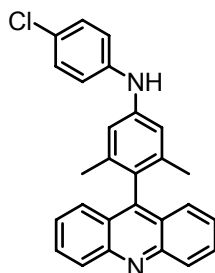
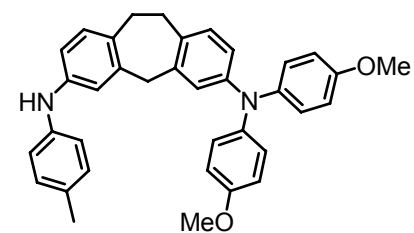
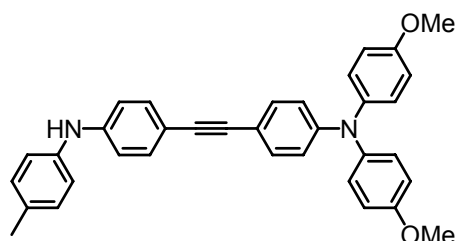
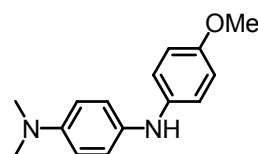
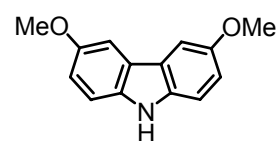
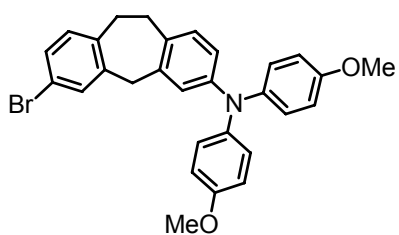
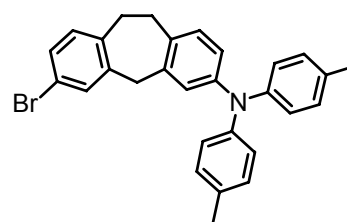
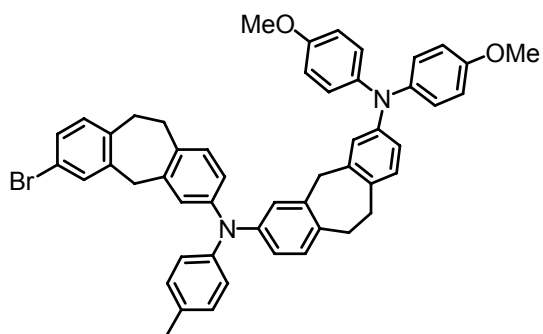
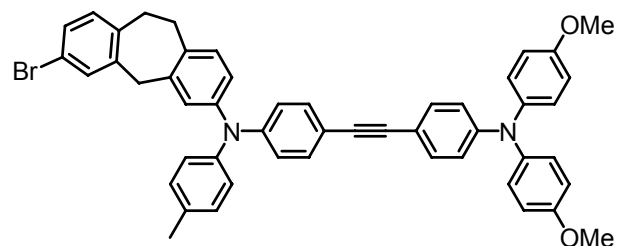
### 6.2 Cascades



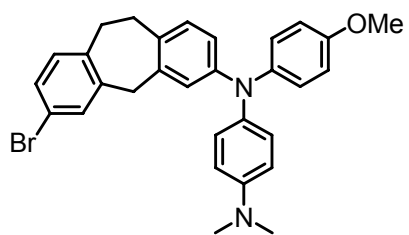
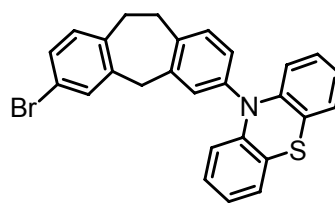
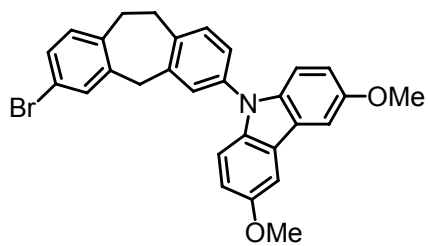


### 6.3 Precursors



**19****20****21****22****23****26****27****28****30****31****32****33****34**



**35****36****37**

## 7 Summary

In the first part of this work a new approach to measure transient absorption spectra of fluorescent compounds by means of laser flash photolysis technique was presented. Generally, the recorded transient absorption signal consists of transient absorption, fluorescence and ground state bleaching. Thus, for fluorescent chromophores a fluorescence correction is indispensable in order to obtain undisturbed absorption decay curves as well as accurate transient absorption spectra. Due to time response characteristics of the PMT detector the fluorescence contribution cannot be corrected by recording the fluorescence separately. Measuring two transient absorption signals with probe light differing in intensity, compounds with quantum yields up to  $\sim 35\%$  can be investigated. This is a major improvement because transient absorption spectroscopy is a powerful method to gain insight into the kinetics and the energy of excited states and information in the time domain of fluorescence are no longer lost.

In the second part the synthesis and the photophysical characterisation of redox cascades were reported. These cascades consist of an acridine acceptor and up to three triarylamine donor subunits. The redox potentials of the triarylamines were tuned by adequate substituents in the para-position of the phenyl ring to ensure a directed redox gradient. Upon photoexcitation a locally excited state or a CT state is populated which then injects a hole onto the adjacent donor and consequently results in a CS state. Fluorescence and transient absorption measurements revealed that HT depends strongly on donor strength and solvent polarity. Formation of a CS state was only observed in case of strong terminal donors or polar solvents. A low lying localised triplet state acts as an energy trap and quenches all CS states even in case of the cascade with the strongest terminal donor in very polar solvents. Furthermore, population of a CS state catalyses the formation of this triplet states which results in a shorter lifetime of the CS state compared to the lifetime of the CT state of the corresponding reference compound.

Compared to redox cascades already reported in literature, the electronic coupling between the redox centres was decreased by sterical as well as electronic effects. To prolong the lifetime of the CS state saturated spacers on the one hand and a perpendicular orientation of the acceptor and the adjacent donor on the other hand were selected. The twisting of the subunits forming the CT state results in a higher degree of charge separation but its contribution to increase the lifetimes of the CS states is of minor importance. The longer lifetime of the CS states can be ascribed to the saturated spacers. Experimental data in combination with calculated values indicate that charge recombination takes place in the

Marcus normal region by a superexchange mechanisms. Although charge recombination of the known cascades is located in the Marcus inverted region, these CS states decay faster than the CS states of the compounds investigated in this work.

## 8 Zusammenfassung

Im ersten Teil der vorliegenden Arbeit wurde eine neue Methode vorgestellt, mit dem transiente Absorptionsspektren von fluoreszierenden Verbindungen mit Hilfe der Laser-Blitzlichtphotolyse aufgenommen werden können. Ein transientes Absorptionssignal setzt sich im Allgemeinen aus transientser Absorption, Fluoreszenz und einer Ausbleichung des Grundzustands zusammen. Daher ist es für fluoreszierende Verbindungen unerlässlich, die Fluoreszenz zu korrigieren, um sowohl einwandfreie Abklingkurven als auch korrekte Spektren zu erhalten. Aufgrund der Charakteristik der Ansprechzeit des Photomultiplier-Detektors kann der Fluoreszenzbeitrag nicht durch ein eigens aufgenommenes Fluoreszenzsignal korrigiert werden. Jedoch können Verbindungen mit einer Fluoreszenzquantenausbeute bis ungefähr 35 % fehlerfrei gemessen werden, sofern das transiente Signal aus zwei Messungen mit unterschiedlicher Weißlichtintensität bestimmt wird. Dieser neue Ansatz zur Ermittlung transienter Absorptionsspektren ist eine entscheidende Verbesserung, da die Laser-Blitzlichtphotolyse eine leistungsstarke Methode zur Ermittlung kinetischer und energetischer Eigenschaften angeregter Zustände darstellt.

Im zweiten Abschnitt wurde die Synthese von Redoxkaskaden vorgestellt und gerichtete Elektronentransferprozesse an diesen Verbindungen untersucht. Die Chromophore bestehen stets aus einem Acridin-Akzeptor und bis zu drei Triarylamin-Untereinheiten als Donoren. Die Redoxpotenziale der Triarylamine können in gewissem Maße durch geeignete Substituenten in *para*-Position der Phenylringe abgestimmt werden, womit ein gerichteter Redoxgradient erzielt wird. Nach Anregung mit Licht geeigneter Wellenlänge wird ein lokal angeregter oder ein CT-Zustand bevölkert. Anschließend wird ein Loch in die benachbarte Donoreinheit injiziert, was schließlich zu einem ladungstrennten Zustand führt. Fluoreszenz- und transiente Absorptionsmessungen zeigen, dass der Lochtransfer in starkem Maße von der Lösungsmittelpolarität sowie der Stärke des terminalen Donors abhängt. Die Ausbildung eines ladungstrennten Zustands konnte nur bei starken terminalen Donoren oder polaren Lösungsmitteln beobachtet werden. Ein energetisch tief liegender lokal angeregter Triplettzustand agiert als energetische Falle und löscht alle ladungstrennten Zustände – selbst im Falle der stärksten Donoruntereinheit in sehr polaren Lösungsmitteln. Darüber hinaus beschleunigt die Bevölkering eines ladungstrennten Zustands die Ausbildung dieses Triplettzustands, was sich in einer kürzeren Lebensdauer dieses ladungstrennten Zustands, verglichen mit dem CT-Zustand der Referenzverbindung, äußert.

Die elektronische Kopplung zwischen den einzelnen Redoxzentren wurde im Vergleich zu ähnlichen bereits bekannten Redoxkaskaden sowohl durch sterische als auch durch elektronische Effekte verringert. Um die Lebensdauer des ladungstrennten Zustands zu verlängern, wurden einerseits gesättigte Einheiten, die die Untereinheiten verbrücken, eingebaut. Andererseits wurde mit Hilfe sterischer Faktoren die Akzeptoreinheit gegenüber dem benachbarten Donor verdrillt, was zwar in einer stärker ausgeprägten Ladungstrennung resultiert, jedoch nur geringfügig zu einer Verlängerung des ladungstrennten Zustands beiträgt. Somit kann die verlängerte Lebensdauer dieses ladungstrennten Zustands eindeutig auf die gesättigten Brückeneinheiten zurückgeführt werden. Experimentelle Daten stimmen mit berechneten Größen dahin gehend überein, dass die Ladungsrekombination in der normalen Marcus-Region über einen Superaustausch-Mechanismus erfolgt. Obwohl diese Rekombination bei den bekannten Kaskaden in der invertierten Marcus-Region erfolgt, werden die entsprechenden ladungstrennten Zustände schneller entvölkert als bei den Verbindungen, die Gegenstand dieses Kapitels waren.

## Publikationen

**Organic mixed valence compounds with *N,N*-dihydrodimethylphenazine redox centres.**  
M. Holzapfel, C. Lambert, C. Selinka, D. Stalke. *Perkin Trans. 2* **2002**, 1553-1561.

**Photoinduced Charge Separation and Recombination in Acridine-Triarylamine Based Redox Cascades.** M. Holzapfel, C. Lambert. *J. Phys. Chem. C*, accepted

## Poster

**Electron Transfer in Redox Cascades with Triarylamine Redox Centres.**  
Marco Holzapfel, Christoph Lambert, Anton Trifonov, Torsten Fiebig, Ulrich-Walter Grummt  
*Towards Molecular Electronics*, Ulm, **2004**.

**Electron Transfer in Redox Cascades with Triarylamine Redox Centres.**  
Marco Holzapfel, Christoph Lambert  
ICSM, Dublin, **2006**.

## Danksagung

An dieser Stelle möchte ich mich bei allen Personen bedanken, die zum Gelingen dieser Arbeit beigetragen haben. Mein besonderer Dank gilt dabei:

*Herrn Dr. Matthias Grüne, Frau Elfriede Ruckdeschel und Frau Christa Künzel*, für die Einweisung in die NMR-Geräte, die Aufnahme der NMR-Spektren sowie die bereitwillige Hilfe bei den alltäglichen Messproblemen.

*Herrn Dr. Michael Büchner, Herrn Fritz Dadrich, Herrn Eugen Ehrlich und Frau Antje Hautzinger*, für die Aufnahme der Massenspektren, die Diskussionen bei der Interpretation sowie ausführliche Erläuterungen bezüglich der Schubstange und der Uni Bielefeld.

*Herrn Dipl.-Ing. Bernd Brunner*, für seine bereitwillige Hilfe bei größeren und kleineren Problemen mit dem Computer. Besonders hervorzuheben ist seine fast endlose Geduld, die nötig ist, um einem völlig Ahnungslosen am PC weiterzuhelfen.

*Herrn Manfred Ludwig*, für die Anfertigung der Glasgeräte.

*Herrn Markus Braun*, für seine schnelle und unkomplizierte Hilfe bei verschiedensten Fragen und Problemen.

*Herrn Michael Ramold*, für die äußerst produktive und kompetente Zusammenarbeit bei einer Vielzahl von Sonderanfertigungen. Ohne sein außerordentliches Engagement und seinen Einsatz wären große Teile dieser Arbeit so nicht durchführbar gewesen.

Allen weiteren Angestellten des Instituts für Organische Chemie, *Herrn Dr. Christian Stadler, Frau Agathe Kempf, Frau Inka Wilhelm, Frau Angela Dreher, Frau Anette Krug, Frau Petra Leckert, Frau Ursula Rüppel, Herrn Alois Ruf, Herrn Matthias Fromm, Herrn Frank Förtsch, Herrn Waldemar Reich, Herrn Herbert Müller, Herrn Wilhelm Heilmann und Herrn Peter Wendinger*, die durch ihre Hilfsbereitschaft meine Arbeit erleichterten.

*Prof. Ingo Fischer und Herrn Michael Schneider*, für ihre Hilfestellungen beim Versuch, die OC mittels einer Ramanzelle in die Luft zu jagen.

*Dr. Eberhard Heller*, für die Einweisung in die mikrowellenunterstützte Synthese sowie die spontane Bereitschaft, Reaktionen in der Mikrowelle des AK Holzgrabe durchführen zu dürfen.

*Herrn Gerhard Rousseau und Dr. Andrew Dick*, für die Zusammenarbeit, um das Transienten-Absorptions-Spektrometer doch noch zum Laufen zu bringen. Besonderer Dank nach Schottland, dass unsere neuesten Erkenntnisse stets zügig in die Software integriert wurden.

*Prof. Ulrich-Walter Grummt und Herrn Alfred Jacobi*, für die äußerst schnelle Durchführung einer Reihe von Testmessungen sowie die Möglichkeit, jenseits des Eisernen Vorhangs den Aufbau der Messanordnung kennen zu lernen.

*Prof. Torsten Fiebig und Dr. Anton Trifonov*, für einige transiente Messungen in unbekanntenen Lösungsmitteln im fs-Bereich.

Besonderer Dank gebührt natürlich allen Mitgliedern des Arbeitskreises Lambert für das entspannte Arbeitsklima und die stete Hilfsbereitschaft bei den Problemen, die im Laufe einer Doktorarbeit auftreten. Insbesondere danke ich:

*Dr. Jürgen Schelter*, für die Vorarbeiten im Themengebiet der Redoxkaskaden und bei allen großen und kleinen Problemen, die der chemische Laboralltag mit sich bringt. Danke auch für die Einführung in die Geheimnisse der Messtechnik und die Hilfestellungen bei Problemen mit Computern.

*Dr. Hongchao Li*, für den „Dibutylether“, den dann jeder Neue im AK bei der ersten Feier mal trinken musste.

*Dr. Volker Kriegisch*, für die gute Zusammenarbeit im Labor, die Organisation der AK-Ausflüge sowie so mancher Grillfete.

*Dr. Stephan Amthor*, für die geduldige und kompetente Hilfe bei verschiedensten Problemen. Egal, ob man mit irgendeiner Software oder mit physikalisch-chemischen Theorien zu kämpfen hatte, er war in allen Belangen stets der richtige Ansprechpartner. Nicht nur ich habe mir Stephan nach seinem Ausscheiden das ein oder andere Mal in den AK zurückgewünscht!

*Dr. Rainer Stahl*, für die Ehre, dass ich mit dem GOE in einem Labor zusammen arbeiten durfte sowie für seine stets äußerst ausgeglichene Art. In Erinnerung werden mir auch die vielen Diskussionen über unsere Probleme bei der Fluoreszenzspektroskopie bleiben. Danken möchte ich nicht zuletzt für die unzähligen Versuche – auch wenn sie letztendlich vergeblich waren – unseren Newcomern die nötige Achtung vor Altdoktoranden einzubläuen. Sein Ausscheiden aus dem AK hat eine Lücke hinterlassen, die bis heute nicht zu schließen war.

*Simone Krakert*, die mein Erbe als Lehramtler im AK erfolgreich fortgeführt hat. Trotz ihrer starken Leistungen im Tor hat es für den AK beim ChemCup nie zum ganz großen Wurf gereicht. Schade, dass es mit einer Doktorarbeit in Würzburg nicht geklappt hat!

*Sascha Heckmann*, für die ausführlichen und immer wiederkehrenden Erläuterungen über all das, was man eigentlich gar nicht wissen will. Danke für die lustige Zeit, in der ich ihn in die Geheimnisse der photophysikalischen Messtechniken einweihen durfte. Nicht zu vergessen die zahlreichen Diskussionen zu verschiedenen Elektronentransfer-Theorien sowie sein äußerst genaues Korrekturlesen!

*Dirk Rausch*, unserem zumindest nach außen hin wirkenden ruhenden Pol des AKs, für die ein oder andere Hilfe beim Umgang mit dem PC.

*Barbara Geiß*, für die Organisation so ziemlich jeder AK-Fete sowie die Planung des Betriebsausfluges und der Instituts-Weihnachtsfeier, die unser AK durchführen musste. Vielen Dank auch für die unzähligen Säuberungsaktionen, ohne die unser Seminarraum wohl nicht mehr zu betreten wäre.

*Christian Müller*, für die tägliche Begrüßung und Verabschiedung. Danke auch für die zahlreichen Versuche, die durch die Kaiser'schen Schwefelverbindungen verseuchte Laborluft mit aromatischen Düften zu verbessern. Natürlich nicht zu vergessen die aufwendige Grafik mit PovRay.



*Dörte Nowak*, für die tägliche Begleitung in die Mensa sowie eine schöne Woche in Dublin. Danke, dass ich durch viele Diskussionen über Synthesen und nicht zuletzt Fluoreszenz-Spektroskopie den Eindruck vermittelt bekam, doch etwas von der Materie zu verstehen.

*Conrad Kaiser*, für seine Hilfe bei verschiedensten Computerproblemen. Vielen Dank nochmals für die Einladung zur perfekt geplanten Hochzeitsfeier im schönen Spessart!

*Ruben Ramon*, für die – wenn zeitlich auch sehr begrenzte – sehr gute Zusammenarbeit im Labor. Nicht nur die Diskussionen von Montag bis Mittwoch über den vergangenen oder spätestens ab Donnerstag über den kommenden Spieltag der Fußball-Bundesliga sorgten für ein sehr entspanntes Arbeitsklima in unserem Labor. Zugegebenermaßen hat es ein Eintracht-Fan neben einem Bayern-Fan sehr schwer.

*Nina Dürrbeck*, auch im Namen von Roswitha, dass ich an sie Nilrot loswerden konnte.

*Tatjana, Vilija, David, André, Jens, Sabine, Christoph* und *Carina* für die Destillation der Lösungsmittel, für Synthesen oder die Bestimmung des ein oder anderen Schmelzpunktes.

*Roswitha Scheblein*, für unzählige nervenaufreibende Synthesen und Säulen. Besonders dankbar bin ich ihr aber für ihr stets offenes Ohr und ihre aufmunternden Worte, die nicht nur bei chemischen Rückschlägen und Problemen nötig waren.

*Marion* und *Thorsten*, die mich durchs Studium begleitet haben, für die Aktivitäten, die mich vom Laboralltag ablenkten sowie für die aufmunternden Worte während meiner Doktorarbeit. Bei Marion möchte ich mich ferner für das Korrekturlesen bedanken.

*Meiner Großmutter*, für ihre großzügige finanzielle Unterstützung, was mir das Studium und die anschließende Doktorarbeit erheblich erleichterte.

Der größte Dank gilt natürlich *meinen Eltern*, für ihren finanziellen und moralischen Rückhalt, ohne den weder mein Studium noch meine Doktorarbeit möglich gewesen wären. Besonders dankbar bin ich ihnen, dass sie mich nach verschiedensten Rückschlägen stets aufgebaut und ermutigt haben, den eingeschlagenen Weg weiterzugehen. Ohne ihren unerschütterlichen Glauben an mich wäre ich heute nicht da, wo ich bin!

## Erklärung

Hiermit erkläre ich an Eides statt, dass ich die Dissertation „Photoinduced Charge Transfer Processes in Triarylamine Based Redox Cascades“ selbstständig angefertigt und keine anderen als die von mir angegebenen Quellen und Hilfsmittel benutzt habe.

Ich erkläre außerdem, dass diese Dissertation weder in gleicher oder anderer Form bereits in einem anderen Prüfungsverfahren vorgelegen hat.

Ich habe früher außer den mit dem Zulassungsgesuch urkundlich vorgelegten Graden keine weiteren akademischen Grade erworben oder zu erwerben versucht.

Würzburg, den 05.10.2007

---

Unterschrift

